IntechOpen

Wastewater and Water Quality

Edited by Taner Yonar

WASTEWATER AND WATER QUALITY

Edited by **Taner Yonar**

Wastewater and Water Quality
http://dx.doi.org/10.5772/intechopen.71219
Edited by Taner Yonar

Contributors

Belal Elgammal, Gehan Mohamed Ibrahim, Şule Camcıoğlu, Baran Ozyurt, Eduardo López-Maldonado, Mercedes T. Oropeza-Guzman, Amira Abdelrasoul, Shahin Layeghpour, Dan Selisteanu, Ion Marian Popescu, Emil Petre, Monica Roman, Dorin Sendrescu, Bogdan Popa, Elena Igorevna Vialkova, Marina Zemlianova, Jin-Hyuk Kim, Young-Seok Choi, Spar Mathews, Patricia Sithebe, Honggui Han, Xiaolong Wu, Junfei Qiao, Philiswa Nomngongo, Berna Kiril Mert, Nihan Goral, Esra Can Dogan, Coskun Aydiner, Ahmed Samir, Shreeshivadasan Chelliapan, Mohammed A. Ajeel, Irma Robles, Luis A. Godinez, Ana Karen Tovar

Notice

First published in London, United Kingdom, 2018 by IntechOpen
eBook (PDF) Published by IntechOpen, 2019
IntechOpen is the global imprint of INTECHOPEN LIMITED, registered in England and Wales, registration number: 11086078, The Shard, 25th floor, 32 London Bridge Street
London, SE19SG – United Kingdom
Printed in Croatia

British Library Cataloguing-in-Publication Data
A catalogue record for this book is available from the British Library

Additional hard and PDF copies can be obtained from orders@intechopen.com

Wastewater and Water Quality
Edited by Taner Yonar

p. cm.

Print ISBN 978-1-78923-620-0

Online ISBN 978-1-78923-621-7

eBook (PDF) ISBN 978-1-83881-539-4

Meet the editor

Dr. Taner Yonar is an associate professor at the Engineering Faculty, Environmental Engineering Department, Uludag University. He received his B.Sc. degree from the Environmental Engineering Department, Uludag University, in 1996. He has M.Sc. (1999) and Ph.D. (2005) degrees in Environmental Technology from the Institute of Sciences, Uludag University. He did his post-doctoral research in the Chemical Engineering and Advanced Materials Department, Newcastle University, UK, in 2011. He teaches graduate- and undergraduate-level courses in environmental engineering on water and wastewater treatment and advanced treatment technologies. He works on advanced oxidation, membrane processes and electrochemical processes. He is the author of over 70 research papers.

Contents

Preface

Protection of water sources has been a major problem for human beings since the industrial revolution. Water demand is also increasing day by day by the increasing population and industrial production. Increasing needs cause increasing water pollution. Briefly, we have to protect our planet not only as a source of water, but also because it is the habitat for many living species.

In this book, necessary theoretical knowledge and experimental results on water and water pollution are given. Its 11 chapters provide a wide variety of topics. Elgammal and Ibrahim discuss the recent drifts in pH-sensitive reverse osmosis membranes for water reuse in their chapter. Parallel to the increasing importance of membrane processes, Nomngongo discusses the membrane process usage potential on wastewater treatment. Kiril Mert, Aydiner, Dogan, and Goral present the efficient removal of micropollutants from wastewater by membrane bioreactors. Camcıoglu and Ozyurt investigate the applications of combined electrocoagulation and electro-oxidation treatment to industrial wastewater. Samir, Ajeel, and Chelliapan evaluate the treatment of textile wastewater using a novel electrocoagulation reactor design in their study. Lopez-Maldonado and Oropeza-Guzman's chapter offers an innovative study on coagulation/flocculation processes using biopolyelectrolytes for water reuse. Popescu, Popa, Sendrescu, Roman, Petre, and Selisteanu discuss distributed control systems for a wastewater treatment plant and also give case study results on advanced control solutions. Kim and Choi present a new design technique for a single-channel pump for wastewater treatment in their study. Mathews and Sithebe evaluate the role of bacteria on the breakdown of recalcitrant polychlorinated biphenyl compounds in wastewater. Han, Qiao, and Wu show an intelligent modeling approach to the prediction of effluent quality of wastewater treatment processes in their chapter. Sustainable sorbent materials obtained from orange peel as an agricultural waste and alternative sorbents for water treatment are presented by Robles, Tovar, and Godinez.

I would like to give my special thanks to Ms. Ivana Glavic for great support during the publishing of this book. I want to thank my mother, wife, and children for their support throughout my life.

Assoc. Prof. Dr. Taner Yonar
Engineering Faculty
Environmental Engineering Department
Uludag University
Bursa, Turkey

Chapter 1

Recent Drifts in pH-Sensitive Reverse Osmosis

Gehan Mohamed Ibrahim and Belal El-Gammal

Additional information is available at the end of the chapter

http://dx.doi.org/10.5772/intechopen.75897

Abstract

Preparation of some smart PAm-ZTS pH-responsive membranes, via reactions between ZTS and PAm under different conditions, was conducted for testing pressure-driven reverse osmosis membranes (PDROMs) in active rejection of Ce^{4+}, Pr^{3+}, Sm^{3+}, Gd^{3+}, Dy^{3+}, and Ho^{3+} ionic lanthanide species in their 3^+ and 4^+ states. Recent theoretical models to designate the membrane operations were mathematically itemized, after selective characterization of the PDROMs. The pH scale response of the membrane was confirmed using static adsorption and hydraulic pervasion result estimations. The flux across the PAm-ZTS membrane decreased with the lowering pH value, with drastic decreases between pH 4 and 7, and was both reversible and durable with pH shifts between ~3 and ~8. At lower pH 3, the individual pores were in a closed-state due to the prolonged structure of the amide chains on the porous surfaces. In contrast, at pH 8, the higher pH value, the membrane pores were in an open-state format, because of the collapsed structures of the amide chains. This grants a clear possible approach for manufacturing some pH-responsive composite membranes and inspires further design for their stimuli-responsive actions by incorporating molecularly designed macromolecules, synthesized by controlled polymerization.

Keywords: pH-responsive membranes, preparation, characterization, morphology, zeta potential, lanthanides, modeling

1. Introduction

Adsorption is the conventional chemical engineering process which is applied in many industries, including oil refineries, petrochemicals, and water and wastewater treatment. Adsorption is an effective separation strategy for the rejection of a wide range of contaminants,

including wastewaters, radioactive waste streams, and separation of radionuclides, but it is not so favorable for the elimination of anions like boron, perchlorates, and nitrates. Adsorption processes would be upgraded by integrating with supplementary processes to obtain hybrid processes with higher removal efficiency [1–5].

Osmosis is a physical technique that has been widely examined by researchers in different branches of science and engineering. Early researchers considered osmosis through naturally occurring materials, and from the mid of the nineteenth century, extraordinary consideration has been given to osmosis through manufactured materials. Following the advance in reverse osmosis over the most recent couple of decades, particularly for forward osmosis applications, the interests in different engineering purposes of osmosis had been impelled. Osmosis, or as it is at present alluded to as forward osmosis, has modern applications in wastewater treatment, sustenance preparing, and seawater/saline water desalination. Other one of a kind of regions of forward osmosis look into incorporate pressure retarding osmosis for era of power from saline and unused water and implantable osmotic pumps for controlled medication discharge [6–8].

2. Different categories of membrane processes

Recently, membrane technology has gained great attention as a powerful separation technique. **Figure 1** shows the main categories of the membrane processes. They are categorized mainly based on the size of the contaminants they can exclude from the input stream. Nanofiltration (NF) is one of the fourth classes of pressure-driven membranes appeared after microfiltration (MF), ultrafiltration (UF), and reverse osmosis (RO). It was first developed in the late 1970s as a variant of reverse osmosis membrane [ROM] with reduced separation efficiency for smaller and fewer charged ions such as sodium and chloride. As the term, NF was not known in the 1970s, such that membrane was initially categorized as either loose/open RO, intermediate RO/UF, or tight UF membrane. The term NF appears to have been first used commercially by the Film-Tec Corporation (now the Dow Chemical Company) in the mid-1980s to describe a new line of membrane products having properties between UF and RO membranes. Owing to the uniqueness and meaningfulness of the word NF, other membrane scientists have begun using it [9–11].

Because of late advancements and advances in osmosis innovation, fascinating film operations, including membrane desalination (MD), pressure retarding osmosis (PRO), and reversed electrodialysis (RED), have developed. These operations are equipped for creating spotless and reasonable power from different waste streams, including brackish water and debilitated water, which generally are viewed as natural liabilities. PRO and RED require blending of a high salinity content (e.g., seawater or brackish water and wastewater, separately) with a low salt content to produce power. MD has demonstrated the possibility to produce freshwater and power as an independent process. Reconciliation of MD with PRO or RED upgrades the execution of these procedures and gives a perfect and practical course to create freshwater and vitality [13–16].

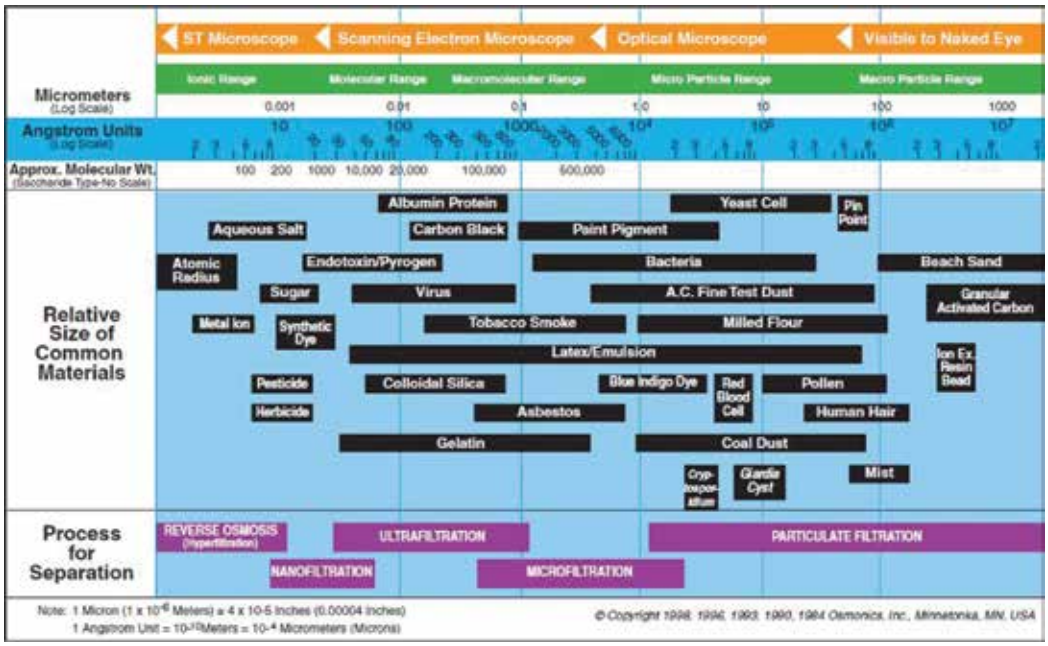

Figure 1. Classification of membrane processes according to separation type, relative size, and approximate molecular weight rejected materials [12].

3. Recent drifts in pH-responsive separation techniques

Recently, membrane technology has gained great attention as a powerful separation technique due to prominent advantages over common processes such as high removal efficiency, low energy consumption, fast kinetic, small footprint, and ease of scale up. They are favored for full-scale applications due to normal operating conditions, high productivity, and low energy consumption. They can efficiently eliminate many contaminants including proteins, macromolecules, natural organic matters (NOMs), dyes, dissolved organic matter (DOM), boron, and compounds responsible for odor and color, from aqueous media. However, the recent achievements for pH-responsive membranes require an ion exchange separation in some cases. **Figure 2** shows a combination between adsorption and membrane separation. The overall removal efficiency of the hybrid process would be enhanced [17–19]. Generally, three different procedures for hybridization of membrane systems with adsorption processes may be found:

- Adsorption treatment before membrane filtration (pretreatment layout)
- Integrated adsorption/membrane processes (IAMPs)
- Adsorption treatment after membrane filtration (post-treatment layout)

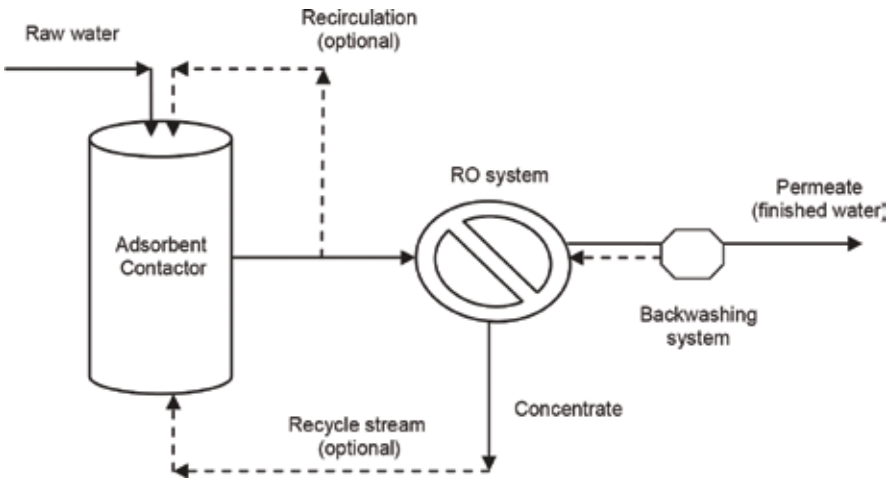

Figure 2. Membrane/adsorption hybrid process with adsorption pretreatment.

The current chapter deals with the adsorption/membrane integrated systems. As could be seen in **Figure 2**, some promising advantages of adsorption/membrane integrated systems could be obtained. They include:

1. Expanding separation efficiency
2. Diminishing process cost
3. Diminished membrane fouling in some cases
4. Straightforwardness of handling and fast control compared to conventional treatments
5. Lower volume of discharge
6. Potential request of beneficial biosorbents
7. Reusability of both membranes and adsorbents
8. Firm removal kinetics
9. Low-energy feed requirements versus adsorption columns, NF and RO systems
10. Low-pressure drop against adsorption columns

4. Fabrication of pH-responsive membranes

Intended for the pre-synthesis of pH-responsive polyacrylamide zirconium titanosilicate (PAm-ZTS) membranes, liquid titanium(IV)chloride (98%), $TiCl_4$, 189.68 [g/mol], 1.728 g/cm^3 (20°C), and zirconium(IV)oxychloride octahydrate powder (>99.5%), $ZrOCl_2.8H_2O$, 321.26752 [g/mol], 1.91 g/cm^3 (20°C), pH value ~1 (50 g/l, H_2O, 20°C), were picked up from Merck Chemicals,

Darmstadt, Germany, while Sigma-Aldrich tetraethyl orthosilicate $(C_2H_5O)_4Si$ 208.33 [g/mol], 0.93 g/cm^3 (20°C), USA was used.

Because of the immense difference between the traditional organic polymers and the corresponding inorganics in their natures and due to strong aggregation of the nanofillers, polymer-inorganic nanocomposite PAm-ZTS membranes cannot be prepared by common schemes such as melt blending and roller mixing. The most frequently secondhand synthesis techniques in the production of nanocomposite membranes can be allocated as three categories [20].

The sol-gel method, the former category secondhand preparation procedure, in which organic monomers, oligomers, or polymers and inorganic nanoparticle precursors are well balanced in solution. The inorganic pioneers were mixed together by gradual addition of tetraethyl orthosilicate, dissolved in equal volumes of bidistilled water and ethyl alcohol with vigorous stirring to zirconium oxychloride octahydrate and titanium tetrachloride solutions, previously dissolved in concentrated hydrochloric acid. The total components are instantly hydrolyzed in an appropriate quantity of water, following to condensation into well-dispersed nanoparticles in the polyacrylamide polymer skeleton with different mole fractions. The reactions' conditions are moderate; usually room temperature, an ordinary atmospheric pressure, and the concentrations of organic and inorganic components are easy to control over the solution. Additionally, the precursor ingredients, as organic and inorganic ingredients could be dispersed in nanometer level in the membranes, and thus the formed membranes are homogeneous. Other techniques as solution mixing and in situ polymerization are used.

5. Characterization of pH-responsive membranes

RO polymerized membranes are different in a couple of characteristics such as material, morphology, transport/separation mechanism, and applications [21–24]. Therefore, a large number of methodologies are required for their characterizations. They can be generally divided into three major tests, that is, methods used for chemical analysis, methods used for physical analysis, and filtration process for assessing membrane separation performance. Depending on the applicable utilization of RO membranes, their stability assessments against chlorination, organic solvent, thermal, and fouling can also be performed to examine their sustainability under specific environments.

Table 1 describes some instrumental methods used in depicting RO membranes with respect to their chemical and physical characteristics, as well as their separation performances and stability. In a wide range, before conducting RO experiments, various techniques can be employed for their characterization in order to obtain a good knowledge of their parameters that are prominent for manufacturing a membrane with the right integration of water flux and solute rejection. For reverse osmosis pH-responsive membranes, zeta potential is well-thought-out as one of the significant parameters to determine the routes and mechanisms that the membranes behave according to its chemical properties.

Property assessment	Instrument/method	Property assessment	Instrument/method
Chemical properties	ATR-FTIR spectroscopy Zeta potential analysis XPS X-ray diffractometry (XRD) Nuclear magnetic resonance (NMR) spectroscopy	Physical properties	SEM/FESEM TEM Atomic force microscopy (AFM) Contact angle analysis PAS
Separation performance	Permeability selectivity	Stability test	Chlorination Solvent Thermal Filtration

Table 1. Assessments on membrane properties and performances based on different analytical instruments/methods.

5.1. Zeta potential

Zeta potential is a surface charge property for RO membranes at different pH environments. The analysis is particularly significant to help recognize the acid–base features of RO membranes and to predict their separation productivity, as well as to consider the fouling propensity of RO at different water pHs [25–27]. Based on the Helmholtz-Smoluchowski equation with the Fairbrother and Mastin approach, zeta potential can be persistent from the measurement of the streaming potential using Eq. (1):

$$\zeta = \frac{\Delta E}{\Delta P} \frac{\mu k}{\varepsilon \varepsilon_{\circ}} \tag{1}$$

where ΔE is the streaming potential, ΔP is the applied pressure, $\boldsymbol{\mu}$ is the solution viscosity, $\boldsymbol{\kappa}$ is the solution conductivity, and ε and $\varepsilon_{\circ}$ are the permittivity of the test solution and free space, respectively. Several assumptions are inherent in this equation. They are (1) flow is laminar, (2) surface conductivity has no effect and has homogeneous properties, (3) width of the flow channel is much larger than the thickness of the electric double layer, and (4) no axial concentration gradient occurs in the flow channel.

The surface zeta potential of ZTS, PAm, and PAm-ZTS, as pH-Responsive membranes, measured at 25°C, are shown in **Figure 3**. Taking a horizontal section at the zero point of charge shows that the isoelectric point of ZTS, PAm, and PAm-ZTS was about 4.01, 5.7, and 7.6, respectively; throughout membrane testing, an electric potential is induced when cations and anions enclosed by the electrical double layer are forced to migrate along with the flow tangential to the ROM surface; in consequence, a potential difference could be initiated. Mostly, the streaming potential of the membrane surface is being measured. The typical pH range applied for determining surface zeta potential of a ROF membrane used to fall within pH 2–12, more preferably, between pH 3 and 9. The pH of the background electrolyte (5 mM KCl, 25°C) can be adjusted by the addition of either an acid, 0.1 M HCl (or HNO_3), or a suitable base electrolyte, 0.1 M NaOH (or KOH) solution. Owing to the workable irreversible change of membrane surface characteristics, it is highly urged to

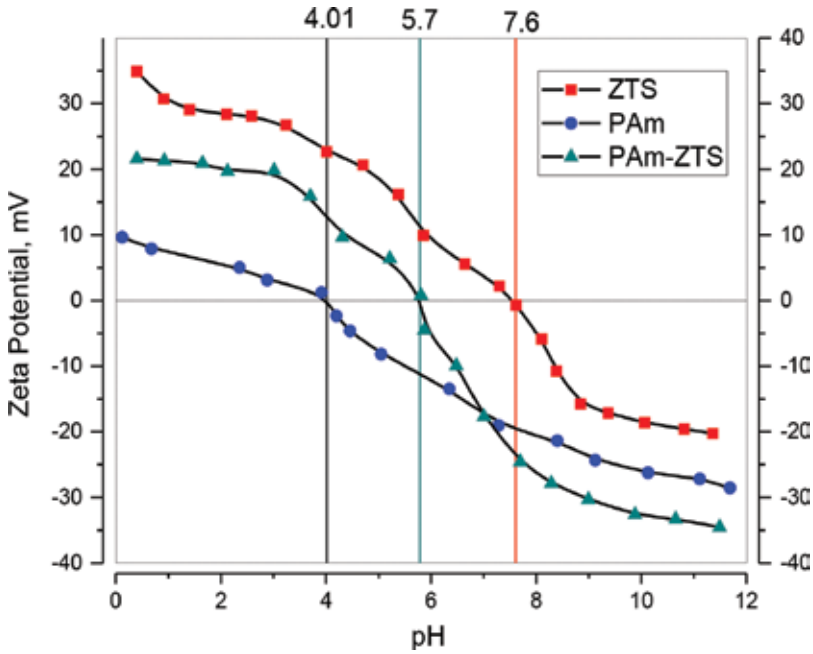

Figure 3. Surface zeta potential as a function of pH for pH-responsive membranes made of ZTS, PAm-ZTS, and Pam, measured at 25°C.

conduct this investigation using two identical freshly prepared ROMs, that is, one for acid titration (pH 6 down to pH 2) followed by another identical membrane for alkali titration (pH 6 up to pH 12).

PAm-ZTS RO membranes tended to have more positive charge owing to the protonation of the amine functional groups. In contrast, the negative charge of RO membranes at higher pHs can be attributed to the loss of functional groups [28–30]. Deprotonation of amine functional groups coupled with either dissociation of the carboxylic acid group or sulfonic acid group on the membrane surface may occur. In brief, in the membranes with organic origin, PAm is more negatively charged than that of that made up of ZTS and PAm-ZTS till pH 7 [25, 31, 32]. Besides showing the positive and negative charge values of a membrane, zeta potential profile can also reveal the isoelectric point (IEP) of the RO membrane at which the membrane surface carries no net electrical charge (i.e., neutral).

Depending on the functional groups of RO surface, a highly positively charged RO membrane could also be prepared, in which this membrane displays a positive zeta potential over a wide range of pH values (pH 2–11). The phenomenon is mainly due to the presence of pendant tertiary amine groups in some polymers used to fabricate the membranes. It was also reported to cause the membrane to be positively charged for pH ranging from 3 to 9 [33, 34]. A summary of the surface zeta potential of some RO membranes made of different monomers at two different pH environments is presented in **Table 2** [25–27].

Type of NF Membrane[a]	IEP (pH)	ζ (mV) at pH 3	ζ (mV) at pH 9
MPF-34 (Koch Membrane Systems)	4.5	~13	~ –34
Desal-5DK (GE Osmonic)	3.9	~18	~ –50
NF 270 (DOW FILMTEC)	3.2	~5	~ –75
BW30 (DOW FILMTEC)	3.6	~2	~ –10
NF90 (DOW FILMTEC)	4.2	~14	~ –24
PIP–TMC–MWCNT NF membrane	2.6	~ –1.2	~ –7
MPD–TMC NF membrane	6.0	~28	~ –11
PIP–TMC–GO NF membrane	5.4	~25	~ –32
PVAm–TMC NF membrane	6.5	~19	~ –12
AEPPS–PIP–TMC NF membrane	4.1	~1.3	~5.6
PES–TA NF membrane[b]	10.7	~32	~6
PIP–*mm*-BTEC NF membrane[b]	–	~28	~4
PEG600–NH_2–TMC NF membrane[b]	~8.9	~19	0

aAEPPS—N-aminoethyl piperazine propane sulfonate, MPD—m-phenylenediamine, *mm*-BTEC—3, 3′, 5, 5′-biphenyl tetraacyl chloride, MWCNT—multi-walled carbon nanotube, GO—graphene oxide, PES–TA—poly (arylene ether sulfone) with pendant tertiary groups, PIP—piperazine, PVAm—polyvinylamine, and TMC—trimesoyl chloride.
bThese NF membranes are positively charged over a wide pH range.

Table 2. Summary of the surface zeta potential of some NF membranes at different pH environments.

It should be noted here that besides surface zeta potential measurement, the conventional titration method can also be employed to evaluate the ion exchange capacity of the RO membrane. Any change in the membrane ion exchange capacity can be related to the amount of charged groups that exist on a membrane.

5.2. Surface topography of PAm-ZTS pH-responsive membranes

In white-LED illumination focused by AFM, as shown in **Figures 4a** and **5a**, the surface topography of the prepared PAm-ZTS was different as the pH of the treatment was switched from three to eight. **Figures 4b** and **5b** explain the three-dimensional image of the pH-responsive membranes. The surface roughness was depicted by the histograms in **Figures 4c** and **5c**, with a broad distribution from less than 50 nm to more than 290 nm, and has a median value of roughly 130 nm in the case of PAm-ZTS treated at pH = 3, while PAm-ZTS treated at pH = 8 has a spread-out distribution between about 20 and 300 nm with an average value of circa 115 nm.

The dissection of **Figures 4a–c** and **5a–c** illuminates the photomicrograph of the cross section in the compact layer morphology of dry/wet phase inversion shear to cast PAm-ZTS asymmetric membrane, in a strained convection dwelling time for 15 s, at pHs 3 and 8, separately. This microstructure had the relatively fit dense skin layer with inconspicuous flaws backed on a highly open nanoporous sublayer containing not only nanovoids but also micro-voids. These

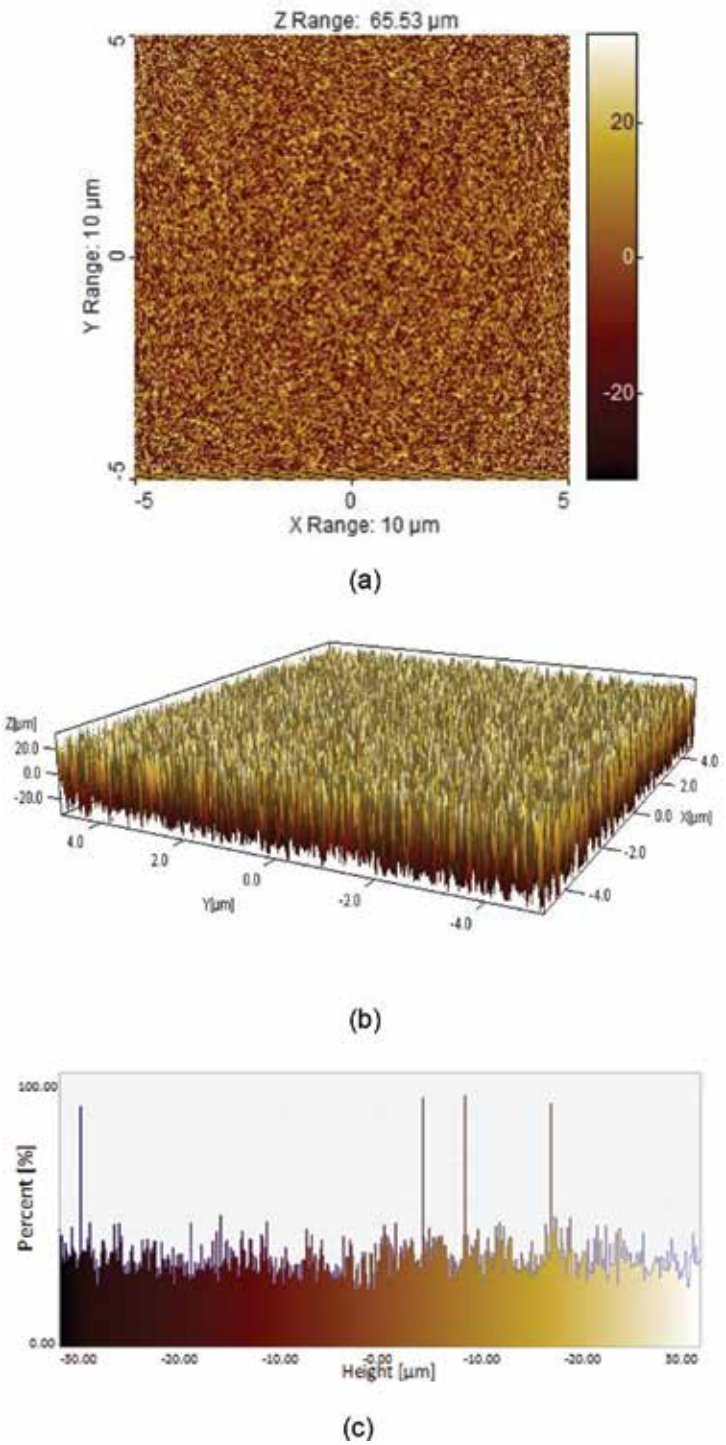

Figure 4. Surface topography of PAm-ZTS as pH-responsive membrane, measured at 25°C after treatment at pH 3.

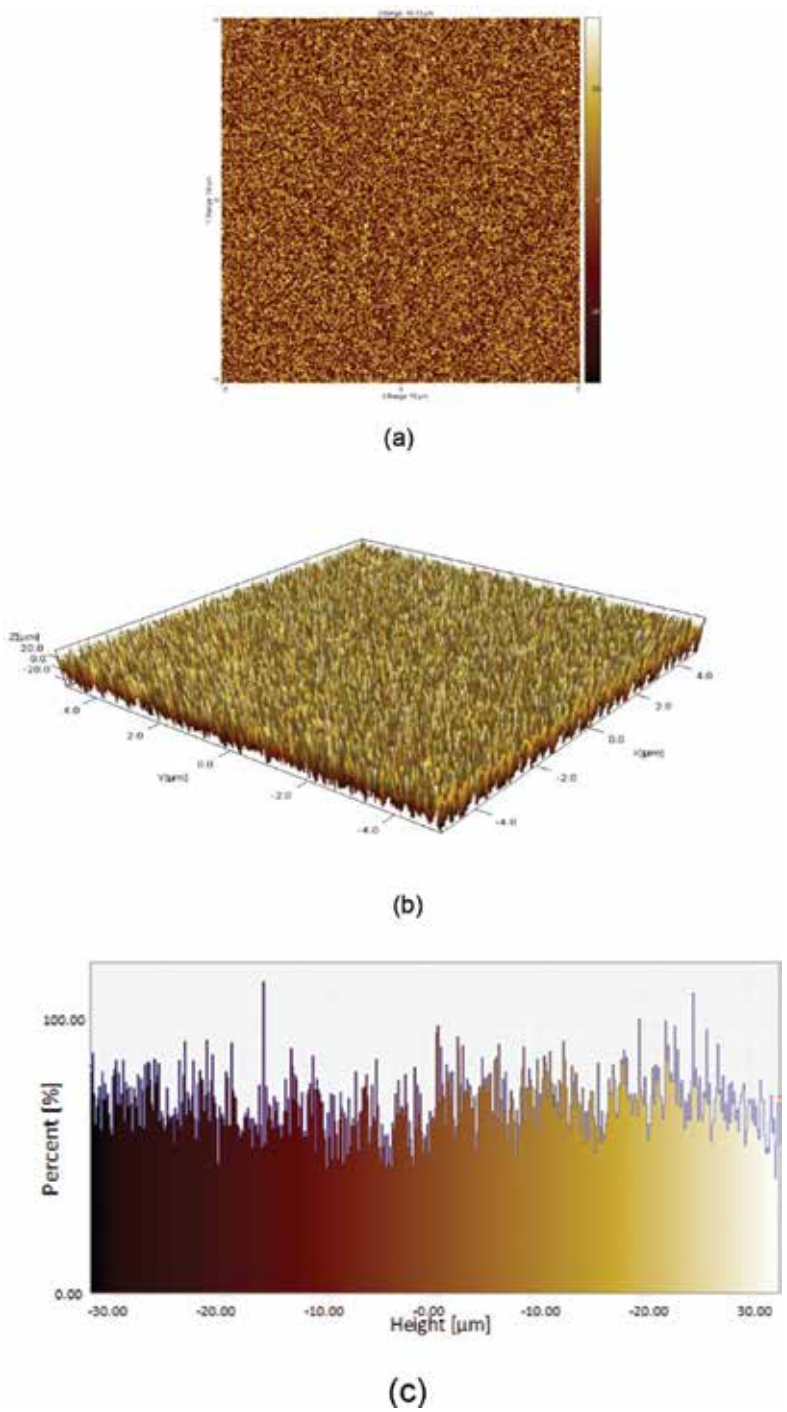

Figure 5. Surface topography of PAm-ZTS as pH-responsive membrane, measured at 25°C after treatment at pH 8.

were truly similar to those found in the aqueous quenched asymmetric ROMs [35–37]. The nanovoids did not span the width of the ROM evoking that these nanovoids are provoked by disparate mechanisms. In this case, the creation nanopores were formulated by intrusion of non-solvent through defects in the surface layer during wet phase separation, in a step for membrane reinforcement. Additionally, no surface pores could be observed on the outer surface of RO membrane, even at 5000X magnifications 5000X magnifications. This indicated that the diameters of any surface pores were at least less than 20 A°, which would be helpful to be applied for reverse osmosis separation rather than ultrafiltration or nanofiltration.

6. Modeling of pressure-driven membranes

The natural water resources contain solids in two forms, suspended and dissolved [16, 38, 39]. Suspended solid-state matters exist in insoluble particulates, debris, seawater microorganisms, silt, or colloids. Dissolved matters are present as ions, preferably as chloride, sodium, calcium, or magnesium. Principally, all desalination plants incorporate two-key treatment steps, sequentially designed to remove suspended and dissolved matters from their sources.

The first step of pretreatment removes the suspended solids from water resources or the naturally occurring soluble solids that may turn into a solid form and precipitates on the ROMs during separation processes. The second step of the RO system separates the dissolved solids from the pretreated saline source water, thereby producing fresh low-salinity water convenient for human utilization agricultural purposes and industrial implementations.

Subsequent pretreatment is designed for the left solids in the source stream; it includes the dissolved minerals. As long as the desalination system is operated in a manner that prevents these minerals from precipitating on the membrane surface, the ROMs could operate and produce freshwater of persistent nature at a high rate deprived of the need to clean these ROMs for long periods.

Notwithstanding pretreatment systems remove most but not all the insoluble solids contained in the saline source water and may not always effectively protect some of the soluble solids from precipitating on the membrane surface, the suspended solids, silt, and natural organic matter (NOM) that remained which may accumulate on ROM surface causing the loss of membrane productivity. In inclusion, saline water contains microorganisms as well as dissolved organics that could serve as food for these microorganisms. Consequently, a biofilm could form and grow on the ROM surface, causing loss of membrane productivity as well.

The protocol of reduction/loss of productivity of ROMs due to agglomeration of suspended solids and NOM, precipitation of dissolved solids, and/or establishment of biofilm on the ROMs surface is known as membrane fouling (MF). Excessive MF is undesirable since it has a negative impact on ROM productivity; it could also result in an increased consumption of energy for salt separation and in deterioration of product water quality.

6.1. External and internal fouling

The classification of the fouling phenomenon depends on the location of the accumulated rejected salts; it can be viewed as [40, 41]:

1. External or "surface" fouling (EF)
2. Internal fouling (IF)

EF involves accumulation of rejected salts on the surface of the membranes by three distinct paths:

- Construction of mineral deposits (scale)
- Construction of cake of rejected solids, particulates, colloids, and other organic and/or inorganic matters
- Biofilm construction, i.e., growth of colonies of microorganisms on the surface of the membranes, rapidly attachable by excretion of extracellular materials

Typically, the three mechanisms can occur in any combination at any given time. However, external membrane fouling of ROMs is most frequently caused by biofouling.

IF is a regular loss of membrane productivity due to changes in its chemical structure either by physical compaction or by chemical degradation. Physical deterioration of the membrane may result from long-term application of feed stream at pressures higher than that designed for the ROMs; they are designed to handle 83 bars for sea water reverse osmosis membranes and/or by their continued setup at source water temperatures above 45°C, the limit of safe membrane operation. Chemical deterioration results from continuous exposure to strong oxidants, e.g., chlorines, bromines, ozones, permanganates, peroxides chemicals, and very strong acids, typically pH < 3 and alkali at pH > 12.

The difference between EF and IF is somewhat clear; EF could be completely reversed by chemical cleaning, while IF causes permanent damage of the micropores, resulting in an irreversible changes.

6.2. Concentration polarization fouling

Concentration polarization (CP) phenomenon entails the formation of a boundary double layer along the membrane surface, with salt concentration considerably higher than that of the starting injected solution as revealed in **Figure 6** [42–44]. C_b is the salt concentration within the boundary layer; C_s is the salt concentration at the inner membrane surface, and C_p is the lower salt content of the freshwater on the pass through side.

As indicated in **Figure 6**, the flow comes to pass in the boundary layers of the feed/concentrate spacers; two different types are encountered: a convective flow of fresh feed solution from the bulk and diffusion flow of repelled drain salts, coming back into the feed flow. In that concern, the semipermeable ROM is designed to give higher rate of convective flow than the diffusion flow, as the salts and particulate solids discarded tend to pile up with highest salt contents on the inner surface of the ROM. The concentration of solid particulates in the boundary layer

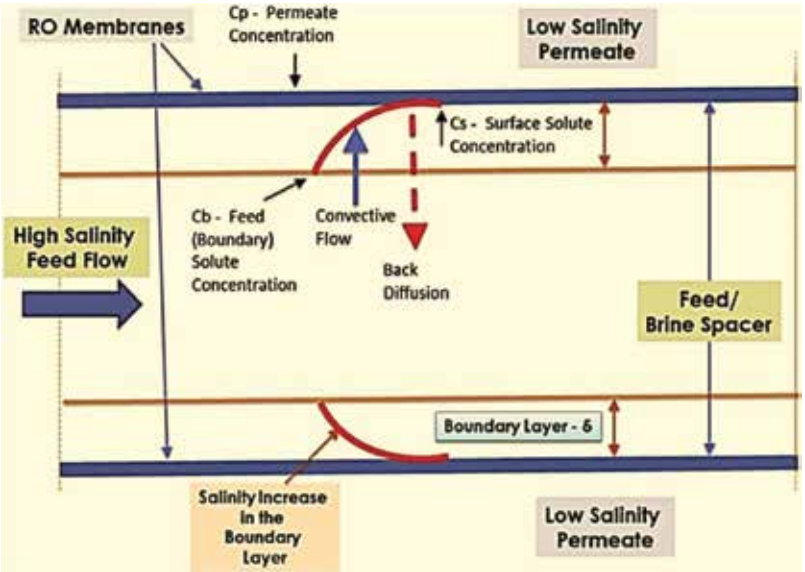

Figure 6. Boundary layers in a membrane-feed spacer. RO, reverse osmosis.

leads to critical negative significances on the ROM function. They include increased osmotic pressure, increased salt extract, creation of hydraulic opposition of water stream, and Induction of scale and fouling on the ROM.

Concentration polarization cannot be evaded; it can only be reduced before taking any corrective measures; concentration polarization should be quantified. This quantification occurs in three separate consecutive paths. They can be emphasized as balancing the chemical and mass balance equations across the boundary layer, balancing the transport equations over the ROM and determination of solute transport equations within the pores of the ROM. System performance can be predicted by simultaneous solution of all these three equations. Based on the type of concentration polarization, there are two classes of models: an osmotic pressure-controlled model and a gel layer-controlling model.

6.3. Osmotic pressure controlled model [OPCM]

In this situation, solute particles form a viscous boundary layer concluded on the surfaces of ROMs [45–47]. Solute concentration increases from the bulk to membrane surface concentration across the mass transfer barrier layer. In this case, the width of the mass transfer boundary layer is constant. At any cross section of the boundary layer for the concentration gradient, $\frac{dc}{dy}$, at the steady state, the solute mass steadiness leads to

$$\left[\left(v_w\, c - v_w\, c_p\right) + D\,\frac{dc}{dy}\right] = 0 \tag{2}$$

where v_w is the permeate flux in $m^3/m^2.s$; c and c_p are the bulk and permeate concentrations in kg/m^3; and D is the solute diffusivity in m^2/s.

Integrating the above equation across the thickness of the mass transfer boundary layer, the governing equation of the flux is obtained as

$$v_w = \left(\frac{D}{\delta}\right)\ln\left(\frac{c_m - c_p}{c\circ - c_p}\right) = k\ln\left(\frac{c_m - c_p}{c\circ - c_p}\right) \tag{3}$$

This equation is well known as the film theory equation. In the above equation, k is the mass transfer coefficient in m/s, δ is the mass transfer boundary layer thickness in m, and c_m, c_p, and c are solute concentrations at the membrane-feed solution interface, in the permeate and in the bulk, generally expressed in kg/m^3, respectively. The mass transfer coefficient is estimated from the following equations depending on the channel geometry and flow regimes. In the rectangular channel, the mass transfer coefficient is estimated using the following Sherwood number relations. For laminar flow (Leveque's equation):

$$Sh = \frac{k\,d_e}{D} = 1.85\left(ReSc\,\frac{d_e}{\mathrm{L}}\right)^{\frac{1}{3}} \tag{4}$$

where, Sh, Re, and Sc are the numbers related to Sherwood, Reynolds, and Schmidt, respectively, d_e is the equivalent diameter in m, and L is the length of the membrane in m. For turbulent flow, Leveque's equation gives rise to (Dittus-Boelter equation):

$$Sh = 0.023(\mathrm{Re})^{0.8}(Sc)^{0.33} \tag{5}$$

In the case of flow through the tube with diameter d in m, the mass transfer coefficient is estimated for laminar flow (Leveque's equation) (Gekas and Hallstrom 1987):

$$Sh = \frac{k\,d}{D} = 1.62\left(ReSc\,\frac{d_e}{\mathrm{L}}\right)^{\frac{1}{3}} \tag{6}$$

In addition, for the turbulent flow, it is calculated from Eq. (5). Now, the transport equation in the flow channel, Eq. (4), must be coupled with the transport law through the porous membrane. It is expressed as Darcy's law:

$$v_w = \mathrm{L}_P\,(\Delta P - \Delta\pi) \tag{7}$$

where $\Delta\pi$ is the osmotic pressure difference between the membrane sides that effectively are related to the quantity of matter, especially the concentration and inversely proportional to the molecular weight of solute; it is a linearly proportional to concentration in the case of a typical salt or lower molecular weight solutes. However, it deviates from linearity in the case of polymers, proteins, and higher molecular weight solutes. In Eq. (2) there are three unknowns, namely, v_w, c_p, and the finally predicted c_m. The comprehensive correlation between the osmotic pressure and concentration, $\pi = ac$, could be pragmatic equation for osmotic pressure difference at the ROM surface as

$$\Delta\pi = \pi_m - \pi_P = a_1[c_m - c_P] + a_2\left[{c_m}^2 - {c_P}^2\right] + a_3\left[{c_m}^3 - {c_P}^3\right] + \ldots\ldots + a_n[c_m n - c_P n] \quad (8)$$

where the constant coefficient is known as the difference between $a_1$and a_{n} and real retention could be defined by c_m and c_P indicated as the coefficients across the ROM phases, respectively, namely, the upstream and downstream phases. Therefore, Eq. (7) can be written in terms of the single parameter c_m using Eq. (2), to reduce the system variables to c_m and v_w, instead of the existing three parameters. The new variables can be attained by solving Eqs. (4) and (6) using an iterative algorithm like the Newton-Raphson equations. This model is known as classic-film model or the osmotic pressure-controlling model.

6.4. Solution diffusion model for RO/NF

The real retention is a partition coefficient, or really the solute flux across the membrane considered using the solution diffusion model described earlier; linear relationship is considered between π and c in the case of salt solution, $\pi = ac$ [42, 43, 48, 49]. In practice, Eq. (6) and the film theory equation, Eq. (4), are only considered. Therefore, the osmotic pressure model could be rewritten as

$$v_w = v_w^o\,[1 - \alpha\,(c_m - c_P)] \quad (9)$$

where

$\alpha = \frac{a}{\Delta p}$ and $v_w^o = L_P\,\Delta P$ are the pure water flux.

The above equation can be equated with the film theory equation and the following equation results:

$$v_w^o\,[1 - \alpha(c_m - c_P)] = k\ln\left[\frac{c_m - c_P}{c\circ - c_P}\right] \quad (10)$$

From the solution diffusion model, the solute flux is written as

$$v_w\,c_P = B(c_m - c_P) \quad (11)$$

where B is a constant. Combining Eqs. (8) and (10), the following equation is obtained:

$$v_w^o\,[1 - \alpha(c_m - c_P)] = B\left[\frac{c_m - c_P}{c_P}\right] \quad (12)$$

The above equation can be simplified as.

$$1 - \alpha c_m + \alpha c_P = \beta\left[\frac{c_m - c_P}{c_P}\right] \quad (13)$$

where $\beta = \frac{\mathrm{B}}{\mathrm{v_w^o}}$

From the above equation, the membrane surface concentration is obtained as

$$c_m = c_P\left[1 + \left(\frac{1}{\beta + \alpha c_P}\right)\right] \tag{14}$$

Putting c_m from the above equation into Eq. (9), we get

$$\frac{\beta v_w \circ}{\alpha c_P + \beta} - k \ln\left[\frac{c_P}{(\alpha c_P + \beta)(c \circ - c_P)}\right] = 0 \tag{15}$$

Once more a trial-and-error formula for c_P is tried using a standard iterative technique.

6.5. Kedem-Katchalsky model [KKM]

KKM is considered as another alternate to osmotic pressure one, in which the imperfect retention of the solutes by the RO/NF/UF membranes is incorporated by a reflection coefficient in the equation of the final output flux [50, 51]:

$$v_w = \mathrm{L}_P(\Delta P - \sigma \Delta \pi) \tag{16}$$

where σ is the reflection coefficient. Using π in the above equation gives rise to the following flux equality:

$$v_w = \mathrm{L}_P\left[\Delta P - a\sigma(c_m - c_P)\right] \tag{17}$$

Turning back to the film theory, the concentration on the ROM surface could be rewritten by

$$c_m = c_P + (c^o - c_P)e^{\frac{v_w}{k}} \tag{18}$$

Combining Eqs. (15) and (17), the following equation is obtained:

$$v_w = \mathrm{L}_P\left[\Delta P - a\sigma\left((c^o - c_P)e\frac{v_w}{k}\right)\right] \tag{19}$$

By means of Eq. (19), c_P could be conveyed in terms of $c_m$by using Eq. (10), followed by solving Eq. (18).

6.6. Modified solution diffusion model [MSDM]

The solute transports across the RO/NF/UF membranes are given by adopting both the convective transport and the diffusive transport of the solutes across the voids of the membranes and writing the corresponding flux equation as [52–54]

$$v_w\, c_P = B(c_m - c_P) + (1 - \sigma)v_w\, c_{av} \tag{20}$$

where

$$c_{av} = \frac{c_m - c_P}{\ln\left(\frac{c_m}{c_P}\right)}$$

By combining Eqs. (4) and (19), we get

$$c_P = \frac{\beta}{v_w}\left[\left(c\circ - c_p\right)e^{\frac{v_w}{k}}\right] + \left[\frac{(1-\sigma)\left(c\circ - c_P\right)e^{\frac{v_w}{k}}}{\ln\left(1+\left(\frac{c\circ - c_P}{c_P}\right)e^{\frac{v_w}{k}}\right)}\right] \tag{21}$$

From the mentioned equations between (16) and (21) in c_m, v_w, and c_P, we can iteratively obtain a system prediction.

The MSDM cons are described by the hypotheses that the mass transfer boundary layer is fully developed, whereas the corresponding entrance length required is substantial. Furthermore, physical properties such as diffusivity and viscosity considerably do not vary with concentration, while mass transfer coefficients are calculated from heat-mass transfer analogies applicable for impervious conduits.

On the other hand, the film theory-based osmotic pressure model presents a simple and quick method for quantifying system performance. In order to overcome these cons, the two-dimensional mass transfer boundary layer equation can be solved, and/or detailed pore flow models can be incorporated. Many studies are available including these intricacies of the model.

6.7. Gel layer-controlling model (GLCM)

In this approximation, the gels of concentrated solutes are deposited over the ROM surface with certain thickness in a uniformly fixed distribution of the solutes, and an outer mass transfer boundary film is formed [52, 55]. In that, the film theory, in which the solute concentration extends from feed concentration and gel concentration undergoing drastic variation in viscosity, diffusivity, and density, can be applied to obtain the equation of permeate flux as

$$v_w = k\ln\left(\frac{c_g}{c^o}\right) \tag{22}$$

7. pH-responsive characteristics of PAm-ZTS membrane

The pH-sensitive characteristics of PAm-ZTS membrane were achieved upon static adsorption modes of Ce^{4+}, Pr^{3+}, Sm^{3+}, Gd^{3+}, Dy^{3+}, and Ho^{3+} using both Langmuir and Freundlich Isotherms, as well as the reverse osmosis dynamic mode.

7.1. Langmuir and Freundlich isotherms

The utilization of Langmuir and Freundlich isotherms to depict the complexation process of binding metal ions in the polymer has previously been investigated using the washing and

enrichment methods of the PEUF process [22, 24]. However, the different metal ions were subjected directly to reverse osmosis in the absence of any binding polymers. In this case, the assumption that the concentration of metal ions in the permeates, C_{pi}, symbolizes the concentration of metal that is free in the solution, Y_i, is prepared.

The Langmuir isotherm equation is given by [20, 56, 57]

$$Q = \frac{Q_{max} Y_i}{K_L + Y_i} \tag{23}$$

where: Q is the amount of metal ion, whereas Q_{max} is the maximum capacity of polymer (mg metal/g membrane).

Y_i is the metal free in solution (mg/l).

K_L is the Langmuir equilibrium constant (mg/l).

Langmuir equation gives a linear form:

$$\frac{1}{Q} = \frac{K_L}{Q_{max}} + \frac{1}{Y_i} + \frac{1}{Q_{max}} \tag{24}$$

The Freundlich isotherm equation is given by

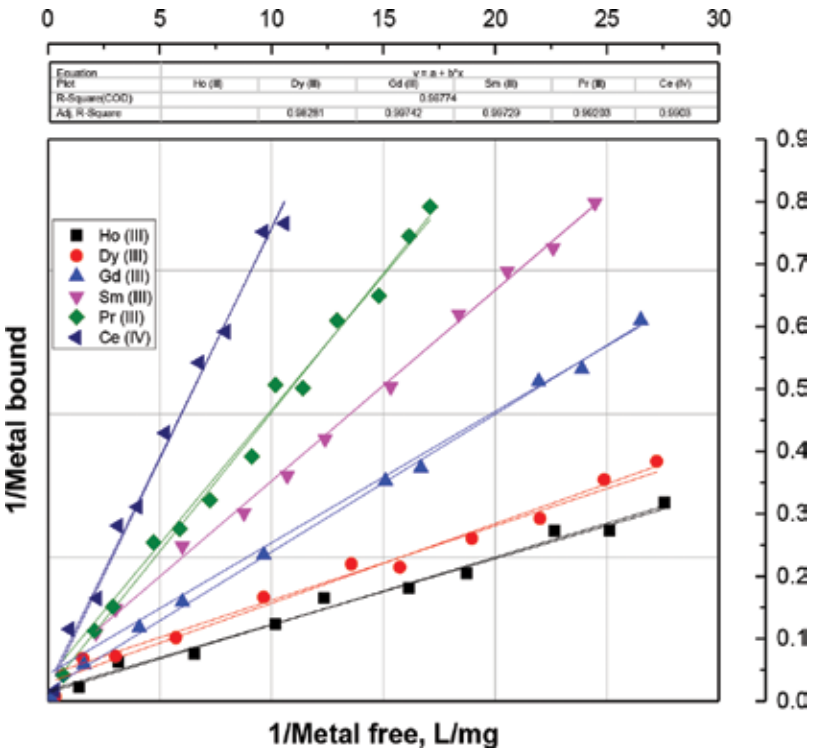

Figure 7. Langmuir isotherm model fits to the experimental data for binding of single metal ions at pH 3.

$$Q = K_F\, Y_i^{n} \tag{25}$$

where Q is the amount of metal ion, K_F is the Freundlich equilibrium constant ($mg^{1-n}\, g^{-1}l^{n}$), Y_i is the metal free in solution (mg/l), and n is a constant. Freundlich equation gives a linear form [58–62]:

$$\ln Q = n \ln Y_i + \ln K_F \tag{26}$$

Figure 7 displays the linear regression fits of the Langmuir isotherm to the data obtained for particular metal ions in solution with PAm at pH 3 upon PAm-ZTS surface. The Langmuir isotherm fitted the test data very well (R^2 values >0.98). **Figure 8** exhibits the fits of the experimental data to the Freundlich isotherm at the same pH. Although this model fits the data intelligently well, the fit was not as good as the Langmuir model. This issue discloses that the Langmuir isotherm offers a better description of the binding of metal ions to PAm-ZTS than the Freundlich isotherm [63–66]. However, for all cases, the Q_{max} asset value was found in the following order [20]:

$Ce^{4+} > Pr^{3+} > Sm^{3+} > Gd^{3+} > Dy^{3+} > Ho^{3+}$

These rates can be applicable when considering the retention of the metal ions during the RO process.

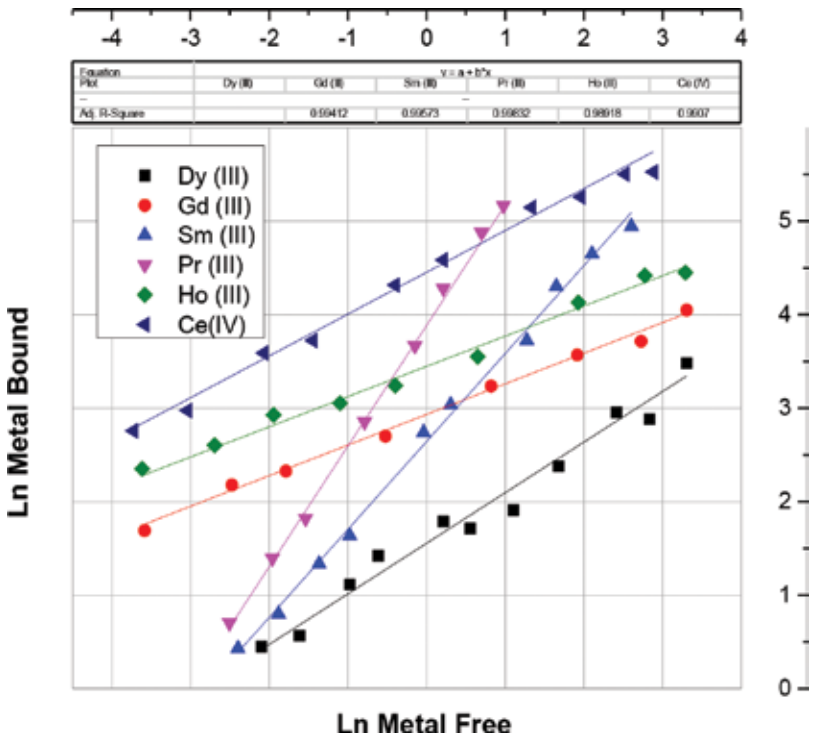

Figure 8. Freundlich isotherm model fits to the experimental data for binding of single metal ions at pH 3.

7.2. Rejection of metal ions

Solute rejections of PAm-ZTS membrane under environmental pH values of 3 and 8 are performed to further evaluate the pH-responsive gating function of membrane. The feed solution is prepared by dissolving Ce^{4+}, Pr^{3+}, Sm^{3+}, Gd^{3+}, Dy^{3+}, and Ho^{3+} in pH buffer with different concentrations mg/l, and the buffers of pH 3 or pH 8 is freshly prepared by adding HCl or NaOH in DI water. The experimental conditions of filtration tests are the same usually used for hydraulic permeability measurements at 0.1 MPa. All the Ce^{4+}, Pr^{3+}, Sm^{3+}, Gd^{3+}, Dy^{3+}, and Ho^{3+} solutions are used as feed solution only within 48 h after preparation. In the filtration test, membranes are conditioned with buffers of pH 3 and pH 8 firstly [67, 68].

Then the permeability of Ce^{4+}, Pr^{3+}, Sm^{3+}, Gd^{3+}, Dy^{3+}, and Ho^{3+} solutions is monitored until the stabilization of membrane is reached and the filtrate is collected. Concentrations of Ce^{4+}, Pr^{3+}, Sm^{3+}, Gd^{3+}, Dy^{3+}, and Ho^{3+} ions in the filtrate solution are measured with Buck Scientific 210 VGP Atomic Absorption Spectrophotometer. The function of examination of the permeate samples for the relevant metal allows the calculation of the observed retention value (R_i) of each metal ion using [9, 42]

$$R_i = \left(1 - \frac{C_{Pi}}{C_{fi}}\right) \times 100 \tag{27}$$

where C_{pi} is the concentration of metal ion, i in the pass through, and C_{fi} is the concentration of metal ion, i in the primary feed solution.

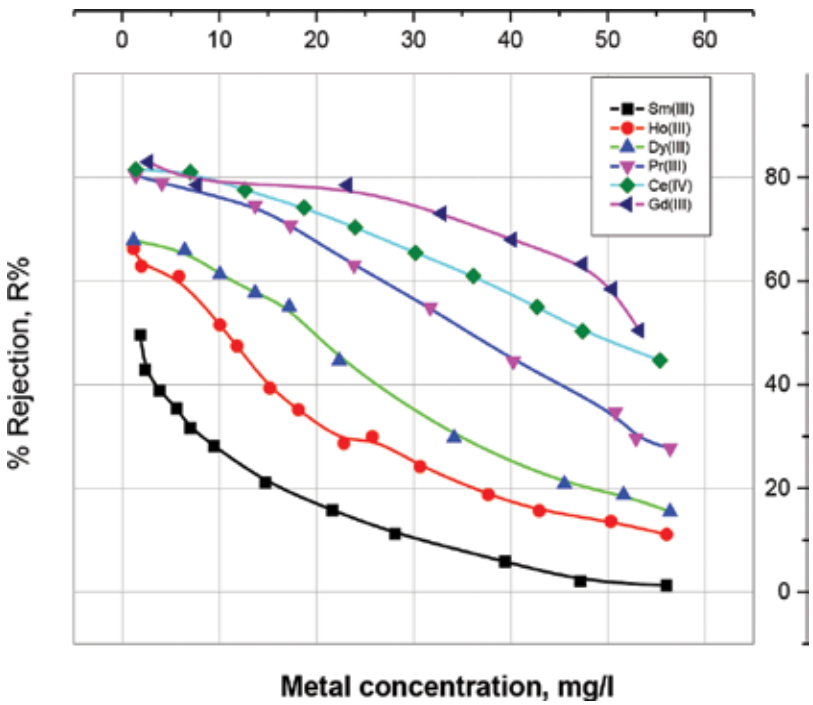

Figure 9. Rejection values of single metal ions at pH 3 for different feed metal concentrations using RO Mode.

Figures 9 and **10** show the rejection coefficient values of single metal ions for different feed metal concentrations using RO Mode at pH ~3 and ~8, respectively. Generally, a high rejection asset value of Ce^{4+}, Pr^{3+}, Sm^{3+}, Gd^{3+}, Dy^{3+}, and Ho^{3+} was observed at low concentrations. Increasing the metal ion content in the feed solution results in a marked decrease in the metal ion rejection, which may be attributed to the closed gates of the membrane. As pH-responsive membrane, PAm-ZTS showed differential rejections according to the pH conditioned. At pH 3, Gd^{3+} and Ce^{4+} were subjected to highest rejection, while Sm^{3+} and Ho^{3+} were rejected with the weakest rates; their rejection coefficients have lowered to less than ten percent at higher concentrations. On the other hand, Pr^{3+} showed the greatest rejection, while Sm^{3+} indicated the quietest rejection. At despicable concentrations, most of the ions are highly rejected at disgusting concentrations that reach about eighty percent. These asset values drop to about thirty to forty percent at higher concentrations. The variation of the rejection as a function of pH in pH-responsive membranes may be explained by the variation of PAm-ZTS conformation because of pH-dependent dissociation of amide hydroxyl. In addition, protonation of amide groups under acidic conditions could be observed [68, 69].

To verify the reversibility and durability of pH-responsive open and closed gating function of the membrane pores, the fluxes of membranes are tested with alternate change of buffer pH between 8 and 3, repeatedly. To characterize the pH-responsive performance, a special coefficient, called pH-responsive coefficient K, is defined as

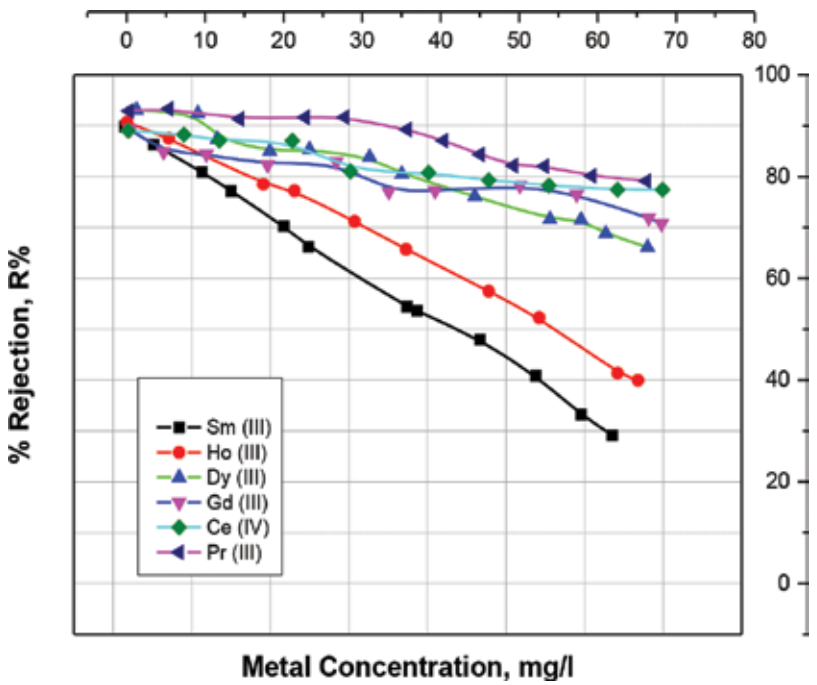

Figure 10. Rejection values of single metal ions at pH 8 for different feed metal concentrations using RO Mode.

$$K = \frac{FLUX_{pH_3}}{FLUXpH_8} \tag{28}$$

where the numerator and denominator represent the transmembrane fluxes at pH 3 and pH 8, respectively. The membrane showed fast response as a function of pH for its potential applications; the fluxes at pH 8 are around 375 l/(m^2 h), while, with changing the feed to pH 3 buffer, the fluxes across the membrane decreased quickly to around 123 l/(m^2 h) within the first recording period, about 40 s. Therefore, the pH-responsive coefficient was about 0.328, indicating a good response of the membrane at the mentioned pHs. This value is mainly a fraction, which contradicts to others found in literature, as other membranes showed a reversed behavior at the same tested pHs [67].

8. Conclusion

A pH-responsive smart PAm-ZTS was prepared by prepared via reactions between zirconium titanosilicate and polyacrylamide under different preparation conditions for testing some lanthanide ions, namely, Ce^{4+}, Pr^{3+}, Sm^{3+}, Gd^{3+}, Dy^{3+}, and Ho^{3+} for their active rejection. The pH response of the membrane was demonstrated using static adsorption and hydraulic permeation results. The water flux of the PAm-ZTS membrane decreased with the decreasing pH value, with the most drastic decrease occurring between pHs 4 and 7, and was both reversible and durable with interchanging pHs between 3 and 8. At pH 3, the membrane pores were in a closed state due to the extended conformation of the amide chains on the pore surfaces. In contrast, at pH 8, the membrane pores were in non-closed state because of the collapsed conformation of the amide chains. The outcomes in this paper afford clear indication to the availability of manufacture and production of pH-responsive composite membranes and can inspire further works on design and preparation of stimuli-responsive membranes through addition of molecularly designed macromolecular additives synthesized by controlled polymerization.

Author details

Gehan Mohamed Ibrahim and Belal El-Gammal*

*Address all correspondence to: belalelgammal@hotmail.com

Faculty of Science, Chemistry Department, University of Bisha, Kingdom of Saudi Arabia

References

[1] El-Naggar IM, Ibrahim GM, El-Gammal B, El-Kady E. Integrated synthesis and characterization of some porous polyacrylamide-based composites for cationic sorption from aqueous liquid wastes. Desalination and Water Treatment. 2014;**52**:6802-6816

[2] El-Gammal B, Ibrahim GM, El-Kholy SH, Shady SA. Ion-exchange equilibrium of cesium/hydrogen ions on zirconium molybdate and zirconium iodomolybdate cation exchangers. Desalination and Water Treatment. 2015;**55**:2121-2143

[3] El-Gammal B, Abdel Hamid M, Ibrahim GM. Ion-exchange properties of ternary CaO-MgO-Al2O3 spinels in pH-controlled aqueous radioactive waste solutions. Desalination and Water Treatment. 2015;**53**:2464-2480

[4] El-Gammal B. Adsorption profiles of some heavy metal ions from aqueous waste solutions using sodium-doped zirconium titanosilicate. Desalination and Water Treatment. 2014;**52**:5952-5964

[5] Khalil T, El-Sweify FH, El-Gammal B, El-Nour FA. Uptake studies of some fission products using ceramic materials. Journal of Radioanalytical and Nuclear Chemistry. 1997;**222**: 61-67

[6] Cheng ZL, Chung TS. Erratum to "mass transport of various membrane configurations in pressure retarded osmosis (PRO)". Journal of Membrane Science. 2017;**539**:358

[7] Chanukya BS, Rastogi NK. Ultrasound assisted forward osmosis concentration of fruit juice and natural colorant. Ultrasonics Sonochemistry. 2017;**34**:426-435

[8] Fischbarg J, Hernandez JA, Rubashkin AA, Iserovich P, Cacace VI, Kusnier CF. Epithelial fluid transport is due to electro-osmosis (80%), plus osmosis (20%). The Journal of Membrane Biology. 2017;**250**:327-333

[9] Khanzada NK, Khan SJ, Davies PA. Performance evaluation of reverse osmosis (RO) pretreatment technologies for in-land brackish water treatment. Desalination. 2017;**406**:44-50

[10] Zaghbani N, Nakajima M, Nabetani H, Hafiane A. Modeling of reverse osmosis flux of aqueous solution containing glucose. Korean Journal of Chemical Engineering. 2017;**34**: 407-412

[11] Shahid MK, Pyo M, Choi YG. Inorganic fouling control in reverse osmosis wastewater reclamation by purging carbon dioxide. Environmental Science and Pollution Research. 2017:1-9

[12] Basile A, Angelo B, Charcosset C. Integrated Membrane Systems and Processes. Newark: Wiley; 2015

[13] Pal P, Chakrabortty S, Nayak J, Senapati S. A flux-enhancing forward osmosis–nanofiltration integrated treatment system for the tannery wastewater reclamation. Environmental Science and Pollution Research. 2017;**24**:15768-15780

[14] Nelson PH. Osmosis and thermodynamics explained by solute blocking. European Biophysics Journal. 2017;**46**:59-64

[15] McCurry DL, Ishida KP, Oelker GL, Mitch WA. Reverse osmosis shifts chloramine speciation causing re-formation of NDMA during potable reuse of wastewater. Environmental Science & Technology. 2017;**51**:8589-8596

[16] Werber JR, Deshmukh A, Elimelech M. Can batch or semi-batch processes save energy in reverse-osmosis desalination? Desalination. 2017;**402**:109-122

[17] Turek M, Mitko K, Piotrowski K, Dydo P, Laskowska E, Jakóbik-Kolon A. Prospects for high water recovery membrane desalination. Desalination. 2017;**401**:180-189

[18] Ali ES, Alsaman AS, Harby K, Askalany AA, Diab MR, Ebrahim Yakoot SM. Recycling brine water of reverse osmosis desalination employing adsorption desalination: A theoretical simulation. Desalination. 2017;**408**:13-24

[19] Touati K, Tadeo F, Elfil H. Osmotic energy recovery from reverse osmosis using two-stage pressure retarded osmosis. Energy. 2017;**132**:213-224

[20] El-Gammal B. Lanthanides diffusion through pH-responsive reverse osmosis membranes. Desalination and Water Treatment. 2014;**52**:4453-4461

[21] Lee J, Choi JY, Choi JS, Chu KH, Yoon Y, Kim S. A statistics-based forward osmosis membrane characterization method without pressurized reverse osmosis experiment. Desalination. 2017;**403**:36-45

[22] Park HM, Jee KY, Lee YT. Preparation and characterization of a thin-film composite reverse osmosis membrane using a polysulfone membrane including metal-organic frameworks. Journal of Membrane Science. 2017;**541**:510-518

[23] Uragami T. Science and Technology of Separation Membranes. Vol. 2. Chichester: John Wiley & Sons; 2017. pp. 274-275

[24] Park SJ, Choi W, Nam SE, Hong S, Lee JS, Lee JH. Fabrication of polyamide thin film composite reverse osmosis membranes via support-free interfacial polymerization. Journal of Membrane Science. 2017;**526**:52-59

[25] Hurwitz G, Guillen GR, Hoek EMV. Probing polyamide membrane surface charge, zeta potential, wettability, and hydrophilicity with contact angle measurements. Journal of Membrane Science. 2010;**349**:349-357

[26] Wilbert MC, Pellegrino J, Zydney A. Bench-scale testing of surfactant-modified reverse osmosis/nanofiltration membranes. Desalination. 1998;**115**:15-32

[27] Elimelech M, Chen WH, Waypa JJ. Measuring the zeta (electrokinetic) potential of reverse osmosis membranes by a streaming potential analyzer. Desalination. 1994;**95**:269-286

[28] Kirby BJ, Hasselbrink EF. Zeta potential of microfluidic substrates: 2 data for polymers. Electrophoresis. 2004;**25**:203-213

[29] Kuo AT, Chang CH, Wei HH. Transient currents in electrolyte displacement by asymmetric electro-osmosis and determination of surface zeta potentials of composite microchannels. Applied Physics Letters. 2008;**92**. DOI: 10.1063/1.2936297

[30] Wang YN, Tang CY. Protein fouling of nanofiltration, reverse osmosis, and ultrafiltration membranes-the role of hydrodynamic conditions, solution chemistry, and membrane properties. Journal of Membrane Science. 2011;**376**:275-282

[31] Salgin S, Salgı U, Soyer N. Streaming potential measurements of Polyethersulfone ultrafiltration membranes to determine salt effects on membrane zeta potential. International Journal of Electrochemical Science. 2013;**8**:4073-4084

[32] Al-Amoudi A, Williams P, Mandale S, Lovitt RW. Cleaning results of new and fouled nanofiltration membrane characterized by zeta potential and permeability. Separation and Purification Technology. 2007;**54**:234-240

[33] Joly L, Ybert C, Trizac E, Bocquet L. Hydrodynamics within the electric double layer on slipping surfaces. Physical Review Letters. 2004;**93**. DOI: 10.1103/PhysRevLett.93.257805

[34] Bukšek H, Luxbacher T, Petrinić I. Zeta potential determination of polymeric materials using two differently designed measuring cells of an electrokinetic analyzer. Acta Chimica Slovenica. 2010;**57**:700-706

[35] Elimelech M, Zhu X, Childress AE, Hong S. Role of membrane surface morphology in colloidal fouling of cellulose acetate and composite aromatic polyamide reverse osmosis membranes. Journal of Membrane Science. 1997;**127**:101-109

[36] Vrijenhoek EM, Hong S, Elimelech M. Influence of membrane surface properties on initial rate of colloidal fouling of reverse osmosis and nanofiltration membranes. Journal of Membrane Science. 2001;**188**:115-128

[37] Tang CY, Kwon YN, Leckie JO. Probing the nano- and micro-scales of reverse osmosis membranes-a comprehensive characterization of physiochemical properties of uncoated and coated membranes by XPS, TEM, ATR-FTIR, and streaming potential measurements. Journal of Membrane Science. 2007;**287**:146-156

[38] Attarde D, Jain M, Singh PK, Gupta SK. Energy-efficient seawater desalination and wastewater treatment using osmotically driven membrane processes. Desalination. 2017;**413**:86-100

[39] Tedesco M, Hamelers HVM, Biesheuvel PM. Nernst-Planck transport theory for (reverse) electrodialysis: II Effect of water transport through ion-exchange membranes. Journal of Membrane Science. 2017;**531**:172-182

[40] Jiang S, Li Y, Ladewig BP. A review of reverse osmosis membrane fouling and control strategies. Science of the Total Environment. 2017;**595**:567-583

[41] Xie Z, Nagaraja N, Skillman L, Li D, Ho G. Comparison of polysaccharide fouling in forward osmosis and reverse osmosis separations. Desalination. 2017;**402**:174-184

[42] Lv L, Xu J, Shan B, Gao C. Concentration performance and cleaning strategy for controlling membrane fouling during forward osmosis concentration of actual oily wastewater. Journal of Membrane Science. 2017;**523**:15-23

[43] Chun Y, Mulcahy D, Zou L, Kim IS. A short review of membrane fouling in forward osmosis processes. Membranes (Basel). 2017;**7**. DOI: 10.3390/membranes7020030

[44] Laqbaqbi M, Sanmartino J, Khayet M, García-Payo C, Chaouch M. Fouling in membrane distillation, osmotic distillation and osmotic membrane distillation. Applied Sciences. 2017;**7**:334

[45] Schulze KD, Hart SM, Marshall SL, O'Bryan CS, Urueña JM, Pitenis AA, Sawyer WG, Angelini TE. Polymer osmotic pressure in hydrogel contact mechanics. Biotribology. 2017. DOI: 10.1016/j.biotri.2017.03.004

[46] de Jesus Junqueira JR, Corrêa JLG, de Mendonça KS, Resende NS, de Barros Vilas Boas EV. Influence of sodium replacement and vacuum pulse on the osmotic dehydration of eggplant slices. Innovative Food Science & Emerging Technologies. 2017;**41**:10-18

[47] Ge Y, Yu F, Tan Y, Zhang X, Liu Z. Comparative Transcriptome sequence analysis of sporulation-related genes of Aspergillus cristatus in response to low and high Osmolarity. Current Microbiology. 2017;**74**:806-814

[48] Zhang M, She Q, Yan X, Tang CY. Effect of reverse solute diffusion on scaling in forward osmosis: A new control strategy by tailoring draw solution chemistry. Desalination. 2017; **401**:230-237

[49] Al-Obaidi MA, Kara-Zaitri C, Mujtaba IM. Scope and limitations of the irreversible thermodynamics and the solution diffusion models for the separation of binary and multicomponent systems in reverse osmosis process. Computers and Chemical Engineering. 2017;**100**:48-79

[50] Merlet RB, Tanardi CR, Vankelecom IFJ, Nijmeijer A, Winnubst L. Interpreting rejection in SRNF across grafted ceramic membranes through the Spiegler-Kedem model. Journal of Membrane Science. 2017;**525**:359-367

[51] Boussouga YA, Lhassani A. Study of mass transfer mechanisms for reverse osmosis and nanofiltration membranes intended for desalination. Journal of Materials and Environmental Science. 2017;**8**:1128-1138

[52] Guo C, Zhou L, Lv J. Effects of expandable graphite and modified ammonium polyphosphate on the flame-retardant and mechanical properties of wood flour-polypropylene composites. Polymers and Polymer Composites. 2013;**21**:449-456

[53] Guha R, Xiong B, Geitner M, Moore T, Wood TK, Velegol D, Kumar M. Reactive micromixing eliminates fouling and concentration polarization in reverse osmosis membranes. Journal of Membrane Science. 2017;**542**:8-17

[54] Xu W, Chen Q, Ge Q. Recent advances in forward osmosis (FO) membrane: Chemical modifications on membranes for FO processes. Desalination. 2017;**419**:101-116

[55] Lin Y-L. Effects of organic, biological and colloidal fouling on the removal of pharmaceuticals and personal care products by nanofiltration and reverse osmosis membranes. Journal of Membrane Science. 2017;**542**. DOI: 10.1016/j.memsci.2017.08.023

[56] El-Kamash AM, El-Gammal B, El-Sayed AA. Preparation and evaluation of cerium(IV) tungstate powder as inorganic exchanger in sorption of cobalt and europium ions from aqueous solutions. Journal of Hazardous Materials. 2007;**141**:719-728

[57] Ibrahim GM, Ahmad MI, El-Gammal B, El-Naggar IM. Selectivity sequence of multivalent lanthanides for their separation on Antimonate based exchangers. Separation Science and Technology. 2011;**46**:2549-2565

[58] Metwally SS, El-Gammal B, Aly HF, Abo-El-Enein SA. Removal and separation of some radionuclides by poly-acrylamide based Ce(IV) phosphate from radioactive waste solutions. Separation Science and Technology. 2011;**46**:1808-1821

[59] Ibrahim GM, El-Gammal B, El-Naggar IM. Synthesis and characterization of novel materials, tin potassium vanadate and zirconium potassium vanadate inorganic multicomponent ion exchangers. Separation Science and Technology. 2011;**46**:664-678

[60] El-Gammal B, Ibrahim GM, El-Nahas HH. Thermodynamic and sorption behavior of U (VI) and Th(IV) on unsaturated polyester - Styrene polymeric beads. Journal of Applied Polymer Science. 2006;**100**:4098-4106

[61] El-Gammal B, Metwally SS, Aly HF, Abo-El-Enein SA. Verification of double-shell model for sorption of cesium, cobalt, and europium ions on poly-acrylonitrile-based Ce(IV) phosphate from aqueous solutions. Desalination and Water Treatment. 2012;**46**:124-138

[62] Ibrahim GM, Ahmad MI, El-Gammal B. Structural development of TMMA and SSQXN-8 as porous chelating resins. Journal of Applied Polymer Science. 2009;**113**:3038-3048

[63] El-Gammal B, Shady SA. Chromatographic separation of sodium, cobalt and europium on the particles of zirconium molybdate and zirconium silicate ion exchangers. Colloids and Surfaces A: Physicochemical and Engineering Aspects. 2006;**287**:132-138

[64] Shady SA, El-Gammal B. Diffusion pathways of sodium and cesium ions in the particles of titanium(IV) antimonate. Colloids and Surfaces A: Physicochemical and Engineering Aspects. 2005;**268**:7-11

[65] El-Gammal B, Allan KF. Ion exchange reversibility of some radionuclides on zirconium Tungstosuccinate and zirconium Tungstosalicylate at their solid-liquid interfaces. Separation Science and Technology. 2012;**47**:131-146

[66] El-Nahas HH, Khalil FH, Ibrahim GM, El-Gammal B. Preparation of unsaturated polyester–styrene beads using gamma irradiation and chemical polymerization routes for use in the recovery of some alkali metal ions. Journal of Applied Polymer Science. 2007; **104**:1149-1160

[67] Oh Y, Armstrong DL, Finnerty C, Zheng S, Hu M, Torrents A, Mi B. Understanding the pH-responsive behavior of graphene oxide membrane in removing ions and organic micropollulants. Journal of Membrane Science. 2017;**541**:235-243

[68] Moula Karimdjy M, Tallec G, Fries PH, Imbert D, Mazzanti M, Karimdjy MM, Tallec G, Fries PH, Imbert D, Mazzanti M. Confinement of a tris-aqua Gd(III) complex in silica nanoparticles leads to high stability and high relaxivity and suppresses anion binding. Chemical Communications. 2015;**51**:6836-6838

[69] Ragavan AJ, Adams DV. Nuclear Materials. Hauppauge: Nova Science Publishers; 2011. pp. 1-46

Chapter 2

Wastewater Treatment Using Membrane Technology

Azile Nqombolo, Anele Mpupa,
Richard M. Moutloali and Philiswa N. Nomngongo

Additional information is available at the end of the chapter

http://dx.doi.org/10.5772/intechopen.76624

Abstract

Water contamination by heavy metals, cyanides and dyes is increasing globally and needs to be addressed as this will lead to water scarcity as well as water quality. Different techniques have been used to clean and renew water for human consumption and agricultural purposes but they each have limitations. Among those techniques, membrane technology is promising to solve the issues. Nanotechnology present a great potential in wastewater treatment to improve treatment efficiency of wastewater treatment plants. In addition, nanotechnology supplement water supply through safe use of modern water sources. This chapter reviews recent development in membrane technology for wastewater treatment. Different types of membrane technologies, their properties, mechanisms advantages, limitations and promising solutions have been discussed.

Keywords: wastewater, membrane technology, nanofiltration, forward osmosis, ultrafiltration, reverse osmosis

1. Introduction

Clean water is important for every living organism to withstand life, but due to rapid increase in growth population and industrialization, there is more demand for clean, safe and drinkable water [1]. About 97% of water is stored in oceans as salty water which is not good for human consumption or agricultural use, only less than 3% water on planet is available for drinking and agricultural use [2]. Most available water is highly contaminated by effluent from agricultural and industrial activity and cannot be consumed therefore water quality and

quantity are the main problems that need to be solved [3]. Removal of contaminants/water pollutants is required as to avoid negative effects on the environment as well as human health [4].

Several techniques have been developed for treatment of wastewater; such methods include reverse osmosis [5] ion exchange [6] gravity [7] and adsorption [8] among others. Adsorption has been widely used to remove water contaminants due to its low cost, available of different adsorbents and easy operation. Different adsorbents that have been used include use of magnetic nanoparticles [9] activated carbon [10], nanotubes [11] and polymer nanocomposites [12]; these can remove different contaminants including heavy metals that are very harmful even at low concentrations. Even though adsorption can remove most of water pollutants, it has some limitations such as lack of appropriate adsorbents with high adsorption capacity and low use of these adsorbents commercially [13]. Hence there has been a need for more efficient techniques such as membrane technology. Membrane separation or treatment process mainly depends on three basic principles, namely adsorption, sieving and electrostatic phenomenon [14]. The adsorption mechanism in the membrane separation process is based on the hydrophobic interactions of the membrane and the solute (analyte). These interactions normally lead to more rejection because it causes a decrease in the pore size of the membrane [15]. The separation of materials through the membrane depends on pore and molecule size [16]. For this reason, various membrane processes with different separation mechanisms have been developed. These include microfiltration (MF), ultrafiltration (UF), nanofiltration (NF), forward osmosis (FO) and reverse osmosis (RO).

Therefore the aim of this chapter is review different membrane technology processes used for treatment of wastewater in the last 5 years (2014–2018). The advantages, challenges/limitations associated with the use of each membrane technology and possible solutions are also discussed briefly.

2. Challenges

Membrane processes such as MF, NF, UF and RO are currently used for water reuse, brackish water and seawater [17]. Polymer based membranes are mostly used membrane material but because polymers such as polysulfone and polyethersulfone, are hydrophobic [18], polymeric membranes are prone to fouling [19]. This leads to blockage of membrane pores and decrease membrane performance [20], also increases operation cost by demanding extra cleaning process. There are factors causing membrane fouling, such as deposition of inorganic components onto the surface membrane/solute absorption pore blocking, microorganism and feed chemistry [21]. This results to either reversible or irreversible membrane fouling [22]. Reversible fouling formed by attachment of particles on the membrane surface, irreversible which occurs when particles strongly attach the membrane surface and cannot be removed by physical cleaning. When there is a formation of strong matrix of the fouled layer with the solute during continuous filtration process will turn reversible fouling to irreversible fouling layer [23].

3. Promising solutions

For polymeric membranes, surface modification of the polymer is essential; such surface modification includes grafting, blending and incorporation of nanomaterials such as TiO_2 [24]), ZnO [25], Al_2O_3 [26], carbon nanotubes [27] and graphene oxide [28]. Among these, graphene oxide membranes (GMs) are very promising in water treatment application such as desalination and wastewater treatment, due to their hydrophilic properties, flexibility and high mechanical strength; GMs have been reported to give wide range of pure water flux [28–32].

4. Membrane processes

4.1. Microfiltration (MF)

Microfiltration is a pressure driven process where separated compounds are 0.1–0.2 μm such as nanoparticles [33, 34]. It is regarded as the first pre-treatment of NF and RO membrane processes. MF removes little or no organic matter; however, when pre-treatment is applied, increased removal of organic material can occur. MF can be used as a pre-treatment to RO or NF to reduce fouling potential [35]. The main disadvantages of MF is that it cannot eliminate contaminants (dissolved solids) that are <1 mm in size. In addition, MF is not an absolute barrier to viruses. However, when used in combination with disinfection, MF appears to control these microorganisms in water [35].

4.2. Ultrafiltration (UF)

Ultrafiltration membrane process can separate compounds between 0.005 ≈ 10 μm which is between MF and RO [36]. UF membranes are highly prominent water filters with low energy consumption in removal of pathogenic microorganisms, macromolecules and suspended maters among others [37]. However, UF has some limitations including its inability to remove any dissolved inorganic substances from water and regular cleaning to maintain high pressure water flow [38]. Mocanu and others developed a synthetic procedure for hybrid ultrafiltration membrane for water treatment. They used wet-phase inversion method with polysulfone and graphene nanoplatelets modified with poly (styrene) to obtain their membranes. ZnO was deposited on one surface of the membrane with polymers that are soluble in water [39]. In the study reported by Igbinigun and others, the modified GO-membrane showed 2.6 times better flux recovery compared to the unmodified membrane and this shows that it is wise to modify membrane with GO to increase flux recovery. They used a simple method known as UV induced amination which has high flux UF membrane found to be resistant to organic fouling, and the resulting membrane can be applied in waste water treatment application. Incorporating hydrophilic materials onto the surface of these polymers will lead to more hydrophilic surface membrane [40].

4.3. Nanofiltration (NF)

NF is capable of removing ions that contribute significantly to the osmotic pressure hence allows operation pressures that are lower than those RO. For NF to be effective pre-treatment is needed for some heavily polluted waters; Membranes are sensitive to free chlorine. Soluble elements cannot be separated from water [41]. In the study reported by Yang and co-workers, PMIA/GO composite nanofiltration membranes were used for water treatment. The prepared composite membrane had greater hydrophilic surface which gave rise to high pure water flux compared to that of the pure polymer (PMIA). The results obtained showed high dye rejection and enhanced fouling resistance to bovine serum albumin (BSA) [42]. Xu and others reported NF membrane for textile wastewater treatment, the prepared membrane displayed good removal of heavy metal ions, common salts and dyes, showing high removal efficiency toward metal ions and cationic dyes [43]. Lin and others reported nanofiltration membranes for dye (Congo red and direct red) and salt rejection, the results showed high dye rejection and low salt rejection which shows the possibility of the salt reuse in FO.

4.4. Forward osmosis (FO)

FO is a natural occurrence where the solvent moves from a region of lower concentration to the region of higher concentration across a permeable membrane [44]. This method is found to be highly efficient with low rate production of brine and is well studied as it promise to solve water problems worldwide, however regeneration of the draw solution is highly expensive for desalination processes hence the use of nanofiltration or reverse osmosis for regeneration of draw solution [45].

4.5. Reverse osmosis (RO)

RO is pressure driven technique used to remove dissolved solids and smaller particles; RO is only permeable to water molecules. The applied pressure on RO must be enough so that water can be able to overcome the osmotic pressure. The pore structure of RO membranes is much tighter than UF, they convert hard water to soft water, and they are practically capable of removing all particles, bacteria and organics, it requires less maintenance [46]. Some disadvantages include the use of high pressure, RO membranes are expensive compared to other membrane processes and are also prone to fouling. In some cases, high level of pretreatment is required [47]. RO has extremely small pores and able to remove particles smaller than 0.1 nm [48]. Huang and others, reported RO membranes coated with azide functionalized graphene oxide hence created smooth, antibacterial and hydrophilic membrane, which removed *Escherichia coli* and reduced BSA fouling [49].

5. Application of membrane technology for wastewater treatment

Zinadini and his group used zinc oxide nanoparticles to coat multiwalled carbon nanotubes (MWCNTs) which were later blended in polyethersulfone (PES) membrane. Incorporation

of ZnO coated MWCNTs increased pure water flux due to the hydrophilic properties added. The results showed increase in antifouling properties as well as decrease in surface roughness brought by the embedded nanoparticle. ZnO/MWCNTs composite membrane showed greater dye removal compared to pure PES membrane [50]. Polymeric membranes in water treatment can reject up to 98% Cd ions through asymmetric polysulfone membrane [51]. Hybrid membranes are also used in removal of water contaminants as they introduce adsorptive capability, photocatalytic and antibacterial capabilities. This will lead to improved water flux and rejection value [52]. Aromatic polyamide is among other polymers that have been used in membrane industries. High pressure membrane includes tight UF, NF and RO, these are operated at high transmembrane pressure (>200 kPa) and low pressure membrane includes lose UF and MF. Usually fouling turn to occur when transmembrane increases, as to maintain flux or when there is decrease in flux [53].

Qiu and others have reported the use of hybrid microfiltration-osmosis membrane bioreactor to remove nitrogen and organic matter in municipal wastewater. Results showed decrease in fouling and reduced bacteria deposition [54]. In the study reported by Ochando-Pulido and others in olive mill wastewater and the rejection efficiency was 99.1% [55]. Microfiltration membrane has been applied in domestic wastewater and the amount percentage recovery of phosphorus was found to be 98.7% [56]. Combination of UF/NF/RO have been used in rendering plant wastewater (RPW) and the rand filtration was used as an effective pre-treatment for UF hence lowering membrane fouling [57]. Another form of membrane called membrane with a molecular weight cut-off (MWCO) was used to treat municipal and industrial wastewater, the obtained results showed complete resistance to irreversible fouling and high dye rejection [58]. UF and NF membranes have been used for waste stream purification also known as backwash water, which is obtained by washing filtration beds from swimming pool water system [59] (**Table 1**).

Matrix/pollutants	Membrane type	Performance	References
Oily water	MF	90.2% removal of organic additives	[60]
Olive mill wastewater	RO	COD rejection 97.5–99.1% and 24–32 L h^{-1} m^{-2} permeate flux	[55]
Domestic wastewater	MF	>97% removal of total nitrogen and total phosphorus	[56]
Nitrogen and phosphorus in microalgae	FO and MF	86–99% removal efficiency for nitrogen 100% for phosphorus	[61]
Chlorophenol	RO	Improved unit performance	[62]
Municipal and industrial wastewater streams	membranes with a molecular weight cut-off (MWCO)	membranes showed complete resistance to irreversible fouling and high rejections of dyes	[58]

Table 1. Membrane applications.

6. Conclusions

This review provides detailed information about the current applications (2014–2018) of the membrane technology for treatment of wastewater. Generally, literature proved that different membrane technologies can be used to treat efficiently wastewaters from different activities. However, membrane fouling and membranes sensitivity to toxicity are the main limitations of the membrane technology. For this reason, Researchers has developed number of ways to overcome membrane technology. These ways include the incorporation of nanomaterials such as graphene oxide and nanometer sized metal oxides (zinc oxide), among others. In overall it can be concluded that membrane technology has been found to be a very promising method for wastewater treatment.

Acknowledgements

I would like to thank National Research Foundation (NRF, grant no. 99270) and Nanotechnology Innovation Centre (UJ Water Node) for providing financial support and the University of Johannesburg for making this study possible by making laboratory facilities available.

Conflict of interest

There is no conflict of interest.

Author details

Azile Nqombolo, Anele Mpupa, Richard M. Moutloali and Philiswa N. Nomngongo*

*Address all correspondence to: pnnomngongo@uj.ac.za

Department of Applied Chemistry, University of Johannesburg, Johannesburg, South Africa

References

[1] Adeleye AS, Conway JR, Garner K, Huang Y, Su Y, Keller AA. Engineered nanomaterials for water treatment and remediation: Costs, benefits, and applicability. Chemical Engineering Journal. 2016;**286**:640-662

[2] Santhosh C, Velmurugan V, Jacob G, Jeong SK, Grace AN, Bhatnagar A. Role of nanomaterials in water treatment applications: A review. Chemical Engineering Journal. 2016; **306**:1116-1137

[3] Bethi B, Sonawane SH, Bhanvase BA, Gumfekar SP. Nanomaterials-based advanced oxidation processes for wastewater treatment: A review. Chemical Engineering and Processing: Process Intensification. 2016;**109**:178-189

[4] Moussa DT, El-Naas MH, Nasser M, Al-Marri MJ. A comprehensive review of electrocoagulation for water treatment: Potentials and challenges. Journal of Environmental Management. 2017;**186**:24-41

[5] Yang Y, Pignatello JJ, Ma J, Mitch WA. Effect of matrix components on UV/H_2O_2 and UV/$S_2O_8^{2-}$ advanced oxidation processes for trace organic degradation in reverse osmosis brines from municipal wastewater reuse facilities. Water Research. 2016;**89**:192-200

[6] Beita-Sandí W, Karanfil T. Removal of both N-nitrosodimethylamine and trihalomethanes precursors in a single treatment using ion exchange resins. Water Research. 2017;**124**:20-28

[7] Carr SA, Liu J, Tesoro AG. Transport and fate of microplastic particles in wastewater treatment plants. Water Research. 2016;**91**:174-182

[8] Hatton TA, Su X, Achilleos DS, Jamison TF. Redox-based electrochemical adsorption technologies for energy-efficient water purification and wastewater treatment. In: Kamalesh K, Sirkar KK, editors. Separations Technology IX: New Frontiers in Media, Techniques, and Technologies. New Jersey Institute of Technology, USA Steven M. Crame, Rensselaer Polytechnic Institute, USA João G. Crespo, LAQV-Requimte, FCT-Universidade Nova de Lisboa, Caparica, Portugal Marco Mazzotti, ETH Zurich, Switzerland Eds, ECI Symposium Series. 2017. http://dc.engconfintl.org/separations_technology_ix/60

[9] Lai GS, Lau WJ, Goh PS, Ismail AF, Yusof N, Tan YH. Graphene oxide incorporated thin film nanocomposite nanofiltration membrane for enhanced salt removal performance. Desalination. 2016;**387**:14-24

[10] Saleh TA, Sarı A, Tuzen M. Optimization of parameters with experimental design for the adsorption of mercury using polyethylenimine modified-activated carbon. Journal of Environmental Chemical Engineering. 2017;**5**(1):1079-1088

[11] Saleh TA. Nanocomposite of carbon nanotubes/silica nanoparticles and their use for adsorption of Pb (II): From surface properties to sorption mechanism. Desalination and Water Treatment. 2016;**57**(23):10730-10744

[12] Lofrano G, Carotenuto M, Libralato G, Domingos RF, Markus A, Dini Gautam RK, Baldantoni D, Rossi M, Sharma SK, Chattopadhyaya MC. Polymer functionalized nanocomposites for metals removal from water and wastewater: An overview. Water Research. 2016;**92**:22-37

[13] Gaouar MY, Benguella B. Efficient and eco-friendly adsorption using low-cost natural sorbents in waste water treatment. Indian Journal of Chemical Technology (IJCT). 2016;**23**(3):204-209

[14] Padaki M, Murali RS, Abdullah MS, Misdan N, Moslehyani A, Kassim MA, Hilal N, Ismail AF. Membrane technology enhancement in oil–water separation. A review. Desalination. 2015;**357**:197-207

[15] Li K, Huang T, Qu F, Du X, Ding A, Li G, Liang H. Performance of adsorption pretreatment in mitigating humic acid fouling of ultrafiltration membrane under environmentally relevant ionic conditions. Desalination. 2016;**377**:91-98

[16] Zhao D, Yu Y, Chen JP. Treatment of lead contaminated water by a PVDF membrane that is modified by zirconium, phosphate and PVA. Water Research. 2016;**101**:564-573

[17] Erkanlı M, Yilmaz L, Çulfaz-Emecen PZ, Yetis U. Brackish water recovery from reactive dyeing wastewater via ultrafiltration. Journal of Cleaner Production. 2017;**165**:1204-1214

[18] Marino T, Blasi E, Tornaghi S, Di Nicolò E, Figoli A. Polyethersulfone membranes prepared with Rhodiasolv® Polarclean as water soluble green solvent. Journal of Membrane Science. 2018;**549**:192-204

[19] Ahmed F, Lalia BS, Kochkodan V, Hilal N, Hashaikeh R. Electrically conductive polymeric membranes for fouling prevention and detection: A review. Desalination. 2016;**391**:1-15

[20] Laohaprapanon S, Vanderlipe AD, Doma BT Jr, You SJ. Self-cleaning and antifouling properties of plasma-grafted poly(vinylidene fluoride) membrane coated with ZnO for water treatment. Journal of the Taiwan Institute of Chemical Engineers. 2017;**70**:15-22

[21] Zinadini S, Gholami F. Preparation and characterization of high flux PES nanofiltration membrane using hydrophilic nanoparticles by phase inversion method for application in advanced wastewater treatment. Journal of Applied Research in Water and Wastewater. 2016;**3**(1):232-235

[22] Ding Q, Yamamura H, Murata N, Aoki N, Yonekawa H, Hafuka A, Watanabe Y. Characteristics of meso-particles formed in coagulation process causing irreversible membrane fouling in the coagulation-microfiltration water treatment. Water Research. 2016;**101**:127-136

[23] Zhao F, Chu H, Zhang Y, Jiang S, Yu Z, Zhou X, Zhao J. Increasing the vibration frequency to mitigate reversible and irreversible membrane fouling using an axial vibration membrane in microalgae harvesting. Journal of Membrane Science. 2017;**529**:215-223

[24] Bet-Moushoul E, Mansourpanah Y, Farhadi K, Tabatabaei M. TiO_2 nanocomposite based polymeric membranes: A review on performance improvement for various applications in chemical engineering processes. Chemical Engineering Journal. 2016;**283**:29-46

[25] Tan YH, Goh PS, Ismail AF, Ng BC, Lai GS. Decolourization of aerobically treated palm oil mill effluent (AT-POME) using polyvinylidene fluoride (PVDF) ultrafiltration membrane incorporated with coupled zinc-iron oxide nanoparticles. Chemical Engineering Journal. 2017;**308**:359-369

[26] Garcia-Ivars J, Iborra-Clar MI, Alcaina-Miranda MI, Mendoza-Roca JA, Pastor-Alcañiz L. Surface photomodification of flat-sheet PES membranes with improved antifouling properties by varying UV irradiation time and additive solution pH. Chemical Engineering Journal. 2016;**283**:231-242

[27] Tijing LD, Woo YC, Shim WG, He T, Choi JS, Kim SH, Shon HK. Superhydrophobic nanofiber membrane containing carbon nanotubes for high-performance direct contact membrane distillation. Journal of Membrane Science. 2016;**502**:158-170

[28] Pandey RP, Shukla G, Manohar M, Shahi VK. Graphene oxide based nanohybrid proton exchange membranes for fuel cell applications: An overview. Advances in Colloid and Interface Science. 2016;**240**:15-30

[29] Chang Y, Shen Y, Kong D, Ning J, Xiao Z, Liang J, Zhi L. Fabrication of the reduced preoxidized graphene-based nanofiltration membranes with tunable porosity and good performance. RSC Advances. 2017;**7**(5):2544-2549

[30] Hu M, Zheng S, Mi B. Organic fouling of graphene oxide membranes and its implications for membrane fouling control in engineered osmosis. Environmental Science & Technology. 2016;**50**(2):685-693

[31] Safarpour M, Vatanpour V, Khataee A. Preparation and characterization of graphene oxide/TiO_2 blended PES nanofiltration membrane with improved antifouling and separation performance. Desalination. 2016;**393**:65-78

[32] Lai L, Xie Q, Chi L, Gu W, Wu D. Adsorption of phosphate from water by easily separable Fe_3O_4@ SiO_2 core/shell magnetic nanoparticles functionalized with hydrous lanthanum oxide. Journal of Colloid and Interface Science. 2016;**465**:76-82

[33] Qu X, Alvarez P, Werber JR, Deshmukh A, Elimelech M. The critical need for increased selectivity, not increased water permeability, for desalination membranes. Environmental Science & Technology Letters. 2016;**3**(4):112-120

[34] Xiaolei Q, Alvarez PJJ, Li Q. Applications of nanotechnology in water and wastewater treatment. Water Research. 2013;**47**(12):3931-3946

[35] Torki M, Nazari N, Mohammadi T. Evaluation of biological fouling of RO/MF membrane and methods to prevent it. European Journal of Advances in Engineering and Technology. 2017;**4**(9):707-710

[36] Qu F, Liang H, Zhou J, Nan J, Shao S, Zhang J, Li G. Ultrafiltration membrane fouling caused by extracellular organic matter (EOM) from *Microcystis aeruginosa*: Effects of membrane pore size and surface hydrophobicity. Journal of Membrane Science. 2014;**449**: 58-66

[37] Krüger R, Vial D, Arifin D, Weber M, Heijnen M. Novel ultrafiltration membranes from low-fouling copolymers for RO pretreatment applications. Desalination and Water Treatment. 2016;**57**(48-49):23185-23195

[38] Zhang L, Zhang P, Wang M, Yang K, Liu J. Research on the experiment of reservoir water treatment applying ultrafiltration membrane technology of different processes. Journal of Environmental Biology. 2016;**37**(5):1007

[39] Mocanu A, Rusen E, Diacon A, Damian C, Dinescu A, Suchea M. Electrochemical deposition of zinc oxide on the surface of composite membrane polysulfone-graphene-polystyrene in the presence of water soluble polymers. Journal of Nanomaterials. 2017;**2017**:11. Article ID: 1401503. DOI: 10.1155/2017/1401503

[40] Igbinigun E, Fennell Y, Malaisamy R, Jones KL, Morris V. Graphene oxide functionalized polyethersulfone membrane to reduce organic fouling. Journal of Membrane Science. 2016;**514**:518-526

[41] Wang N, Liu T, Shen H, Ji S, Li JR, Zhang R. Ceramic tubular MOF hybrid membrane fabricated through in situ layer-by-layer self-assembly for nanofiltration. AIChE Journal. 2016;**62**(2):538-546

[42] Yang M, Zhao C, Zhang S, Li P, Hou D. Preparation of graphene oxide modified poly (m-phenylene isophthalamide) nanofiltration membrane with improved water flux and antifouling property. Applied Surface Science. 2017;**394**:149-159

[43] Xu YC, Wang ZX, Cheng XQ, Xiao YC, Shao L. Positively charged nanofiltration membranes via economically mussel-substance-simulated co-deposition for textile wastewater treatment. Chemical Engineering Journal. 2016;**303**:555-564

[44] Ong CS, Al-anzi B, Lau WJ, Goh PS, Lai GS, Ismail AF, Ong YS. Anti-fouling double-skinned forward osmosis membrane with zwitterionic brush for oily wastewater treatment. Scientific Reports. 2017;**7**(1):6904

[45] Blandin G, Verliefde AR, Comas J, Rodriguez-Roda I, Le-Clech P. Efficiently combining water reuse and desalination through forward osmosis—Reverse osmosis (FO-RO) hybrids: A critical review. Membranes. 2016;**6**(3):37

[46] Wood AR, Justus K, Parigoris E, Russell A, LeDuc P. Biological inspiration of salt exclusion membranes in mangroves toward fouling-resistant reverse osmosis membranes. The FASEB Journal. 2017;**31**(1 Supplement):949-942

[47] Liu G, Han K, Ye H, Zhu C, Gao Y, Liu Y, Zhou Y. Graphene oxide/triethanolamine modified titanate nanowires as photocatalytic membrane for water treatment. Chemical Engineering Journal. 2017;**320**:74-80

[48] Yan HM, Cao CY, Bai G, & Bai W: Seawater desalination technology route and analysis of production capacity for large commercial nuclear power plant. In: International Conference Pacific Basin Nuclear Conference. Singapore: Springer; 2016. pp. 865-872

[49] Huang X, Marsh KL, McVerry BT, Hoek EM, Kaner RB. Low-fouling antibacterial reverse osmosis membranes via surface grafting of graphene oxide. ACS Applied Materials & Interfaces. 2016;**8**(23):14334-14338

[50] Zinadini S, Rostami S, Vatanpour V, Jalilian E. Preparation of antibiofouling polyethersulfone mixed matrix NF membrane using photocatalytic activity of ZnO/MWCNTs nanocomposite. Journal of Membrane Science. 2017;**529**:133-141

[51] Gao J, Sun SP, Zhu WP, Chung. Green modification of outer selective P84 nanofiltration (NF) hollow fiber membranes for cadmium removal. Journal of Membrane Science. 2016;**499**:361-369

[52] Li M, Wang W, Teng K, Xu Z, Li C, Shan M, Yanng C, Qian X, Jiao X. Manipulating F/O ratio of fluorinated graphene oxide to improve permeability and antifouling properties of poly (vinylidene fluoride) hybrid membranes. Journal of Nanoscience and Nanotechnology. 2017;**17**(12):8935-8945

[53] Jia Z, Hao S, Liu Z. Synthesis of $BaSO_4$ nanoparticles with a membrane reactor: Parameter effects on membrane fouling. Journal of Membrane Science. 2017;**543**:277-281

[54] Qiu G, Zhang S, Raghavan DSS, Das S, Ting YP. The potential of hybrid forward osmosis membrane bioreactor (FOMBR) processes in achieving high throughput treatment of municipal wastewater with enhanced phosphorus recovery. Water Research. 2016;**105**:370-382

[55] Ochando-Pulido JM, Stoller M, Víctor-Ortega MD, Martínez-Férez A. Analysis of the fouling build-up of a spiral wound reverse osmosis membrane in the treatment of two-phase olive mill wastewater. Chemical Engineering Transactions. Italian Association of Chemical Engineering-AIDIC. 2016;**47**:403-408

[56] Zuo K, Chen M, Liu F, Xiao K, Zuo J, Cao X, Zhang X, Liang P, Huang X. Coupling microfiltration membrane with biocathode microbial desalination cell enhances advanced purification and long-term stability for treatment of domestic wastewater. Journal of Membrane Science. 2018;**547**:34-42

[57] Racar M, Dolar D, Špehar A, Košutić K. Application of UF/NF/RO membranes for treatment and reuse of rendering plant wastewater. Process Safety and Environmental Protection. 20171;**05**:386-392

[58] Bengani-Lutz P, Zaf RD, Culfaz-Emecen PZ, Asatekin A. Extremely fouling resistant zwitterionic copolymer membranes with ~1 nm pore size for treating municipal, oily and textile wastewater streams. Journal of Membrane Science. 2017;**543**:184-194

[59] Łaskawiec E, Madej M, Dudziak M, Wyczarska-Kokot J. The use of membrane techniques in swimming pool water treatment. Journal of Ecological Engineering. 2017;**18**(4):130-136

[60] Chang Q, Zhou JE, Wang Y, Liang J, Zhang X, Cerneaux S, Wang X, Zhu Z, Dong Y. Application of ceramic microfiltration membrane modified by nano-TiO_2 coating in separation of a stable oil-in-water emulsion. Journal of Membrane Science. 2014;**456**: 128-133

[61] Praveen P, Heng JYP, Loh KC. Tertiary wastewater treatment in membrane photobioreactor using microalgae: Comparison of forward osmosis & microfiltration. Bioresource Technology. 2016;**222**:448-457

[62] Al-Obaidi MA, Li JP, Kara-Zaitri C, Mujtaba IM. Optimisation of reverse osmosis based wastewater treatment system for the removal of chlorophenol using genetic algorithms. Chemical Engineering Journal. 2017;**316**:91-100

Chapter 3

Efficient Removal Approach of Micropollutants in Wastewater Using Membrane Bioreactor

Berna Kırıl Mert, Nihan Ozengin,
Esra Can Dogan and Coskun Aydıner

Additional information is available at the end of the chapter

http://dx.doi.org/10.5772/intechopen.75183

Abstract

In the recent past years, micropollutants that are pharmaceutically active compounds (PhACs) have been used extensively and have been discovered in raw sewage, wastewater treatment plants, effluents, surface, and groundwater with concentrations from ng/L to several μg/L. Even though many of these compounds are still not determined online, monitoring technology improvements progressed. Today's wastewater treatment plants are not constructed to remove these micropollutants yet. Conventional activated sludge processes are used in the treatment of municipal wastewater but are not specifically designed for the removal of micropollutants. The remaining pharmaceuticals mix into surface waters. At that stage, they can adversely affect the aquatic environment and may cause issues for drinking water production. As the conventional methods are insufficient for removing the micropollutants, other alternative treatment methods can be applied such as coagulation-flocculation, activated carbon adsorption (powdered activated carbon and granular activated carbon), advanced oxidation processes, membrane processes, and membrane bioreactor. It has been observed that membrane bioreactor (MBR) can achieve higher and more consistent micropollutants removal. The removal of micropollutants is based on physicochemical properties of micropollutants and the conditions of treatment. Due to recent technical innovations and cost reductions of the actual membranes, the membrane bioreactor takes attention. In this study, membrane bioreactor experiments for micropollutants in drinking use, wastewater, and surface waters were investigated in detail based on literature investigations, and the feasibility of this method was evaluated.

Keywords: wastewater, removal, micropollutant, membrane bioreactor

1. Introduction

Pharmaceutical wastewater is one of the most important gateways of emerging pollutants (such as synthetic hormones including corticosteroids) to enter water bodies. During the last years, numerous studies have documented the presence of many of these substances at the level of microgram or nanogram per liter in raw water (i.e., stream/source water), in wastewater effluents, and even in finished drinking waters [1, 2]. As a consequence, pharmaceuticals are entering in the trophic chain and causing adverse ecological and human health effects [3].

Pharmaceuticals are not regulated at the moment in the EU, but the 2013 amendment of the Environmental Quality Standards Directive (2008/105/EC) contains a mechanism to collect high-quality data on concentration of compounds of environmental concern, the so-called watchlist. This list includes diclofenac, 17-beta-estradiol (E2), and 17-alpha-ethinylestradiol (EE2). For compounds on this list, it is likely that regulations will be developed in the future. This would mean that additional treatment of wastewater will be necessary to comply with these regulations [4].

Membrane bioreactor (MBR) technique is a promising alternative to conventional treatment, [5, 6], and its usage is increasingly for municipal wastewater treatment and reuse, and great concerns have been raised to some emerging trace pollutants found in aquatic environment in the last decade, notably the pharmaceuticals [7]. In that sense, recently a pilot MBR was innovatively applied leading to removal efficiencies over 95% of the chemical oxygen demand (COD). Furthermore, other lab-scale MBR studies have been focused not only in the removal of the bulk organic matter but also in the elimination of the specific organic micropollutants present in the raw wastewater [1].

In this study, we present a comprehensive review of the studies carried out in the literature with MBR of micropollutant residues in different wastewaters, and it is expected that these pollutants, which are highly biologically active and difficult to biodegrade, shed light on treatment strategies to improve biodegradation.

2. Sources of pharmaceutical micropollutants in the aquatic environment

Pharmaceuticals are important and indispensable elements of modern life. They are used in humans and animals, in agriculture and in water culture. The presence of pharmaceuticals in the environment first attracted the attention of the scientific community and the public in the 1970s. However, until the 1990s, little has been done about the presence, behavior, and effects of pharmaceuticals in the environment. During this time, environmental pollutants such as heavy metals, polycyclic hydrocarbons, dioxins, furans, pesticides, and detergents have been extensively studied. Endocrine system drugs and lipid-lowering drugs have been on the rise since the 1990s. After this date, many studies have been done in the USA and Europe for hormones and other pharmaceuticals [8–10].

An important reason why so much care is taken with pharmaceutical products is that they have to produce a biological effect. They are made as stable as possible so that they can be stored for a long time and easily swallowed. The membranes are lipophilic enough to cross the membranes, and in order to reach the sites of action—especially those taken orally—drugs must be resistant to enzymes and must not hydrolyze at acidic pH values. They must be stable and have high mobility in liquid phase [11–13].

Because of these properties, active pharmaceutical ingredients/conversion products can be bioaccumulated and can cause effects in aquatic or terrestrial ecosystems.

The intake of drug active substances occurs in various ways. Starting from humans and animals, the active pharmaceutical ingredients reach the wastewater, soil, and groundwater and, if adequate treatment is not done, reach our drinking water. Pharmaceutical products can be roughly divided into two: medicinal products and veterinary drugs used by humans. Veterinary medicines are used in farm animal breeding and poultry production. Medicinal products used by humans reach sewage through urea and feces and from there to wastewater treatment plant. If xenobiotics are taken as an example, there are three possible behaviors of the substance: (i) the substance is completely mineralized to water and CO_2 (e.g., aspirin). (ii) The substance is lipophilic and does not easily fragment. So, some of the material is kept in clay. (iii) The substance is metabolized to a more hydrophobic than lipophilic form but becomes resistant. It cannot be removed in the treatment plant, and it is thrown away with wastewater and mixed with the receiving waters. If the metabolites are still biologically active, they also affect the aquatic organisms in the environment. Possible materials in clay, if the mud is laid on the field, may affect microorganisms and the useful ones. Medicinal substances used to support growth of animals in the stables are mostly fertile. These substances can affect soil organisms. The hydrophilic materials in the sewage sludge, which are scattered in the mouth, reach the aquatic environment by infiltrating with rain [11–13].

Pharmaceutical substances used for animals in the field are thrown directly to the ground via urea and feces. High local concentration affects soil organisms. It is also possible that medicinal substances spread over the surface are mineralized to the ground or reach the groundwaters.

They are used in fish farms and are directly confused with the receiving waters because the best way to treat fish with antibiotics and other medicines is to use feed additives. Because most of the feed additives are not eaten by the fish, they fall from the cages and accumulate in the seabed. These substances can affect aquatic organisms. An unknown part of the medical goods sold for human use is thrown into the toilet as waste by people and reaches the treatment plant by interfering with the sewage system [14–17].

Micropollutants consist of a vast and expanding array of anthropogenic as well as natural substances. These include pharmaceuticals, personal care products, steroid hormones, industrial chemicals, pesticides, and many other emerging compounds. Micropollutants are commonly present in waters at trace concentrations, ranging from a few ng/L to several μg/L. The "low concentration" and diversity of micropollutants not only complicate the associated detection and analysis procedures but also create challenges for water and wastewater treatment processes [2].

Sources of micropollutants in the environment are diverse, and many of these originate from mass-produced materials and commodities. **Table 1** summarizes the sources of the major categories of micropollutants in the aquatic environment.

Pharmaceuticals are thoroughly used to cure the diseases in humans and as veterinary drugs. These biologically active chemicals are treated as emerging contaminant due to their persistence and potential harmful impact on the aquatic ecosystem.

These refractory emerging contaminants (RECs) (analgesics, anti-inflammatories, antiepileptics, and antibiotics) fall into the class of endocrine-disrupting compounds, which continually enters into the aquatic environment in small concentration.

They remain active even in low concentrations and deteriorate water quality and have an adverse impact on the ecosystem and human health. The most common and persistent pharmaceutical products in the aquatic environment are summarized below.

2.1. Antibiotics

In recent years, global consumption and the use of antibiotics increase to >30% [18]. Antibiotics are generally treated as pseudo-persistent compound because of its continuous introduction in environment. The existence and release of antibiotics are inclined to be of specific concern since

Category	Important subclasses	Major sources	Nonexclusive
Pharmaceuticals	[a]NSAIDs, lipid regulator, anticonvulsants, antibiotics, β-blockers, and stimulants	Domestic wastewater (from excretion) Hospital effluents Runoff from [b]CAFOs and aquaculture	Sources that are not exclusive to individual categories include industrial wastewater (from product manufacturing discharges) Landfill leachate (from improper disposal of used, defective, or expired items)
Personal care products	Fragrances, disinfectants, UV filters, and insect repellents	Domestic wastewater (from bathing, shaving, spraying, swimming, etc.)	
Steroid hormones	Estrogens	Domestic wastewater (from excretion) Runoff from CAFOs and aquaculture	
Surfactants	Nonionic surfactants	Domestic wastewater (from bathing, laundry, dishwashing, etc.)	
Industrial chemicals Pesticides	Plasticizers, fire retardants Insecticides, herbicides, and fungicides	Industrial wastewater (from industrial cleaning discharges) Domestic wastewater (by leaching out of the material) Domestic wastewater (from improper cleaning, runoff from gardens, lawns, roadways, etc.) Agricultural runoff	

[a]NSAIDs, Nonsteroidal anti-inflammatory drugs.
[b]CAFOs, concentrated animal feeding operations.

Table 1. Sources of micropollutants in the aquatic environment.

they are designed to kill and inhibit the growth of microorganism; thus, they will hinder the activity of beneficial microbes in wastewater treatment plant (WWTP) operation and involved in their removal. Moreover, for constant exposure to antibiotics, microbial community stay in wastewater improves resistant mechanism more readily than the rest of another microbial world. The presence of numerous antibiotic compounds was identified in untreated wastewater in both aqueous and solid phases. Overall, occurrence and persistence of antibiotics in water bodies increase concern; almost 90% of antibiotics consumed by human body were discharged via urine and feces [19].

2.2. Therapeutic hormones

Therapeutic hormones are the synthetic analog of animal or plant natural hormones, which affect the endocrine system and have impacts on human and animal health. The most frequently found hormones in the environment are estrogens. A synthetic estrogenic steroid is used as a birth control agent and in estrogen substitution therapies. Thus, estrogen and its metabolite become the abundant class of emerging pharmaceutical contaminants. The metabolite of 17b-ethinyl estradiol and estrone (E1) is one of the most powerful EDCs creating impacts in aquatic organisms. Their presence in the river environment causes adverse reproductive and developmental effect in nontargeted organisms [20]. Several studies confirmed that the presence of estrogen in both influent and effluent of municipal wastewater treatment plants at a concentration ranges from 5 to 188 ng/L and between 0.3 and 12.6 ng/L, respectively [19, 21].

2.3. Analgesic pharmaceuticals

Analgesic is the widely used drug for pain relaxation and to treat fever. Drugs belonging to the class of analgesics such as naproxen acetaminophen, ibuprofen, diclofenac, and meprobamate were treated as significant environment pollutants due to their persistence in the aquatic environment [22]. Almost, 15% of ibuprofen was excreted after administration and 26% as its metabolite. The metabolite of ibuprofen is more toxic to aquatic organisms than parental compound [23]. The presence of ibuprofen, diclofenac, naproxen, gemfibrozil, and hydrochlorothiazide in the river shows a concentration range from 2 to 18 ng/L. The occurrence of these xenobiotic compounds in natural water bodies represents a significant concern for human health as little information is available on the effect of long-term ingestion of these compounds through drinking water [19].

2.4. By-product and metabolites

Pharmaceutical compounds pass on a set of biochemical transformation in human and animal body and form polar, hydrophilic, and biologically active metabolites, which are discharged through urine and feces and enter WWTP. These active metabolites are accumulated in tissues of aquatic organisms. They have the potential to bind covalently to their cellular protein and may evoke an immune response or exert toxic effects [25]. These metabolites are reported to be 50% more toxic than their parental compounds. The poorly metabolized parental pharmaceutical substances undergo a transformation and affect the action of microbial community present in

the WWTP. These metabolites are persistent due to their weaker sorption potential and high mobility and, thus, detected in environmental samples [26].

Literature reported that the concentration of the metabolite in influent and effluent of WWTP is often higher than their parental compounds, and their fate depends on the environmental conditions such as salinity, temperature, pH, and microbial diversity [19, 27].

Many studies on removal of pharmaceutical compounds from wastewater have been conducted, and many treatment technologies of hospital wastewater treatment have been developed.

Treatment of pharmaceutical residues using MBR processes was discussed in the following sections.

3. General features of MBR systems

Membranes have been used for many years as biological treatment (aerobic and anaerobic) and solid–liquid separation methods in physical applications. Nowadays, these methods are increasingly attracted to the name of membrane bioreactors combined with biological wastewater treatment [28]. Membrane bioreactor technology is emerging as a mature technology around the world with many full-scale installations for municipal and different wastewater treatments [29–31]. The reactor is operated in a similar manner to a conventional activated sludge process, and there is no need for tertiary stages such as secondary purification and sand filtration. Low-pressure membrane filters such as microfiltration (MF) or ultrafiltration (UF) are used to separate wastewater from the activated sludge [32].

Several factors have been reported that may affect contamination in MBR membrane properties such as floc size, mixed liquid viscosity, mixed liquid viscosity, pH, solubility, associated polymeric compounds (EPS), pore size, porosity, surface charge, roughness, and hydrophilicity/hydrophobicity. Operating parameters such as hydraulic retention time (HRT), solid retention time (SRT), and food/mass (F/M) ratio do not have a direct effect on membrane contamination [33, 34]. They affect more sludge properties and therefore sludge filtration properties. Organic contamination is caused by contamination of the membrane during active sludge filtration compared to inorganic pollution [35].

3.1. MBR configuration

There are two membrane-type alternatives: the first option is submerged MBR configuration such as operating under a vacuum, instead of direct pressure. This configuration may be named immersed as the membrane is placed directly into the liquid. The second option is sidestream MBR configuration such as operating under pressure. In this approach, the membrane is separated from the bioreactor, and a pump is required for pushing the bioreactor effluent into the membrane system and permeates through the membrane. This configuration may be named external cross flow membrane. Flat sheet (FS) and hollow fiber (HF) membranes are generally used for submerged MBR configuration [36]. The two main MBR configurations involve either submerged membranes or external circulation (sidestream configuration) (**Figure 1**) [32].

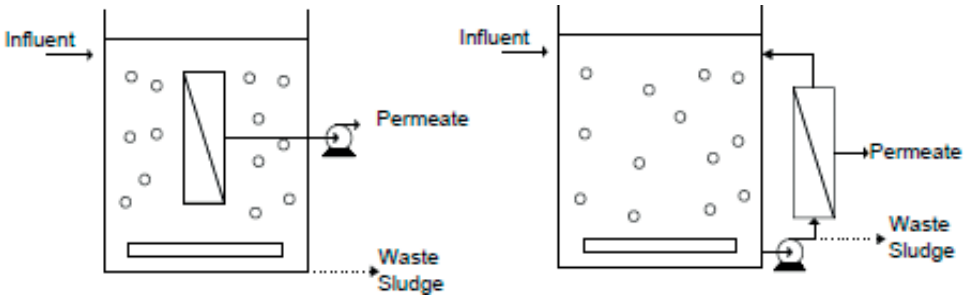

Figure 1. Configuration of MBR systems: (a) submerged (immersed) MBR and (b) sidestream (external) MBR configuration (adapted from [32, 37]).

Since submerged MBRs operate at lower operating fluxes, they have greater hydraulic efficiency due to greater permeability. Working with low flux is important in submerged MBR because this application minimizes membrane contamination or plugging. Membrane blockage is one of the major disadvantages of MBRs and requires cleaning mechanisms that increase cost and make operation difficult. While submerged MBRs require lower pumping costs than external MBRs, they require more aeration. The reason is that the aeration is the main method to prevent membrane clogging. In addition, low flux studies in submerged MBRs require more membrane surface area (and hence greater initial investment cost) when based on constant permeate flux production. Despite these disadvantages, however, the selected and implemented configuration for medium- and large-scale municipal wastewater treatment is the internal submerged MBR [38].

By the year 1990s, this existing accumulation has been rapidly increased by the MBR applications which are made as academic and field studies. MBR producers are Kubota from Japan, Zenon from Canada, Mitsubishi Rayon, and US Filtration [36, 39, 40] (**Table 2**).

Items	Zenon	Mitsubishi Rayon	Tianjin Motimo	Kubota[b]	Shanghai Zizheng
(1) Membrane module properties					
Polymer	PVDF	PE	PVDF	PE	PVDF
Filtration type	UF	MF	MF	MF	MF
Module	Hollow fiber	Hollow fiber	Hollow fiber	Flat sheet	Flat sheet
Hydrophilic	Yes	Yes	Yes	Yes	Yes
Outside diameter (mm)	1.95	—	1.00	490 (width)	460 (width)
Inside diameter (mm)	0.92	—	0.65	1000 (height)	1010 (height)
Fiber length (mm)	1650	663.5	1010	6 (thickness)	7 (thickness)
Pore size (μm)	0.04	0.4	0.2	0.4	0.2
Surface area (m^2)	23/module	105/module	20/module	0.8/panel	0.7/panel
Normal flux ($L/(m^2h)$	25.5	10.3–16.7	15	25.5	20–30

Items	Zenon	Mitsubishi Rayon	Tianjin Motimo	Kubota[b]	Shanghai Zizheng
(2) MBR performance					
[a]MLSS (g/L)	12–30		<15	15–30	10–30
Aeration per module (m^3/h)	14	57–73	—		0.6/panel
SRT (d)	10–100		<60	>40	40
Sludge yield (kg MLSS/kg BOD)	0.1–0.3		—		0.26
BOD effluent (mg/L)	<2	2–6	—	3–5	
NH_3 effluent (mg/L)	<0.3		—	<2	<2
Cleaning method	Back pulse and relax	Relax	—	Relax	
Cleaning frequency (min/min)	0.5/15	2/12		1/60	
Recovery method	Chemical soak	Chlorine backwash		Chlorine backwash	
Recovery frequency	≥3 months	≥3 months		≥6 months	
Recovery location	Drained cell or in situ	In situ		In situ	

[a]MLSS, Mixed liquor suspended solids.
[b]Although Kubota was not found very active in China, it was still referenced here in order to compare flat-sheet membranes made in China and those made in other countries.

Table 2. Summary comparison of membranes used in full-scale MBRs and MBR performance (adapted from [39, 41, 42]).

3.2. Design and operating parameters

A number of parameters must be considered in order to activate an economically appropriate MBR system. These include membrane selection, membrane performance (permeate flow, transmembrane pressure, viscosity), biological performance of microorganisms (biomass concentration, ESS, HBS, F/M ratio), and economic factors (energy consumption, sludge treatment, and disposal cost). These parameters can influence each other, and a positive change can be observed in the other parameter by changing one parameter. For example, a high biomass concentration requires a long CIS, which in turn reduces the cost of sludge disposal and sludge disposal. On the other hand, at high sludge age, the cost of energy also increases as the sludge reaches a viscous structure, which leads to the decomposition of the organic fraction and the amount of oxygen needed to grow the microorganism [43–45].

These designed and operational parameters are used to design the reactor and to be able to differentiate in different configurations applied to the process, to give formulas which are used in the general working principles of MBRs, also in the definition and calculation.

The amount of liquid drained from the surface area of the membrane is called flux. MBRs are mostly 10–100 LMH flux values.

3.3. Advantage and disadvantage of MBR

The best feature of MBRs is that they can easily convert existing activated sludge systems into MBR systems. This can be accomplished by placing submerged membranes in the aeration tank [46]. Membrane bioreactor is separating biological treatment of microorganisms and secondary cleaners from one site to another. The feed water is mixed with the biomass, the mixture is filtered from the membrane, and the biomass is separated from the treated water. Conventional activated sludge (CAS) units compared to the same operational conditions to provide better recovery efficiency in the MBR. Using MBR has many advantages [22, 47] (**Table 3**).

At higher MLSS concentrations, the ability to work at higher SRT than conventional treatments, reduced biomass yield, higher quality waste, less hydraulic residence time and lower area footprint generation are advantages of MBRs compared to CAS units [48]. This means a small reactor volume and a reduction in the initial investment cost. They are also more resistant to sudden different hydraulic and organic loads and better respond to existing sustainability criteria for municipal wastewater systems [49]. Biomass separation is independent of the ability of the activated sludge to precipitate as it is achieved by microfiltration or ultrafiltration; in other words, there is no need for final sedimentation, no sludge swelling, and sedimentation problems caused by filament growth. Due to high MLSS concentrations, excess organic loading can be done in the system. MBRs are less likely to be negatively affected by nitrification or by business problems related to the toxic effects of toxic organisms [50]. Since the sludge from the membrane system is less than the conventional system, the storage requirement is also reduced [51].

MBRs are becoming increasingly common throughout the world, despite the fact that they can reduce their investment and operating costs and produce effluent that cannot be used despite their different reuse areas. One of the biggest causes of this is the clogging of the wastes, and the transmembrane pressure (TMP) increases to provide a constant flux. Occlusions may occur at the membrane surface or within the membrane pores. Membrane clogs

MBR	CAS
Meets sensitive discharge standards	Cannot meet sensitive discharge standards
Decreased reactor volume and foot print	Large area is required for the secondary clarifier
Used as a pretreatment for reverse osmosis (RO) and nanofiltration (NF) with good effluent quality	Less quality effluent is obtained
Complete retention of bacterial flocs by the membrane	Needs disinfection step
Biomass retention is achieved by the membrane	Biomass retention is accomplished by gravity
Operated at elevated solid retention time (SRT)	Usually operates with low SRT
Better removal efficiency for slowly biodegradable micropollutants	The low SRT in ASP cannot allow this
High MLSS (10–15 g L^{-1}) and low feed to microorganism ratio (F/M)	MLSS is about four times less than that of MBR
Long SRT and high MLSS imply low sludge yield	Low SRT and low MLSS imply high sludge yield

Table 3. Comparison of MBR and CAS (adapted from [52]).

are roughly divided mechanically into two: recycled (removal of the surface gel and cake layer by aeration or physical backwash) and irreversible (removal of dissolved or colloidal substances in the adsorptive pore accumulation and clogging by chemical cleaning) [53]. MLSS, particle size distribution, soluble microbial by-products, extracellular polymeric materials, viscosity, pore size, porosity, surface energy, electrical charge, hydrophilic/hydrophobic properties parameters are affecting clogging [54]. The formation of cake, which is unavoidable on the membrane surface, is one of the factors that cause the membrane to become contaminated. In a general system, the sidestream of the MBR shows a higher tendency to pollute than the submerged MBR. The reason is that the sidestream MBR needs high pump energy to generate high flux which will cause repetition of pollution when compared to the submerged MBR [37]. Tank reduces production, increases operating and maintenance costs, and requires a special extra cleaning and backwashing. Membrane replacement is challenging. There are more than 10 years of MBR systems. On the other hand, there are many systems that change after 4 years. The main causes are often pollution problems. When contamination is combined with high transmembrane pressure, this contamination is most irreversible, and therefore the chemical cleaning frequency should be increased. This leads to an increase in operating cost by reducing membrane life [51].

The main contributors to energy costs in MBR are sludge transfer, permeate production, and aeration which is often exceeding 50% of total energy consumption. Energy consumption of membrane-related modules was in the range of 0.5–0.7 kWh/m^3, and specific energy consumption for membrane aeration in flat sheet was 33–37% which was higher than in a hollow fiber system. Submerged membranes in MBR reduces the pumping energy requirement to 0.007 kWh/m^3 of permeate compared with sidestream membrane (3.0 kWh/m^3). Future trend of MBR might be focused on two aspects which are reduction of energy demand and membrane fouling [55].

4. Micropollutant treatment studies with MBR applications

Many analgesics such as ibuprofen, diclofenac, naproxen, and ketoprofen; lipid regulators such as bezafibrate and gemfibrozil; and carbamazepine for antiepileptic drugs were frequently found to be removed at concentrations above 1.0 mg/L in domestic wastewater and in MBR procedures [22].

While the removal rates of microcontaminants in MBR vary from one compound to another, these removal rates, sludge retention time (SRT), biomass concentration, temperature, pH value, class of microcontaminants and hydrophobicity, chemical structure, pKa etc. as well as their physico-chemical properties. The hydrophobic components are removed from the liquid phase by adsorption and, possibly, when the SRT is sufficiently high, to be removed between the biodegradation processes [56–58]. The compactness of the MBR system, the high organic load that can be applied, and the high SRT give good results in removing micropollutant [48]. When the pH value of the wastewater changes, it may affect the removal of micropollutants in the negative direction. On the other hand, the role of pH on sorption has been related with the dissociation of certain micropollutants (through the acid dissociation constant pKa), which can result in the generation of positively charged compounds (prone to interact with the negatively

charged surface of sludges) or anions (low interaction). Thus, the cationic species would be adsorbed by van der Waals-type interactions [59].

Wastewater temperature also plays an important role. WWTP with an average temperature of 15–20°C can be better suited for micropollutants such as in cold countries, which are often below 10°C in the USA. Summer and winter affect seasonal temperature changes, micro-degradation, and biodegradation [60]. Sorption has been correlated inversely with temperature in the case of the hormone 17α-ethinyl estradiol (EE2), with a reduction of Kd values of 20–25% when the temperature was increased from 10 to 30°C [59].

Studies have shown that compounds such as ibuprofen and antiseptic powder, methyl paraben, and galaxolide, an analgesic drug in hospital wastewater, do not have significant differences in effluent efficiency with activated sludge processes and MBR. MBR system was found to be efficient for hormones (e.g., estriol, testosterone, androstenedione) and certain pharmaceuticals (e.g., acetaminophen, ibuprofen, and caffeine) with approximately 99% removal [61, 62]. Experimental investigations show that the removal of such compounds from wastewater is 30–50% superior to that of conventional activated sludge process. In addition, the removal efficiencies of some compounds such as mefenamic acid, indomethacin, diclofenac, and gemfibrozil in MBR were 40%, 40%, 65%, and 32–42% [63, 64]. However, biodegradable erythromycin, TCEP, trimethoprim, naproxen, diclofenac, carbamazepine, and nonylphenoxyacetic acid have not been removed [47]. This is comparable to the results of previous studies which indicated very low elimination rates of diclofenac and carbamazepine in WWTP due to their recalcitrant nature processes in Germany. Hydrophilic compounds such as MBRs, acetaminophen, atenolol, iopromide, and sulfamethoxazole (calculated logP <2) (with the exception of sulfamethoxazole (> 62%) are more efficient than hydrophobic compounds. Hydrophobic compounds (calculated log P > 2) can largely be removed by active sludge biosorption in the MBR and in the middle, and longer holding scoops are formed in the bioreactor, resulting in a higher removal yield from the CAS process. However, some hydrophilic microspheres such as carbamazepine and diclofenac tend to be highly resistant to biological degradation in the treatment of CAS and MBR. The retention time of the hydrophilic and persistent micropollutants in the bioreactor is the same as the retention time of hydraulic retention (HRT), as the micropollutants can freely permeate MF and UF membranes. The duration of hydraulic retention in the MBR and the prolongation of the retention time of the sludge are dependent on the compound biosorption of some hydrophobics for the activated sludge, and it can be seen that the pollutants can improve the biodegradation [2, 65].

In the comparison between the two MBR modules used in this study (plate and frame versus hollow fiber), no difference in target compound removal was found [60, 65]. Some results can be negative efficiency. For example, González-Pérez et al. (2017) have worked on the system that has been operated with complex nitrification and ensured that the biodegradable organic material due to circulation is effectively retained [66]. By reducing the concentration increase in the diclofenac (DCF) in the aerobic bioreactor, negative removal efficiencies for DCF have been obtained. This was not observed in the anoxic reactor.

Membrane bioreactor applications for these pollutants in different wastewaters are presented in detail given in **Table 4**.

Operation mode/membrane configuration	Volume (L)/ temperature (°C)	Substrate	MLSS (g SS/L) Organic loading rate (kg COD/m^3.d)	Removal (%)			Reference
Full scale (VRM) Pilot Scale (Clear-box) PES membrane Plate and frame	350 L 4 °C	Syntetic wastewater	5 g/L		Full Scale	Pilot Scale	[67]
				Diltiazem	100	0	
				Acetaminophen	100	>95%	
				Estrone	10	100%	
				Carbamazepine	0	0	
Anoxic + aerobic hollow fiber (MF) PVDF Membrane submerged	5 L 25°C (±5°C)	Real wastewater	7 – 11 g/L 0.1 grBOD/grMLVSS	Bezafibrate Ketaprofen Furosemide Atenolol Propranolol Diltiazen Roxithromyan Clarithromyun Naproxen Ciprofloxacin Levofloxacin Tetracycline Triclosan Triclocarban	93 87 68 58 50 57 51 46 97 36 47 52 84 42		[63]
Anaerobic reactor+ external / hollow fiber Hybrid aerobic MBR	176 L 20 – 22 °C	Synthetic wastewater	0,6 g/L 1.7 grCOD/L.d	Sulfamed hoxazole Trimethoprim	> 84%		[68]
Anoxic+Aerobic+MBR 3,6m^3 + 8,8 m^3 + 3,5 m^3 Flat sheet (MF)			6,3 – 7.1 gr/L TSS 75 – 77 % VSS 0.83 – 0.98 kgCOD/m^2d	Ibuprofen Naproxen Ketoprofen Diclofenac$_A$ Diclofenac$_B$	98.12 98.2 92.26 20.70 -18.75		[66]
Flat Sheet MF Hallow Fiber UF + PAC	MF_{MBR} ➔ 30 L UF_{MBR} ➔ 185 L 20 – 22 °C	Synthetic wastewater	3gr$_{VSS}$/L 400 mgCOD/L 0.4 gr COD/L	Trimethoprim	MF% 50	UF % 40	[69]

Operation mode/membrane configuration	Volume (L)/ temperature (°C)	Substrate	MLSS (g SS/L) Organic loading rate (kg COD/m^3.d)	Removal (%)			Reference
				Sulfamed hoxazole	80	70	
				Erythromycin	80	90	
				Carbamazepine	0	0	
				Roxithromyan	70	> 95	
				Aceclofenac	30	60	
				Naproxen	90	90	
				Ibuprofen	90	> 95	
				Ethynilestradiol	90	> 90	
				Estradiol	95	> 95	
				Naproxen	98.2		
				Ketoprofen	92.26		
				$Diclofenac_A$	20.70		
				$Diclofenac_B$	-18.75		
Lab scale hollow fiber membrane model	3.2 L	PVDF submerged	1.66 gVSS/L 2.16 g+COD/Lday	Levo	98.7		[1]
				Betha-V	97.8		
				Betha-D	99.6		
				Medro	93.4		
Pilot-scale PES UF submerged flat sheet		Hospital effluent	2 g/L	Carbamazepine	−6		[70]
				Trimethoprim	96		
				Sulfamethoxazole	7		
				Atenolol	99		
(4.7 m^3) Microfiltration (MF) Flat Sheet (FS) membrane Module (3.6 m^3) Hollow fiber (HF) ultrafiltration membrane External configuration	20±2 °C	Real wastewater			FS MBR	HF MBR	[22]
				Analgesics and anti-inflammatory drugs			
				Ibuprofen	99.2	99.5	

http://dx.doi.org/10.5772/intechopen.75183

Operation mode/membrane configuration	Volume (L)/ temperature (°C)	Substrate	MLSS (g SS/L) Organic loading rate (kg COD/m^3.d)	Removal (%)			Reference
				Naproxen	90.7	91.6	
				Ketoprofen	43.9	44.0	
				Diclofenac	65.8	62.6	
				Mefenamic	40.5	35.5	
				Propyphenazone	64.5	60.7	
				Acetaminophen	99.8	99.9	
				Indomethacin	41.4	39.7	
				Anti-histamines			
				Ranitidine	44.2	29.5	
				Loratidine	<10	33.5	
				Famotidine	64.6	47.4	
				Anti-epileptic drug			
				Carbamazepine	<10	<10	
				Psychiatric drugs			
				Fluoxetine	98.0	98.0	
				Antibiotics			
				Erythromycin	43.0	25.2	
				Sulfamethoxazole	80.8	78.3	
				Ofloxacin	95.2	91.3	
				Trimethoprim	66.7	47.5	
				ß-blockers			
				Atenolol	76.7	69.5	
				Sotalol	53.1	30.4	
				Metoprolol	44.2	29.5	

Operation mode/membrane configuration	Volume (L)/ temperature (°C)	Substrate	MLSS (g SS/L) Organic loading rate (kg COD/m^3.d)	Removal (%)			Reference
				Propranolol	77.6	65.5	
				Hypoglycaemic agents			
				Glibenclamide	95.6	82.2	
				Lipid regulator and cholesterol lowering statin drugs			
				Gemfibrozil	42.2	32.5	
				Bezafibrate	90.3	88.2	
				Pravastatin	86.1	83.1	
				Hydrochlorothiazide	<10	<10	
Full-scale hollow fiber		Raw wastewater	7.5–8.5 g/L	Ibuprofen	~100		[71]
				Diclofenac	43		
				Carbamazepine	24		
				Sulfamethoxazole	60		
				Trimethoprim	30		
				Estrone,	~100		
				Estriol	~100		
				BisphenolA	~100		
Lab-scale hollow fiber submerged UF modüle		Synthetic wastewater	8.6–10 g/L	Ibuprofen	96.7		[72]
				Diclofenac	17.3		
				Paracetamol	95.1		
				Carbamazepine	13.4		
				Linuron	21.1		

http://dx.doi.org/10.5772/intechopen.75183

Operation mode/membrane configuration	Volume (L)/ temperature (°C)	Substrate	MLSS (g SS/L) Organic loading rate (kg COD/m^3.d)	Removal (%)		Reference
				Sulfamethoxazole	91.9	
				Ketoprofen	70.5	
				17β-estradiol	99.4	
				17α- ethynilestradiol	93.5	
				Triclocarban	>98.4	
				Naproxen	40.1	
				Bisphenol A	90.4	
				Sulfamethoxazole	91.9	
				Nonylphenol	99.3	
				Atrazine	4.4	
Flate and frame- type hollow fiber	1 m^3/d	Domestic wastewater		Hormones	Good	[60]
				Acetaminophen	99	
				Ibuprofen	99	
				Caffeine	99	
				Others	low	
A pilot-scale MBR flat-sheet membranes submerged	21 L	Municipal, hospital, and industrial wastewater		Aceclofenac Carbamazepine Diclofenac Enalapril Trimethoprim	~ 50 ~ 0 ~80 > 95 > 95	[49]
Flat- sheet (MF) membrane submerged MBR	21L (20 ± 2 °C)	Real wastewater (municipal, hospital and industrial)		***Analgesics and anti-inflammatory drugs***		[22]
				Naproxen	99.3	
				Ketoprofen	91.9	
				Ibuprofen	99.8	

Operation mode/membrane configuration	Volume (L)/ temperature (°C)	Substrate	MLSS (g SS/L) Organic loading rate (kg COD/m^3.d)	Removal (%)		Reference
				Diclofenac	87.4	
				Indomethacin	46.6	
				Acetaminophen	99.6	
				Mefenamic acid	74.8	
				Propyphenazone	64.6	
				Anti-ulcer agents		
				Ranitidine	95.0	
				Psychiatric drugs		
				Paroxetine	89.7	
				Antiepileptic drugs		
				Carbamazepine	-	
				Antibiotics		
				Ofloxacin	94.0	
				Sulfamethoxazole	60.5	
				Erythromycin	67.3	
				B-blockers		
				Atenolol	65.5	
				Metoprolol	58.7	
				Diuretics		
				Hydrochlorothiazide	66.3	
				Hypoglycaemic agents		
				Glibenclamide	47.3	
				Lipid regulator and cholesterol lowering statin drugs		

http://dx.doi.org/10.5772/intechopen.75183

Operation mode/membrane configuration	Volume (L)/ temperature (°C)	Substrate	MLSS (g SS/L) Organic loading rate (kg COD/m^3.d)	Removal (%)			Reference
				Gemfibrozil	89.6		
				Bezafibrate	95.8		
				Clofibric acid	71.8		
				Pravastatin	90.8		
Full-scale flat sheet		Hospital effluent		Ibuprofen	>80		[73]
				Carbamazepine	<20		
				Diclofenac	<20		
MBR Concept A	10 °C		10 g/L		Concept A	Concept B	[74]
MBR Concept B	10 °C		10 g/L				
				Paracetamol	>99	>99	
				Ibuprofen	>99	98.5	
				Ketoprofen	90.1	81.3	
				Naproxen	>97	90.2	
				Caffeine	99.7	99.5	
				Tetracycline	>95	>95	
				Atenolol	70.8	69.1	
				Bisoprolol	41.9	21.7	
				Metoprolol	18.8	20.1	
				Sotalol	-27.7	-33.0	
				Furosemide	16.3	5.6	
				Hydrochlorothiazide	27.5	2.4	
Pilot-scale MBR hollow fiber PVDF	1.3 m^3	Hospital wastewater	less than 13 g/L	Diclofenac Sulfamethoxazole Trimethoprim		0 0 0	[75]

Operation mode/membrane configuration	Volume (L)/ temperature (°C)	Substrate	MLSS (g SS/L) Organic loading rate (kg COD/m^3.d)	Removal (%)			Reference
				Carbamazepine		0	
				Tramadol		0	
				Naproxen		23.6	
				Propanolol		34.2	
				Ibuprofen		100	
				17b-Estradiol		100	
				Triclosan		100	
				Gemfibrozil		0	
Laboratory-scale MBR	Feed tank (50 L) MBR (15 L)		2.15 gCOD/L/d	Amelotin (AMTN)		20-40	[76]
Pilot-scale Anoxic+Aerobic MBR	Anoxic (13.8 L) Aerobic (11.7 L) hollow fiber Ultrafiltration membrane (18 ± 3 °C)		Anoxic (4.1 ± 0.5 and 2.7 ± 0.3 g/L) Aerobic (2.4 ± 0.8 g/L (MLSS))	Atenolol	Pilot	Full Scale	[77]
				Sulfamethoxazole	> 80	> 80	
				Caffeine	~ 60	> 80	
				Naproxen	~ 90	> 90	
				Ibuprofen	> 80	> 90	
				Paracetamol	> 90	> 90	
				Trimethoprim	> 90	> 90	
				Primidone	~ 60	~ 70	
				Diclofenac	~ 20	0	
				Gemfibrozil	~ 20	~ 60	
				Carbamapazine	~ 90	> 90	
				DEET	0	0	
				Diuron	~ 80	> 90	
				Polyparaben	~ 30	> 90	
				Amtriptyline	> 90	> 90	
				Estrone	0	~ 30	
				Androsterone	> 90	> 90	
				Etiocholanolone	> 90	> 90	
				Triclosan	> 90	> 90	
				Triclocarban	~ 60	~ 60	
					> 90	~ 50	

Table 4. Membrane bioreactor applications for micropollutants in various wastewaters.

http://dx.doi.org/10.5772/intechopen.75183

5. Integration of MBRs with other technologies

Membrane bioreactors (MBRs) have recently emerged with integrated MBR systems, along with other treatment technologies. The purposes of the integrated MBR are to improve qualities of permeates, mitigate membrane fouling, and enhance the stability of the treatment process. Recent studies have provided improvements in the degradation of micropollutants using integrated

Integrated technology of MBR	Advantages	Disadvantages and limitations
Advanced oxidation processes/electrocoagulation-MBR	Effective in removal of recalcitrant contaminants (pharmaceutical wastewater) Effective in removing colors Reduces the production of excess sludge Easy to operate Reduce membrane fouling	High capital and operational cost Not effective in treatment of wastewater with high TSS
FO-MBR	Produce good effluent quality Phosphorus recovery Low energy consumption as compared to conventional MBR Low fouling tendency compared to RO Effective in removal of trace organic contaminants Fouling is largely reversible Effective in treatment of wastewater with high TSS as compared to RO	Uncertainly of stability of membrane Increasing salinity/salt accumulation might decrease the microbial kinetics and water flux
RO-MBR	Low fouling tendency Cost of RO membrane is cheaper than FO membrane Low energy consumption as compared to conventional MBR	Not effective in treatment of high-salinity wastewater compared to FO
Membrane distillation	Enhances biodegradation of recalcitrant compounds Low sludge yield Higher effluent quality Excellent process stability Cost-effective compared to RO process Smaller footprint	Low removal of COD
Biofilm/bio-entrapped MBR	Reduces the concentration of suspended solids Reduce membrane fouling Improve nitrification and denitrification processes	Membrane fouling might be severe at the later stage of treatment
Granular MBR	Improve nitrification and denitrification processes High shock resistance capacity Reduce membrane fouling Smaller footprint	Membrane fouling might be severe at the later stage of treatment Long start-up period of granule formation

Table 5. Advantages and disadvantages of various integrated MBRs in wastewater treatment technology [55].

processes. There are several methods to reduce the membrane fouling of MBR such as optimization of HRT and SRT which were discussed in some review papers. These processes containing biofilm carriers, suspended/attached growth system, or cross-linked enzyme aggregates showed better removal of micropollutants, even on recalcitrant compounds such as CBZ [78].

The advantages and disadvantages of various integrated systems, such as advanced oxidation processes (AOPs) [79], reverse osmosis (RO-MBRs) [64], forward osmosis (FO-MBRs) [80], membrane distillation (MDBRs) [81], microbial fuel cells (MBR-MFCs) [7], anaerobic (AnMBRs) [82], biofilm (BF-MBR) [83], and granular (GMBR) membrane bioreactors [84] to demonstrate their ability to reduce membrane contamination, are given in the **Table 5**. Combined MBR process configurations and conventional biological therapies, as an alternative, resulted in more consistent results. As shown in the studies, the removal efficiency of each of the micropollutants is different for the different membrane technologies. The value ranges from close to zero to almost complete removal. For example, the removal efficiency of carbamazepine is less than 20% with ASP and MBR and up to 93% with MBR-NF and higher than 99% with MBR-RO, MBR-PAC, and MBR-GAC [52]. The use of combinations of different complementary technologies has produced promising results. Nonetheless, there is a lack of a holistic understanding of the nature of pollutants, their interactions, and some predictable relationships between the best available specific technologies. More practice is needed to evaluate the hybrid MBR systems proposed in the treatment of micropollutants [48].

6. Conclusions

In recent years, pharmaceutical products have been a cause for concern due to the persistence of their presence in aquatic environments. Drugs are known to be involved in a variety of aquatic environments, including domestic wastewater, hospital discharges, sewage treatment plants, and water treatment plants.

Pharmaceutical products can preserve their original concentrations and structures, or they can be mobilized for life in water matrices and converted to other active (or inactive) compounds. The presence of micropollutants in aqueous environments is an increasing concern due to their potentially harmful effects on aquatic life. Since this situation poses a serious danger to the environment, the treatment of these pollutants is very important.

As it is clear from this work, today's CAS is not sufficient for the destruction of many pharmaceutical substances in the wastewater of the AAT. For these pollutants, the use of MBR systems developed by adding membranes to CAS systems has begun to be used, and these are often more effective at removing pollutant concentrations than traditional biological treatment systems. MBR technology has become a reliable and valuable option with many advantages. However, in addition to its advantages, membrane fouling is a major obstacle to the development of these systems. To this end, it will be useful to focus on the reduction of energy demand and membrane contamination during operation, along with the development of integrated MBR systems, with future research. Further work is needed to assess which system actually makes more cost–benefit and to investigate the toxicity of micropollutants and the effect of working conditions after processing.

Author details

Berna Kırıl Mert[1]*, Nihan Ozengin[2], Esra Can Dogan[3] and Coskun Aydıner[4]

*Address all correspondence to: bkiril@sakarya.edu.tr

1 Sakarya University, Faculty of Engineering, Department of Environmental Engineering, Sakarya, Turkey

2 Uludag University, Faculty of Engineering, Department of Environmental Engineering, Bursa, Turkey

3 Kocaeli University, Faculty of Engineering, Department of Environmental Engineering, Kocaeli, Turkey

4 Gebze Technical University, Environmental Engineering Department, Gebze, Kocaeli, Turkey

References

[1] Fernández RL, Martínez L, Villaverde S. Membrane bioreactor for the treatment of pharmaceutical wastewater containing corticosteroids. Desalination. 2012;**300**:19-23. DOI: 10.1016/j.desal.2012.05.032

[2] Luo Y. Guo W, Ngo HH, Nghiem LD, Hai FI, Zhang J, Liang S, Wang XC. A review on the occurrence of micropollutants in the aquatic environment and their fate and removal during wastewater treatment. Science of the Total Environment. 2014;**473–474**:619-641. DOI:10.1016/j.scitotenv.2013.12.065

[3] Miège C, Choubert JM, Ribeiro L, Eusèbe M, Coquery M. Fate of pharmaceuticals and personal care products in wastewater treatment plants – Conception of a database and first results. Environmental Pollution. 2009;**157**:1721-1726. DOI: 10.1016/j.envpol.2008.11.045

[4] Hofman-Caris CHM, Siegers WG, Merlen K van de, Man AWA de, Hofman JAMH. Removal of pharmaceuticals from WWTP effluent: Removal of EfOM followed by advanced oxidation. Chemical Engineering Journal. 2017;**327**:514-521. DOI:10.1016/j.cej.2017.06.154

[5] Hai FI, Yamamoto K, Lee CH. Membrane Biological Reactors: Theory, Modeling, Design, Management and Applications to Wastewater Reuse. IWA Publishing, 2014, London. eISBN:9781780401331

[6] Zaviska FO, Drogui P, Grasmick A, Azais A, Héran M. Nanofiltration membrane bioreactor for removing pharmaceutical compounds. Journal of Membrane Science. 2013;**429**:121-129. DOI: 10.1016/j.memsci.2012.11.022

[7] Li C, Cabassud C, Reboul B, Guigui C. Effects of pharmaceutical micropollutants on the membrane fouling of a submerged MBR treating municipal wastewater: Case of continuous pollution by carbamazepine. Water Research. 2015;**69**:183-194. DOI: 10.1016/j.watres.2014.11.027

[8] Vergili İ, Kaya Y, Gönder B, Barlas H. İlaç aktif maddelerinin sucul çevrede bulunuşları, davranışları ve etkileri. Ulusal Su Günleri 2005, 28–30 Eylül, Trabzon (in Turkish)

[9] Kümmerer K. Introduction: Pharmaceuticals in the Environment. In: Kümmerer K. editor. Pharmaceuticals in the Environment. Berlin, Heidelberg: Springer; 2001. DOI: 978–3–662-04634-0_1 http://www.epa.gov/esd/chemistry/pharma/kummer/intro.pdf

[10] Daughton CG, Ternes TA. Pharmaceuticals and personal care products in the environment: Agents of subtle change. Environmental Health Perspectives Supplements. 1999; **107**(56):907-938

[11] Wasser-wissen.de. Das Internetportal für Wasser und Abwasser, Institut für Umweltverfahrenstechnick – Universität Bremen. 2000. ISSN 1614–0362

[12] Halling–Sorensen B, Nors Nielsen S, Lanzky PF, Ingerslev F, Holten Lützhoft HC, Jorgensen SE. Occurence, fate and effects of pharmaceutical substances in the environment: A review. Chemosphere. 1998;**36**(2):357-393

[13] Ternes TA. Occurence of drugs in german sewage treatment plants and rivers. Water Research. 1998;**32**(11):3245-3260

[14] Heberer T. Occurence, fate and removal of pharmaceutical residues in the aquatic environment: A review of recent research data. Toxicology letters. 2002;**131**:5-17 https://doi.org/10.1016/S0378-4274(02)00041-3

[15] Reddersen K, Heberer T, Dünnbier U. Identification and significance of phenazone drugs and their metabolites in ground-and drinking water. Chemosphere. 2002;**49**:539-544 https://doi.org/10.1016/S0045-6535(02)00387-9

[16] Dietrich DR, Webb SF, Petry T. Hot spot pollutants: Pharmaceuticals in the environment. Toxicology Letters. 2002;**131**:1-3. https://dx.doi.org/10.1016/S0378-4274(02)00062-0

[17] Mersmann P. Transport und Sorptionsverhalten der Arzneimittelwirkstoffe Carbamazepin, Clofibrinsäure, Diclofenac, Ibuprofen und Propyphenazon in der wassergesättigten und ungesättigten Zone. Dissertation am Institut für Angewandte Geowissenschaften der Technischen Universität Berlin. 2003; http://dx.doi.org/10.14279/depositonce-708

[18] Gelbrand H, Miller-Petrie M, Pant S, Gandra S, Levinson J, Barter D, White A, Laxminarayan R, Ganguly N, Kariuki S. The state of the World's. Antibiotics. Wound Healing Southern Africa. 2015;**8**(2):30-34

[19] Tiwari B, Sellamuthu B, Ouarda Y, Drogui P, Tyagi RD, Buelna G. Review on fate and mechanism of removal of pharmaceutical pollutants from wastewater using biological approach. Bioresource Technology. 2017;**224**:1-12. DOI:10.1016/j.biortech.2016.11.04

[20] Gross-Sorokin MY, Roast SD, Brighty GC. Assessment of feminization of male fish in English rivers by the environment Agency of England and Wales. Environmental Health Perspectives. 2005;**114**(S-1):147-151

[21] Joss A, Andersen H, Ternes T, Richle PR, Siegrist H. Removal of estrogens in municipal wastewater treatment under aerobic and anaerobic conditions: Consequences for plant

optimization. Environmental Science & Technology. 2004;**38**(11):3047-3055. DOI: 10.1021/es0351488

[22] Radjenovic´ J, Petrovic´ M, Barceló D. Fate and distribution of pharmaceuticals in wastewater and sewage sludge of the conventional activated sludge (CAS) and advanced membrane bioreactor (MBR) treatment. Water Research. 2009;**43**(3):831-841 https://doi.org/10.1016/j.watres.2008.11.043

[23] Evgenidou EN, Konstantinou IK, Lambropoulou DA. Occurrence and removal of transformation products of PPCPs and illicit drugs in wastewaters: A review. Sci. Total Environ. 2015;**505**:905-926. https://doi.org/10.1016/j.scitotenv.2014.10.021

[24] Valcarcel Y, Alonso SG, Rodriguez-Gil JL, Maroto RR, Gil A, Catala M. In river- and drinking-water of the Madrid region in Spain. Chemosphere. 2011;**82**(7):1062-1071 https://doi.org/10.1016/j.chemosphere.2010.10.041

[25] Zhou S, Chan E, Duan W, Huang M, Chen Y. Drug bioactivation covalent binding to target proteins and toxicity relevance. Drug Metabolism Reviews. 2005;**37**(1):41-213 https://doi.org/10.1081/DMR-200028812

[26] Zuehlke S, Duennbier U, Heberer T. Investigation of the behavior and metabolism of pharmaceutical residues during purification of contaminated ground water used for drinking water supply. Chemosphere. 2007;**69**(11):1673-1680. https://doi.org/10.1016/j.chemosphere.2007.06.020

[27] Marques CR, Abrantes N, Goncalves F. Life-history traits of standard and autochthonous cladocerans: II. Acute and chronic effects of acetylsalicylic acid metabolites. Environ. Toxicology. 2004;**19**(5):527-540. DOI: 10.1002/tox.20060

[28] Judd S. The status of membrane bioreactor technology. Trends in Biotechnology. 2008;**26**(2) DOI:10.1016/j.tibtech.2007.11.005

[29] Krzeminski P, Leverette L, Malamis S, Katsou E. Membrane bioreactors: A review on recent developments in energy reduction, fouling control, novel configurations, LCA and market prospects. Journal of Membrane Science. 2017;**527**:207-227. https://doi.org/10.1016/j.memsci.2016.12.010

[30] Wu Y, Huang X, Wen X, Chen F. Function of dynamic membrane in self-forming dynamic membrane coupled bioreactor. Water Science and Technology. 2005;**51**(6–7):107-114

[31] Lesjean B, Huisjes EH. Survey of the European MBR market: Trends and perspectives. Desalination. 2008;**231**:71-81. https://doi.org/10.1016/j.desal.2007.10.022

[32] Melin T, Jefferson B, Bixio D, Thoeye C, WDe W, JDe K, JVder G, Wintgens T. Membrane bioreactor technology for wastewater treatmentand reuse. Desalination. 2006;**187**:271-282. DOI: 10.1016/j.desal.2005.04.086

[33] Meng F, Chae SR, Drews A, Kraume M, Shin HS, Yang F. Recent advances in membrane bioreactors(MBRs): Membrane fouling and membrane material. Water Research. 2009;**43**: 1489-1512. DOİ:10.1016/j.watres.2008.12.044

[34] Meng F, Zhang S, Oh Y, Zhou Z, Shin HS, Chae SY. Fouling in membrane bioreactors: An updated review. Water Research. 2017;**114**:151-180. DOI: 10.1016/j.watres.2017.02.006

[35] Erşahin ME. Application of Dynamic Membranes in Anaerobic Membrane Bioreactor Systems. Istanbul Technıcal Unıversıty Graduate School of Scıence Engıneerıng and Technology, Delft Unıversıty of Technology Graduate School of Cıvıl Engıneerıng and Geoscıences. Ph.D. Thesıs. October 2015

[36] Cinar Ö, Kizilet A, Isik O, Ćemanović A, Veral MA, Duman S. A review on dynamic membrane bioreactors: Comparison of membrane bioreactors and different support materials, Transmembrane pressure. ICENS-International Conference on Engineering and Natural Sciences. 24-28 May 2016 Sarajevo

[37] Mutamim NSA, Noor ZZ, Hassan MAA, Yuniarto A, Olsson G. Membrane bioreactor: Applications and limitations in treating high strength industrial wastewater. Chemical Engineering Journal. 2013;**225**:109-119. DOI: 10.1016/j.cej.2013.02.131

[38] Judd SJ. The development of the membrane bioreactor Technology for Sewage Treatment in the UK, School of Water Sciences. In: Cranfield University. 2002

[39] Judd S. The MBR Book Principles and Applications of Membrane Bioreactors in Water and Wastewater Treatment. Oxford, UK: Elsevier; 2006. ISBN: 978–0–08-096682-3

[40] Radjenovic J, Matosic M, Mijatovic I, Petrovic M, Barceló D. Membrane bioreactor (MBR) as an advanced wastewater treatment technology. Handbook of Environment Chemical. 2008;**5**:37-101. DOI: 10.1007/698_5_093

[41] Wang Z, Wu Z, Mai S, Yang C, Wang X, An Y, Zhou Z. Research and Applications of Membrane Bioreactors in China: Progress and Prospect. Separation and Purification Technology. 2008;**62**:249-263 DOI: 10.1016/j.seppur.2007.12.014

[42] Yang W, Cicek N, Ilg J. State-of-the-art of membrane bioreactors: Worldwide research and commercial applications in North America. Journal of Membrane Science. 2006;**270**:201-211. DOI: 10.1016/j.memsci.2005.07.010

[43] Atay B. Hidrokarbon İçeren Tuzlu Atıksuların Membran Biyoreaktör (Mbr) ile Ön Arıtma Sonrası Nanofiltrasyon (Nf) ve Ters Osmoz (To) Membranları ile İleri Arıtımının Araştırılması. Istanbul Teknik Üniversitesi Fen Bilimleri Estitüsü. Yüksek Lisans Tezi, Haziran 2010 (in Turkish)

[44] Yurtsever A. Tekstil Endüstrisi Atıksularının Anaerobik ve Aerobik Membran Biyoreaktörlerle Arıtılabilirliği ve Tıkanma Özelliklerinin İncelenmesi. Yıldız Teknik Üniversitesi Fen Bilimleri Enstitüsü. Doktora Tezi. İstanbul, 2016. (in Turkish)

[45] Visvanathana C, Choudharya MK, Montalboa MT, Jegatheesan V. Landfill leachate treatment using thermophilic membrane bioreactor. Desalination. 2007;**204**(1–3):8-16. https://doi.org/10.1016/j.desal.2006.02.028

[46] Bacaksız AM. Anaerobik Membran Biyoreaktörde (AnMBR) Membran Kirlenme Mekanizmalarının Araştırılması: İlaç Endüstrisi Uygulaması. İstanbul Üniversitesi Fen Bilimleri Enstitüsü. Yüksek Lisans Tezi. Mayıs. 2014

[47] Clara M, Sternn B, Gans O, Martinez E, Kreuzinger N, Kroiss H. Removal of selected pharmaceuticals, fragrances and endocrine disrupting compounds in a membrane bioreactor and conventional wastewater treatment plants. Water Research. 2005;**39**:4797-4807. https://doi.org/10.1016/j.watres.2005.09.015

[48] Cecconet D, Molognoni D, Callegari A, Capodaglio AG. Biological combination processes for efficient removal of pharmaceutically active compounds from wastewater: A review and future perspectives. Journal of Environmental Chemical Engineering. 2017;**5**:3590-3603. DOI: 10.1016/j.jece.2017.07.020

[49] Celiz MD, Pérez S, Barceló D, Aga DS. Trace analysis of polar pharmaceuticals in wastewater by LC-MS-MS: Comparison of membrane bioreactor and activated sludge systems, Journal of Chromatographic Science. 2009;**47**:19-25. http://dx.doi.org/10.1093/chromsci/47.1.19.yy

[50] Özgü YN. Membran Biyoreaktörü ile (MBR) Evsel Atıksu Arıtımı. Süleyman Demirel Üniversitesi Fen Bilimleri Enstitisü. Doktora Tezi. Isparta 2007. (in Turkish)

[51] Wozniak T. MBR design and operation using MPE-technology (membrane performance enhancer). Desalination. 2010;**250**:723-728. DOI: 10.1016/j.desal.2008.11.030

[52] Besha AT, Gebreyohannes AY, Tufac RA, Bekeled DN, Curciob E, Giornob L. Removal of emerging micropollutants by activated sludge process and membrane bioreactors and the effects of micropollutants on membrane fouling: A review. Journal of Environmental Chemical Engineering. 2017;**5**:2395-2414. DOI: 10.1016/j.jece.2017.04.027

[53] Huang X, Gui P, Qian Y. Effect od sludge retention time on microbial behavior in a submerged membrane bioreactor. Process Biochemistry. 2001;**36**:1001-1006 https://doi.org/10.1016/S0032-9592(01)00135-2

[54] Gao W, Liang H, Maa J, Han M, Chen Z, Han Z, Li G. Membrane fouling control in ultrafiltration technology for drinking water production: A review. Desalination. 2011; **272**(1–3):1-8 https://doi.org/10.1016/j.desal.2011.01.051

[55] Neoh CH, Noor ZZ, Mutamim NSA, Lim CK. Green technology in wastewater treatment technologies: Integration of membrane bioreactor with various wastewater treatment systems. Chemical Engineering Journal. 2016;**283**:582-594. DOI: 10.1016/j.cej.2015.07.060

[56] Cirja M, Ivashechkin P, Schaeffer A, Philippe F, Corvini X. Factors affecting the removal of organic micropollutants from wastewater in conventional treatment plants (CTP) and membrane bioreactors (MBR). Reviews in Environmental Science and Biotechnology. 2008;**7**:61-78 https://doi.org/10.1007/s11157-007-9121-8

[57] Basile A, Introduction GF. A review of membrane reactors. USA: John Wiley & Sons, ltd. 2011. DOI: 10.1002/9780470977569.ch

[58] Tran NH. Karina yew-Hoong gin. Occurrence and removal of pharmaceuticals, hormones, personal care products, and endocrine disrupters in a full-scale water reclamation plant. Science of the Total Environment. 2017;**599–600**:1503-1516. DOI: 10.1016/j.scitotenv.2017.05.097

[59] Alvarino T, Suarez S, Lema J, Omil F. Understanding the sorption and biotransformation of organic micropollutants in innovative biological wastewater treatment technologies. Science of the Total Environment. 2018;**615**:297-306. https://doi.org/10.1016/j.scitotenv.2017.09.278

[60] Hai FI, Yamamoto K, Nakajima F, Fukushi K. Recalcitrant industrial wastewater treatment by membrane bioreactor (MBR). In: Gorley S, editor. Handbook of Membrane Research: Properties, Performance and Applications. New York: Nova Science Publishers; 2010 pp. 67-104. http://dx.doi.org/10.1002/chin.201133280

[61] Kim SD, Cho J, Kim IS, Vanderford BJ, Snyder SA. Occurrence and removal of pharmaceuticals and endocrine disruptors in south Korean surface, drinking, and waste waters. Water Research. 2007;**41**:1013-1021. http://dx.doi.org/10.1016/j. watres.2006.06.034

[62] Boonstra S. Behaviour of Pharmaceutically Active Compounds in Contact with Reactive Media in Simulated Ground Water. Ontario, Canada: A thesis presented to the University of Waterloo in fulfillment of the thesis requirement for the degree of Master of Science in Earth Sciences Waterloo; 2008

[63] Park J, Yamashita N, Park C, Shimono T, Takeuchi DM, Tanaka H. Removal characteristics of pharmaceuticals and personal care products: Comparison between membrane bioreactor and various biological treatment processes. Chemosphere. 2017;**179**:347-358. DOI: 10.1016/j.chemosphere.2017.03.135

[64] Verlicchi P, Galletti A, Petrovic M, Barcelo D. Hospital effluents as a source of emerging pollutants: An overview of micropollutants and sustainable treatment options. Journal of Hydrology. 2010;**389**:416-428 https://doi.org/10.1016/j.jhydrol.2010.06.005

[65] Chon K, KyongShon H, Cho J. Membrane bioreactor and nanofiltration hybrid system for reclamation of municipal wastewater: Removal of nutrients, organic matter and micropollutants. Bioresource Technology. 2012;**122**:181-188. DOI: 10.1016/j.biortech.2012.04.048

[66] González-Pérez DM, Pérez JI, Gómez MA. Behaviour of the main nonsteroidal anti-inflammatory drugs in a membrane bioreactor treating urban wastewater at high hydraulic-and sludge-retention time. Journal of Hazardous Materials. 2017;**336**:128-138. DOI: 10.1016/j.jhazmat.2017.04.059

[67] Komesli OT, Muz M, Ak MS, Bakırdere S, Gökçay CF. Comparison of EDCs removal in full and pilot scale membrane bioreactor plants: Effect of flux rate on EDCs removel in short SRT. Journal of Environmental Management. 2017;**203**:847-852. DOI: 10.1016/j. jenvman.2016.06.004

[68] Alvarino T, Torregrosa N, Omil F, Lema JM, Suarez S. Assessing the feasibility of two hybrid MBR systems using PAC for removing macro and micropollutants. Journal of Environmental Management. 2017;**203**:831-837. DOI: 10.1016/j.jenvman.2016.03.023

[69] Alvarino T, Suárez S, Garrido M, Lema JM, Omil F. A UASB reactor coupled to a hybrid aerobic MBR as innovative plant configuration to enhance the removel of organic micropollutants. Chemosphere. 2016;**144**:452-458. DOI: 10.1016/j.chemosphere.2015.09.016

[70] Kovalova L, Siegrist H, Singer H, Wittmer A, McArdell CS. Hospital wastewater treatment by membrane bioreactor: Performance and efficiency fo organic micropollutant elimination. Environmental Science & Technology. 2012;**46**:1536-1545. DOI: 10.1021/es203495d

[71] Trinh T, van den Akker B, Stuetz RM, Coleman HM, Le-Clech P, Khan SJ. Removal of trace organic chemical contaminants by a membrane bioreactor. Water Science and Technology 2012;**66**:1856-1863. DOI: 10.2166/wst.2012.374

[72] Tadkaew N, Hai FI, McDonald JA, Khan SJ, Nghiem LD. Removal of trace organics by MBR treatment: The role of molecular properties. Water Research. 2011;**45**:2439-2451. https://doi.org/10.1016/j.watres.2011.01.023

[73] Beier S, Cramer C, Koster S, Mauer C, Palmowski L, Schroder H. Full scale membrane bioreactor treatment of hospital wastewater as forerunner for hot-spot wastewater treatment solutions in high density urban areas. Water Science and Technology. 2011;**63**:66-71. DOI: 10.2166/wst.2011.010

[74] Arola K, Hatakka H, Mänttäri M, Kallioinen M. Novel Process Concept Alternatives for Improved Removal of Micropollutants in Wastewater Treatment. Separation and Purification Technology. 2017;**186**:333-341. DOI: 10.1016/j.seppur.2017.06.019

[75] Prasertkulsak S, Chiemchaisri C, Chiemchaisri W, Itonaga T. Yamamoto. Removals of pharmaceutical compounds from hospital wastewater in membrane bioreactor operated under short hydraulic retention time. Chemosphere. 2016;**150**:624-631. http://dx.doi.org/10.1016/j.chemosphere.2016.01.031

[76] Navaratna D, Elliman J, Cooper A, Shu L, Baskaran K, Jegatheesan V. Impact of herbicide Ametryn on microbial communities in mixed liquor of a membrane bioreactor (MBR). Bioresource Technology 2012;**113**:181-190. https://doi.org/10.1016/j.biortech.2011.12.018

[77] Phan HV, Hai FI, McDonald JA, Khan SJ, Zhang R, Price WE, Broeckmann A, Nghiem LD. Nutrient and trace organic contaminant removal from wastewater of a resort town: Comparison between a pilot and a full scale membrane bioreactor, International Biodeterioration and Biodegradation 2015;**102**:40-48. http://dx. doi.org/10.1016/j.ibiod.2015.02.010

[78] Grandclement C, Seyssiecq I. Piram, Anne, Wong-Wah-Chung P, Vanot G, Tiliacos N, Roche N, Doumenq P. From the conventional biological wastewater treatment to hybrid processes, the evaluation of organic micropollutant removal: A review. Water Research. 2017;**111**:297-317 http://dx.doi.org/10.1016/j.watres.2017.01.005

[79] Shahbeig H, Mehrnia MR, Mohammadi AR, Moghaddam PE, Rouin MR. Pharmaceutical Wastewater Treatment Using Membrane Bioreactor-Ozonation System. Water and Environment Journal. 2017. Print; ISSN 1747–6585. DOI:10.1111/wej.12222

[80] Zhang Q, Jie YW, Loong WLC, Zhang J, Fane AG, Kjelleberg S, Rice SA, McDougald D. Characterization of biofouling in a lab-scale forward osmosis membrane bioreactor (FOMBR). Water Research. 2014;**58**:141-151. https://doi.org/10.1016/j.watres.2014.03.052

[81] Phattaranawik J, Fane AG, Pasquier ACS, Bing W, Wong FS. Experimental study and design of a submerged membrane distillation bioreactor. Chemical Engineering and Technology. 2009;**32**:38-44. DOI: 10.1002/ceat.200800498

[82] Smith AL, Stadler LB, Love NG, Skerlos SJ, Raskin L. Perspectives on anaerobic rmembrane bioreactor treatment of domestic wastewater: A critica review. Bioresource Technology. 2012;**122**:149-159. DOI: 10.1016/j.biortech.2012.04.055

[83] Subtil EI, Mierzwa JC, Hespanhol I. Comparison between a conventional membrane bioreactor (C-MBR) and a biofilm membrane bioreactor (BF-MBR) for domestic wastewater treatment. Brazilian Journal of Chemical Engineering. 2014;**31**:683-691. https://dx.doi.org/10.1590/0104-6632.20140313s00002890

[84] Zhao X, Chen ZL, Wang XC, Shen JM, Xu H. PPCPs removal by aerobic granular sludge membrane bioreactor. Applied Microbiology and Biotechnology. 2014;**98**(23):9843-9848 https://doi.org/10.1007/s00253-014-5923-0

Chapter 4

Applications of Combined Electrocoagulation and Electrooxidation Treatment to Industrial Wastewaters

Baran Özyurt and Şule Camcıoğlu

Additional information is available at the end of the chapter

http://dx.doi.org/10.5772/intechopen.75460

Abstract

In recent years, it is aimed to reuse wastewater to form an economical input and to manage it sustainably without threatening human life and ecosystem. High pollutant removal yield from wastewaters was achieved using electrocoagulation method without adding any chemical coagulant or flocculants, thus reducing the amount of sludge. However, electrocoagulation (EC) is an inefficient method for the removal of stable and dissolved organic pollutants. Electrooxidation (EOx), which was evaluated as one of the most promising technologies for the treatment of wastewater containing soluble organic compounds, can directly and indirectly oxidize small organic pollutants. Although electrooxidation provides full mineralization of the organic matter, if suspended solids are present, energy consumption is increased. Since EC is a fast but incomplete process and EOx is a complete but slow process, combining the two processes offers a practical hybrid. In this chapter, mechanisms and applications of EC, EOx, and their combinations will be widely discussed.

Keywords: wastewater treatment, electrocoagulation, electrooxidation, combined, simultaneous, sequential, hybrid, integrated

1. Introduction

Water pollution seriously affects the ecosystems and availability of healthy freshwater [1]. The preservation of water resources is one of the most important issues of the twenty-first century [2]. Nowadays, sources of safe drinking water are limited and under stress [3]. The main problems encountered are population growth, rapid decline of forest areas, urbanization, climate change due to global warming, and industrialization [1]. Large amounts of raw water were consumed by industrial processes for various purposes [4]. Consequently, wastewater is

produced in large quantities [4]. Wastewaters are composed of a complex mixture of different organic and inorganic compounds, which may be toxic and difficult to degrade [4]. The most common inorganic water pollutants are heavy metals, nitrates, sulfates, phosphates, fluorides, and chlorides, which have serious hazardous effects [3]. The organic pollutants found in wastewaters may be generalized as insecticides, herbicides, fungicides, polycyclic aromatic hydrocarbons, phenols, biphenyls, halogenated aromatic hydrocarbons, formaldehyde, detergents, oils, greases, normal hydrocarbons, alcohols, aldehydes, ketones, proteins, lignin, and pharmaceuticals [3]. These pollutants remain either in dissolved, in colloidal, or in suspended form [3]. Mostly, wastewater treatment is carried out by conventional wastewater treatment processes [5]. Conventional wastewater treatment technologies could be categorized as physical processes including screening, flotation, filtration, and sedimentation [6]; chemical processes such as coagulation/flocculation, chlorination, adsorption, and ion exchange [6]; biological processes, i.e., activated sludge, aerated lagoons, and membrane bioreactors [2].

However, it is difficult to degrade the complex refractory organic pollutants in the wastewater by biological methods [7, 8]. In addition, physical–chemical methods are not always effective due to formation of additional pollution caused by the unreacted chemicals and difficulties of treatment of large amount of toxic sludge produced during conventional wastewater treatment [3–5, 9, 10]. With the strict environmental regulations on wastewater discharge, there is a need to develop efficient technologies and approaches at large scale for the treatment and management of industrial wastewater so that clean water quality can be maintained and amount increased while environmental protection and sustainability are achieved [1–5, 8, 11–13]. There has been an increasing interest in the use of electrochemical wastewater treatment technologies, such as electrodeposition [14], electrodisinfection [15], electro-Fenton [16], electrosorption [17], EOx [4] and EC [1] and their sequential [8, 18], and simultaneous [19, 20] combinations for the treatment of industrial wastewaters in recent years.

The foundations of electrochemical water treatment were laid in 1889 [11]. Electrocoagulation for drinking water was first carried out by Fred E. Stuart in 1946 [11, 21]. With the increasing interest in the second half of the twentieth century, many investigations were made on the topic [11]. Among others, EC and EOx methods are the electrochemical technologies that researchers are most interested in regarding water and wastewater treatment [2, 5, 11]. EC is based on the principle that coagulant species including hydroxide precipitates are produced in situ by electrolytic oxidation of the sacrificial anodic material, which is dissolved as ions by electric current applied through metal electrodes such as aluminum and iron [1, 22]. Thus, the EC method is more advantageous than the coagulation/flocculation method in which metal salts and polyelectrolytes are used as coagulants/flocculants in terms of sludge formation [23, 24]. EC aims to remove particles from the wastewater by destabilizing/neutralizing the repulsive forces that keep the particles suspended in the water [2]. When the repulsive forces are neutralized, suspended particles can be separated more easily from water by forming larger particles that can precipitate [2]. EC also provides the removal of pollutants by simultaneous cathodic reactions, either by deposition on the cathode or by flotation based on the formation of hydrogen gas at the cathode [1]. In recent years, EC was reported as an easy-to-operate, efficient, and economical method. Strengths of EC method can be summarized as follows; it requires simple equipment and operating conditions and does not require additional chemicals; treated water is

http://dx.doi.org/10.5772/intechopen.75460

colorless, odorless, and clear; the amount of the sludge formation is low which can be easily stabilized and dehydrated; compared with chemical coagulation, the effluent contains less total dissolved solids; and the gas bubbles produced in the cathode allow the pollutants to be separated easily by floating them to the surface. However, weaknesses of EC method can be listed as follows: sacrificial electrodes need to be replaced regularly, formation of an impermeable film layer on the cathode may reduce the efficiency of the process and it is inefficient for the removal of persistent dissolved organic pollutants.

With regard to the treatment of effluents polluted with organic compounds, biological oxidation is the most economical process, but the presence of toxic or biorefractive molecules may prevent this approach [25]. Despite chemical oxidation using chlorine, ozone or hydrogen peroxide is currently used for the oxidation of biorefractive contaminants to harmless or biodegradable products; in some reactions, the intermediate products remain in the solution and may cause similar or higher toxicity than the initial compounds [25]. EOx can completely degrade many harmful organic pollutants before they reach the receiving environment [4]. EOx is based on in situ production of oxidants either directly at the surface of the electrodes or indirectly from the chemical compounds in the treated water during treatment [4]. EOx may occur either through direct oxidation with hydroxyl radicals produced on the anode surface or indirectly through oxidants such as chlorine, hypochlorous acid, and hypochlorite or hydrogen peroxide/ozone formed at electrodes [13]. The hydroxyl radicals can oxidize substantially all of the organic compounds with an oxidation rate 109 times higher than that of ozone [26]. The oxidation power of chlorine and other anode-formed oxidants remains low compared to the hydroxyl radicals and as a result it does not allow many pollutants to be effectively oxidized to carbon dioxide and water [13]. Electrode material selection is very important because it affects process selectivity and efficiency [12]. Electrode material must have the properties such as resistance to erosion, corrosion and formation of passivation layers, high electrical conductivity, selectivity and catalytic activity, low cost, and durability. Noble metal electrodes; metal alloys electrodes; mixed metal oxide electrodes which are also referred as dimensionally stable anodes (DSAs) such as Ti/Ta_2O_5-IrO_2, Ti/SnO_2-IrO_2, Ti/RuO_2-IrO_2, Ti/Sb-SnO_2, Ti/SnO_2-Sb_2O_5-RuO_2, and Ti/TiO_2-IrO_2; carbon and graphite electrodes; and boron-doped diamond (BDD) electrodes are some examples of the electrode materials used in recent wastewater treatment studies [27]. Strengths of EOx method can be summarized as follows: it requires simple equipment and operating conditions, totally mineralizes persistent organic pollutants, has low electrode maintenance cost, and forms disinfecting compounds. However, EOx method has some weaknesses such as: it is inefficient for the removal of suspended solids, and formation of an impermeable film layer on the cathode may reduce the efficiency of the process.

Since EC is a fast but incomplete process and EOx is a complete but slow process, coupling the two processes offers a practical hybrid [26]. EC has the ability to remove pollutants quickly but not completely. EOx is able to remove pollutants slowly but consistently. Sequential and simultaneous operations are combining the best abilities of EC and EOx processes with fast and complete pollutant removal [26]. This chapter focuses on effects of operating parameters on EC and EOx, pollutant removal mechanisms, and recent applications of these methods and their sequential and simultaneous combinations.

2. Electrocoagulation mechanism and operation

2.1. Mechanism

In the EC process, coagulant species are produced in situ using the electrical dissolution of sacrificial anode, usually made of iron or aluminum by electric current applied between metal electrodes [1]. At the anode, metal is oxidized into cations as shown in Eqs. (1)–(3).

$$Al_{(s)} \rightarrow {Al_{(aq)}}^{3+} + 3e^- \tag{1}$$

$$Fe_{(s)} \rightarrow {Fe_{(aq)}}^{2+} + 2e^- \tag{2}$$

$${Fe_{(aq)}}^{2+} + O_2 + 2H_2O \rightarrow {Fe_{(aq)}}^{3+} + 4OH^- \tag{3}$$

In the case of high anode potential, following reactions may occur as shown in Eqs. (4) and (5).

$$2H_2O \rightarrow O_{2(g)} + 4H^+ + 4e^- \tag{4}$$

$$2Cl^- \rightarrow Cl_{2(g)} + 2e^- \ (in\ the\ presence\ of\ Cl^-\ anions) \tag{5}$$

Chlorine formation may lead to the formation of hypochlorous acid, an oxidizing agent which may contribute to the oxidation of dissolved organic compounds as shown in Eq. (6) [1].

$$Cl_{2(g)} + H_2O \rightarrow HClO + H^+ + Cl^- \tag{6}$$

At the cathode, hydrogen gas and hydroxyl anions are formed by the reduction of water as shown in Eq.(7).

$$2H_2O + 2e^- \rightarrow H_{2(g)} + 2OH^- \ (at\ alkaline\ conditions) \tag{7}$$

The amount of dissolved metal at the anode can be calculated using Faraday's law as shown in Eq. (8).

$$m = \frac{ItM}{zF} \tag{8}$$

where m is the mass of metal in g, t is the electrolysis time in s, I is the electric current in A, M is the atomic weight of the electrode material in g/mole, z is the number of electrons transferred, and F is Faraday's constant (96486 C/mole). The most common phenomenon for metal cations released from the anode is the formation of non-soluble and easily precipitable metal hydroxide sweep flocs which have large surface areas beneficial for a rapid adsorption of soluble organic compounds and trapping of colloidal particles as shown in Eqs. (9)–(13) [1].

$${Al_{(aq)}}^{3+} + 3H_2O \rightarrow Al(OH)_3 + 3H^+ \tag{9}$$

$$Al(OH)_3 + H_2O \rightarrow {Al(OH)_4}^- + H^+ \ (at\ pH > 9) \tag{10}$$

$${Fe_{(aq)}}^{2+} + 2OH^- \rightarrow Fe(OH)_2 \tag{11}$$

$$4Fe(OH)_2 + O_2 + H_2O \rightarrow 4Fe(OH)_3 \tag{12}$$

$$Fe(OH)_3 + OH^- \rightarrow \left[Fe(OH)_4\right]^- (at\ pH > 9) \tag{13}$$

Removal mechanisms of various pollutants involve physical removal of dissolved pollutants during precipitation, adsorption, and complexation [1]; electrooxidation [28] or electroreduction [29] of the electro-active ion or molecules on the anode or the cathode; the direct adsorption of pollutants on the electrodes [30]; the compression of the double layer of a colloidal particle [31]; charge neutralization; and colloid entrapment [1].

2.2. Operating parameters

The parameters affecting the effectiveness of the EC process are operating conditions such as the current density, operating time, pH, conductivity, and electrode properties [22]. The bubble density affects system hydrodynamics, which determine the mass transfer between pollutants, coagulant, and gas microbubbles, and determines the collision rate of the coagulated particles resulting in flock formation [1].

The current density determines the coagulant dosage at the anode and the formation of hydrogen gas at the cathode. Unnecessarily high current values may negatively affect the EC efficiency as coagulant overdosage can reverse the charge of the colloids and redistribute them, reducing coagulation efficiency and also reducing electrode lifetime [1].

pH is an important factor affecting EC performance, particularly the coagulation mechanism, since it governs the hydrolyzed metal species formed in electrolyte media [32]. Adsorption and coagulation depend on pH in particular. The superficial charge of Al or Fe precipitates can be explained by the adsorption of charged soluble monomeric species on their own hydroxide precipitates [1]. For Al and Fe electrodes, the amount of insoluble aluminum hydroxide increases sharply with increasing pH from 4.5 to 7 [1]. For a pH above 10, amorphous metal hydroxide is absent. For acidic influent, effluent pH after EC treatment would increase but can decrease for alkaline influent, which is due to the buffering effect of EC [11].

Lower amounts of energy are consumed with decreasing the gap between electrodes. As the distance between electrodes becomes lower, the amount of generated gas bubbles increases, thus leading to a high mass transfer as well as to a high reaction rate between the coagulants and pollutants [1].

Applied potential difference of galvanostatic EC operation depends strongly on conductivity and ionic strength of the wastewater. Applied potential difference decreases with increasing electrolytic conductivity due to the decrease of ohmic resistance of wastewater [1]. Consequently, the energy consumption per unit volume of treated wastewater is reduced as shown in Eq. (14).

$$SEEC\left(kWh/m^3\right) = \frac{IVt}{V_E} \tag{14}$$

where SEEC is the specific electrical energy consumption, I is the electric current in A, V is the applied potential difference in V, t is the electrolysis time in h, and V_E is the volume of treated wastewater in L.

2.3. Applications of electrocoagulation

In this section, recent studies on the application of EC method in the treatment of different wastewaters and pollutants such as chemical oxygen demand (COD), total organic carbon (TOC), total phosphate (TP), phenol, oil and grease (O&G), biochemical oxygen demand (BOD_5), and total suspended solids (TSS) are presented. Ranges and optimum values of operating parameters, pollutant removal efficiencies, energy consumption, and operating cost values of previously published work are given in **Table 1**. It has been reported that EC

Ref.	Wastewater	Electrode material	Parameters	Research ranges for parameters	Optimum conditions	Results at optimum conditions
[33]	Olive mill (real)	Al	Electrolysis time (min)	3–20	15	Color removal: 91% COD removal: 83% Phenol removal: 87% SEEC: 2.63 kWh/kg COD_r Operating cost: 0.27 €/kg COD_r
			Current density (A/m^2)	10–4000	250	
			NaCl concentration (g/L)	0.5–3	2	
			Initial pH	2–10	4.2	
[34]	Textile (synthetic)	Al	Current density (A/m^2)	100–400	300	Turbidity removal: 90% Color removal: 97% SEEC: 19.5 kWh/kg dye removed
			Inlet flow rate (L/h)	15–60	15	
			Initial concentration (mg/L)	50–300	< 300	
			Initial pH	2.3–8.8	7.74	
			Residence time (min)	5–55	35	
[35]	Dairy (real)	Al	Electrolysis time (min)	0–60	30	COD removal: 74.56% BOD_5 removal: 96.28% Turbidity removal: 98.91% SEEC: 3.36 kWh/m^3
			Initial pH	2–12	7	
			Current density (mA/cm^2)	2.5–35	14	
			NaCl concentration (g/L)	0–2	1	
[22]	Pulp and paper (real)	Al or Fe	Electrode material	Al-Fe	Al	COD removal: 65.33% Color removal: 100% Turbidity removal: 98.61% TSS removal: 97.06% SEEC: 8.82 kWh/kg COD
			Electrical conductivity (mS/cm)	2.3–4.2	2.72	
			pH	3–12	5.82	
			Temperature (°C)	10–50	22.62	
			Electrolysis time (min)	5–45	10.83	
			Current intensity (A)	0.5–1.8	1.22	

Ref.	Wastewater	Electrode material	Parameters	Research ranges for parameters	Optimum conditions	Results at optimum conditions
[36]	Car wash (real)	Al or Fe	Electrode material	Al-Fe	Fe	COD removal: 88% O&G removal: 90% Cl^- removal: 50% Operating cost: 0.6 \$/m^3 Sludge: 2.1 kg/ m^3
			pH	2–10	8	
			Current density (mA/cm^2)	0.1–5	3	
			Operating time (min)	5–50	30	
[37]	Industrial estate (real)	Fe	Current density (mA/cm^2)	10–50	30	COD removal: 62.5% SEEC: 42.44 kWh/m^3 Energy cost: 1.91 €/m^3 Sludge: 1.91 g/g COD
			Na_2SO_4 concentration (mM)	1–7	3	
			Initial pH	3.12–8.83	6	

Table 1. EC treatment results of various wastewaters for selected examples in the literature.

treatment is an effective method in removing organic matter, turbidity, color, phenol, phosphate, heavy metals, pharmaceuticals, O&G from wastewater.

3. Electrooxidation mechanism and operation

3.1. Mechanism

EOx may occur either by direct oxidation of pollutants using hydroxyl or hydroperoxyl radicals produced on anode surface or by an indirect process where oxidants like chlorine, hypochlorous acid, and hypochlorite or hydrogen peroxide/ozone are formed at electrodes. Direct anodic oxidation of pollutants and formation of indirect oxidizing agents occur according to the reactions given in Eqs. (15)–(24) [26, 38, 39].

$$H_2O + S \rightarrow S[OH]^{\bullet} + H^+ + e^- \tag{15}$$

$$R + S[OH]^{\bullet} \rightarrow S + RO + H^+ + e^- \tag{16}$$

$$H_2O + S + Cl^- \rightarrow S[ClOH]^{\bullet} + H^+ + 2e^- \tag{17}$$

$$R + S[ClOH]^{\bullet} \rightarrow S + RO + H^+ + Cl^- \tag{18}$$

$$H_2O + S[OH]^{\bullet} \rightarrow S + O_2 + 3H^+ + 3e^- \tag{19}$$

$$H_2O + S[OH]^{\bullet} \rightarrow S + H_2O_2 + H^+ + e^- \tag{20}$$

$$S[OH]^{\bullet} + H_2O_2 \rightarrow S + HO_2^{\bullet} + H_2O \tag{21}$$

$$O_2 + S[OH]^{\bullet} \rightarrow S + O_3 + H^+ + e^- \tag{22}$$

$$H_2O + S[ClOH]^{\bullet} + Cl^- \rightarrow Cl_2 + S + O_2 + 3H^+ + 4e^- \tag{23}$$

$$H_2O + S[ClOH]^{\bullet} + Cl_2 \rightarrow S + ClO_2 + 3H^+ + 2Cl^- + e^- \tag{24}$$

Indirect oxidation of pollutants occurs according to the reactions given in Eqs. (25)–(29) [26].

$$2Cl^- \rightarrow Cl_{2(g)} + 2e^- \tag{25}$$

$$Cl_2 + H_2O \rightleftarrows HClO + H^+ + Cl^- \tag{26}$$

$$HClO \rightleftarrows H^+ + ClO^- \tag{27}$$

$$H_2O + R + ClO^- + H^+ \rightarrow RO + H_3O^+ + Cl^- \tag{28}$$

$$6ClO^- + 3H_2O \rightarrow 2ClO_3^- + 4Cl^- + 6H^+ + \frac{3}{2}O_2 + 6e^- \tag{29}$$

Chlorate is usually an unwanted product in the effluent, and its formation could also prevent the use of EOx in various applications [25]. At the cathode, hydrogen gas and chloride anions are formed as shown in Eqs. (30)–(32).

$$2H_3O^+ + 2e^- \rightarrow H_2 + 2H_2O(at\ acidic\ conditions) \tag{30}$$

$$2H_2O + 2e^- \rightarrow H_2 + 2OH^-(at\ alkaline\ conditions) \tag{31}$$

$$ClO^- + H_2O + 2e^- \rightarrow Cl^- + 2OH^- \tag{32}$$

Here S symbolizes the active sites of the anode surface, and R represents the organic matter. To evaluate the selectivity of an anode material, competition between the oxidation of organic materials and the oxygen formation (the side reaction) at the anode (Eq. (4)) must be taken into account [12]. Oxygen formation is typically considered to be an undesirable side reaction in the electrochemical wastewater treatment because it affects the efficiency of the process and significantly increases the operating costs [25].

Removal mechanisms of various pollutants involve diffusion of pollutants from the bulk solution to the anode surface and direct oxidation at the anode surface either partially or completely [12] and generation of a strong oxidizing agent (i.e., chlorine) at the anode surface and indirect oxidation of pollutants in the bulk solution.

3.2. Operating parameters

Among the variables that are usually studied in EOx treatment, the current density is one of the most frequently referenced terms since it affects the rate of reactions [12]. It should be noted that an increase in current density will not necessarily result in an increase in oxidation efficiency or oxidation rate [12]. The use of higher current densities usually leads to higher operating costs due to the increase in energy consumption.

It should be noted that although there is no agreement on the effect of the conductivity on the overall oxidation efficiency, the cell voltage is reduced for a given current density as the conductivity of the electrolyte increases [12]. For this reason, the electrochemical oxidation process is more cost-effective if the treated wastewater already has a high conductivity [12].

When reactions are carried out in chloride-containing media, the pH value may affect the rate of oxidation because it determines the primary active chloro species present in the effluent [12]. During indirect oxidation, chlorine evolution occurs at the anode (Eq. (25)). At pH values lower than 3.3, the primary active chloro species is Cl_2, while at higher pH values, it forms HClO at pH <7.5 (Eq. (26)) and ClO^- at pH >7.5 (Eq. (27)). Operation at strongly acidic conditions is favorable since chlorine is the strongest oxidant followed by HClO and ClO^-, respectively [12]. Depending on the electrolytic cell design, desorption of chlorine from reaction medium may prevent its action as an oxidizing agent. Thus, neutral or mildly alkali medium may be preferred since HClO and ClO^- species remain almost unaffected by desorption of gases and they can act as oxidizing reagents in the whole volume of wastewater [40].

3.3. Applications of electrooxidation

This section briefly describes the treatment of different wastewater types by EOx method in the last few years. **Table 2** shows a general insight on minimum, maximum, and optimum values of operating parameters, pollutant reduction, energy consumption, and operating cost of EOx

Ref.	Wastewater	Electrode material	Parameters	Research ranges for parameters	Optimum conditions	Results at optimum conditions
[41]	Pulp and paper industry (real)	Anode: Catalytic oxide coated titanium Cathode: Stainless steel	Current density (A/dm^2)	2.5–5	2.5	COD removal: 67.99% SEEC: 37.67 kWh/kg COD
			NaCl concentration (g/L)	1–5	3	
[42]	Textile (real)	Graphite	Initial pH	4–10	4	COD removal: 90.78% Color removal: 96.27% SEEC: 23.58 kWh/kg COD
			Current density (A/m^2)	27.78–138.89	27.78	
			NaCl concentration (g/L)	0–2	2	
			Electrolysis time (min)	10–130	110	
[43]	Olive mill (real)	Anode: Ti/Pt mesh Cathode: Ti mesh	Electrolysis time (h)	1–24	5	COD removal: 100% TOC removal: 78% Phenol removal: 100% SEEC: 451.25 kWh/m^3 Energy cost: 6.02 $/kg COD
			Mixing rate (rpm)	0–600	0	
			Dilution ratio	1/5–5/5	1/5	
			pH	2–8	4.5–4.7	
			Type of support electrolyte	Na_2SO_4, KCl, NaCl	NaCl	
			Concentration of support electrolyte (mM)	0.25–1.25	0.25	
			Current density (mA/cm^2)	2.5–15	7.69	
			Temperature (°C)	10–50	10	

Ref.	Wastewater	Electrode material	Parameters	Research ranges for parameters	Optimum conditions	Results at optimum conditions
[44]	Pharmaceutical (synthetic)	Anode: BDD Cathode: Stainless steel	Current density (mA/cm^2)	1.56–6.25	6.25	TOC removal: 80% SEEC: 2.34 kWh/g TOC
[45]	Industrial park sewage (real)	Anode: Mesh-structure plate Cathode: Mesh-structure Ti plate	Anode material	Ti/PbO_2, Ti/RuO_2, Ti/RuO_2-IrO_2	Ti/PbO_2	COD: 60 mg/L Color: 20 CU SEEC: 4.12 kWh/ton Operating cost: 0.57 $/ton
			Current density (mA/cm^2)	2–15	5	

Table 2. EOx treatment results of various wastewaters for selected examples in the literature.

treatment. By evaluating the previously published studies, it has been concluded that EOx is a remarkable treatment method in terms of organic matter, turbidity, color, phenol, total Kjeldahl nitrogen (TKN), and O&G removal efficiencies.

4. Combined electrocoagulation and electrooxidation mechanism and applications

4.1. Mechanism

As stated in Section 1, EC is a fast but incomplete process, while EOx is a complete but slow process; coupling the two processes proposes a functional hybrid. COD removal mechanism of a combined EC and EOx process can be summarized as follows: production of metal ions; hydrolysis of metal ions to generate metal hydroxides and/or polyhydroxides in appropriate pH; generation of bubbles of oxygen and hydrogen gases at the anode and the cathode, respectively, which provides the flotation of coagulated pollutants; destabilization of colloidal pollutants and trapping of destabilized colloidal particles to form flocks; removal of pollutants by precipitation [46]; formation of adsorbed hydroxyl radicals on anode surface [39]; degradation of organic pollutants by direct oxidation of adsorbed hydroxyl radicals; generation of indirect oxidizing agents such as chlorine, hypochlorite, and hydrogen peroxide near the anode; and electrochemical combustion of organic pollutants by indirect oxidizing agents [26].

4.2. Applications of combined electrocoagulation and electrooxidation

In the recent years, application of combined treatment has been successfully achieved in the removal of different kinds of pollutants either by sequential EOx treatment of the electrocoagulated

Ref.	Wastewater	Electrode material	Parameters	Research ranges for parameters	Optimum conditions	Results at optimum conditions
[48]	Dairy (synthetic)	Anode: Al Cathode: Ti/Pt	Current density (A/m^2)	0–75	50	COD removal: 54.16% TP removal: 42.9% Turbidity removal: 37%
			Electrolysis time (min)	0–5	2	
			Initial pH	4–11	6.6	
			NaCl concentration (g/L)	0–2	1.5	
[49]	Anaerobic reactor effluent (real)	Anode: MP RuO_2/Ti Cathode: MP stainless steel Sacrificial electrode: BP Al	pH	5–10	7	Ammonia removal: 98% TP removal: 98% COD removal: 72%
			Current intensity (A)	1–3	3	
			Detention time (min)	10–60	60	
[50]	Pharmaceutical (synthetic)	Anode: MP stainless steel Cathode: MP stainless steel	pH	4.5–10.9	10.9	Diclofenac sodium removal: 84% COD removal: 80%
[20]	Olive mill (real)	Anode: RuO_2/Ti Cathode: Stainless steel Sacrificial electrodes: BP Al	pH	3–9	4	COD removal: 96% BOD_5 removal: 93.6% Phenol removal: 94.4% Color removal: 91.4% Turbidity removal: 88.7% TSS removal: 97% O&G removal: 97.1% BOD_5/COD: 0.46
			Current density (mA/cm^2)	5–40	40	
			NaCl concentration (g/L)	0.5–3	1	
			H_2O_2 concentration (mg/L)	0–2000	1000	
			Detention time (min)	5–30	30	
[19]	Textile (real)	Anode: MP Ti/IrO_2 Cathode: MP Ti Sacrificial electrode: BP Al or Fe	Sacrificial electrode material	Al-Fe	Al	COD removal: 93.5% TSS removal: 97% Color removal: 97.5% BOD_5 removal: 90% Turbidity removal: 96% Phenol removal: 99% TP removal: 97% Operating cost: 1.69 US $/$m^3$
			Electrolysis time (min)	20–90	90	
			Current intensity (A)	0.2–1	0.6	
			pH	5–10	6	
			Interelectrode distance (cm)	0.5–1.5	1	
			Stirring speed (rpm)	250–750	500	

Ref.	Wastewater	Electrode material	Parameters	Research ranges for parameters	Optimum conditions	Results at optimum conditions
[26]	Pulp and paper mill (real)	Anode: MP graphite Cathode: MP graphite Sacrificial electrode: BP Al or Fe	Electrode material	Al-Fe	Al	COD removal: 87% Color removal: 100% Turbidity removal: 100% SEEC: 31.6 kWh/kg COD Operating cost: 1.33 $/m^3
			Initial pH	3–9	6	
			Electrical conductivity (mS/cm)	3–7	5	
			Temperature (°C)	10–30	20	
			Current intensity (A)	0.5–1.5	1	

Table 3. Simultaneous EC-EOx treatment results of various wastewaters for selected examples in the literature.

effluent or simultaneous EC and EOx treatment with an appropriate electrode configuration. The aim of sequential EC-EOx is to propose a new approach that combines the synergistic effects of the two methods [47]. Simultaneous EC-EOx offers a hybrid system integrating monopolar (MP) EOx and bipolar (BP) EC in a single reactor that also provides all the advantages of sequential EC-EOx [19]. Recent studies on combined EC-EOx treatment of different kinds of wastewater are presented in **Tables 3** and **4**.

Ref.	Wastewater	Electrode material	Parameters	Optimum conditions	Results at optimum conditions
[18]	Textile (synthetic)	EC: Al	Current density (mA/cm^2)	30	COD removal: ~94% SEEC: 0.02 kWh/g
			Treatment time (min)	5	
		EOx: Graphite	Current density (mA/cm^2)	0.91	
			Treatment time (min)	425	
[8]	Industrial park (real)	EC: Fe	pH	8	Color removal: 100% Turbidity removal: 100% COD removal: 100% BOD_5 removal: 100%
			Current density (A/m^2)	800	
			Treatment time (min)	30	
		EOx: Anode: BDD Cathode: Fe	pH	8	
			Current density (A/m^2)	800	
			Treatment time (min)	150	
[51]	Car wash (real)	EC: Anode: Fe Cathode: Stainless steel	Electrolysis time (min)	6	COD removal: > 97% SEEC: 12 kWh/m^3
			Current density (mA/cm^2)	2	
		EOx: Anode: BDD Cathode: Stainless steel	Electrolysis time (min)	90	
			Current density (mA/cm^2)	10	
[47]			Current density (A/dm^2)	0.6	

Ref.	Wastewater	Electrode material	Parameters	Optimum conditions	Results at optimum conditions
	Dairy (real)	EC: Al			Turbidity removal: 100% Color removal: 90.4% COD removal: 66.4%
			Operating time (min)	6	
		EOx: platinized titanium	Current density (A/dm^2)	1.4	
			Operating time (min)	15	
[52]	Cardboard (real)	EC: Al	Current density (mA/cm^2)	7.5	Turbidity removal: 98.7% TOC removal: 86.4% COD removal: 85.3%
			Operating time (min)	60	
			Initial pH	7	
		EOx: Anode: BDD Cathode: Stainless steel	Current density (mA/cm^2)	100	
			Operating time (min)	180	
			Initial pH	7.2	
			Na_2SO_4 concentration (g/L)	5	
[53]	Soft drink (real)	EC: Copper	Current density (mA/cm^2)	51	COD removal: 85% TOC removal: 75% TP removal: 89% Total nitrogen: 84% Color removal: 100%
			Initial pH	8	
			Time (min)	20	
		EOx: Anode: Niobium substrate BDD Cathode: Copper	Current density (A/m^2)	30	
			pH	6	
			Time (h)	6	
[54]	Soluble coffee industrial plant (real)	EC: Anode: Al Cathode: Graphite	Current density (A/m^2)	149.2	Color removal: 100% COD removal: 89% TOC removal: 72% SEEC: 45.28 kWh/m^3 BOD_5/COD: 0.6
			Initial pH	7.98	
			Treatment time (min)	62	
		EOx: Anode: Graphite Cathode: Al	Current density (A/m^2)	500	
			Treatment time (min)	53	

Table 4. Sequential EC-EOx treatment results of various wastewaters for selected examples in the literature.

5. Conclusion

Due to the increasing need for freshwater resources and the large number of pollutants produced by the industries, it becomes more and more important to treat and reuse wastewater. For this purpose, effective, economical, and easy-to-operate wastewater treatment technologies need to be developed. Because of the fact that electrochemical treatment methods have various

advantages, they are still investigated extensively. Besides being simple and effective, they are able to remove almost all kinds of pollutants at the same time. They are also eco-friendly and clean due to in situ generation of metal hydroxides and hydroxyl radicals. Many EC and EOx studies have been published on the treatment of industrial wastewaters such as olive mill, textile, dairy, pulp and paper, tannery, pharmaceutical, bilge, refinery, slaughterhouse, food processing, potato chips manufacturing, and leather. It is reported that EC and EOx methods have been successfully applied for removing COD, BOD, oil, phenol, lignin, phosphate, arsenic, color, turbidity, chromium, sulfate, total coliforms, boron, nickel, copper, and pharmaceuticals from wastewaters. Recent studies were briefly presented in this chapter, and it is observed that a minimum of 54.16% COD, 90.4% color, 90% BOD, 37% turbidity, 94.4% phenol, 42.9% phosphate, 72% TOC, and 97% TSS removal efficiencies and a maximum of 45.28 kWh/m^3 SEEC were achieved by applying combined treatment. Since EC is a fast and efficient method for wastewaters containing suspended solids but also an inefficient method for the removal of persistent dissolved organic pollutants and EOx is able to mineralize persistent organic pollutants completely but also a slow and energy-consuming method for the removal of suspended solids, combining these two processes offers a practical hybrid by taking advantage of the synergistic effects. According to the results, it can be concluded that combined EC-EOx process is an efficient alternative for industrial wastewater treatment in terms of pollutant removal and more research on applications to the industrial wastewaters are required.

Acknowledgements

This research was supported by Ankara University Scientific Research Projects Coordination Unit [grant numbers 16B0443001 and 14 L0443005].

Author details

Baran Özyurt and Şule Camcıoğlu*

*Address all correspondence to: camcioglu@eng.ankara.edu.tr

Faculty of Engineering, Department of Chemical Engineering, Ankara University, Tandogan, Ankara, Turkey

References

[1] Hakizimana JN, Gourich B, Chafi M, Stiriba Y, Vial C, Drogui P, Naja J. Electrocoagulation process in water treatment: A review of electrocoagulation modeling approaches. Desalination. 2017;**404**:1-21. DOI: 10.1016/j.desal.2016.10.011

[2] Moussa DT, El-Naas MH, Nasser M, Al-Marri MJ. A comprehensive review of electrocoagulation for water treatment: Potentials and challenges. Journal of Environmental Management. 2017;**186**:24-41. DOI: 10.1016/j.jenvman.2016.10.032

[3] Gupta VK, Ali I, Saleh TA, Nayak A, Agarwal S. Chemical treatment technologies for waste-water recycling—An overview. RSC Advances. 2012;**2**(16):6380-6388. DOI: 10.1039/C2RA20340E

[4] Särkkä H, Bhatnagar A, Sillanpää M. Recent developments of electro-oxidation in water treatment—A review. Journal of Electroanalytical Chemistry. 2015;**754**:46-56. DOI: 10.1016/j.jelechem.2015.06.016

[5] Zheng T, Wang J, Wang Q, Meng H, Wang L. Research trends in electrochemical technology for water and wastewater treatment. Applied Water Science. 2017;**7**(1):13-30. DOI: 10.1007/s13201-015-0280-4

[6] Camcioglu S, Ozyurt B, Zeybek Z, Hapoglu H. Experimental application of one step ahead advanced pH control to water-based paint wastewater treatment. Journal of the Faculty of Engineering and Architecture of Gazi University. 2016;**31**(3):656-665. DOI: 10.17341/gummfd.52934

[7] Camcioglu S, Ozyurt B, Hapoglu H. MIMO control application for pulp and paper mill wastewater treatment by electrocoagulation. Desalination and Water Treatment. 2017;**93**: 200-213. DOI: 10.5004/dwt.2017.21065

[8] Linares-Hernández I, Barrera-Díaz C, Bilyeu B, Juárez-GarcíaRojas P, Campos-Medina E. A combined electrocoagulation–electrooxidation treatment for industrial wastewater. Journal of Hazardous Materials. 2010;**175**(1):688-694. DOI: 10.1016/j.jhazmat.2009.10.064

[9] Afzal A, Pourrezaei P, Ding N, Moustafa A, Hwang G, Drzewicz P, Kim E, Perez-Estrada LA, Ayala PC, Liu Y, El-Din MG. Physico-chemical processes. Water Environment Research. 2011;**83**(10):994-1091. DOI: 10.2175/106143011X13075599869173

[10] Camcıoğlu Ş, Özyurt B, Doğan İC, Hapoğlu H. Application of response surface methodology as a new PID tuning method in an electrocoagulation process control case. Water Science and Technology. 2017;**76**(12):3410-3427. DOI: 10.2166/wst.2017.506

[11] Chen G. Electrochemical technologies in wastewater treatment. Separation and Purification Technology. 2004;**38**(1):11-41. DOI: 10.1016/j.seppur.2003.10.006

[12] Anglada A, Urtiaga A, Ortiz I. Contributions of electrochemical oxidation to waste-water treatment: Fundamentals and review of applications. Journal of Chemical Technology and Biotechnology. 2009;**84**(12):1747-1755. DOI: 10.1002/jctb.2214

[13] Oturan MA, Aaron JJ. Advanced oxidation processes in water/wastewater treatment: Principles and applications. A review. Critical Reviews in Environmental Science and Technology. 2014;**44**(23):2577-2641. DOI: 10.1080/10643389.2013.829765

[14] Tonini GA, Ruotolo LAM. Heavy metal removal from simulated wastewater using electrochemical technology: Optimization of copper electrodeposition in a membraneless fluidized bed electrode. Clean Technologies and Environmental Policy. 2017;**19**(2):403-415. DOI: 10.1007/s10098-016-1226-8

[15] Ghernaout D, Ghernaout B. From chemical disinfection to electrodisinfection: The obligatory itinerary? Desalination and Water Treatment. 2010;**16**(1–3):156-175. DOI: 10.5004/dwt.2010.1085

[16] Nidheesh PV, Gandhimathi R. Removal of Rhodamine B from aqueous solution using graphite–graphite electro-Fenton system. Desalination and Water Treatment. 2014;**52**(10–12):1872-1877. DOI: 10.1080/19443994.2013.790321

[17] Huang CC, Su YJ. Removal of copper ions from wastewater by adsorption/electrosorption on modified activated carbon cloths. Journal of Hazardous Materials. 2010;**175**(1):477-483. DOI: 10.1016/j.jhazmat.2009.10.030

[18] Raju GB, Karuppiah MT, Latha SS, Parvathy S, Prabhakar S. Treatment of wastewater from synthetic textile industry by electrocoagulation–electrooxidation. Chemical Engineering Journal. 2008;**144**:51-58. DOI: 10.1016/j.cej.2008.01.008

[19] Naje AS, Chelliapan S, Zakaria Z, Abbas SA. Enhancement of an electrocoagulation process for the treatment of textile wastewater under combined electrical connections using titanium plates. International Journal of Electrochemical Science. 2015;**10**(6):4495-4512

[20] Esfandyari Y, Mahdavi Y, Seyedsalehi M, Hoseini M, Safari GH, Ghozikali MG, Kamani H, Jaafari J. Degradation and biodegradability improvement of the olive mill wastewater by peroxi-electrocoagulation/electrooxidation-electroflotation process with bipolar aluminum electrodes. Environmental Science and Pollution Research. 2015;**22**(8):6288-6297. DOI: 10.1007/s11356-014-3832-5

[21] Stuart FE. Electronic water purification progress report on the electronic coagulator—A new device which gives promise of unusually speedy and effective results. Water Sewage. 1946;**84**:24-26

[22] Camcioglu S, Ozyurt B, Hapoglu H. Effect of process control on optimization of pulp and paper mill wastewater treatment by electrocoagulation. Process Safety and Environment Protection. 2017;**111**:300-319. DOI: 10.1016/j.psep.2017.07.014

[23] Kabdaşlı I, Arslan-Alaton I, Ölmez-Hancı T, Tünay O. Electrocoagulation applications for industrial wastewaters: A critical review. Environmental Technology Reviews. 2012;**1**(1):2-45. DOI: 10.1080/21622515.2012.715390

[24] Butler E, Hung YT, Yeh RYL, Suleiman Al Ahmad M. Electrocoagulation in wastewater treatment. Water. 2011;**3**(2):495-525. DOI: 10.3390/w3020495

[25] Sirés I, Brillas E, Oturan MA, Rodrigo MA, Panizza M. Electrochemical advanced oxidation processes: Today and tomorrow. A review. Environmental Science and Pollution Research. 2014;**21**(14):8336-8367. DOI: 10.1007/s11356-014-2783-1

[26] Özyurt B, Camcıoğlu Ş, Hapoglu H. A consecutive electrocoagulation and electrooxidation treatment for pulp and paper mill wastewater. Desalination and Water Treatment. 2017;**93**:214-228. DOI: 10.5004/dwt.2017.21257

[27] Shestakova M, Sillanpää M. Electrode materials used for electrochemical oxidation of organic compounds in wastewater. Reviews in Environmental Science and Bio/Technology. 2017;**16**(2):223-238. DOI: 10.1007/s11157-017-9426-1

[28] Kumar PR, Chaudhari S, Khilar KC, Mahajan SP. Removal of arsenic from water by electrocoagulation. Chemosphere. 2004;**55**(9):1245-1252. DOI: 10.1016/j.chemosphere.2003.12.025

[29] Zongo I, Leclerc JP, Maïga HA, Wéthé J, Lapicque F. Removal of hexavalent chromium from industrial wastewater by electrocoagulation: A comprehensive comparison of aluminium and iron electrodes. Separation and Purification Technology. 2009;**66**(1):159-166. DOI: 10.1016/j.seppur.2008.11.012

[30] Emamjomeh MM, Sivakumar M, Varyani AS. Analysis and the understanding of fluoride removal mechanisms by an electrocoagulation/flotation (ECF) process. Desalination. 2011; **275**(1):102-106. DOI: 10.1016/j.desal.2011.02.032

[31] Harif T, Khai M, Adin A. Electrocoagulation versus chemical coagulation: Coagulation/flocculation mechanisms and resulting floc characteristics. Water Research. 2012;**46**(10): 3177-3188. DOI: 10.1016/j.watres.2012.03.034

[32] Malakootian M, Mansoorian HJ, Moosazadeh M. Performance evaluation of electrocoagulation process using iron-rod electrodes for removing hardness from drinking water. Desalination. 2010;**255**(1):67-71. DOI: 10.1016/j.desal.2010.01.015

[33] Hanafi F, Assobhei O, Mountadar M. Detoxification and discoloration of Moroccan olive mill wastewater by electrocoagulation. Journal of Hazardous Materials. 2010;**174**(1):807-812. DOI: 10.1016/j.jhazmat.2009.09.124

[34] Amour A, Merzouk B, Leclerc JP, Lapicque F. Removal of reactive textile dye from aqueous solutions by electrocoagulation in a continuous cell. Desalination and Water Treatment. 2016;**57**(48–49):22764-22773. DOI: 10.1080/19443994.2015.1106094

[35] Benaissa F, Kermet-Said H, Moulai-Mostefa N. Optimization and kinetic modeling of electrocoagulation treatment of dairy wastewater. Desalination and Water Treatment. 2016;**57**(13):5988-5994. DOI: 10.1080/19443994.2014.985722

[36] Gönder ZB, Balcıoğlu G, Vergili I, Kaya Y. Electrochemical treatment of carwash wastewater using Fe and Al electrode: Techno-economic analysis and sludge characterization. Journal of Environmental Management. 2017;**200**:380-390. DOI: 10.1016/j.jenvman.2017.06.005

[37] Yavuz Y, Ögütveren ÜB. Treatment of industrial estate wastewater by the application of electrocoagulation process using iron electrodes. Journal of Environmental Management. 2018;**207**:151-158. DOI: 10.1016/j.jenvman.2017.11.034

[38] Israilides CJ, Vlyssides AG, Mourafeti VN, Karvouni G. Olive oil wastewater treatment with the use of an electrolysis system. Bioresource Technology. 1997;**61**(2):163-170

[39] Körbahti BK, Artut K. Electrochemical oil/water demulsification and purification of bilge water using Pt/Ir electrodes. Desalination. 2010;**258**(1):219-228. DOI: 10.1016/j.desal.2010.03.008

[40] Canizares P, Paz R, Lobato J, Sáez C, Rodrigo MA. Electrochemical treatment of the effluent of a fine chemical manufacturing plant. Journal of Hazardous Materials. 2006; **138**(1):173-181. DOI: 10.1016/j.jhazmat.2006.05.056

[41] Soloman PA, Basha CA, Velan M, Balasubramanian N. Electrochemical degradation of pulp and paper industry waste-water. Journal of Chemical Technology and Biotechnology. 2009;**84**(9):1303-1313. DOI: 10.1002/jctb.2176

[42] Bhatnagar R, Joshi H, Mall ID, Srivastava VC. Electrochemical oxidation of textile industry wastewater by graphite electrodes. Journal of Environmental Science and Health, Part A. 2014;**49**(8):955-966. DOI: 10.1080/10934529.2014.894320

[43] Kul S, Boncukcuoğlu R, Yilmaz AE, Fil BA. Treatment of olive mill wastewater with electro-oxidation method. Journal of the Electrochemical Society. 2015;**162**(8):G41-G47. DOI: 10.1149/2.0451508jes

[44] García-Montoya MF, Gutiérrez-Granados S, Alatorre-Ordaz A, Galindo R, Ornelas R, Peralta-Hernández JM. Application of electrochemical/BDD process for the treatment wastewater effluents containing pharmaceutical compounds. Journal of Industrial and Engineering Chemistry. 2015;**31**:238-243. DOI: 10.1016/j.jiec.2015.06.030

[45] Zhu R, Yan C, Zhou M, Wang J. Industrial park wastewater deeply treated and reused by a novel electrochemical oxidation reactor. Chemical Engineering Journal. 2015;**260**:427-433. DOI: 10.1016/j.cej.2014.09.029

[46] Camcioglu S, Canan Pekel L, Polat K, Hapoglu H. Experimental design of wastewater treatment with electro-coagulation. Management of Environmental Quality: An International Journal. 2014;**25**(1):86-95. DOI: 10.1108/MEQ-03-2013-0020

[47] Chakchouk I, Elloumi N, Belaid C, Mseddi S, Chaari L, Kallel M. A combined electrocoagulation-electrooxidation treatment for dairy wastewater. Brazilian Journal of Chemical Engineering. 2017;**34**(1):109-117. DOI: 10.1590/0104-6632.20170341s20150040

[48] Bensadok K, El Hanafi N, Lapicque F. Electrochemical treatment of dairy effluent using combined Al and Ti/Pt electrodes system. Desalination 2011;**280**(1):244-251. DOI: 10.1016/j.desal.2011.07.006

[49] Mahvi AH, Ebrahimi SJAD, Mesdaghinia A, Gharibi H, Sowlat MH. Performance evaluation of a continuous bipolar electrocoagulation/electrooxidation–electroflotation (ECEO–EF) reactor designed for simultaneous removal of ammonia and phosphate from wastewater effluent. Journal of Hazardous Materials. 2011;**192**(3):1267-1274. DOI: 10.1016/j.jhazmat.2011.06.041

[50] Ghatak HR. Comparative removal of commercial diclofenac sodium by electro-oxidation on platinum anode and combined electro-oxidation and electrocoagulation on stainless steel anode. Environmental Technology. 2014;**35**(19):2483-2492. DOI: 10.1080/09593330.2014.911357

[51] Panizza M, Cerisola G. Applicability of electrochemical methods to carwash wastewaters for reuse. Part 2: Electrocoagulation and anodic oxidation integrated process. Journal of Electroanalytical Chemistry. 2010;**638**(2):236-240. DOI: 10.1016/j.jelechem.2009.11.003

[52] Gengec E. Treatment of highly toxic cardboard plant wastewater by a combination of electrocoagulation and electrooxidation processes. Ecotoxicology and Environmental Safety. 2017;**145**:184-192. DOI: 10.1016/j.ecoenv.2017.07.032

[53] Linares Hernández I, Barrera Díaz C, Valdés Cerecero M, Almazán Sánchez PT, Castañeda Juárez M, Lugo Lugo V. Soft drink wastewater treatment by electrocoagulation–electrooxidation processes. Environmental Technology. 2017;**38**(4):433-442. DOI: 10.1080/09593330.2016.1196740

[54] Ibarra-Taquez HN, GilPavas E, Blatchley ER, Gómez-García MÁ, Dobrosz-Gómez I. Integrated electrocoagulation-electrooxidation process for the treatment of soluble coffee effluent: Optimization of COD degradation and operation time analysis. Journal of Environmental Management. 2017;**200**:530-538. DOI: 10.1016/j.jenvman.2017.05.095

Chapter 5

Intelligent Modeling Approach to Predict Effluent Quality of Wastewater Treatment Process

Hong-Gui Han, Xiao-Long Wu, Lu Zhang and Jun-Fei Qiao

Additional information is available at the end of the chapter

http://dx.doi.org/10.5772/intechopen.74984

Abstract

Monitoring of effluent quality remains a challenge to the wastewater treatment process (WWTP). In order to provide a reliable tool for the online monitoring of effluent quality, an intelligent modeling approach, which consists of online sensors and an effluent quality predicting plant, is developed to predict effluent quality in this chapter. The intelligent modeling approach, based on a self-organizing fuzzy neural network (SOFNN), is able to enhance the modeling performance by organizing the structure and adjusting the parameters simultaneously. The experimental studies of intelligent modeling approach have been performed on several systems to verify the effectiveness. The comparison with other existing methods has been made and demonstrated that the intelligent modeling approach is of better performance.

Keywords: intelligent modeling approach, effluent quality, wastewater treatment process, fuzzy neural network

1. Introduction

In recent years, due to the increasingly severe situation of the wastewater treatment, more and more stringent wastewater effluent limits and regulations have been implemented to reduce the negative impact to the water bodies and the environment [1–3]. Therefore, it is important and desirable to predict the effluent quality in real time, since infrequent and inaccurate measurements of the effluent parameters may lead to poor system performances, large operational cost and wrong management decisions [4–6]. How to design the predictor,

which can conduct an appropriate action to realize the accurate monitor and adjust to the dynamic operational stations, is still a challenging work [4, 7].

Conventionally, the measurement of the effluent quality indices can be performed by off-line or online instruments [8, 9]. However, the measurement time of the off-line or online measurement is long, for it requires several minutes to hours [10, 11]. The dynamic conditions in biological treatment processes such as the complex activated sludge process make the measurement challenging [12]. Therefore, prediction modeling method based on online sensors causes great attention. Wen et al. used an equation, derived from the material balance, to calculate the suspended solid concentration, and then employed to predict the treatment results through the sludge [13]. Yu et al. proposed two mechanism models, which were based on linear regression analyses of experimental results from two anaerobic filters, to predict the effect of recirculation on effluent quality of anaerobic filters [14]. The prediction ability was verified by several experiments, and superior results were realized. Bhowmick et al. presented a mathematical model based on the dynamic wave method, to simulate the effluent quality of the treatment system [15]. The abovementioned methods have realized the online prediction of the effluent quality. However, considering the complexity and nonlinearity of WWTP, it is reasonable to design the adaptive prediction model to improve the accuracy of the online prediction.

To improve the adaptive ability of the online prediction model, intelligent method, based on data-driven approach, has caused extensive concern [16, 17]. Zhao et al. presented a partial least-squares-based extreme learning machine to enhance the estimate performance in terms of accuracy and reliability for effluent quality indices [18]. The experimental results showed that the proposed prediction model could effectively capture the input-output relationship with favorable performance. Pai et al. applied five types of gray models to predict suspended solids, chemical oxygen demand and *pH* in the effluent from a wastewater treatment plant [19]. The results revealed that the gray models could predict the industrial effluent variation successfully. To improve the model accuracy, Perendeci et al. used a neural fuzzy model, based on an adaptive network-based fuzzy inference system, to estimate the effluent chemical oxygen demand by the related process variables [20]. Acceptable correlation coefficient (0.8354) and root mean square error (0.1247) were found between estimated and measured values of the system output variable, effluent chemical oxygen demand. However, considering the dynamic properties of WWTP, it is difficult to determine the reasonable fuzzy rules in this adaptive network-based fuzzy inference system. Aimed at this problem, Han et al. designed a flexible structure radial basis function neural network (FS-RBFNN) and applied it to estimate the water quality [21]. This FS-RBFNN could vary its structure dynamically in order to maintain the prediction accuracy, but it had poor interpretability.

Considering the learning ability of neural network and the interpretability of rule-based fuzzy systems, an intelligent method, based on self-organizing fuzzy neural network (SOFNN), is developed to realize the online prediction of the effluent indices. The main advantages of this prediction model are summarized as follows. First, an efficient second-order algorithm is designed to adjust the parameters of SOFNN, which enables to improve

http://dx.doi.org/10.5772/intechopen.74984

the learning capability. Second, the structure of SOFNN can be self-organized based on the relative importance index of each rule in the learning process. The fuzzy rules can be generated or pruned automatically to reduce the computational complexity and improve the generalization power of SOFNN.

2. Wastewater treatment process

WWTP is a large nonlinear system subject to large perturbations in influent flow rate and pollutant load, together with uncertainties concerning the composition of the incoming wastewater. It is also a complex reaction process, which contains biological, physical and chemical reactions. The most popular technology for wastewater treatment is the activated sludge process (ASP). The simplified flow chart of ASP is shown in **Figure 1**, where a primary sedimentation tank, a biochemical reaction tank and a secondary sedimentation tank are consisted. First of all, the dynamically changing influent flows into the primary sedimentation tank to remove the suspended solids. Then, the wastewater gets further processed in the biochemical reaction unit. In this unit, nitrification and denitrification are composed to achieve biological nitrogen removal. After that, the standard wastewater is discharged from the top of the secondary sedimentation tank, and the sludge is returned to the biochemical reaction unit from the bottom of the secondary sedimentation tank. During the reaction process, numerous process variables are contained to influence the treatment performance.

Effluent quality, taken as an important performance evaluation to reflect the treatment results, can provide a basis for water treatment plant management decisions to minimize the microbial risks and optimize the treatment operation. Standard effluent quality requires that the effluent organisms, such as effluent ammonia nitrogen, effluent total nitrogen and effluent suspended solid, remain in the required limits. Although the effluent quality indices can be measured directly by laboratory analysis, a significant time delay problem, which may range from a matter of minutes to a few days, is always unavoidable. This lack of suitable real-time process variable information limits the effective operation of effluent quality. Therefore, an online prediction model is essential to support water quality parameters. Since an approach based on neural networks does not make any assumptions about the functional relationship between the dependent and independent variables, it is suitable for capturing functional relationships between bacterial levels and other variables.

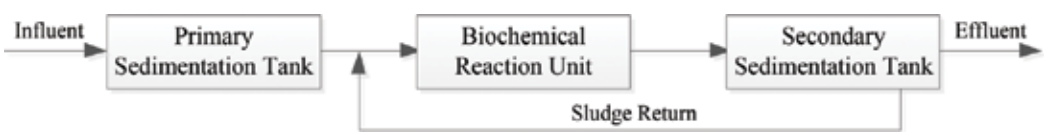

Figure 1. Simplified flow chart of ASP.

3. Intelligent modeling approach based on SOFNN

An intelligent method based on SOFNN is proposed to predict the effluent ammonia nitrogen (S_{NH}) in urban WWTP. The main challenges are the selection of the principal process variables, the construction of the model structure and the adjustment of the model parameters.

3.1. Selection of principal process variables

To determine the principal process variables of the effluent S_{NH}, the mechanism analysis is firstly applied to determine the related process variables, and then principal component analysis (PCA) is introduced to lower the dimension of the original process variables. This method has the advantage of extracting the important information from the coupling process variables and reducing the computational complexity of prediction models.

For the effluent S_{NH}, the mechanism models are described as:

$$\frac{dS_{NH}}{dt} = v_{1,NH_4} \cdot (\rho_1 + \rho_2 + \rho_3) - \left(\frac{1}{Y_A} + i_{N,BM}\right) \cdot \rho_{16} - v_{17,NH_4}\rho_{17}, \tag{1}$$

where

$$v_{1,NH_4} = -\left(1 - f_{s_1}\right) \cdot i_{N,S_F} - f_{S_1} \cdot i_{N,S_1} + i_{N,X_S}, \tag{2}$$

$$v_{17,NH_4} = -f_{X_1} \cdot i_{N,X_1} - \left(1 - f_{X_1}\right) \cdot i_{N,X_s} + i_{N,BM}, \tag{3}$$

$$\rho_1 = K_h \cdot \eta_k \cdot \frac{k_{O_2}}{k_{O_2} + S_{O_2}} \cdot \frac{S_{NO_3}}{K_{NO_3} + S_{NO_3}} \cdot \frac{{}^{X_S}/_{X_H}}{K_X + {}^{X_S}/_{X_H}} \cdot X_H, \tag{4}$$

$$\rho_2 = K_h \cdot \eta_{NO_3} \cdot \frac{k_{O_2}}{k_{O_2} + S_{O_2}} \cdot \frac{S_{NO_3}}{K_{NO_3} + S_{NO_3}} \cdot \frac{{}^{X_S}/_{X_H}}{K_X + {}^{X_S}/_{X_H}} \cdot X_H, \tag{5}$$

$$\rho_3 = K_h \cdot \frac{S_{O_2}}{K_{O_2} + S_{O_2}} \cdot \frac{{}^{X_S}/_{X_H}}{K_X + {}^{X_S}/_{X_H}} \cdot X_H, \tag{6}$$

$$\rho_{16} = \mu_{AUT} \cdot \frac{S_{O_2}}{K_{O_2} + S_{O_2}} \cdot \frac{S_{PO_4}}{K_P + S_{PO_4}} \cdot \frac{S_{NH_4}}{K_{NH_4} + S_{NH_4}} \frac{S_{NH_4}}{K_{ALK} + S_{ALK}} \cdot X_{AUT}, \tag{7}$$

$$\rho_{17} = b_{AUT} \cdot X_{AUT}. \tag{8}$$

where Y_A is the autotrophic bacteria yield coefficient of chemical oxygen demand, $i_{N,BM}$, $i_{N,S1}$, $i_{N,XS}$ and $i_{N,X1}$ are the parameters of nitrogen content, f_{s1} is the proportion of inert chemical oxygen demand in granular matrix, f_{X1} is the proportion of inert chemical oxygen demand in oxide, K_h is the water solubility rate function, μ_{AUT} is the maximum growth rate, X_S is the slowly biodegradable substrate, K_{NO3} is the subsaturation coefficient of nitrate, K_{NH4} is the autotrophic bacteria subsaturation coefficient of nitrogen, K_{O2} is the heterotrophic bacteria

subsaturation coefficient of oxygen, K_{NO3} is the heterotrophic bacteria subsaturation coefficient of nitrate, K_S is the heterotrophic bacteria subsaturation coefficient of *COD*, K_P is the phosphorus storage saturation coefficient, X_P is the particulate products arising from biomass decay, X_H is the water solubility, b_{AUT} is the decay rate, K_{ALK} is the growth factor of alkalinity, S_{O2} is the dissolved oxygen, S_{NO3} is the nitrate, S_{PO4} is the total phosphorus, S_{ALK} is the alkalinity and X_{AUT} is the autotrophic concentration.

According to the mechanism models in Eqs. (1)–(8), it can be concluded that the related process variables to the effluent SNH are S_{NO3}, X_S, S_{O2}, S_{PO4}, S_{ALK}, X_{AUT} and X_H. Combining with the real data collected from urban WWTP, oxidation-reduction potential (*ORP*), total suspended solids (*TSS*), temperature (*T*), PH, influent ammonia nitrogen ($S_{NH,i}$) and effluent nitrate nitrogen ($S_{NO,e}$) are also considered as the influencing variables of the effluent S_{NH}. Then, PCA is utilized to select the principal variables from the 13 related variables.

For reducing the dimension of the process variables, the first important thing is to remove the abnormal data according to the standard deviation calculation formula

$$\sigma_i = \sqrt{\sum_{j=1}^{l} \left(u_{j,i} - \overline{u}_i\right)^2} \Big/ l, \tag{9}$$

where σ_i is the standard error and $\bar{u}_i$ is the average value of the *i*th column sample data; the error between the sample and the average value is shown as $v_i = u_i\text{-}\bar{u}_i$ (i = 1, 2,…, 13), if v_i satisfies

$$|v_i| > 3\sigma_i, \tag{10}$$

it is considered as abnormal data and then, it is removed. Due to the fact that the 13 columns of process variables have different magnitudes, data normalization processing should be conducted

$$u_{inorm} = \frac{u_i - u_{i\min}}{u_{i\max} - u_{i\min}}, \tag{11}$$

where u_{inorm} is the value after normalization and $u_{i\min}$ and $u_{i\max}$ are the minimum and maximum of the *i*th column sample data, respectively. After the normalization treatment, all the sample data are within [0, 1]. It is worth noting that the testing outputs should be anti-normalized to the original ranges.

Then, the covariance matrix **S** is calculated and decomposed according to their singular values into matrices **V** and **Λ**

$$\mathbf{S} = \begin{bmatrix} r_{11} & r_{12} & \cdots & r_{1,m} \\ r_{21} & r_{22} & \cdots & r_{2,m} \\ \vdots & \vdots & \vdots & \vdots \\ r_{m,1} & r_{m,2} & \cdots & r_{m,m} \end{bmatrix}, \tag{12}$$

$$\mathbf{S} = \mathbf{V}\mathbf{\Lambda}\mathbf{V}^{\mathrm{T}}, \tag{13}$$

where $r_{m,m}$ is the correlation coefficient and $\mathbf{\Lambda}$ is a diagonal matrix of the eigenvalues associated with the eigenvectors contained in the columns of matrix $\mathbf{V}$. The contribution rate of each component is calculated by $\mathbf{\Lambda}$, the principal component factor loading matrix $\mathbf{P}$ is then calculated according to $\mathbf{\Lambda}$ and $\mathbf{V}$. The projected matrix $\mathbf{T}$ in the new space is defined as

$$\mathbf{T} = \mathbf{X}\mathbf{P}^{\mathrm{T}} + \mathbf{E}, \tag{14}$$

where matrix $\mathbf{E}$ is used to detect misbehavior in the modeling process.

3.2. Self-organizing fuzzy neural network

To predict the effluent S_{NH} through the principal process variables, a multi-input and single-output SOFNN is developed. The structure of the fuzzy neural network is shown in **Figure 2**.

The mathematical description of this multi-input and single-output fuzzy neural network is given below:

$$\hat{g} = \mathbf{W}\mathbf{v}, \tag{15}$$

where $\hat{g}$ is the output of the output layer, $\mathbf{W} = [w_1, w_2, \ldots, w_P]$ are the weights between the output layer and the normalized layer, P is the number of neurons in the normalized layer and $\mathbf{v}$ is the output of the normalized layer and for a fuzzy model

$$\hat{g} = \mathbf{W}\mathbf{v} = \frac{\sum_{l=1}^{P} w_l e^{-\sum_{i=1}^{k} \frac{(x_i - c_{il})^2}{2\sigma_{il}^2}}}{\sum_{j=1}^{P} e^{-\sum_{i=1}^{k} \frac{(x_i - c_{ij})^2}{2\sigma_{ij}^2}}}, \tag{16}$$

where v_l is the output of the lth normalized neuron and $\mathbf{v} = [v_1, v_2, \ldots, v_P]^{\mathbf{T}}$ and

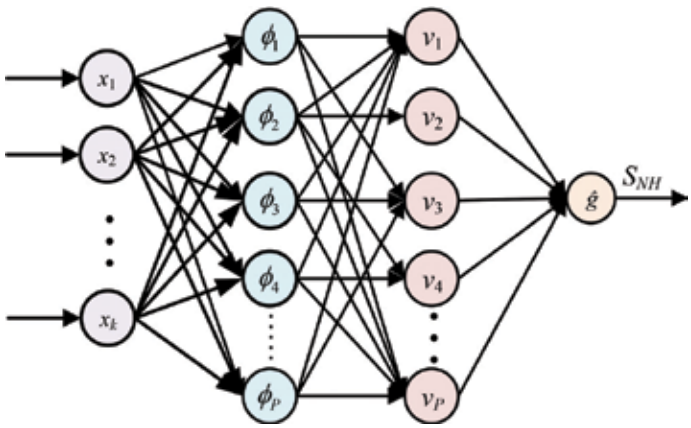

Figure 2. The structure of fuzzy neural network.

$$v_l = \frac{\phi_l}{\sum_{j=1}^{P} \phi_j} = \frac{e^{-\sum_{i=1}^{k} \frac{(x_i - c_{il})^2}{2\sigma_{il}^2}}}{\sum_{j=1}^{P} e^{-\sum_{i=1}^{k} \frac{(x_i - c_{ij})^2}{2\sigma_{ij}^2}}}, \quad j = 1, 2, \ldots, P; \;\; l = 1, 2, \ldots, P, \tag{17}$$

The number of neurons in the radial basis function (RBF) layer is equal to the number of neurons in the normalized layer, and ϕ_j is the output value of the jth RBF neuron

$$\phi_j = \prod_{i=1}^{k} A_j^i(x_j) = \prod_{i=1}^{k} e^{-\frac{(x_i - c_{ij})^2}{2\sigma_{ij}^2}} = e^{-\sum_{i=1}^{k} \frac{(x_i - c_{ij})^2}{2\sigma_{ij}^2}}, \;\; i = 1, 2, \ldots, k; \;\; j = 1, 2, \ldots, P, \tag{18}$$

$\mathbf{c}_j = [c_{1j}, c_{2j}, \ldots, c_{kj}]$ and $\boldsymbol{\sigma}_j = [\sigma_{1j}, \sigma_{2j}, \ldots, \sigma_{kj}]$ are the vectors of centers and widths of the jth RBF neuron, respectively, and

$$u_i = x_i, \;\; i = 1, 2, \ldots, k, \tag{19}$$

where $\mathbf{x} = [x_1, x_2, \ldots, x_k]$ is the input vector of the input layer and $\mathbf{U} = [u_1, u_2, \ldots, u_k]$ is the input of the RBF layer.

Following the computation procedure in the Levenberg-Marquardt algorithm, the updated rule of the adaptive second-order algorithm for the parameters in fuzzy neural network is given by

$$\boldsymbol{\Theta}(t+1) = \boldsymbol{\Theta}(t) + (\boldsymbol{\Psi}(t) + \lambda(t) \times \mathbf{I})^{-1} \times \boldsymbol{\Omega}(t), \tag{20}$$

where $\boldsymbol{\Psi}(t)$ is the quasi-Hessian matrix, $\boldsymbol{\Omega}(t)$ is the gradient vector, $\mathbf{I}$ is the identity matrix which is employed to avoid the ill condition in solving inverse matrix and $\lambda(t)$ is the adaptive learning rate defined as:

$$\lambda(t) = \mu(t)\lambda(t-1), \tag{21}$$

$$\mu(t) = \left(\tau^{\min}(t) + \lambda(t-1)\right)/(\tau^{\max}(t) + 1), \tag{22}$$

where $\tau^{\max}(t)$ and $\tau^{\min}(t)$ are the maximum and minimum eigenvalues of $\boldsymbol{\Psi}(t)$, respectively, $(0 < \tau^{\min}(t) < \tau^{\max}(t), 0 < \lambda(t) < 1,)$ and the variable vector $\boldsymbol{\Theta}(t)$ contains three kinds of variables: the output parameter matrix $\mathbf{W}$, the center vector $\mathbf{c}$ and the width vector $\boldsymbol{\sigma}$

$$\boldsymbol{\Theta}(1) = \left[w_1(1), \cdots, w_3(1), \cdots, w_P(1), \mathbf{c}_1(1), \cdots, \mathbf{c}_j(1), \cdots, \mathbf{c}_P(1), \boldsymbol{\sigma}_1(1), \cdots, \boldsymbol{\sigma}_j(1), \cdots, \boldsymbol{\sigma}_P(1)\right]. \tag{23}$$

In this adaptive second-order optimization algorithm, the output parameter matrix $\mathbf{W}$, the center vector $\mathbf{c}$ and the width vector $\boldsymbol{\sigma}$ can be optimized simultaneously. The quasi-Hessian matrix $\boldsymbol{\Psi}(t)$ and the gradient vector $\boldsymbol{\Omega}(t)$ are accumulated as the sum of related submatrices and vectors.

$$\mathbf{\Psi}(t) = \mathbf{j}^T(t)\mathbf{j}(t), \tag{24}$$

$$\mathbf{\Omega}(t) = \mathbf{j}^T(t)e(t), \tag{25}$$

$$e(t) = y(t) - \widehat{g}(t), \tag{26}$$

where $e(t)$ is the error between the output layer and the real output at time t, and the Jacobian vector $\mathbf{j}(t)$ is calculated as:

$$\mathbf{j}(t) = \left[\frac{\partial e(t)}{\partial w_1(t)}, \cdots, \frac{\partial e(t)}{\partial w_2(t)}, \cdots, \frac{\partial e(t)}{\partial w_P(t)}, \frac{\partial e(t)}{\partial \mathbf{c}_1(t)}, \cdots, \frac{\partial e(t)}{\partial \mathbf{c}_j(t)}, \cdots, \frac{\partial e(t)}{\partial \mathbf{c}_P(t)}, \frac{\partial e(t)}{\partial \mathbf{\sigma}_1(t)}, \cdots, \frac{\partial e(t)}{\partial \mathbf{\sigma}_j(t)}, \cdots \frac{\partial e(t)}{\partial \mathbf{\sigma}_P(t)}\right]. \tag{27}$$

The elements of the Jacobian vector $\mathbf{j}(t)$ are given as:

$$\frac{\partial e(t)}{\partial w_p(t)} = -v_p(t), \quad p = 1, 2, \cdots, P, \tag{28}$$

$$\frac{\partial e(t)}{\partial \mathbf{c}_j(t)} = \left[\frac{\partial e(t)}{\partial c_{1j}(t)}, \frac{\partial e(t)}{\partial c_{2j}(t)}, \cdots, \frac{\partial e(t)}{\partial c_{kj}(t)}\right], \tag{29}$$

$$\frac{\partial e(t)}{\partial c_{ij}(t)} = -\frac{2w_j(t) \times v_i(t) \times \left[x_i(t) - c_{ij}(t)\right]}{\sigma_{ij}(t)}, \quad i = 1, 2, \cdots, k, \tag{30}$$

$$\frac{\partial e(t)}{\partial \mathbf{\sigma}_j(t)} = \left[\frac{\partial e(t)}{\partial \sigma_{1j}(t)}, \frac{\partial e(t)}{\partial \sigma_{2j}(t)}, \cdots, \frac{\partial e(t)}{\partial \sigma_{kj}(t)}\right], \tag{31}$$

$$\frac{\partial e(t)}{\partial \sigma_{ij}(t)} = -\frac{w_j(t) \times v_i(t) \times \left\|x_i(t) - c_{ij}(t)\right\|^2}{\sigma_{ij}^2(t)}. \tag{32}$$

With Eqs. (28)–(32), all the elements of the Jacobian vector $\mathbf{j}(t)$ can be calculated. Then, the quasi-Hessian matrix $\mathbf{\Psi}(t)$ and the gradient vector $\mathbf{\Omega}(t)$ are obtained from Eqs. (24)–(25), so as to apply the updated rule (20) to parameter adjustment. From the former analysis, some remarks are emphasized.

To grow or prune the structure of the fuzzy neural network, relative importance index is utilized. The values of relative importance index can be used to determine the proportion of output values in a multiple regression equation. The relative importance index of each neuron in the normalized layer is defined as:

$$R_k(t) = \frac{\sum_{l=1}^{P} a_{kl}(t) \times b_l(t)}{\sum_{k=1}^{P}\sum_{l=1}^{P} a_{kl}(t) \times b_l(t)}, k = 1, 2, \cdots, P, \tag{33}$$

where $R\ k(t)$ is the relative importance index of the kth normalized neuron at time t; the regression coefficients $\mathbf{B}(t) = [q\ 1(t),\ b\ 2(t),\ldots,\ b\ P(t)]^{\mathrm{T}}$ and $\mathbf{A}(t) = [\mathbf{a}\ 1(t),\ \mathbf{a}\ 2(t),\ldots,\ \mathbf{a}\ P(t)]$ ($\mathbf{a}\ l = [a\ 1\ l(t),\ldots,\ a\ Pl(t)]^{\mathrm{T}}$) can be calculated as:

$$\mathbf{A}(t) = \left[(\mathbf{Z}(t))^{\mathrm{T}}\mathbf{Z}(t)\right]^{-1}(\mathbf{Z}(t))^{\mathrm{T}}\widehat{\mathbf{I}}(t) = (\mathbf{Z}(t))^{\mathrm{T}}\widehat{\mathbf{I}}(t), \tag{34}$$

$$\mathbf{B}(t) = \left[(\mathbf{Z}(t))^{\mathrm{T}}\mathbf{Z}(t)\right]^{-1}(\mathbf{Z}(t))^{\mathrm{T}}\widehat{\mathbf{G}}(t) = (\mathbf{Z}(t))^{\mathrm{T}}\widehat{\mathbf{G}}(t), \tag{35}$$

where $\mathbf{A}(t)$ is $P\times P$ and $\mathbf{B}(t)$ is $P\times 1$, $\hat{\mathbf{G}}(t) = [\hat{g}(t), \hat{g}(t-1), \ldots, \hat{g}(t\text{-}N + 1)]^{\mathrm{T}}$ and

$$\mathbf{Z}(t) = \mathbf{S}(t)\widehat{\mathbf{S}}(t), \tag{36}$$

$$\widehat{\mathbf{I}}(t) = \mathbf{S}(t)\mathbf{\Delta}(t)\widehat{\mathbf{S}}(t), \tag{37}$$

$\mathbf{S}(t) = [\xi\ 1, \xi\ 2, \ldots, \xi\ P]$ is the eigenvectors of $\hat{\mathbf{I}}(t)(\hat{\mathbf{I}}(t))^{\mathrm{T}}$, $\hat{\mathbf{S}}(t) = [\zeta\ \mathbf{1}, \zeta\ 2, \ldots, \zeta P]$ is the eigenvectors of $(\hat{\mathbf{I}}(t))^{\mathrm{T}}\hat{\mathbf{I}}(t)$, $\mathbf{\Delta}(t)$ is the singular matrix of $\hat{\mathbf{I}}(t)$, $\hat{\mathbf{I}}\ l(t) = [w\ l(t)\times v_l(\mathbf{x}(t)), w\ l(t)\times v_l(\mathbf{x}(t-1)), \ldots, w\ l(t)\times v_l(\mathbf{x}(t\text{–}T + 1))]^{\mathrm{T}}$ and T is the preset number of sample. The relative importance index of each normalized neuron represents the contribution of each normalized neuron to each output neuron.

Before introducing the self-organizing mechanism, the error of the output is defined as:

$$E(\mathbf{\Theta}(t)) = \frac{1}{2}\times (y(t)\text{-}\widehat{g}(t))^2, \tag{38}$$

where $y(t)$ and $\hat{g}_q t)$ are the desired and real output values.

The procedure of the proposed self-organizing mechanism is given as follows:

1. Growing phase.

If $E(\mathbf{\Theta}(t))$ is larger than $E(\mathbf{\Theta}(t-1))$, a new neuron will be inserted to the normalized layer. The parameters of the new normalized neuron are designated by the normalized neuron with the largest relative importance index

$$R_m(t) = \max \mathbf{R}(t), \tag{39}$$

$\mathbf{R}(t) = [R\ 1(t), R\ 2(t), \ldots, R_P(t)]$, $R_m(t)$ is the mth normalized neuron with the largest relative importance index. The parameters of new normalized neuron are designed as:

$$\mathbf{c}_{new}(t) = \mathbf{c}_{P+1}(t) = \frac{1}{2}(\mathbf{c}_m(t) + \mathbf{x}(t)), \tag{40}$$

$$\mathbf{\sigma}_{new}(t) = \mathbf{\sigma}_{P+1}(t) = \mathbf{\sigma}_m(t), \tag{41}$$

$$w_{new}(t) = y(t) - \widehat{g}(t)/e^{-\sum_{i=1}^{k}\frac{(u_i(t)-c_{inew}(t))^2}{2\sigma^2_{inew}(t)}}, \tag{42}$$

where $\mathbf{c}_{new}(t)$ and $\mathbf{\sigma}_{new}(t)$ are the center vector and width vector of the new normalized neuron, respectively, $w_{new}(t)$ is the weight of new normalized neuron, $\mathbf{c}_m(t)$ and $\mathbf{\sigma}_m(t)$ are the center vector and width vector of the mth normalized neuron, respectively.

2. Pruning phase.

In the training process, if $E(\mathbf{\Theta}(t))$ is less than $E(\mathbf{\Theta}(t-1))$ and

$$R_h(t) \le R_r, \tag{43}$$

$R_r \in (0, E_0)$ is the threshold, where

$$R_h(t) = \min \mathbf{R}(t). \tag{44}$$

Then, the hth normalized neuron will be pruned and the parameters of remaining normalized neuron will be updated

$$\mathbf{c}'_{h'}(t) = \mathbf{c}_{h'}(t), \tag{45}$$

$$\mathbf{\sigma}'_{h'}(t) = \mathbf{\sigma}_{h'}(t), \tag{46}$$

$$w_{h'}(t) = \frac{w_{h'}(t)e^{-\sum_{i=1}^{k}\left(u_i(t)-c_{i,h'}(t)\right)^2/2\sigma^2_{i,h'}(t)} + w_h^q(t)e^{-\sum_{i=1}^{k}\left(u_i(t)-c_{i,h}(t)\right)^2/2\sigma^2_{i,h}(t)}}{e^{-\sum_{i=1}^{k}\left(u_i(t)-c_{i,h'}(t)\right)^2/2\sigma^2_{i,h'}(t)}}, \tag{47}$$

$$\mathbf{c}'_h(t) = 0, \tag{48}$$

$$\mathbf{\sigma}'_h(t) = 0, \tag{49}$$

$$\mathbf{w}'_h(t) = 0, \tag{50}$$

where the h'th normalized neuron is nearest to the hth normalized neuron with the smallest Euclidean distance, $\mathbf{w}_h{}'(t)$ and $w_{h'}(t)$ are the hth weight vector and the h'th weight vector after pruning the hth normalized neuron, respectively, $\mathbf{c}_h{}'(t)$ and $\mathbf{\sigma}_h{}'(t)$ are the center vector and width vector of the hth normalized neuron after the neuron is pruned, respectively, and $\mathbf{c}'_{h'}(t)$ and $\mathbf{\sigma}'_{h'}(t)$ are the center vector and width vector of the h'th normalized neuron after the neuron is pruned, respectively.

4. Simulation results and analysis

In this section, the effectiveness of the proposed intelligent modeling method based on SOFNN is evaluated. A brief introduction to experimental setup is provided before the experimental results are detailed.

4.1. Experimental setup

The performance of the online prediction for the effluent S_{NH} depends heavily on the determination of the input variables. Based on the analysis of PCA and the work experience of the

experts in urban WWTP, five process variables have been chosen as the input variables to develop the intelligent method: S_{PO4}, ORP, S_{O2}, *TSS* and *PH*, respectively. S_{PO4} is an important index of the effluent, *ORP* reflects the concentration of oxide, S_{O2} is an important indicator to the growth of organic matter and the nitrification reaction, *TSS* stands for the degree of wastewater treatment and *PH* stands for the acid-base property of the wastewater. The input variables determined for the effluent S_{NH} are listed in **Table 1**. The detailed selection process and analyzation process are shown in [22]. Meanwhile, the online measurement instruments used for obtaining the process values are also displayed.

CHM-301 is the S_{PO4} detector, AODJ-QX6530 is the portable *ORP* probe, WTW oxi/340i is the portable S_{O2} probe, 7110 MTF-FG is the *TSS* analyzer and pH 700 is the *PH* detector.

Taking advantage of the abovementioned analysis, an experimental hardware is set up. Anaerobic-anoxic-oxic (A^2/O) treatment process with the online sensors is employed in urban WWTP (shown in **Figure 3**). In this experimental hardware, online sensors, effluent S_{NH} models based on fuzzy neural network are schematically shown.

The online sensors consist of five parts: TP detector, *ORP* probe, S_O probe, *TSS* analyzer and *PH* detector. The output signals from the sensors are integrated and connected to programmable logical controller (PLC, S7-200) for transmitting primary indictors. The PLC system is interfaced with equipped sensors and collected reliable data in form of 4-20mA electrical signals with a fast response time. Moreover, the PLC system has been connected through a serial port (RS 232, Siemens AG) of the host computer, which uses the real-time data to calculate the values of key variables and also stores the data in form of local file. The sensors are operated in continuous/online measurement mode, and the historical process data are routinely acquired and stored in the data acquisition system. The process data are periodically collected from the reactor to check whether the system is operating as scheduled during the experiments. Then, after preprocessing, the data are applied to the proposed SOFNN method. In SOFNN, five neurons are determined in the input layer based on the analyzed related process variables S_{PO4}, ORP, S_{O2}, *TSS* and *PH*. According to the experienced experts, there are 10 neurons in both RBF layer and normalized layer initially, and then the neurons in normalized layer are self-organized based on the relative importance index to guarantee the prediction accuracy. The number of output neuron is one, which represents the predicted effluent S_{NH}.

Variables	Units	Main apparatus and instrument
S_{PO4} (total phosphorus)	mg/L	CHM-301
ORP (oxidation reduction potential)	—	AODJ-QX6530
S_{O2} (dissolved oxygen)	mg/L	WTW oxi/340i
TSS (total suspended solid)	mg/L	7110 MTF-FG
PH	—	pH 700

Table 1. The principal variables' measurement with online sensors.

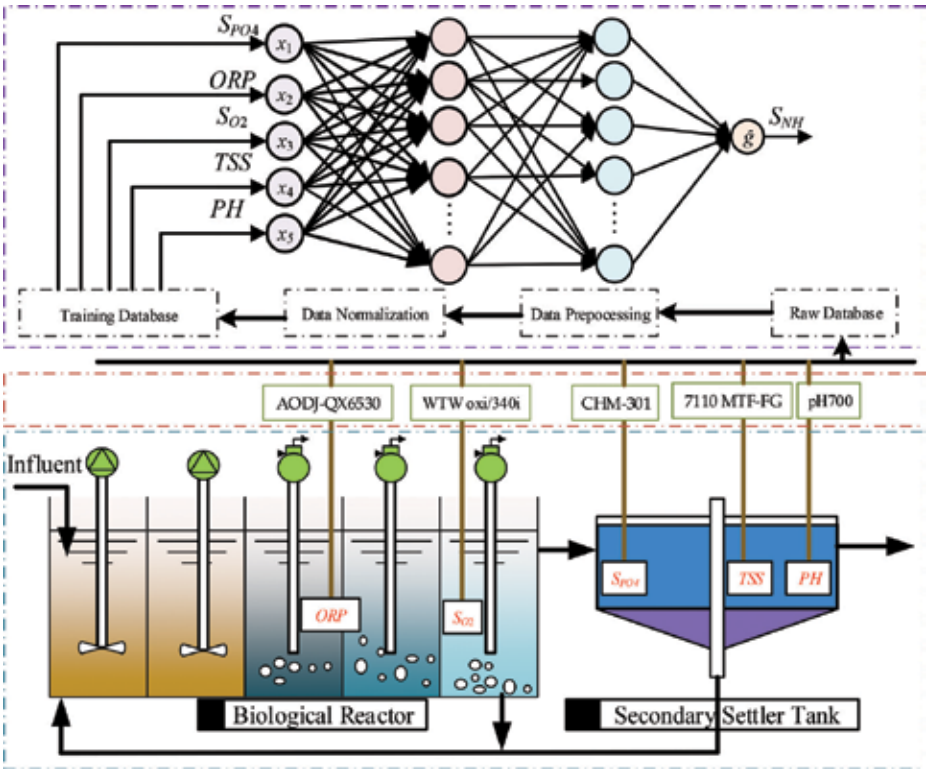

Figure 3. Experiment diagram of the online modeling.

4.2. Experimental results

An intelligent modeling method based on the proposed SOFNN is proposed to predict the effluent S_{NH} concentration by the determined principal process variables. All data are collected on a daily basis and covered all four seasons. The daily frequency of measurements is considered sufficient because of the long residence times in WWTP. To guarantee the efficiency in this soft-computing method, all variables are normalized and denormalized by taking advantage of the maximum and minimum values before and after application. The input-output water quality data were collected from a real-world wastewater treatment plant (Beijing, China) over the year 2014. After deleting the abnormal data, 280 samples were obtained and normalized; 140 samples from 1/5/2014 to 30/9/2014 were taken as the training data while the remaining 140 samples from 1/10/2014 to 30/11/2014 were employed as testing data.

The error measures for the effluent NH_4 are 0.1 mg/L confidence limits. Both the mean testing RMSE $\sqrt{\sum_{n=1}^{N}\left(y_n(t)-\widehat{g}_n(t)\right)^2/N}$ and the mean predicting accuracy $\left(\sum_{t=1}^{Days}(1-e(t)/\widehat{g}(t))/Days\right)$ are utilized as the performance indices to assess the modeling performance, where N is the number of samples.

The predicting results and the predicting error of the effluent S_{NH} concentration are shown in **Figures 4–6**. Additionally, to show the performance of SOFNN clearly, **Table 2** shows the network structure, the mean testing RMSE and the mean accuracy in comparison with other methods.

The prediction results of the effluent S_{NH} based on SOFNN are displayed in **Figures 4–6**. The training RMSE of the effluent S_{NH} is shown in **Figure 4**; it can be observed that the final value can reach 0.02. In **Figure 5**, the predicted results are displayed, both the SOFNN outputs and real outputs. The predicted outputs based on SOFNN can approximate the real outputs with little errors. Meanwhile, the errors are displayed in **Figure 6**, which remain in the range of

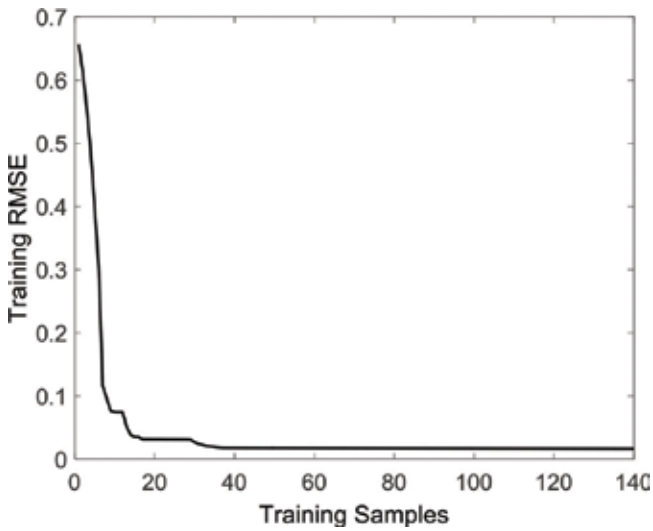

Figure 4. The training RMSE.

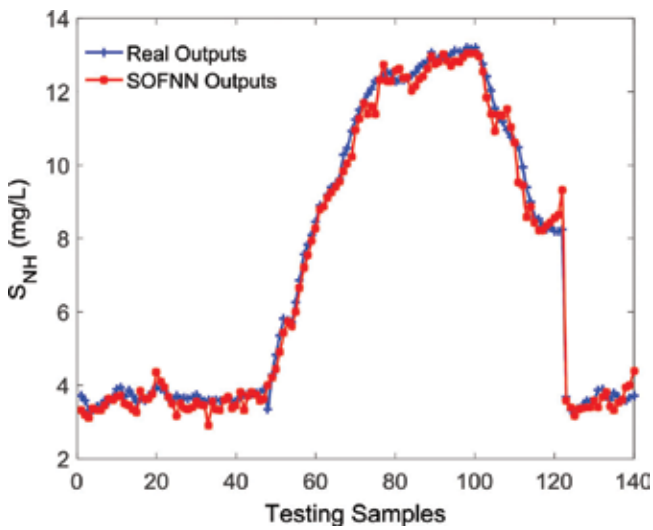

Figure 5. The testing results of the effluent S_{NH}.

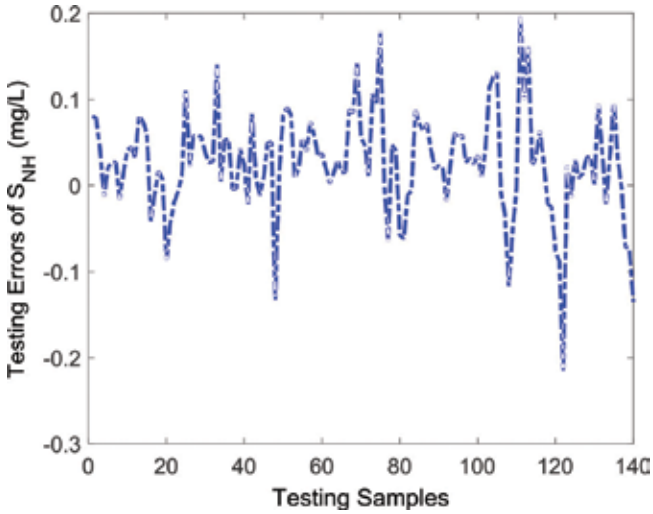

Figure 6. The testing errors of the effluent S_{NH}.

Methods	No. of final normalized neurons	Mean testing RMSE	Mean accuracy (%)
SOFNN (adaptive learning rate)	**13**	**0.103**	**97.94**
SOFNN (fixed learning rate)	**13**	**0.112**	**97.76**
SOFNN-ACA [23]	19	0.162	96.76
FAOS-PFNN [24]	25	0.221	95.58
GP-FNN [25]	19	0.191	96.18
Mathematic model [12]	—	0.772	84.56

Table 2. Performance comparison between different methods.

± 0.3. From this figure, it can be observed that the proposed adaptive fuzzy neural network has the superior prediction ability by using S_{PO4}, ORP, S_{O2}, *TSS* and *PH* as the inputs.

In addition, the results of SOFNN are also compared with other modeling methods, SOFNN with fixed learning rate, the self-organizing fuzzy neural network with adaptive computation algorithm (SOFNN-ACA)[23], fast and accurate online self-organizing fuzzy neural network (FAOS-PFNN) [24], growing-and-pruning fuzzy neural network (GP-FNN)[25] and the mathematic model [12].

Table 2 indicates that the proposed SOFNN can achieve with compact structure than other compared methods, the number of the final normalized neurons is 13. Higher mean accuracy is acquired by this proposed SOFNN with adaptive learning rate (mean accuracy value is 97.94%), which is higher than the proposed SOFNN-ACA [23], FAOS-PFNN [24], GP-FNN [25] and the mathematic model [12]. This means that this proposed SOFNN with

adaptive learning rate has the ability to improve the accuracy of approximating the global optimization parameters during the learning process. The detailed testing samples are shown in **Tables 3–9**.

2.18	2.55	2.21	2.73	3.00	2.81	2.75	2.83	2.94	3.17
2.70	3.24	3.13	3.32	3.43	2.74	2.82	2.59	2.47	2.20
2.39	2.32	2.60	2.23	2.53	2.11	2.10	2.73	2.54	2.58
2.70	2.65	2.78	2.67	2.83	2.72	2.99	2.83	2.98	2.73
3.05	3.00	2.76	2.38	2.88	2.95	3.04	2.97	3.36	2.75
3.42	3.03	3.41	3.23	3.08	2.97	3.09	3.03	2.95	3.06
2.76	2.24	2.58	2.60	2.88	2.32	2.55	2.60	2.27	1.92
1.82	1.73	2.51	2.33	2.53	2.21	2.65	2.19	2.85	2.23
2.48	1.94	1.97	1.52	1.67	1.60	1.43	1.53	1.57	1.57
1.54	1.69	1.44	1.21	1.19	1.11	1.00	1.00	0.90	0.80
0.68	0.62	0.54	0.52	0.47	0.44	0.35	0.34	0.30	0.30
0.27	0.29	0.28	0.25	0.25	0.23	0.23	2.24	2.27	0.27
2.18	2.55	2.21	2.73	3.00	2.81	2.75	2.83	2.94	3.17
2.70	3.24	3.13	3.32	3.43	2.74	2.82	2.59	2.47	2.20

Table 3. Testing inputs S_{PO4}.

−17.43	−16.54	−16.79	−15.13	−17.18	−28.20	−35.76	−43.97	−51.53	−57.17
−63.07	−71.01	−76.85	−82.49	−87.81	−91.91	−95.37	−98.19	−101.14	−104.21
−97.80	−89.28	−80.69	−77.49	−71.98	−73.83	−68.64	−67.23	−71.14	−80.82
−97.61	−103.57	−108.32	−112.16	−115.49	−117.99	−120.05	−121.65	−123.12	−122.67
−121.20	−119.79	−120.75	−108.44	−56.21	−49.86	−48.84	−49.22	−46.34	−51.40
−48.01	−54.99	−52.94	−49.67	−47.75	−45.95	−46.21	−45.63	−45.76	−36.40
−11.73	−12.11	−6.09	−39.74	−15.25	−13.01	−11.28	−10.25	−13.33	−22.24
−31.66	−41.28	−51.47	−60.63	−66.27	−62.36	−61.34	−57.11	−60.89	32.05
39.55	37.56	38.33	37.69	37.43	36.66	35.89	34.48	33.07	31.08
30.76	27.62	26.47	33.33	−27.82	−43.26	−55.95	−63.90	−71.85	−78.90
−84.09	−88.90	−94.22	−96.97	−99.28	−102.42	−105.50	−108.64	−112.10	−115.56
−117.99	−121.07	−124.47	−126.84	−129.21	−133.06	−135.43	−137.09	−138.95	−140.94
−142.67	−144.02	−144.85	−146.52	−147.48	−147.99	−149.02	−150.62	−151.90	−153.63
−155.49	−157.28	−159.08	−158.76	−160.87	−163.24	−165.94	−170.17	−172.79	−174.78

Table 4. Testing inputs ORP.

7.64	6.35	4.34	2.63	1.84	1.54	1.34	1.33	1.41	1.73
1.77	1.86	1.97	2.41	2.77	2.92	2.80	3.76	5.62	6.02
6.11	6.04	5.91	6.12	5.90	5.22	4.02	3.43	2.71	2.30
2.36	2.59	2.77	3.30	3.49	3.77	4.02	4.22	4.16	4.28
5.59	7.49	7.97	7.93	7.64	6.91	6.54	6.35	6.35	6.60
6.57	6.75	6.84	6.83	6.88	7.10	7.17	7.11	7.07	7.84
7.95	7.65	7.36	7.96	7.80	5.98	4.08	2.72	2.04	1.87
2.10	3.20	4.75	5.59	5.95	6.22	6.54	7.12	7.75	5.97
7.67	6.55	6.09	6.09	6.40	6.63	6.92	6.85	6.67	6.78
7.05	7.35	7.63	7.77	0.81	0.81	0.84	0.86	0.89	0.86
0.99	1.14	0.73	0.68	0.65	0.68	0.66	0.56	0.50	0.53
0.55	0.54	0.49	0.49	0.48	0.49	0.48	0.51	0.53	0.50
0.53	0.57	0.54	0.54	0.59	0.62	0.53	0.52	0.49	0.50
0.51	0.52	0.45	0.43	0.46	0.46	0.46	0.48	0.51	0.47

Table 5. Testing inputs S_{O2}.

2.83	2.72	2.83	2.77	2.81	2.82	2.74	2.77	2.78	2.77
2.78	2.78	2.80	2.80	2.75	2.79	2.77	2.83	2.79	2.79
2.78	2.76	2.80	2.81	2.80	2.85	2.80	2.82	2.90	2.81
2.81	2.78	2.90	2.81	3.17	2.80	2.92	2.85	2.80	2.82
2.82	2.89	2.91	2.80	2.79	2.81	2.82	2.88	2.84	2.83
2.82	2.82	2.80	2.82	2.83	2.87	2.77	2.82	2.82	2.82
2.81	2.84	2.83	2.83	2.86	2.77	2.73	2.78	2.80	2.79
2.81	2.80	2.74	2.81	2.81	2.78	2.87	2.83	2.87	2.88
2.86	2.82	2.95	2.89	2.88	2.90	2.89	2.95	2.90	2.92
2.93	2.89	2.93	2.90	2.82	2.82	2.81	2.80	2.77	2.82
2.80	2.84	2.81	2.82	2.79	2.78	2.85	2.78	2.73	2.74
2.78	2.71	2.77	2.84	2.87	2.86	2.90	2.88	2.90	2.84
2.80	2.88	2.85	2.82	2.78	2.78	2.79	2.81	2.78	2.75
2.75	2.71	2.76	2.75	2.77	2.72	2.71	2.71	2.74	2.68

Table 6. Testing inputs *TSS*.

7.93	7.93	7.93	7.93	7.92	7.91	7.90	7.89	7.88	7.87
7.86	7.86	7.85	7.85	7.84	7.84	7.84	7.85	7.85	7.85
7.85	7.85	7.86	7.86	7.86	7.86	7.86	7.86	7.87	7.87
7.86	7.86	7.86	7.86	7.86	7.86	7.86	7.86	7.86	7.86
7.87	7.87	7.87	7.88	7.91	7.92	7.92	7.92	7.92	7.92
7.91	7.91	7.91	7.90	7.90	7.90	7.90	7.90	7.90	7.90
7.95	7.95	7.95	7.89	7.90	7.91	7.92	7.92	7.92	7.92
7.91	7.90	7.90	7.90	7.89	7.89	7.89	7.89	7.89	7.93
8.02	8.02	8.02	8.02	8.02	8.01	8.01	8.01	8.01	8.01
8.01	8.00	8.00	7.99	8.02	8.02	8.02	8.01	8.01	8.01
8.00	7.99	7.98	8.00	8.01	8.02	8.02	8.02	8.01	8.00
7.99	8.00	8.00	8.00	8.00	8.01	8.00	8.00	7.99	7.99
7.99	7.99	7.99	7.99	7.99	7.99	8.00	8.01	8.00	8.00
8.00	8.01	8.01	8.01	8.01	8.00	8.00	8.00	7.99	7.99

Table 7. Testing inputs *PH*.

3.22	3.24	3.25	3.25	3.34	3.33	3.41	3.33	3.38	3.44
3.46	3.44	3.41	3.38	3.47	3.61	3.56	3.95	3.67	3.81
3.82	3.97	3.63	3.52	3.51	3.70	3.61	3.61	3.47	3.67
3.26	3.29	3.26	3.20	3.24	3.37	3.50	3.85	3.75	3.81
3.61	3.66	3.65	3.65	3.66	3.66	3.62	2.98	3.64	4.31
4.90	5.42	5.77	5.95	6.35	6.82	7.27	7.62	8.08	8.20
8.38	8.50	8.78	9.02	9.32	9.26	9.99	10.16	10.54	11.11
11.38	11.71	11.77	11.97	11.76	12.41	12.77	12.52	12.52	12.59
12.65	12.35	12.41	11.95	12.15	12.17	12.24	12.37	12.76	12.89
12.88	13.19	12.93	12.58	12.92	12.65	12.68	12.81	12.68	12.89
12.82	12.43	11.73	11.17	10.87	11.30	11.12	11.16	10.59	10.14
9.11	9.02	8.75	8.95	8.83	8.58	8.64	8.88	8.90	9.07
8.97	9.35	3.22	3.28	3.33	3.32	3.36	3.37	3.30	3.36
3.37	3.45	3.49	3.40	3.44	3.39	3.51	3.58	3.53	3.70

Table 8. Testing outputs S_{NH}.

3.72	3.58	3.31	3.32	3.42	3.46	3.57	3.54	3.68	3.88
3.93	3.67	3.86	3.70	3.56	3.64	3.58	3.72	3.80	3.94
3.88	3.84	3.65	3.56	3.72	3.62	3.66	3.64	3.68	3.74
3.62	3.59	3.60	3.58	3.59	3.58	3.59	3.65	3.59	3.55
3.70	3.74	3.76	3.76	3.78	3.82	3.88	3.34	4.27	4.84
5.35	5.83	5.78	5.73	6.27	6.86	7.56	7.83	8.09	8.45
8.89	8.88	9.18	9.41	9.50	9.64	10.27	10.46	10.94	11.25
11.50	11.73	11.92	12.09	12.28	12.34	12.41	12.54	12.49	12.28
12.32	12.32	12.37	12.45	12.51	12.67	12.77	12.84	13.07	12.88
12.92	12.93	12.96	13.01	13.12	13.09	13.08	13.19	13.17	13.21
13.03	12.76	12.41	12.02	11.57	11.33	11.18	10.96	10.78	10.62
10.50	9.95	9.39	8.99	8.59	8.53	8.35	8.26	8.31	8.19
8.19	8.25	3.69	3.32	3.30	3.38	3.43	3.57	3.56	3.59
3.86	3.88	3.71	3.59	3.79	3.67	3.58	3.58	3.64	3.72

Table 9. Real outputs S_{NH}.

5. Conclusion

In this chapter, an intelligent method is designed to realize the online prediction of the effluent S_{NH}. Based on SOFNN, the proposed model could capture the correlation between the effluent S_{NH} and the principal process variables and construct the modeling structure automatically. The effectiveness of the proposed intelligent modeling method is evaluated in a WWTP. Experimental simulations and results analysis are provided to show the superior prediction performance.

Author details

Hong-Gui Han[1,2]*, Xiao-Long Wu[1,2], Lu Zhang[1,2] and Jun-Fei Qiao[1,2]

*Address all correspondence to: rechardhan@sina.com

1 College of Electronic and Control Engineering, Beijing University of Technology, Beijing, China

2 Beijing Key Laboratory of Computational Intelligence and Intelligent System, Beijing, China

References

[1] Jasinska EJ, Goss GG, Gillis PL, et al. Assessment of biomarkers for contaminants of emerging concern on aquatic organisms downstream of a municipal wastewater discharge. Science of the Total Environment. 2015;**530**:140-153

[2] Du B, Price AE, Scott WC, et al. Comparison of contaminants of emerging concern removal, discharge, and water quality hazards among centralized and on-site wastewater treatment system effluents receiving common wastewater influent. Science of the Total Environment. 2014;**466**:976-984

[3] Mailler R, Gasperi J, Coquet Y, et al. Study of a large scale powdered activated carbon pilot: Removals of a wide range of emerging and priority micropollutants from wastewater treatment plant effluents. Water Research. 2015;**72**:315-330

[4] Marques R, Rodríguez-Caballero A, Oehmen A, et al. Assessment of online monitoring strategies for measuring N2O emissions from full-scale wastewater treatment systems. Water Research. 2016;**99**:171-179

[5] Goldstein RER, Micallef SA, Gibbs SG, et al. Detection of vancomycin-resistant enterococci (VRE) at four US wastewater treatment plants that provide effluent for reuse. Science of the Total Environment. 2014;**466**:404-411

[6] Gong T, Zhang X. Detection, identification and formation of new iodinated disinfection byproducts in chlorinated saline wastewater effluents. Water Research. 2015;**68**:77-86

[7] Haimi H, Mulas M, Corona F, et al. Data-derived soft-sensors for biological wastewater treatment plants: An overview. Environmental Modelling & Software. 2013;**47**:88-107

[8] Liu Y, Pan Y, Sun Z, et al. Statistical monitoring of wastewater treatment plants using variational Bayesian PCA. Industrial & Engineering Chemistry Research. 2014;**53**(8):3272-3282

[9] Symonds EM, Breitbart M. Affordable enteric virus detection techniques are needed to support changing paradigms in water quality management. CLEAN–Soil, Air, Water. 2015;**43**(1):8-12

[10] Zou X, Kang M, Li A, et al. Spray inlet proton transfer reaction mass spectrometry (SI-PTR-MS) for rapid and sensitive online monitoring of benzene in water. Analytical Chemistry. 2016;**88**(6):3144-3148

[11] Li WW, Yu HQ, He Z. Towards sustainable wastewater treatment by using microbial fuel cells-centered technologies. Energy & Environmental Science. 2014;**7**(3):911-924

[12] Kaelin D, Manser R, Rieger L, et al. Extension of ASM3 for two-step nitrification and denitrification and its calibration and validation with batch tests and pilot scale data. Water Research. 2009;**43**(6):1680-1692

[13] Wen X, Xing C, Qian Y. A kinetic model for the prediction of sludge formation in a membrane bioreactor. Process Biochemistry. 1999;**35**(3):249-254

[14] Yu H, Wilson F, Tay JH. Prediction of the effect of recirculation on the effluent quality of anaerobic filters by empirical models. Water Environment Research. 2000; **72**(2):217-224

[15] Bhowmick A, Irvine K, Jindal R. Mathematical modeling of effluent quality of cha-Am municipality wastewater treatment pond system using PCSWMM. Journal of Water Management Modeling. 2017

[16] Rodriguez A, Quiroz G, Femat R, et al. An adaptive observer for operation monitoring of anaerobic digestion wastewater treatment. Chemical Engineering Journal. 2015;**269**:186-193

[17] Qasaimeh A, Qasaimeh M, Salem ZA, et al. Adaptive Sugeno fuzzy clustering system for intelligent monitoring of inorganic materials in wastewater aeration tanks. Research Journal of Environmental Toxicology. 2015;**9**(6):290

[18] Zhao L, Wang D, Chai T. Estimation of effluent quality using PLS-based extreme learning machines. Neural Computing and Applications. 2013;**22**(3–4):509-519

[19] Pai TY. Gray and neural network prediction of effluent from the wastewater treatment plant of industrial park using influent quality. Environmental Engineering Science. 2008; **25**(5):757-766

[20] Perendeci A, Arslan S, Çelebi SS, et al. Prediction of effluent quality of an anaerobic treatment plant under unsteady state through ANFIS modeling with on-line input variables. Chemical Engineering Journal. 2008;**145**(1):78-85

[21] Han HG, Chen Q, Qiao JF. An efficient self-organizing RBF neural network for water quality prediction. Neural Networks. 2011;**24**(7):717-725

[22] Zhou S, Wu Y. Improving the prediction of ammonium nitrogen removal through struvite precipitation. Environmental Science and Pollution Research. 2012;**19**(2):347-360

[23] Han H, Wu XL, Qiao JF. Nonlinear systems modeling based on self-organizing fuzzy-neural-network with adaptive computation algorithm. IEEE Transactions on Cybernetics. 2014;**44**(4):554-564

[24] Wang N, Er MJ, Meng X. A fast and accurate online self-organizing scheme for parsimonious fuzzy neural networks. Neurocomputing. 2009;**72**(16):3818-3829

[25] Han H, Qiao J. A self-organizing fuzzy neural network based on a growing-and-pruning algorithm. IEEE Transactions on Fuzzy Systems. 2010;**18**(6):1129-1143

Chapter 6

Treatment of Textile Wastewater Using a Novel Electrocoagulation Reactor Design

Ahmed Samir Naje, Mohammed A. Ajeel,
Peter Adeniyi Alaba and
Shreeshivadasan Chelliapan

Additional information is available at the end of the chapter

http://dx.doi.org/10.5772/intechopen.76876

Abstract

This study explored the best operating conditions for a novel electrocoagulation (EC) reactor with the rotating anode for textile wastewater treatment. The influence of operating parameters like interelectrode distance (IED), current density (CD), temperature, pH, operating time (RT) and rotation speed on the removal efficiency of the contaminant was studied. A comparative study was done using conventional model with static electrodes in two phases under same textile wastewater. The findings revealed that the optimal conditions for textile wastewater treatment were attained at RT = 10 min, CD = 4 mA/cm^2, rotation speed = 150 rpm, temperature = 25°C, IED = 1 cm and pH = 4.57. The removal efficiencies of color, biological oxygen demand (BOD), turbidity, chemical oxygen demand (COD) and total suspended solid (TSS) were 98.50, 95.55, 96, 98 and 97.10%, respectively, within the first 10 min of the reaction. The results of the experiment reveal that the newly designed reactor incorporated with cathode rings and rotated anode impellers provide a superior treatment efficiency within a short reaction time. The novel EC reactor with a rotating anode significantly enhanced textile wastewater treatment compared to the conventional model. The values of adsorption and passivation resistance validated the pollutants removal rate.

Keywords: rotated anode reactor, textile wastewater, electrode consumption, electrocoagulation

1. Introduction

Electrocoagulation (EC) process involves in situ coagulant formation with sacrificial anode dissolution. Generally, the anode is prepared using iron or aluminum (Al) [1, 2]. The metal ions

interact to generate insoluble OH^- ions. The generated insoluble hydroxides adsorb the contaminants from the solution either by electrostatic attraction or complexation before the coagulation [3, 4]. Lessening of the electrodes' internal resistance drop (IR-drop) is one of the most essentials toward reducing the total cost of EC operation to enhance the current performance by enhancing the state of turbulence. Both oxygen and hydrogen gas emerged near the cathode and anode as soon as each gas bubble nucleates. The bubbles are like insulating spherical figures, generating a film that fouls oxide over the electrode surface (passivation effects). This issue increases the total electrical resistance of the cell, thereby needing a superior quantity of electrical energy to attain the optimal removal [5]. To moderate the bubble accumulation, the electrolyte flow around the electrodes must be augmented for the bubbles to be pushed out [6].

To proffer solution to these, the current EC reactor with rotating anode was conducted to enhance the reactors' overall efficiency [7]. Additionally, the leading objective of the present work is to study the treatment of textile wastewater using a novel EC reactor under optimum operating conditions and to compare the performance with that of conventional EC reactor.

2. Materials and methods

2.1. Wastewater characteristics

The wastewater used for the present study was obtained from one of the foremost textile industries in Babylon (Iraq). For dyeing of fabrics, the industry employs Imperon Violet KB (CAS #: 6358-46-9). **Table 1** presents the major characteristics of the textile wastewater, while **Table 2** shows the properties of the employed Imperon Violet KB.

2.2. EC rotating anode reactor

Figure 1 illustrates the new EC reactor employed in the current study. The reactor (10 L working volume) was made from Perspex and has a cylindrical form stirred tank setting (total length = 500 mm; inner diameter = 174 mm; external diameter = 180 mm). To keep the impeller structure and sustain the rotation of the electrode, a 32-mm-diameter rotating shaft was attached to a regulating speed motor. The motor is a DC electrical type and offers a number of steady-state speeds in the range of 0–1000 rpm. The electrodes were produced from the aluminum substance; the rotating anode comprises ten impellers. All the impellers have four rods (diameter = 12 mm, length = 30 mm) each and ten rings, which were employed as the cathode. Every one of the ring (thickness = 12 mm, internal diameter = 134 mm, diameter = 172 mm) was serially organized, maintaining 30 mm distance of apart. The entire active surface area is 500 cm^2; the reactor comprises three equally spaced baffles to establish the cathode rings by terminating the rotation and tangential flow arrangements of the mass fluid. The endorsed surface area-to-volume ratio ranges from 5 to 45 m^2/m^3 [8]. In the current model, the ratio was minimized (to 5 m^2/m^3) with the aid of a small area of the electrode for treatment of a great wastewater volume. The patent novelty filing was performed with application number PI 2015702202.

Parameters	Values
Electrical conductivity (μS/cm)	1455
Turbidity (NTU)	396
Total suspension solid, TSS (mg/L)	3270
Total dissolved solid, TDS (mg/L)	1250
Dissolved oxygen, DO (mg/L)	0.72
pH	4.50
Chlorides, Cl^- (mg/L)	35
Sulfate (mg/L)	678
Phosphate (mg/L)	7.2
Nitrates (mg/L)	11
Phenols (mg/L)	335
Oil and grease (mg/L)	3.2
BOD (mg/L)	112
COD (mg/L)	990

Table 1. Characteristics of textile wastewater.

2.3. Experimental procedure

The performance of EC process was determined based on color removal, TSS and COD. The experiment was initially performed by investigating the influence of CD and the anode rotation speed. The overall competence of the reactor was investigated using three major variables: overall rotation speed of the anode, CD and processing time. The value of RT of 10–30 min was maintained. Three values of CD (4, 6 and 8 mA/cm^2) with different steady-state anode rotation speed (75, 150 and 250 rpm) were observed at room temperature (25–27°C). The selection of the current densities was based on some initial studies, which show an insignificant change in the total removal efficiency when the value of CD exceeds 8 mA/cm^2. For all the runs, a 10 L sample was used for the EC process, and nine different batches of EC runs were performed. Upon concluding each run, a primary sample was removed, and the cells were washed with a 5% HCl solution for 10 min and subsequently washed using a sponge. The anode and cathode were linked to the positive and negative parts of DC power supply (YIZHAN, 0–6 A; 0-40 V, China). 30 V was used as the main voltage was for each experiment. For voltage measurement, a voltmeter was attached to the cell in parallel. For each run, the current was kept constant by using a variable resistance and monitored using an ammeter. For each iteration, the samples were left to settle for 30 min and subsequently filtered. About 100 ml of supernatant sample was collected for examination and analysis in replicates. The same parameters were examined for the entire replicated sample.

Color	Imperon Violet KB
Chemical structure	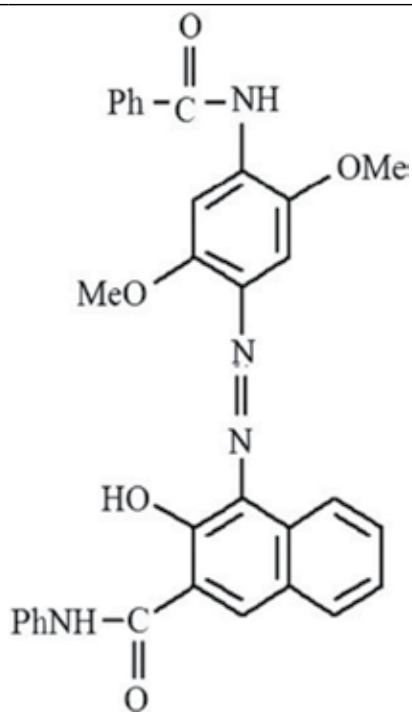
Chemical formula	$C_{32}H_{26}N_4O_5$
The molecular weight (g/mol)	546.57
λ_{max} (nm)*	533

*Absorbance of 0.34 at 533.

Table 2. Properties of Imperon violet KB.

The experiment was performed using four different sets of operating conditions to obtain best parameters. The influence of pH on the EC system was investigated at varying pH values (5–10 by addition of 0.5 M NaOH). Some secondary electrolytes like Na_2SO_4 and NaCl (0.0, 0.02, 0.05 and 0.10 kg/m^3) were added to the wastewater toward investigating the effect of electrolyte support on the removal efficiency. The influence of temperature was studied, ranging from 25 to 45°C using water circulation to sustain the temperature as the EC process proceeds. The IED between the cathode rings and anode impellers were attained for various distance (1, 1.5 and 2 cm). At the end of experimentation, the best operating condition was determined again in triplicate to confirm the accuracy of the EC operation and repeatability for treatment of textile wastewater pollutants. For comparison study using same textile wastewater, the results of the conventional model with parallel electrodes in two phases have been observed by our previous works using EC alone by aluminum plates [9] and on enhancing of EC process by combining with electro-oxidation (EO) using titanium plates [10].

http://dx.doi.org/10.5772/intechopen.76876

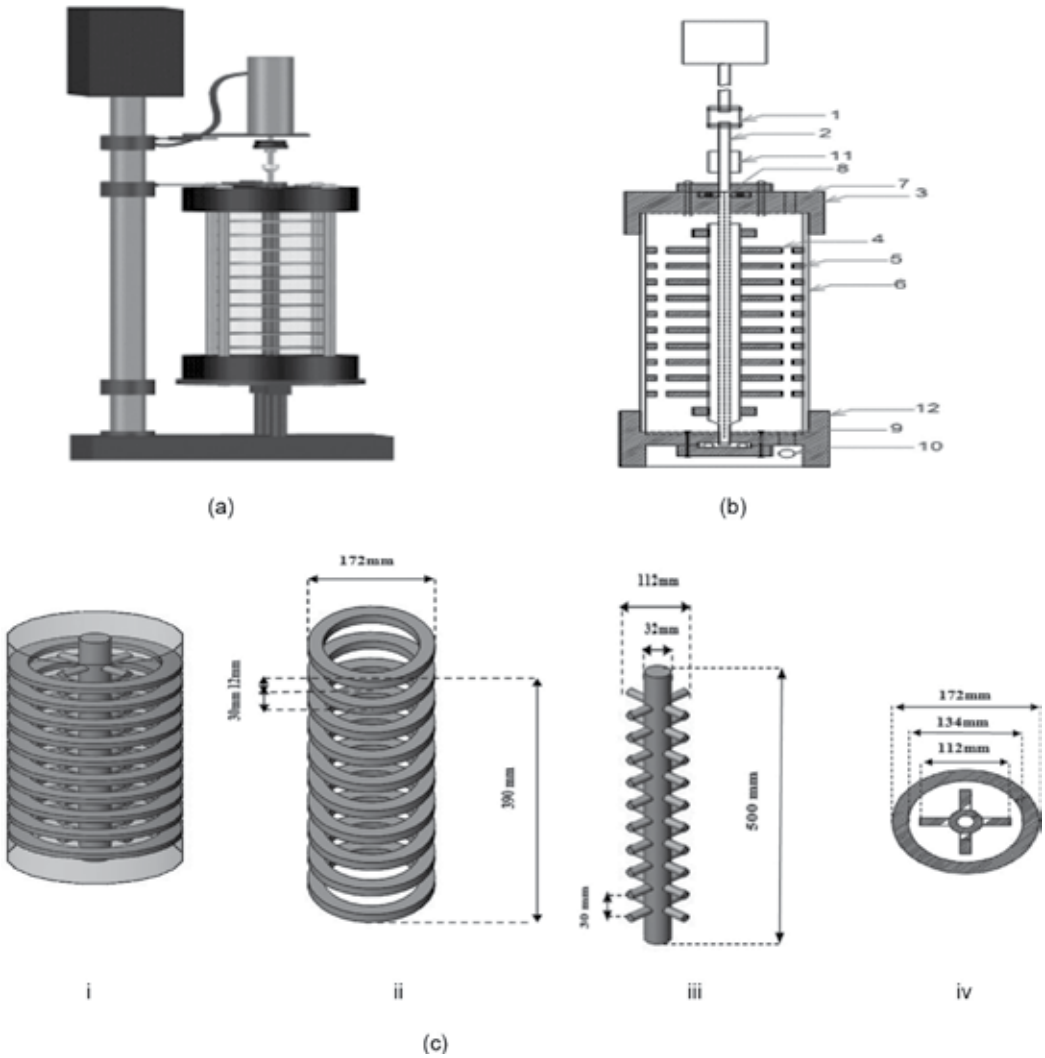

Figure 1. (a) Illustration of EC rotating anode setup. (b) Representation of the EC rotating anode system: (1) motor variable speed, (2) stainless steel shaft (D = 32 mm), (3) Teflon flange cover (upper) (H = 100 mm, D = 280 mm), (4) impeller anode aluminum rod (D = 12 mm, L = 30 mm, no = 4), (5) aluminum ring cathode (T = 12 mm, d.In = 132 mm, D.Out =1 72 mm, no = 10), (6) Perspex reactor (L = 500 mm, d.In = 174 cm, D.Out = 180 mm), (7) upper ports (D = 10 mm, no = 3), (8) ball bearing, (9) thrust bearing, (10) lower port (D = 10 mm), (11) zoom couping and (12) Teflon flange cover (lower) (D = 280 mm, H = 100 mm). (c) Electrode configurations: (i) cathode and anode, (ii) anode impellers, (iii) cathode rings and (iv) top view of cathode rings and impeller anode.

The passivation and adsorption phenomenon was also investigated using the electrochemical impedance spectroscopy. The experiment was performed using AC signal potential amplitude maintained at 10 mV, and the observed frequency range was 0.01–10^5 Hz. A potentiostat was employed to carry out the electrochemical impedance assays. The impedance experiments were performed in a single-partition, three-electrode system, consisting of an Al electrode

(1:25 of the original size) as the working electrode, a platinum wire as a counter electrode and Ag/AgCl (3 M KCl) electrode as a reference electrode.

2.4. Chemical analysis

The efficiency of the new EC reactor for the entire treatment was analyzed based on color removal performances, TSS and COD. For every iteration, the electrical potential was kept constant at 30 V. The COD was determined using a Closed Reflux-Titrimetric technique. The determination of TDS and TSS was performed using gravimetric technique. The phenol content was determined using HPLC. ODS Hypersil C18 column (4.6 mm×150 mm×5 μm) at 25 was employed for separation of aromatic and phenolic compounds with the aid of water/acetonitrile (40/60, v/v) being the mobile phase. The flow rate of the mobile phase and the injection volumes was 1 mL/min and 5 μL. 254 nm detection wavelength was used. The samples were subjected to filtration by using a 0.25 μm membrane filter. The amount of grease and oil (G&O) was determined using solvent extraction technique. The amount of dissolved oxygen (DO) and BOD was determined using DO meter. The turbidity, conductivity and pH were also determined in the present study. The color was analyzed through absorbance using a UV–Vis spectrophotometer with a wavelength corresponding to the peak absorbance value for the textile effluence (533 nm). The sample filtration was carried out with the aid of Whatman 934 AH filter. The rotating anode speed was monitored using a microprocessor digital meter. The ion was analyzed using ionic chromatography ICS-2000. The whole analytical works were performed based on the prescribed procedures in the standard techniques [11]. The determination of color removal, TSS and COD was done using formulas stated by [12–15] among others.

2.5. Sludge compaction analysis

The sludge of the textile wastewater was allowed to sit for 1 h to boost the alliance of the sediments. The two concentrations of cationic polymer (LPM 3135 polymer, 10 and 40 mg/L) were examined to enhance the settling process. The volume of the space engaged by the solid (mL) was measured at fixed time intervals. The weight of the wet residue (the solid portion) was determined, after which the samples were dried for approximately 24 h at 100°C to obtain the whole residual solids. The specific resistance to filtration (SRF) and the cake-dry solid was estimated to properly depict the dewater capability of the sludge using Buchner funnel filtration with pressure (0.015 mPas). The SRF formula (in m/kg) is defined as [16].

$$RF(SRF) = (2KbPA^2)/\mu a_w \quad (1)$$

where P is the pressure during sludge filtration (mPas), A is the filtered area, μ is the viscosity of the filtrate (N.s/m^2), a_w is the weight of the solid per unit volume of filtrate (kg/m^3) and Kb is the slope of the *V* vs. t/*V* plot. Whatman glass fiber filter (Grade 934-AH) was used. Measuring and estimating dryness of the general cake were performed by the following equation:

$$\text{Sludge dryness (\%)} = 100 \times \left[(m_3 - m_1)/(m_2 - m_1)\right] \quad (2)$$

where m_1 and m_2 are the mass of the cup (with the membrane) after and before the filtration process and m_3 is the mass of the same cup after the drying for 24 h at 100°C.

A sludge volume index (SVI) was implemented to decide the settling properties of the sludge suspensions. The SVI (mL/g) is the volume (in mm) used by 1 g of a suspension subject to 30 min of settling [11]. The SVI is defined as.

$$SVI = VD_{30}/TSS \tag{3}$$

where TSS is the concentration of suspended solids (g/L) and VD_{30} is the volume of settled sludge after 30 min (mL/L).

2.6. Economic analysis

The total operating costs for treatment of wastewater process include electricity, equipment, chemical usage, labor, maintenance and sludge disposal. For EC process, the major costs of operation include the cost of electricity and electrode material. In this study, the cost of chemical supplements and sludge disposal was added as well. The total cost of operation (TCO) was computed using [3].

$$TCO = a\,C_{energy} + b\,C_{electrode} + d\,C_{sludge} + e\,C_{chemicals} \tag{4}$$

$$C_{energy} = UIRT/V \tag{5}$$

$$C_{electrode} = M_w\,I\,RT/ZFV \tag{6}$$

where C_{energy} = denotes intake of energy per cubic meter of wastewater (kWh/m^3); $C_{electrode}$ = intake of electrode for treatment of 1 m^3 of wastewater (kg/m^3); C_{sludge} = quantity of sludge per m^3 of wastewater (kg/m^3); $C_{chemical}$ = amount of chemicals (kg/m^3).; a = total cost of electricity (about 0.075US$/kWh); b = cost of iron or aluminum (2.5US$/kg); d = sludge disposal cost excluding the drying and including transportation (0.06US$/kg); e = cost of chemicals that can be added: LPM 3135 polymer (3.0US$/kg), NaOH (0.5US$/kg), Na_2SO_4 (0.25US$/kg) and NaCl (0.06US$/kg); U = voltage; I = intensity of the current; RT = EC electrolysis time; V = textile wastewater working volume; M_w = molar mass of the iron (55.84 g/mol) or aluminum (26.98 g/mol); Z = quantity of electrons moved (3); F = Faraday constant (96,500 C/mol).

The operating expense was computed according to the Iraqi market prices for the year 2017. For EC rotating anode, the total consumption of electrical energy was estimated as follows:

$$C_{energy}\,(kWh/m^3) = \left(C_{energy}\right)_S + \left(C_{energy}\right)_M \tag{7}$$

where $(C_{energy})_M$ signifies the rate at which the DC motor anode rotation consumed electrical energy and $(C_{energy})_S$ signifies the amount of electrical energy consumed by the reacting system

(electricity received by the cathode and the anode because of DC power supply). The values of $(C_{energy})_M$ and $(C_{energy})_S$ were determined from Eq. (5).

3. Results and discussion

3.1. Efficiency and reproducibility of the novel EC reactor

The investigations of the best parameters have been discussed in our previous research [17]. The major EC operation in the textile wastewater was executed in triplicate to confirm the efficiency and reproducibility of the application when the best operating conditions (CD = 4 mA/cm^2, temperature = 25°C, RT = 10 min, pH = 4. 57, rotation speed = 150 rpm and d_e = 1 cm) are used. The performance of the novel EC system was investigated based on the levels of BOD, Al, color, phenols, turbidity, COD, G&O, TDS, DO, nitrates, sulfate, phosphate and TSS. The summary of the results of the parameters is shown in **Figure 2** and **Table 3**. The EC operation exhibited 97.1% total removal efficiency of COD. After the EC treatment process, the G&O and BOD_5 in the wastewater had values of 0.1 and 5 mg/L, respectively. The hydrophobic capacity of G&O resulted in a higher affinity combining with the H_2 bubbles created at the cathode. The (G&O)-H_2 complex gathered on the surface of the liquid, which could be skimmed with ease [18].

The proposed EC design enables superior efficiencies and simultaneously reduces energy consumption in comparison with other reports. Un and Aytac [12] studied textile wastewater treatment by EC process in a packed-bed electrochemical reactor. They reported 96.88% removal efficiency for COD and observed that the color was almost completely removed after 1 h of EC

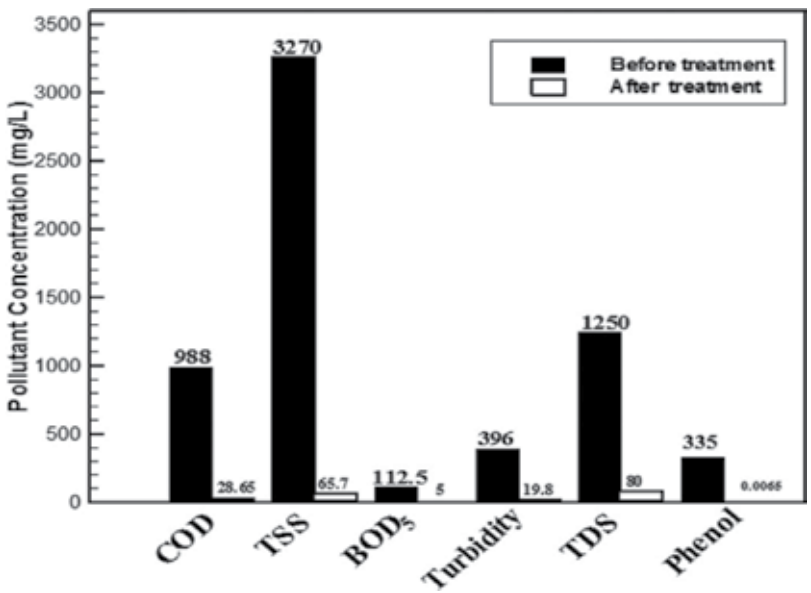

Figure 2. The removal efficacy of several parameters of the textile wastewater using the best operating condition.

Parameters	Raw effluent	Treated effluent	Allowable limit (EPA) 1996	Removal (%)
Electrical conductivity (μS/cm)	1455	2000	ID	—
Initial pH	4.57	4.57	—	—
Final pH	—	6.92	6–8	—
Energy consumption (kwh/m^3)	—	0.966	—	—
Electrode consumption (kg/m^3)	—	0.038		—
Sludge production (kg/m^3)		1.44		
Polymer consumption (kg/m^3)		0.01		
O&G (mg/L)	3	0.1	5–40	96.66
BOD_5 (mg/L)	112.5	5.00	5–45.5	95.55
COD (mg/L)	988	28.65	20–500	97.10
TSS (mg/L)	3270	65.70	60–300	98.00
Color observance at 533 NM	0.3400	0.0051	ID	98.50
TDS (mg/L)	1250	80.00	5–180	93.60
Turbidity (NTU)	396	19.80	15–50	96.00
DO (mg/L)	0.7	14.5	4.5–15	
Sulfate (mg/L)	678	17.00	ID	97.50
Phosphate (mg/L)	7.2	0.23	ID	96.80
Nitrates (mg/L)	11	0.2	ID	98.18
Phenols (mg/L)	335	0.0065	10	99.99
Chlorides Cl^- (mg/L)	33	0.4	ID	—
Aluminum (mg/L)	1.50	6.00	—	—
Electrical energy cost (US$/$m^3$)	—	0.072	—	—
Electrode consumption cost (US$/$m^3$)	—	0.095	—	—
Sludge disposition cost (US$/$m^3$)	—	0.086	—	—
Polymer cost (US$/$m^3$)	—	0.030	—	—
Total operating cost (US$/$m^3$)	—	0.283	—	—

Table 3. Efficiency and reproducibility of EC rotating anode in textile wastewater treatment using the best operating conditions (CD = 4 mA/cm^2, temperature = 25°C, rotation speed = 150 rpm, RT = 10 min, pH = 4.57, d_e = 1 cm).

operation. However, in this work, the 97% COD removal efficiency was obtained after 10 min reaction. Merzouk et al. [15] also studied the textile wastewater treatment using electro-flotation and EC using a batch reactor (electrode gap = 1 cm, conductivity = 2.1 μS/cm, pH = 7.6 and density = 11.55 mA/cm^2). With the best operating conditions, the obtained results are as follow: TSS = 85.5%, color = 93%, COD = 79.7%, BOD_5 = 88.9% and turbidity = 76.2%. Comparing with

the above results, this study utilizes only EC under the best operating conditions and exhibits superior removal efficiencies: TSS 98%, color >98%, BOD_5 = 95.55%, COD 97% and turbidity = 96%. In recent time, El-Ashtoukhy et al. [19] examined phenol removal from wastewater generated from oil refinery using a fixed-bed anode electrochemical reactor consisting random Al raschig rings. At pH = 7, CD = 8.59 mA/cm^2 and concentration of NaCl = 1 g/L, around 80% phenol reduction was observed after 2 h using 40 mg/L as the primary phenol concentration.

In this study, the concentration of primary phenol is 350.0 mg/L, and after 10 min, about 99.99% was extracted, while 0.009 mg/L of phenol remains with the cured wastewater. Furthermore, Martinez-Delgadillo et al. (2012) investigated Cr (VI) reduction to Cr (III) with the aid of Fe (II) in a rotating ring iron electrode. Their report shows up to 99.9% removal of Cr (VI) between 22 and 42 min contact time at an angular velocity ranging from 0 to 230 rpm (at 5 A). In the current study, the optimal reaction time and current were 10 min and 2 A, to confirm the reduction in power consumption and low cost of operation. Moreover, this work also reports high TDS removal efficiency (93.6%) when the best set of operating parameters were used, and the phosphate concentration was decreased to 0.23 from 7.2 mg/L. The Al electrode suspension displayed a rise in the whole dissolved concentration to 6.00 from 1.5 mg/L during the operation. In comparison with the quality standards of global textile wastewater [20, 21], the findings support the analysis of the efficacy of the EC system for treatment of textile wastewater for various usages. The outcomes show that the COD, turbidity, TDS, BOD and DO are all lower than the acceptable limit. Conversely, the generally pH level of the treated effluence was basic (6.9 ± 0.04) to some extent, which is under the acceptable limit. Similarly, the oil and grease, as well as the total phenols, fall under the acceptable limit. Under optimal conditions, the real electrode consumption was 0.038 kg/m^3, while the energy consumption was 0.966 kWh/m^3, 0.9 kWh/m^3 for DC power supply consumption and 0.066 kWh/m^3 for DC motor of rotating anode. For settling metallic sludge study after adding 0.01 kg/m^3 LPM3135 polymers, a 5% sludge dryness and 63 mL/g SVI were noted in the course of the analysis. The sludge production was 1.44 kg/m^3. Furthermore, the SRF utilized in these investigations was (4.6×10^{12}m/kg). The results revealed that the main cost of the treatment operation per m^3 [Eq. (4)] of wastewater, using the best set of operating parameters, is roughly 0.283 US$.

3.2. Comparison performance of the EC rotating anode with the conventional model

Table 4 shows a comparative study between EC rotating anode and the conventional static electrodes in two-phase EC process alone and EC-EO process depending on the results of each model at the optimal conditions. Each model has the same optimal applied current to volume ratio (0.2 A/L). Although the EC model with rotating anode has the lowest surface area to volume ratio (5 m^2/m^3), it can be seen that this reactor model obtained the best removal efficiency of contaminant textile wastewater (COD, TSS and the color). The minimum reaction time (10 min) was achieved by EC model with rotating anode compared with a conventional model in two phases (90 min) which demonstrated the activity of electrodes for the treatment and reduced significantly the energy consumption to 0.966 kwh/m^3. Furthermore, the rotation speed of anode affects the energy consumption by reducing the main voltage and passivation films. The EC process with rotating anode showed excellent treatment without setting the initial pH or using supporting electrolyte. The electrode consumption and sludge production were less than the conventional model with static electrodes. As for the operating costs, the

EC model with rotating anode was lower than the conventional model with static electrodes (EC rotating anode = 0.283US$/$m^3$, while conventional static electrode including EC = 1.76 US$/$m^3$ and EC-EO =1.69 US$/$m^3$).

3.3. Passivation and adsorption phenomenon

Electrochemical impedance spectroscopy is one of the most effective methods for investigation of electrochemical constraints of the electrolyte/electrode interface [22–24]. The impedance method was employed to study the effect of color adsorption on the Al anode and rotation speed (rpm) of the electrode on electrode passivity. The electrolyte was real textile effluence, and the potential of 0 V vs. Ag/AgCl, and frequency ranging from 0.01 to 10^5 Hz, was used for performance evaluation of the electrolyte/anode interface. **Figure 3(a)** presents the Nyquist plot for the anode at varying speed of rotation (0, 75, 100 and 150 rpm). Two semicircles were detected at low frequencies and high frequencies. **Figure 3(b)** presents the best fits for the Al electrode impedance spectra. The fitting parameters comprise the solution resistance (R_s) in parallel with a combination of the double-layer capacitance (C_{dl}) and impedance of the faradic reaction. On the other hand, the faradic reaction impedance comprises passivation resistance (R_{ct}), accompanied by adsorption capacitance (C_{ads}) and adsorption resistance (R_{ads}) [25–28]. **Table 5** summarizes the impedance parameters. Temporarily, the first semicircle diameter signifies the values of R_{ct}, and the diameter of the second semicircle signifies the values of R_{ads}.

Parameters	EC rotating anode	EC static electrode	EC-EO static electrode
Materials	Al-Al	Mp Al-Bp Al	Mp Ti-Bp Al
COD removal (%)	97.10	92.60	93.50
TSS removal (%)	98.00	96.40	97.00
Color removal (%)	98.50	96.50	97.50
Initial pH	Natural	6.00	6.00
Conductivity (μS/cm)	2000	1980	1910
Current/volume ratio (A/L)	0.2	0.2	0.2
Surface area/volume ratio (m^2/m^3)	5	12	12
RT (min)	10	90	90
Electrode consumption (kg/m^3)	0.038	0.1	0.087
Energy consumption (kwh/m^3)	0.966	8.49	9.00
Sludge production (kg/m^3)	1.44	3.50	2.88
NaOH (kg/m^3)	No add	1.26	1.20
NaCl (kg/m^3)	No add	0.1	No add
Operation cost (US$/$m^3$)	0.283	1.76	1.69

Table 4. Comparison of the EC rotating anode with the conventional model static electrode (EC alone and EC-EO) at optimal conditions.

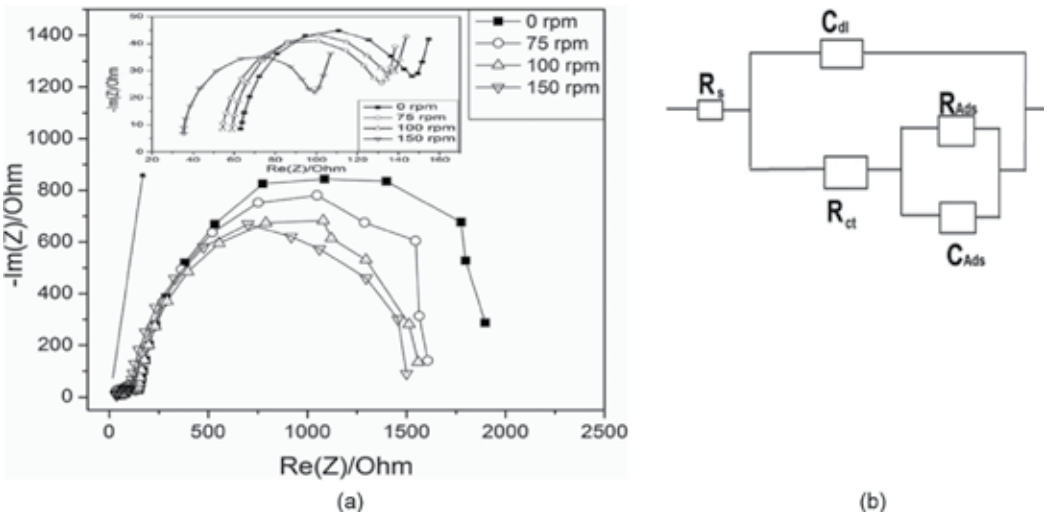

Figure 3. (a) Nyquist plots of the Al anode in an aqueous textile wastewater solution at 25°C temperature and varying electrode speed of rotation. (b) Equivalent circuits utilized to fit the Nyquist plots.

Rotation speed (rpm)	R_s(Ω)	R_{ct}(Ω)	C_{dl}(μF)	R_{ads} (Ω)	C_{ads}(μF)
0	63.30	96.98	0.128	1774	7.18
75	56.90	88.89	0.129	1531	7.36
100	59. 08	90.00	0.145	1369	7.13
150	40.54	41.65	0.412	1151	8.31

Table 5. Electrochemical impedance data extracted from the Nyquist plots at varying speed of rotation (rpm).

From **Table 5** and **Figure 3(a)**, it is clear that the values of R_{ct} and R_{ads} significantly declined with a rise in the rotation speed of the Al anode from 0 attaining the lowest value at 150 rpm. Therefore, the fouling rate of the anode was lessened, and the rate of adsorption of color to the interface of the anode increased at 150 rpm. Conversely, the highest values of the adsorption capacitance and double-layer capacitance were observed at 150 rpm. This elucidates the improvement in the rate of removal upon rotating the anode at 150 rpm as the EC experiment proceeds. It also confirms that the designed model can be a panacea to the limitation of the previous model.

4. Conclusions

The use of novel EC reactor in textile wastewater treatment exhibits a higher removal efficiency than the erstwhile models. The efficiency of the textile effluence pollutant removal with high values was achieved using a lower CD, precisely 4 mA/cm^2, at initial reaction period (10 min) at 1 cm interelectrode distance (IED) and 150 rpm anode rotation speed. A rise in the value of CD enhanced the efficiency of EC process in the treatment of textile wastewater. The setting of the

solution pH to increase the solution temperature and the addition of any chemicals (Na_2SO_4 or NaCl) is not required. The economic viability of the operation of the reactor is influenced by the parameters. The energy and electrode consumption of the EC increases as the CD increases. The optimal energy and electrode consumptions were 0.038 kg/m^3 and 0.966 kWh/m^3, which led to the lower cost of operation (0.283US$/m^3). The novel EC reactor with rotating anode significantly enhanced the textile wastewater treatment by improving the pollutant removal rate, reducing reaction time of treatment, without any additional chemicals during the process, and reducing the operation cost compared to conventional model (EC and EC-EO). It was found that the passivation phenomenon reduced with the increased rotation speed of anode, which enhanced the EC process performance and validated the novel reactor design.

Acknowledgements

The authors thank Babylon Textile Plant, Iraq, for supplying the textile wastewater. They also thank for Almuthana University Iraq and Ministry of Higher Education Iraq for funding this research.

Conflict of interest

The authors whose names are listed in the beginning of this chapter certify that they have no affiliations with or involvement in any organization or entity with any financial interest (such as honoraria; educational grants; participation in speakers' bureaus; membership, employment, consultancies, stock ownership or other equity interest; and expert testimony or patent-licensing arrangements) or nonfinancial interest (such as personal or professional relationships, affiliations, knowledge or beliefs) on the subject matter or materials discussed in this manuscript.

Author details

Ahmed Samir Naje[1]*, Mohammed A. Ajeel[2], Peter Adeniyi Alaba[3] and Shreeshivadasan Chelliapan[4]

*Address all correspondence to: ahmednamesamir@yahoo.com

1 Department of Architect Engineering, College of Engineering, Almuthana University, Almuthana Governorate, Iraq

2 Al-Karkh University of Science, Baghdad, Iraq

3 Department of Chemical Engineering, Covenant University, Sango-Ota, Ogun-State, Nigeria

4 Department of Engineering, Razak Faculty of Technology and Informatics, Universiti Teknologi Malaysia, Malaysia

References

[1] Chen G. Electrochemical technologies in wastewater treatment. Separation and Purification Technology. 2004;**38**:11-41

[2] Mook WT, Ajeel MA, Aroua MK, Szlachta M. The application of iron mesh double layer as anode for the electrochemical treatment of reactive black 5 dye. Journal of Environmental Sciences. 2016;**54**:184-195

[3] Dalvand A, Gholami M, Joneidi A, Mahmoodi NM. Dye removal, energy consumption and operating cost of electrocoagulation of textile wastewater as a clean process. CLEAN–Soil, Air, Water. 2011;**39**:665-672

[4] Ajeel MA, Aroua MK, Daud WHAW. Preparation and characterization of carbon black diamond composite electrodes for anodic degradation of phenol. Electrochimica Acta. 2015;**153**:379-384

[5] Martínez A, Urios A, Blanco M. Mutagenicity of 80 chemicals in Escherichia coli tester strains IC203, deficient in OxyR, and its oxyR+ parent WP2 uvrA/pKM101: Detection of 31 oxidative mutagens. Mutation Research/Genetic Toxicology and Environmental Mutagenesis. 2000;**467**:41-53

[6] Mollah MY, Morkovsky P, Gomes JA, Kesmez M, Parga J, Cocke DL. Fundamentals, present and future perspectives of electrocoagulation. Journal of Hazardous Materials. 2004;**114**:199-210

[7] Martinez-Delgadillo S, Mollinedo-Ponce H, Mendoza-Escamilla V, Gutiérrez-Torres C, Jiménez-Bernal J, Barrera-Diaz C. Performance evaluation of an electrochemical reactor used to reduce Cr(VI) from aqueous media applying CFD simulations. Journal of Cleaner Production. 2012;**34**:120-124

[8] Holt P, Barton G, Mitchell C. Electrocoagulation as a wastewater treatment. The Third Annual Australian Environmental Engineering Research Event, Vol. 1000. 1999. pp. 41-46

[9] Naje AS, Chelliapan S, Zakaria Z, Abbas SA. Treatment performance of textile wastewater using electrocoagulation (EC) process under combined electrical connection of electrodes. International Journal of Electrochemical Science. 2015;**10**:5924-5941

[10] Naje AS, Chelliapan S, Zakaria Z, Abbas SA. Enhancement of an electrocoagulation process for the treatment of textile wastewater under combined electrical connections using titanium plates. International Journal of Electrochemical Science. 2015;**10**:4495-4512

[11] APHA, Standard Methods for the Examinations of Water and Wastewater. 20th Edition, American public Health association. Washington DC: American Water Works Association and Water Environmental federation; 1998. p. 20

[12] Un UT, Aytac E. Electrocoagulation in a packed bed reactor-complete treatment of color and cod from real textile wastewater. Journal of Environmental Management. 2013;**123**:113-119

[13] Bayar S, Yıldız YŞ, Yılmaz AE, İrdemez Ş. The effect of stirring speed and current density on removal efficiency of poultry slaughterhouse wastewater by electrocoagulation method. Desalination. 2011;**280**:103-107

[14] Aoudj S, Khelifa A, Drouiche N, Hecini M, Hamitouche H. Electrocoagulation process applied to wastewater containing dyes from textile industry. Chemical Engineering and Processing: Process Intensification. 2010;**49**:1176-1182

[15] Merzouk B, Madani K, Sekki A. Using electrocoagulation–electroflotation technology to treat synthetic solution and textile wastewater, two case studies. Desalination. 2010;**250**: 573-577

[16] Djedidi Z, Khaled JB, Cheikh RB, Blais J-F, Mercier G, Tyagi RD. Comparative study of dewatering characteristics of metal precipitates generated during treatment of monometallic solutions. Hydrometallurgy. 2009;**95**:61-69

[17] Naje AS, Chelliapan S, Zakaria Z, Abbas SA. Electrocoagulation using a rotated anode: A novel reactor design for textile wastewater treatment. Journal of Environmental Management. 2016;**176**:34-44

[18] Asselin M, Drogui P, Brar SK, Benmoussa H, Blais J-F. Organics removal in oily bilgewater by electrocoagulation process. Journal of Hazardous Materials. 2008;**151**:446-455

[19] El-Ashtoukhy E, El-Taweel Y, Abdelwahab O, Nassef E. Treatment of petrochemical wastewater containing phenolic compounds by electrocoagulation using a fixed bed electrochemical reactor. International Journal of Electrochemical Science. 2013;**8**:1534-1550

[20] EPA. Best Management Practices for Pollution Prevention in the Textile Industry. Ohio, USA: EPA; 1996

[21] Naje AS, Chelliapan S, Zakaria Z, Ajeel MA, Alaba PA. A review of electrocoagulation technology for the treatment of textile wastewater. Reviews in Chemical Engineering. 2017;**33**:263-292

[22] Brett CM, Brett AO, Electrochemistry P. Methods and Applications. Oxford: Oxford University Press; 1993

[23] Oliveira SCB, Oliveira-Brett AM. Voltammetric and electrochemical impedance spectroscopy characterization of a cathodic and anodic pre-treated boron doped diamond electrode. Electrochimica Acta. 2010;**55**:4599-4605

[24] Ajeel M, Aroua MK, Daud WMAW. Reactivity of carbon black diamond electrode during the electro-oxidation of Remazol brilliant blue R. RSC Advances. 2015;**169**:46-51

[25] Sakharova A, Nyikost L, Pleskov Y. Adsorption and partial charge transfer at diamond electrodes—I. Phenomenology: An impedance study. Electrochimica Acta. 1992;**37**: 973-978

[26] Hernando J, Lud SQ, Bruno P, Gruen DM, Stutzmann M, Garrido JA. Electrochemical impedance spectroscopy of oxidized and hydrogen-terminated nitrogen-induced conductive ultrananocrystalline diamond. Electrochimica Acta. 2009;**54**:1909-1915

[27] Bo Z, Wen Z, Kim H, Lu G, Yu K, Chen J. One-step fabrication and capacitive behavior of electrochemical double layer capacitor electrodes using vertically-oriented graphene directly grown on metal. Carbon. 2012;**50**:4379-4387

[28] Ajeel MA, Aroua MK, Daud WMAW, Mazari SA. Effect of adsorption and passivation phenomena on the electrochemical oxidation of phenol and 2-chlorophenol at carbon black diamond composite electrode. Industrial & Engineering Chemistry Research. 2017;**56**:1652-1660

Chapter 7

Innovation of Coagulation-Flocculation Processes Using Biopolyelectrolytes and Zeta Potential for Water Reuse

Eduardo A. López-Maldonado and
Mercedes T. Oropeza-Guzmán

Additional information is available at the end of the chapter

http://dx.doi.org/10.5772/intechopen.75898

Abstract

The coagulation-flocculation process is one of the conventional technologies used for the treatment of different types of industrial wastewater. The zeta potential is a key parameter that allows to determine the effective pH, the type and the correct biopolyelectrolyte dose to return the water quality using coagulation-flocculation. In this chapter, we present the application of a natural cationic biopolyelectrolyte (chitosan) to make the separation and recovery of cellulose fiber more efficient and to increase the reuse of treated water from the pulp and paper industry. The result of the coagulation-flocculation test at pH 5.4 and a chitosan dose = 10 mg/L shows that the treated water has the following values: biochemical oxygen demand = 150 mg O_2/L, turbidity = 5 FAU, total suspended solids = 2 mg/L, chemical oxygen demand = 200 mg/L and hardness = 250 mg $CaCO_3$/L. The quality of water obtained allows its discharge to a natural water body, in which it is possible to continue with a biological treatment stage, or to reuse the treated water for the manufacture of paper. Additionally, this coagulation-flocculation process can be coupled to an advanced oxidation process to increase the quality of the water and mineralize the content of organic material.

Keywords: zeta potential, wastewater treatment, biopolyelectrolytes, coagulation-flocculation

1. Introduction

The issue regarding the quality and use of water has several aspects: the first option is the most common and of greater importance, than a simple view, which becomes the vital liquid

to survive and perform daily activities. Its quality directly affects the health and well-being of society [1]. The second corresponds to the use of water as the main raw material for the manufacture of some products and the operation of production processes. The interaction of water with the environment is influenced by the water quality that both society and the industrial sector confer on water.

Each type of industry has a particular interest in the care of water quality and its reuse, which is why day by day, they require new strategies to treat and recycle the wastewater they generate in the different production processes [1]. Water quality is affected by various chemical substances that dissolve in water used in each stage of the manufacturing process.

In general, the main pollutants that are identified in the industrial wastewater are suspended particles, organic matter, heavy metals, the hardness of the water and fats and oils [2]. One of the pollutants frequently present in the industrial wastewater is suspended particles or solids. According to the nature of the production processes, the particles in suspension can be organic and inorganic and can be present in different particle sizes. The content of organic matter in industrial wastewater is attributed to the organic compounds (colorants, additives, nutrients, carbohydrates, etc.) that can be biodegradable or difficult to be degraded, and that are incorporated into the water at the time of use [3]. The levels of concentration in which these contaminants or undesirable substances are present in the wastewater are directly related to the operating conditions of the productive processes. The presence of these pollutants in the water causes an impact on the efficiency of the production processes, limits the reuse of water, increases the consumption of clean water, the discharge of the wastewater generated contaminates the water bodies, and this implies sanctions to the industry for exceeding the maximum permissible limits at the effluent discharge point [3].

There is an urgent need of environmentally friendly and cheaper technologies to eliminate the chemical toxicants from wastewater to improve the water quality.

Several methods that have been developed to eliminate these present pollutants from wastewater are as follows: reverse osmosis, solvent extraction, coagulation-flocculation, membrane separation, chemical precipitation, advanced oxidation processes, ion exchange, evaporation, electrolysis [4–6], photochemical [7], activated sludge [8], anaerobic and aerobic treatment [9, 10], electrodialysis [11], ultrasonic treatment [12], magnetic separation [13] and adsorption [14–16].

As part of the integral management of water in the industry, the development of environmentally friendly technologies is involved. In this chapter, we propose one of the strategies to restore the water quality (decontaminate, purify, remove undesirable substances for a specific use), which consists of the application of natural functional polymeric materials in physicochemical/electrochemical systems for the elimination of contaminants [17]. One of the simple and efficient methods for the separation of various types of contaminants is coagulation-flocculation, in which chemical substances are used as synthetic coagulant-flocculating agents (polyelectrolytes) [18]. However, in order to employ the different renewable sources, which are rich in polymeric materials and available in the region, as shrimp waste from the fishing industry will be used as a raw material for the production of functional polyelectrolytes and give it an added value. Due to the type of interactions that occur at a molecular level between the contaminants and the polyelectrolytes in the coagulation-flocculation processes, the zeta

http://dx.doi.org/10.5772/intechopen.75898

potential measurements are key to determine the best operating conditions and understand the mechanisms of interface (contaminant-biopolyelectrolyte). In this chapter, the physicochemical characterization of six types of industrial wastewater is presented. Due to the complexity and variety of the contaminants present in these types of wastewater, only the wastewater treatability results of the pulp and paper industry are presented.

2. Experimental

2.1. Wastewater sampling

In this chapter, the physicochemical characterization of six types of industrial wastewater and how to develop a treatment strategy for water recovery and how to add value to the byproducts formed are presented. The wastewater sampling protocol was followed as recommended by Mexican sampling standard (NMX-AA-003-1980). Residual water samples were taken from the nixtamalization industry (nejayote) that is dedicated to the manufacture of corn products and their derivatives. Another sample was collected from a candy factory that generates wastewater with a high content of dyes and suspended particles. The third case corresponds to a company dedicated to the recycling of cellulose and paper, which uses well water for its paper and cardboard manufacturing process. Another type of water sample was collected from the industry that is dedicated to the collection of hazardous waste that contains a greater proportion of oil and water. Finally, there is the sector dedicated to the metalworking industry and the semiconductor industry. Tested parameters were: total solids (TS), total dissolved solids (TDS), total suspended solids (TSS), turbidity, color, particle size, electrical conductivity (EC), zeta potential (ζ), total phosphorous (TP), biological oxygen demand (BOD_5), chemical oxygen demand (COD), total organic carbon (TOC) and total nitrogen (TN). Tests were carried out following the current Mexican standard procedures that are equivalent to those published by EPA (AWWA standard methods, respectively).

2.2. Extraction of chitosan biopolyelectrolyte

Chitosan (Ch) was obtained from waste shrimp shells using the adapted method proposed by the authors Goycoolea et al. [19].

2.3. Zeta potential = f (pH) profiles of the industrial wastewater and chitosan

Zeta Potential from wastewater and biopolyelectrolyte data was recorded on a Stabino Particle Charge Mapping (Microtrac). The measurements were done at ambient temperature in Teflon cuvettes. Influence of pH on the zeta potential behavior of each biopolyelectrolytes was studied within a pH range of 2–11 with 0.1 M NaOH and 0.1 M HCl [20].

2.4. Wastewater coagulation-flocculation tests using chitosan

The performance of cationic chitosan biopolyelectrolyte in the coagulation-flocculation of wastewater from the cellulose and paper recycling industry was carried out using 20 mL of residual water at pH 5.4 and in different doses of chitosan extracted from the shrimp shells.

After each addition of chitosan, the mixture of residual water with chitosan was stirred at 200 rpm for 2 min and subsequently at 50 rpm for 20 min. For the evaluation of the quality of the treated water, a sample of the supernatant was extracted [21].

3. Results and discussion

Tables 1 and **2** show the physicochemical characterization of the six types of industrial wastewater. The values of the main residual water quality parameters such as BOD_5, COD, alkalinity, hardness, pH, electrical conductivity, content of dissolved and suspended solids, settleable solids, temperature, turbidity, nitrogen and total phosphorus, heavy metals are shown. Of these normative parameters, the environmental legislation dictates which ones must comply, considering the type of industry and body of discharge of residual water. Additionally, other non-regulated parameters, which are fundamental to understand and operate the coagulation-flocculation process, such as particle size, turbidity, total organic carbon, biodegradability and zeta potential [21]. The measurement of these parameters is key to implement the design and sequence of an industrial wastewater treatment train to achieve the best quality of treated water.

In all types of wastewater, the regulated parameters exceed the maximum permissible limits, both for their discharge to the water receiving bodies and for their reuse. One of the main pollutants present in industrial wastewater is the content of dissolved and suspended solids, where these can be organic and inorganic depending on the source of the wastewater. Generally, the first stage of a wastewater treatment train consists of the elimination of the suspended particles; this is where the coagulation-flocculation processes are applied. Considering the main interactions that occur between the suspended particles and the coagulant-flocculant agents, the zeta potential is a key parameter to determine the surface charge density of the suspended particles and the polyelectrolytes, as well as the optimum dose to perform the solid-liquid separation of the suspended particles.

Figure 1 shows the $\zeta = f(pH)$ profiles of each type of industrial wastewater, metalworking, candy factory, nejayote, recycled oils, recycled cellulose and paper. These profiles show that all the wastewater has negative zeta potential values at $pH > 5$, while at $pH < 5$, zeta potential values are close to neutrality or positive. With exception, the wastewater from the electroplating processes shows positive zeta potential values at $pH < 6.0$, and at $pH > 7.0$ presents negative zeta potential values. As expected, in order to carry out a coagulation-flocculation process in an efficient way, it is necessary to add a polyelectrolyte with a positive charge to neutralize the negative charge of the wastewater from the pulp and paper industry. The monitoring of the zeta potential value with respect to the polyelectrolyte dose in the wastewater allows to construct the coagulation-flocculation operation curves, and this ensures that the operators of the wastewater treatment plants avoid the problem of overdosing of coagulant-flocculant agents and save on the consumption of chemical substances [22]. In this chapter, the capacity of a biopolyelectrolyte extracted from the shrimp waste for the clarification of wastewater from the cellulose and paper recycling industry was evaluated. This was done with the aim of increasing the reuse potential of the treated water and improving the efficiency of solid-liquid separation processes for the recovery of cellulose fiber present in industrial wastewater.

Parameter	Nixtamalization wastewater	Parameter	Candy Industry wastewater
Temperature (°C)	38	Temperature (°C)	26
Sedimentable solids, SS (mL/L)	850	SS (mL/L)	25
Total Dissolved Solids, TDS (mg/L)	47,200	TDS (mg/L)	12,743
Total Suspended Solids, TSS (mg/L)	2000	TSS (mg/L)	2342
Turbidity (FAU)	1500	Turbidity (FAU)	1676
Alkalinity (mg/L $CaCO_3$)	1025	Alkalinity (mg/L $CaCO_3$)	500
Electric conductivity, EC (mS/cm)	5.42	EC (mS/cm)	1.30
ζ (mV)	−10.5	ζ (mV)	−25.7
Particle size of dissolved part (nm)	100–600	Particle size of dissolved part (nm)	300–800
Color (Pt-Co)	8580	Color (Pt-Co)	6572
pH	10.0–12.0	pH	6.7
Chemical Oxygen Demand, COD (mg O_2/L)	28,450	COD (mg O_2/L)	786
Total Organic Carbon, TOC (mg C/L)	9836	TOC (mg C/L)	250
Biochemical Oxygen Demand, BOD_5 (mg O_2/L)	2700	BOD_5 (mg O_2/L)	653
Total Phosphorus, TP (mg P/L)	1321	TP (mg P/L)	142
Total Nitrogen, TN (mg N/L)	418	TN (mg N/L)	120
Biodegradability (BOD_5/COD)	0.27	Biodegradability (BOD_5/COD)	0.83
Parameter	**Recycled cellulose and paper wastewater**	**Parameter**	**Recycled oils wastewater**
Temperature (°C)	35	Temperature (°C)	28
Chlorides (mg/L)	900	Zn (mg/L)	10.2
Total hardness (mg/L)	3800	Cu (mg/L)	12.2
Alkalinity (mg/L $CaCO_3$)	850	Alkalinity (mg/L $CaCO_3$)	100
Fats and oils (mg/L)	11	Fats and oils (mg/L)	6732
TSS (mg/L)	500	TSS (mg/L)	15,000
TDS (mg/L)	3500	TDS (mg/L)	3500
SS (mL/L)	438	SS (mL/L)	438
Turbidity (FAU)	560	Turbidity (FAU)	350
EC (mS/cm)	1.00	EC (mS/cm)	2.00
ζ (mV)	−25.8	ζ (mV)	−2.1

Parameter	Recycled cellulose and paper wastewater	Parameter	Recycled oils wastewater
Particle size (nm)	500	Particle size (nm)	750
Color (Pt-Co)	3000	Color (Pt-Co)	2340
pH	5.4	pH	7.63
COD (mg O_2/L)	8000	COD (mg O_2/L)	43,650
TOC (mg C/L)	1890	TOC (mg C/L)	5200
BOD_5 (mg O_2/L)	4000	BOD_5 (mg O_2/L)	17,500
Total Nitrogen, TN (mg N/L)	88	Biodegradability (BOD_5/COD)	0.4
Total Phosphorus, TP (mg P/L)	16		
Biodegradability (BOD_5/COD)	0.5		

Table 1. Physicochemical characterization of industrial wastewater: Nixtamalization, recycled cellulose and paper and recycled oils wastewater.

Parameter	Electroplating wastewater	Parameter	Metalworking wastewater
Temperature (°C)	25	Temperature (°C)	32
Sn (mg/L)	4854	Zn (mg/L)	7.78
Pb (mg/L)	1044	Ni (mg/L)	41.57
Fe (mg/L)	683	Cr (mg/L)	7.44
TSS (mg/L)	4510	Cd (mg/L)	0.47
Turbidity (FAU)	2990	SS (mg/L)	9
EC (mS/cm)	74	Fats and oils (mg/L)	465.66
ζ (mV)	26	TSS (mg/L)	3352.63
Particle size (nm)	346	Turbidity (FAU)	2990
Color (Pt-Co)	6742	EC (mS/cm)	327
pH	0.8	ζ (mV)	−10.0
COD (mg O_2/L)	1432	Particle size (nm)	678
TOC (mg C/L)	125	Color (Pt-Co)	2500
BOD_5 (mg O_2/L)	30	pH	7.36
TN (mg N/L)	50.6	COD (mg O_2/L)	64,800
Biodegradability (BOD_5/COD)	0.02	TOC (mg C/L)	3858
		BOD_5 (mg O_2/L)	2857
		TN (mg N/L)	316.8
		Biodegradability (BOD_5/COD)	0.04

Table 2. Physicochemical characterization of industrial wastewater: Electroplating and metalworking wastewater.

http://dx.doi.org/10.5772/intechopen.75898

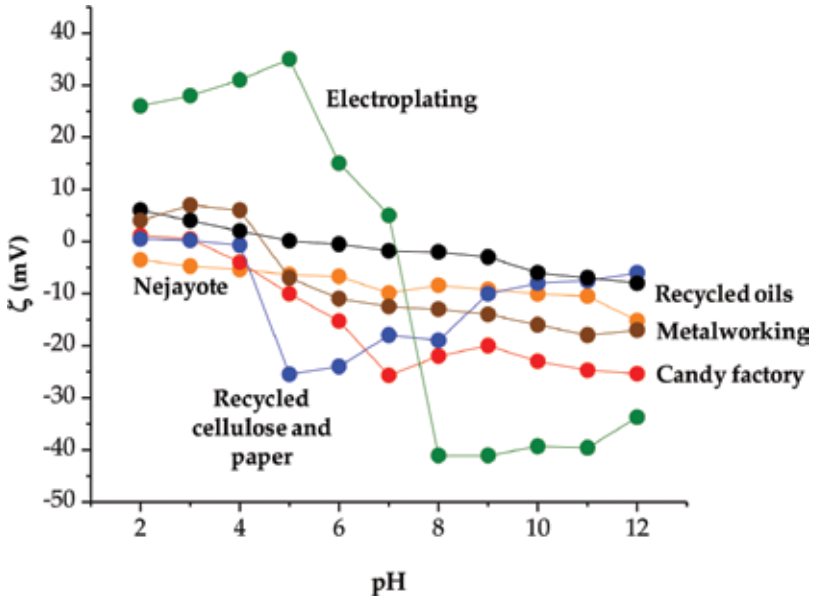

Figure 1. ζ = f (pH) profiles from industrial wastewater: Candy factory, metalworking, recycled oils, nejayote, electroplating and recycled cellulose and paper.

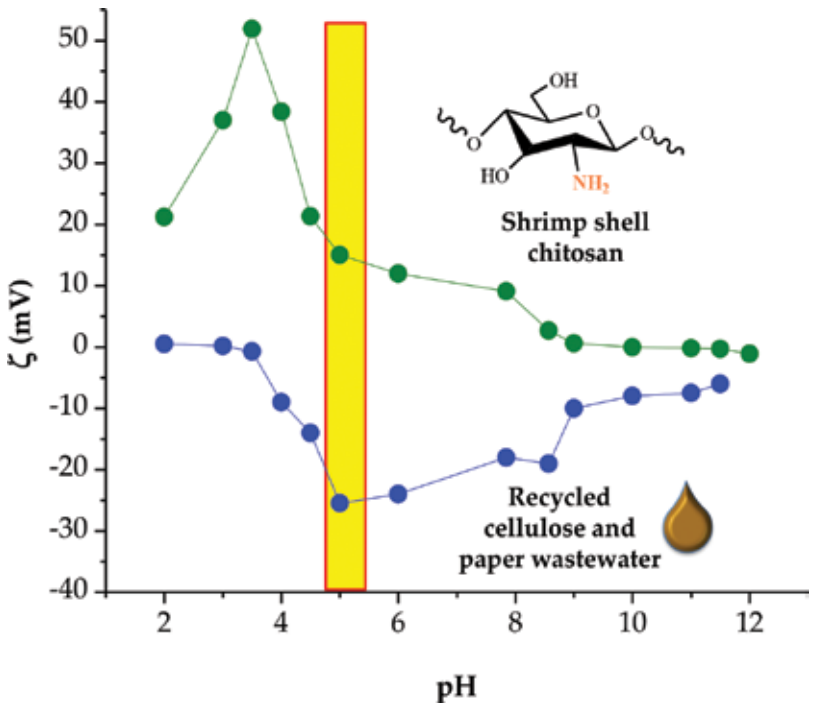

Figure 2. ζ = f (pH) profiles of recycled cellulose and paper wastewater and chitosan.

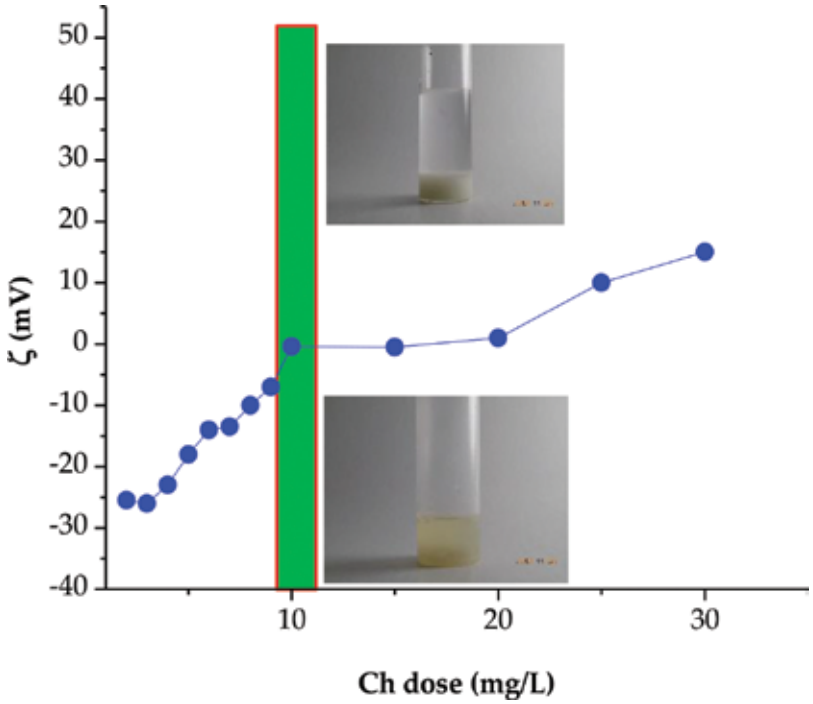

Figure 3. ζ = f (chitosan dose) in coagulation-flocculation tests from recycled cellulose and paper wastewater.

Figure 2 shows the variation of zeta potential with respect to the pH of the wastewater and chitosan. The zeta potential value of the wastewater shows that the suspended particles have a negative surface charge density at pH 5–9. The ζ = f (pH) profile shows that at pH = 4.0 and pH > 10.0, the wastewater has two isoelectric points (ζ = 0). The stability of the particles to remain suspended is due to the value of the negative zeta potential (ζ = −25.5 mV). In order to destabilize the dispersion of cellulose fiber particles, the addition of a cationic coagulant-flocculant agent that allows the neutralization of the negative surface charge is necessary. The wastewater at pH 5.4 has a ζ = −25.5 mV and the chitosan ζ = 15.0 mV, the dosage of chitosan at this pH by pure electrostatic interaction ensures its reaction.

In **Figure 3**, it is shown that the zeta potential value of the wastewater from cellulose and paper industry increases linearly as the dose of chitosan increases (ζ = −25.5 mV to ζ = −5.1 mV), reaching the isoelectric point at a dose of 10 mg/L chitosan. The water treated at pH 5.4 with chitosan has a value of BOD_5 = 150 mg O_2/L, turbidity = 5 FAU, TSS = 2 mg/L, COD = 200 mg/L and hardness = 250 mg $CaCO_3$/L, and the treated water with these physicochemical characteristics can be discharged into the municipal sewer system or reused as process water.

4. Conclusions

The wastewater generated by industries is becoming more complex and difficult to treat to restore its quality and reuse it. The coagulation-flocculation process has become one of the

most used technologies to remove suspended particles, dyes and heavy metals; however, one of the trends consists of the substitution of synthetic coagulant-flocculant agents with biopolyelectrolytes. This leads to the development of environmentally friendly technologies, and take advantage of the waste that contains biodegradable polymeric materials and with high potential for its application in the elimination of toxic pollutants from industrial wastewater. In this chapter, the wastewater treatment of the cellulose and paper industry was carried out through a coagulation-flocculation process using a dose of 10 mg/L chitosan at pH 5.4. Through the zeta potential measurements, the pH = 5.4 at which the chitosan and the wastewater have an opposite electric charge was determined, and the best dose of chitosan to maximize the recovery of cellulose fiber and obtain the best quality of treated water.

Acknowledgments

The authors thank the Autonomous University of Baja California for the financing granted for the development of this project (UABC-PTC-668).

Conflict of interest

The authors state that there is no conflict of interest.

Author details

Eduardo A. López-Maldonado[1]* and Mercedes T. Oropeza-Guzmán[2]

*Address all correspondence to: elopez92@uabc.edu.mx

1 Faculty of Chemical Sciences and Engineering, Autonomous University of Baja California, Tijuana, Mexico

2 Graduate and Research, Center of the Technical Institute of Tijuana, Tijuana, México

References

[1] Muralikrishna IV, Manickam V, editors. Environmental Management: Science and Engineering for Industry. United States: Elsevier; 2017. pp. 295-336

[2] Cahoon LB, Mallin MA. Water quality monitoring and environmental risk assessment in a developing coastal region, southeastern North Carolina. In: Ahuja S, editor. Monitoring Water Quality. Amsterdam: Elsevier; 2013. pp. 149-169

[3] Suthar S, Sharma J, Chabukdhara M, Nema A. Water quality assessment of river Hindon at Ghaziabad, India: Impact of industrial and urban wastewater. Environmental Monitoring and Assessment. 2010;**165**:103-112

[4] Ali A, Saeed K. Phenol removal from aqueous medium using chemically modified banana peels as low-cost adsorbent. Desalination and Water Treatment. 2015;**57**:11242-11254

[5] Gupta VK, Ali I. Removal of endosulfan and methoxychlor from water on carbon slurry. Environmental Science & Technology. 2008;**42**:766-770

[6] Wojnarovits L, Foldvary CM, Takacs E. Radiation-induced grafting of cellulose for adsorption of hazardous water pollutants: A review. Radiation Physics and Chemistry. 2010;**79**:848-862

[7] Fox MA, Dulay MT. Heterogeneous photocatalysis. Chemical Reviews. 1993;**93**:341-357

[8] Bromley-Challenor KCA, Knapp JS, Zhang Z, Gray NCC, Hetheridge MJ, Evans MR. Decolorization of an azo dye by unacclimated activated sludge under anaerobic conditions. Water Research. 2000;**34**:4410-4418

[9] dos Santos AB, Cervantes FJ, van Lier JB. Review paper on current technologies for decolorisation of textile wastewaters: Perspectives for anaerobic biotechnology. Bioresource Technology. 2007;**98**:2369-2385

[10] Shen H, Wang YT. Biological reduction of chromium by E. Coli. Journal of Environmental Engineering. 1994;**120**:560-572

[11] Ali I, Khan TA, Asim M. Removal of arsenic from water by electrocoagulation and electrodialysis techniques. Separation & Purification Reviews. 2011;**40**:25-42

[12] Suzuki Y, Maezawa A, Uchida S. Utilization of ultrasonic energy in a photocatalytic oxidation process for treating waste water containing surfactants. Japanese Journal of Applied Physics. 2000;**39**:2958-2961

[13] Karapinar N. Magnetic separation of ferrihydrite from wastewater by magnetic seeding and high-gradient magnetic separation. International journal of mineral processing. 2003;**71**:45-54

[14] Gupta VK, Ali I. Removal of endosulfan and methoxychlor from water on carbon slurry. Environmental Science & Technology. 2008;**42**:766-770

[15] Hashem FS, Amin MS. Adsorption of methylene blue by activated carbon derived from various fruit peels. Desalination and Water Treatment. 2016;**57**:22573-22584

[16] Hossain MA, Ngo HH, Guo WS, Nguyen TV. Removal of copper from water by adsorption onto banana peel as bioadsorbent. International Journal of GEOMATE. 2012;**2**:227-234

[17] Chitanu GC, Carpov A. Ecologically benign polymers: The case of maleic polyelectrolytes. Environmental Science and Technology. 2002;**36**:1856-1860

[18] Abiola Oladoja N. Headway on natural polymeric coagulants in water and wastewater treatment operations. Journal of Water Process Engineering. 2015;**6**:174-192

[19] Goycoolea F, Agullo E, Mata R. Sources and processes of obtaining. In: Pastor de Abram A, editor. Chitin and Chitosan: Obtaining, Characterization and Applications. 1ra ed.

San Miguel, Peru: Fondo editorial de la Pontificia Universidad Catolica del Perú; 2004. pp. 103-154

[20] López-Maldonado EA, Ochoa-Terán A, Oropeza-Guzmán MT. A multiparameter colloidal titrations for the determination of cationic polyelectrolytes. Journal of Enviromental Protection. 2012;**3**:1559-1570. DOI: 10.4236/jep.2012.311172

[21] López-Maldonado EA, Oropeza-Guzman MT, Jurado-Baizaval JL, Ochoa-Terán A. Coagulation–flocculation mechanisms in wastewater treatment plants through zeta potential measurements. Journal of Hazardous Materials. 2014;**279**:1-10

[22] López-Maldonado EA, Oropeza-Guzman MT, Ochoa-Terán A. Improving the efficiency of a coagulation-flocculation wastewater treatment of the semiconductor industry through zeta potential measurements. Journal of Chemistry. 2014;**2014**:1-10

Chapter 8

The Role of Bacteria on the Breakdown of Recalcitrant Polychlorinated Biphenyls (PCBs) Compounds in Wastewater

Spar Mathews and Patricia Sithebe

Additional information is available at the end of the chapter

http://dx.doi.org/10.5772/intechopen.75400

Abstract

Pseudomonas aeruginosa was used to assess their potentials to degrade PCBs at concentrations of 1.0 μg/mL. An aliquot of 1.0 μL of the bacterial suspension with an optical density of 1.0 at 600 nm was used as an inoculum of the assay. Isolates were analysed for their ability to degrade PCB (Aroclor 1260) by measuring a shift in the wavemax using Cary 300 UV-visible spectrophotometer for a period of 96 hours. The presence /absence of the compounds was checked using high performance liquid chromatography (HPLC) UFLC Shimadzu using florescence detector pump RF-20A and system gold column C18 (CTO-20A) after 96 h. PCBs were extracted from wastewater samples from both Gaborone and Mafikeng using the Quick, Easy, Cheap, Effective, Rugged, and Safe (QuEChERS) extraction kit, and analysis was performed using the gas chromatography mass spectrometer (GC-MS). The bacteria were able to degrade these compounds under different pH values of 5.0, 7.0, 8.0, and 9.0 and temperatures of 20, 27, 30, and 35°C. Degradation occurred at the most at 35°C and the least at 20°C for PCB samples that were used in the study. The bacteria strain was able to completely degrade Aroclor 1260 that was incoperated into the wastewater samples within 96 h. This was shown by a shift in the wavelength from 224 to 270 nm, which indicated that Aroclor 1260 was degraded and therefore forming a chlorobenzoate derivative. From this finding, it can be concluded that the sewage water samples did not possess PCB (Aroclor 1260) after treatment with bacteria and can be safely recycled.

Keywords: *Pseudomonas aeruginosa*, sewage water, PCBs, recycled, breakdown

1. Background

One of the key areas in sustainable development entails the promotion of environmental management and introduction of new technologies to treat large quantities of waste. This includes treatment of wastewater for recycling purposes [1]. The adverse effects of global warming have mostly been experienced by countries in Africa, resulting in scarcity of water as a natural resource. This has prompted a great global concern to recycle and conserve water, especially in sub-Saharan Africa where the problem of water scarcity has affected most countries [2]. South Africa is faced with freshwater scarcity, which is exacerbated by its increasing demand, pollution, unsustainable use, and climate change [3].

The presence of chemicals in the environment calls for quantification of such so as to come up with a risk analysis posed by these chemicals [4, 5]. According to Guillen et al., substances such as pharmaceuticals, perfluorinated acids, perfluorosulfonates, PAHs, PCBs, pesticides, and surfactants are mostly found in wastewater [4]. Ying et al. also noted that the presence of pharmaceutically active compounds in wastewater is a major concern [6]. Several methods may be used to determine quantitatively, these substances from wastewater, which is mainly from sewage treatment plants [6]. According to Ying et al., although much research has been done regarding the removal of these substances, it was mainly on activated sludge and no work has been done on wastewater [6].

Some strains of organism *Acinetobacter* have the ability to degrade pollutants such as biphenyls from wastewater [7]. *Enterobacter cloacae* secretes an emulsifier that increases the hydrophobicity of the bacterial cell surface and also neutralizes the surface charge of cells [8]. This as a result increases the ability of the bacteria to degrade PCBs [8, 9]. Biosurfactants are also effective at extremes of temperature, pH, and salinity [9, 10], a property that is essential in the biodegradation of PCBs as they are hydrophobic organic compounds [11]. This property causes these recalcitrant compounds to be removed through physico-chemical means or treatments, limited bioavailability to microorganisms, and limited availability to oxidative and reductive chemicals when applied in treatments [8].

This study is very important in contributing toward addressing sustainable development goal 6. With the global emphasis of conservation of natural resources and the three Rs, that is, reduce, reuse, and recycle, this research is very important. The research is my original proposal which was stimulated by quite a number of issues, such as the scarcity of water although there is a lot of water that is being let to waste. Also the high prevalence of cancer cases with no direct link to water but with a view to eliminate the possibility of such cancer causing chemicals with direct attention on PCBs, from sewage which in most cases the effluent is released into the environment.

2. Brief literature

2.1. Physio-chemical properties of polychlorinated biphenyls (PCBs)

Polychlorinated biphenyls (PCBs) consist of two benzene rings with a carbon-to-carbon bond between carbon 1 on one ring and carbon 1 on the other ring [12]. PCBs have varying number of chlorines in their structure [12–14], as shown in **Figure 1**.

http://dx.doi.org/10.5772/intechopen.75400

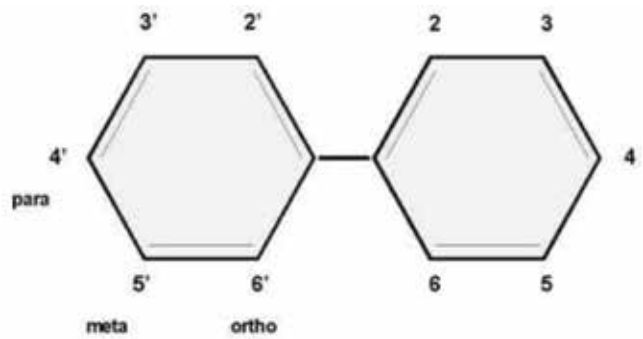

Figure 1. Structure of PCBs (*source*: [14]).

Toxicity of PCBs is dependent upon the number of chlorines present on the biphenyl structure and their position, that is, the co-planar congeners [13, 14]. The PCB congeners that have been deemed to be highly toxic were those that had chlorine atoms attached to the 3,4-ortho positions, followed by those with 5–10 chlorine atoms in the para and meta positions [13].

PCBs toxicity has been largely associated with their structure. This has resulted in PCBs being placed into categories, namely coplanar or non-*ortho*-substituted "*arene*" substitution patterns or noncoplanar or *ortho*-substituted congeners [15]. The coplanar group members are characterized by a fairly rigid structure, with the biphenyl rings in the same plane giving them a molecule structure similar to polychlorinated dibenzo-p-dioxins (PCDDs) and polychlorinated dibenzofurans. Based on this structure, this group of PCBs act in the same way as these molecules as an agonist of the aryl hydrocarbon receptor (AhR) in organisms [16]. This group of PCBs is considered contributors to overall dioxin toxicity [16].

On the other hand, the other group of PCBs, noncoplanar PCBs, has chlorine atoms at the *ortho* positions. According to Ross [17], they have not been found to activate the AhR and are not considered part of the dioxin group; however, they have been implicated in having some neurotoxic and immunotoxic effects, although at levels much higher than normally associated with dioxins, and thus of much less concern to regulatory bodies [18, 19].

According to Rudel et al. PCBs are very stable compounds and do not decompose readily [18]. Their chemical inability to oxidize and reduce in the natural environment gives them this characteristic; they have a long half-life (8–15 years) and are insoluble in water, thus the recalcitrant property [18]. The biodegradability (and solubility in water) of PCBs is also dependent upon the number of chlorine molecules it has [12, 13]. The more chlorine molecules contained in a compound renders that compound less biodegradable [12]. PCBs are mostly hydrophobic; some are less hydrophilic [20, 21]. These properties result in bioaccumulation of these compounds as they do no dissolve in water, and thus, they render them difficult to be biodegraded [12, 14, 20, 22].

2.2. Elimination of PCBs

Although the Stockholm Convention on Persistent Organic Pollutants (POPs) (of which PCBs are part of) signed in 2001 was aimed at eliminating and/or restricting the production and use of POPs [23], more of these ubiquitous substances are still being introduced into the

environment through various human activities [24]. Water has become a widely used environmental matrix for monitoring POPs [20, 25, 26], although most studies on PCBs have been carried out on contaminated soils than water [27].

The destruction of PCBs by chemical, thermal, and biochemical processes is extremely difficult and presents the risk of generating extremely toxic dibenzodioxins and dibenzofurans through partial oxidation [12, 16, 27].

2.3. Effects of polychlorinated biphenyls (PCBs) on human health

PCB mixtures have been associated with cancer incidents in animals from long time back [17, 28, 29]. PCBs were found to induce liver tumors, thyroid adenomas, intestinal metaplasia, and adenocarcinomas in rats and mice [29]. Exposure to some environmental chemicals such as DDT and PCBs has been associated with a drop in sperm count, breast cancer, testicular cancer, and hypospadias, which are all associated with endocrine disruption caused by these chemicals [30]. This comes as a result of some PCB congeners being able to occupy thyroid receptors, thus interrupting their action [17, 30].

PCBs accumulate in the fats of organisms and get passed on from one organism to the other in food chains [31, 32], thus causing bioaccumulation. They get entry into the human body and animals through the skin, lungs, and gastrointestinal tract [13]. PCBs then get distributed to various parts of the body via blood and accumulate in different tissues [31, 33]. The effects of PCBs on humans depend on age, sex, and part of the body affected by chemicals [13]. The liver, as the major organ for removal of toxins in the body, is usually highly affected by PCBs [13, 29]. Humans become exposed to PCBs through consumption of contaminated fish, meat, and dairy products [28] and also through grains grown in PCB contaminated soils [13, 28]. PCBs have been isolated from human milk and serum [31, 34] and have been found to have effects on breastfed children leading to low IQ and endocrine-related ailments [28, 31, 34]. Some studies have shown an increase in cancer mortality in workers exposed to PCBs [13].

2.4. Biodegradation

Biodegradation is the metabolic ability of microorganisms to transform or mineralize organic contaminants into less harmful, non-hazardous substances, which are integrated into natural biochemical cycles [27, 35]. Specific bacteria having bio-degradative potential for various chemical substances in wastewater as well as raw water may be used to treat water [35] for purposes of safe recycling. Bacteria, unlike other organisms, have the ability to interact better with man-made and naturally occurring compounds, which result in such compounds being changed structurally and eventually degraded [35]. This is in a way a better cleanup strategy that can be used in the cleanup of wastewater as it is environment friendly [35]. Use of mixed population of microbes is usually recommended as it has been seen to yield faster results as the two different microbes attack different parts through different mechanisms resulting in effective breakdown of the toxic compound [21, 33]. This activity also creates a condition of co-metabolism [33].

PCBs may not be readily biodegradable, but studies have shown that some bacteria species such as *Vibrio cholera*, *Acinetobacter 1woffnii*, *Aeromonas hydrophila*, *Pseudomonas aeruginosa*, *Pseudomonas putida*, *Rhodococcus* sp., *Bacillus* sp., and *Burkholderia* sp. have the ability to breakdown these compounds, although it is through a very long route [11, 13, 21, 36, 37, 51]. This may be achieved through co-metabolism and mineralization [8, 35]. They use of a metabolic pathway similar in all these bacteria, which comprise four steps catalyzed by enzymes BphA, BphB, BphC, and BphD [37]. The pathway, according to Petric et al., is initiated by insertion of two oxygen atoms at the carbon positions 2, 3 of one aromatic ring [37]. This is followed by dehydrogenation meta-cleavage and hydrolysis forming a 5-carbon compound [37]. The process follows a biphenyl catabolic pathway [37].

2.5. Biodegradation of xenobiotic compounds

According to Heider and Rabus, xenobiotic compound due to its recalcitrant nature is hard to break down [38]. The recalcitrant nature of these compounds is a result of the complexity of its chemical composition [8]. Breakdown of these compounds occurs when enzymes act on certain groups present in the compound [38]. The halocarbons, for example, the halogen group, are targeted, with enzymes such as oxygenases playing a major role in their breakdown [8]. The enzymes target the bonds such as ester-, amide-, or ether bonds present in the compounds leading to break down of these compounds [39, 40]. The enzymes may target the aliphatic chains and in aromatic compounds, the aromatic components may be targeted [40]. The mode of attack as well as the site depends primarily on the action of enzyme, its concentration, and favorable conditions [40]. According to Abor-Amer [40], the xenobiotics do not act as a source of energy to microbes and as a result, they are not degraded while the presence of a suitable substrate induces its breakdown [39]. These substrates are known as co-metabolites, and the process of degradation is known asco-metabolism [39]. Gratuitous metabolism is another process in which xenobiotics serve as substrates and are acted upon to release energy [8].

The processes described cannot be achieved through the use of *Moringa oleifera* in treating wastewater to remove PCBs. It is evident from literature that the removal of these compounds using plant protein has not been fully studied [52]. Plant protein has been found to be slightly efficient with the reduction of fecal coliforms and other bacteria [41, 42], which has made Moringa treatment to be applicable. The use of *Moringa oleifera* seed powder in water treatment plants has been found to target mainly microorganisms, thus reducing turbidity [43]. Although this mode of water treatment has been used, especially in rural areas of the developing countries, synthetic polymers, aluminum sulfate, ferric chloride, and poly aluminum chlorides used together with this powder have been reported to be unsafe [41, 43, 44]. The action of *Moringa oleifera* seed powder has been reported to be based on the ability of the protein contained in the seeds to be able to form coagulants, which reduce water turbidity by acting on coliforms [45]. The bacteria found to be mainly involved in biodegradation of POPs and PCBs have been found mostly not to be coliforms [11, 13]. After treating water with Moringa seed powder, 10^1–10^5 of bacteria is left [45]. Taking into cognizance that Moringa is a tree, sustainability of tree growth and productivity, which relies on environmental conditions, may not be viable. This will therefore affect production and maintenance of the Moringa tree

species, given the global warming and related environmental problems. Growing of bacteria indoors is quite sustainable, when compared to growth of plants although Lea argues that propagation is affordable [44].

3. Materials and method

3.1. Sample collection

Water released from the wastewater treatment plant (effluent) was obtained from Notwane Sewage Treatment Plant situated in Gaborone, Botswana. It was collected from the sampling site in sterile 250 ml Duran bottles and immediately placed on ice in a cooler box with ice. The samples were taken to the Department of Biological Sciences, North-West University, Mafikeng for analysis. Samples were analyzed within 24 h of sampling. The treatment plant treats 40,000 m^3 per day of sewage.

3.2. Biodegradation of PCBs in wastewater by isolate *Pseudomonas aeruginosa*

In the study carried out by the author, out of the many bacteria stated in literature, only *Pseudomonas aeruginosa* isolated from the wastewater sampled during the study was used. The water samples were divided into two parts, one part was sterilized by autoclaving at 121°C for 15 min and the other half was left unsterilized. The wastewater samples were treated with Aroclors of polychlorinated biphenyls (PCBs) obtained from SUPELCO Solutions Within™, USA, through Lehlabile Scientific, South Africa. The PCBs were supplied as Aroclors. Aroclor 1242 (Lot No. LB8851), 1248 (Lot No. LB88969), and 1260 (Lot No. LB92109) in 1 ml ampoules at concentration 1000 μg/ml dissolved in isooctane were used in this study. The purity for each Aroclor was not stated.

To each 100 ml wastewater sample in a 250 ml flask, 10 μl of polychlorinated biphenyls Aroclors mixture, herein referred to as PCBs, was added. The sterilized wastewater samples were inoculated with a colony of the 18 h old culture of the test organism, which was identified as *Pseudomonas aeruginosa* (with accession number from the gene bank of CP 006832 in a study carried out in 2014). Non-sterilized wastewater without bacterial inoculation (Control 1) and sterilized wastewater without inoculation (Control 2) were both treated with PCBs and were the controls. The flasks were wrapped with aluminum foil to exclude light and were incubated at 30°C in the dark in a rotary shaker at 150 rpm [46]. A 5 ml was aseptically taken at 24 h intervals from each setup/flask for detection of PCBs using HPLC and spectral changes were checked at 200–800 nm using Cary 300 UV-visible spectrophotometer, for a period of 96 h.

Analysis for PCB using HPLC was carried out as described by Roy et al. with some modifications [46]. A 1 ml was sampled from each setup to check for residual PCB at 24 h interval. The compounds were extracted by adding 10 ml each of dichloromethane and acetone. The mixture was incubated in a rotary shaker for 24 h at 30°C. After incubation, the mixture was centrifuged for 10 min at 12,000 rpm at 4°C using a Hermle Z326k high speed microcentrifuge, Labortechnik GmbH (LASEC, South Africa). The extra water was pipetted and 4 g

http://dx.doi.org/10.5772/intechopen.75400

of anhydrous sodium sulfate mixed with a PCB-containing solvent to remove residual water. The extract was concentrated to 1.5 ml using a rotary evaporator Stuart RE300DB, LASEC, South Africa and filtered with 0.45 μm PTFE syringe filters. Extracts were analyzed by high performance liquid chromatography (HPLC) UFLC Shimadzu using a florescence detector pump RF-20A and system gold column C18 (CTO-20A). The excitation level was set at 254 nm, emission level at 390 nm. The mobile phase used was a mixture of acetonitrile and water (80:20) as described by Roy et al. [46]. Data analysis was computed using real-time analysis. All chemicals used were of HPLC grade supplied by Sigma Aldrich through Lehlabile Scientific, South Africa.

4. Results

4.1. Degradation of PCBs by *Pseudomonas aeruginosa*

Samples of wastewater from the Notwane Sewage Treatment Plant were used in this study to find out the degree of biodegradation of PCBs in wastewater un-inoculated and inoculated with the test organism. Spectral changes (a shift in wavelength (λ_{max}) in nm), detected using the UV-visible spectrophotometer, were used as an indication that the compounds were broken down into new products. The results of the wavemax (λ_{max}) nm obtained are presented in **Figure 2**.

The results shown by chromatogram indicated that there was a shift in λ_{max} from 224 to 270 nm in 0 h of incubation to 96 h of incubation at 30°C on a rotary shaker in the dark. These results were obtained using a Cary 300 UV-visible spectrophotometer at a wavelength range of 200–800 nm. The results were an indication that isolates *Pseudomonas aeruginosa* was able to degrade Aroclor 1260 into chlorobenzoates and derivatives, which have wavelength ranging from 244 to 270 nm, hence the shift in wavelength.

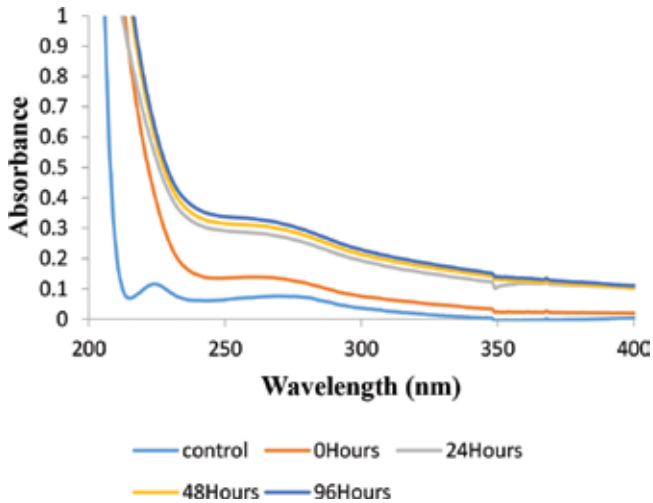

Figure 2. Spectral changes of PCB degradation in water inoculated with isolate *Pseudomonas aeruginosa*.

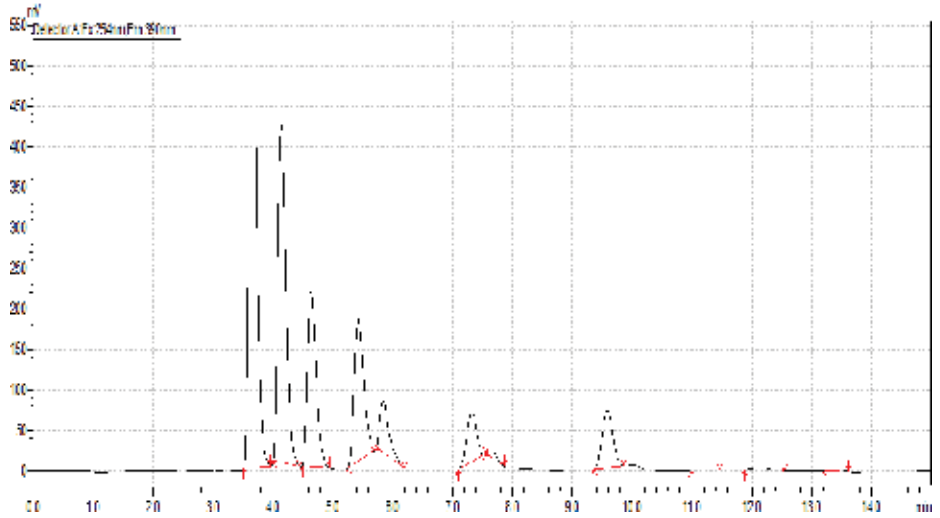

Figure 3. HPLC chromatogram for PCBs standard using a florescence detector method at 10 µl injection volume.

4.2. Results from high performance liquid chromatography (HPLC)

HPLC chromatogram depicted differences in picks obtained for the experiments, the controls, and the standards. Although concentrations were not determined, no PCBs were detected by HPLC after 96 h of incubation. This was an indication that the bacteria degraded the compounds, hence the chromatogram shown in **Figure 4**. The chromatogram obtained for the experiments was compared with the chromatogram for the PCB standard using the retention times for the compounds in the standard, which was represented in **Figure 3**. The results for

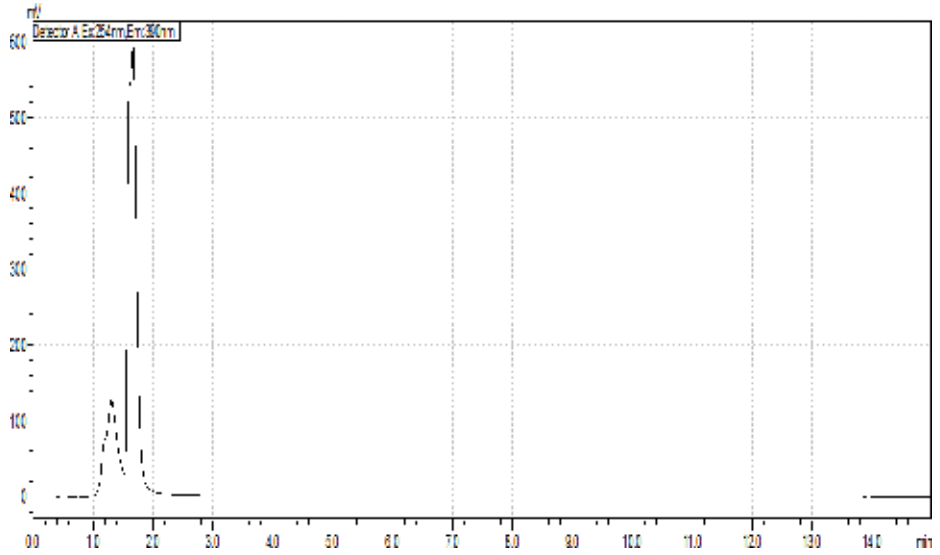

Figure 4. Chromatogram for PCB biodegradation experiment after 96 h of incubation.

PCB standard presented in **Figure 3** showed that there were several compounds in the Aroclor; thus, the many picks, which are not found when the same treatment was extended to the experiment, resulted in **Figure 4**.

The chromatogram shows that the components of the standard had retention times ranging from 3.647 to 13.119 min. The components picked by the instrument are indicated by the red line marking the beginning and ending of the peak. The instrument could not detect the actual names of the compounds though.

The wastewater was sterilized and thereafter inoculated with the test organism and PCBs mixture added. **Figure 4** shows that no peaks were picked by the HPLC. This is an indication that the polychlorinated biphenyls added to the wastewater were completely broken down by isolate *Pseudomonas aeruginosa* resulting in complete elimination.

Representation of **Figure 4** is a clear indication that there were no detectable amounts of compounds after Aroclor was subjected to bacterial treatment. The compounds were broken down in 5 days. There are no peaks shown as compared to the chromatogram shown in **Figure 3**.

5. Discussion

The wavelength maximum (λ_{max}) observed after 96 h ranged from 264 to 269 nm on average for PCBs (**Figure 2**). These results indicated that the PCBs were broken down forming new products with different wavelength and thus the change. This implies that the bacteria were able to use them as their sole source of carbon; thus, the biodegradation of the PCBs added to wastewater. The shifts are an indication of the presence of initial ring oxidation metabolites and ring fission metabolites [19, 47]. PCBs first get degraded into chlorobenzoates [47] that have been found to have λ_{max} ranging from 210 to 214 nm in the B-band and 244 to 270 nm in the C-band when dissolved in water [48], a range that was observed in the results obtained after 24 h of culturing the organism used in this study in PCBs Aroclor mixture, results of which are shown in **Figure 2**. The results depicted that the bacteria was able to breakdown the PCBs, which were similar to results in a similar studies by Vrchotova et al. and Seeger et al. [47, 49]. In their studies [47, 49], the product chlorobenzoate was biodegraded into benzoate and eventually pyruvate and acetyladehyde, which are essential in the tricarboxylic cycle (TCA) [47, 49].

The HPLC run confirmed that the compound was biodegraded by the bacteria isolate *Pseudomonas aeruginosa* as presented in **Figures 3** and **4**, which was also proved by Heider and Rabus, Roy et al. and Raja et al. [38, 46, 50] in their studies. No PCB compound was detected after 96 h of exposure to the bacteria in wastewater.

6. Conclusion

Pseudomonas aeruginosa, isolated from wastewater in the Notwane Sewage Treatment Plant was successfully used in biodegradation of recalcitrant polychlorinated biphenyls (PCBs). This having been successfully employed at the micro level, and further tests can be carried out to

validate the results obtained in this study. With this recommendation in place, it is ideal to say that employing bacteria in the biodegradation processes of recalcitrant PCBs will be highly cost effective as it is a biotechnological process. The process will enable developing countries to employ effective but easy to maintain at a cost effective mode means of wastewater treatment. This wholly will also enable these countries to address the problem of water shortage at the same time practicing water conservation strategies. This is in a way contributing toward addressing the sustainable development goals (SDGs). With the findings from this study, a recommendation for further experimentation on a larger scale is made so as to safely recycle the sewage water for purposes of redirecting to Gaborone dam. This in a way will aid in curbing the problem of water shortage, of course, taking into consideration other factors, such as total coliforms, *Escherichia coli,* and other pathogenic organisms and chemicals. These have to be within the expected standards according to Botswana Bureau of Standards (BOBS) limits as well as international World Health Organization (WHO) standards.

Acknowledgements

My gratitude goes to the Department of Biological Sciences at North-West University, Mafikeng Campus for financial support while carrying out the study. I extend my gratitude to Professor C.N. Ateba, Professor N.P. Sithebe, and Dr. K. Sichilongo for all their support and guidance. I would like to thank the Ministry of Basic Education of Botswana for providing me time to carry out the research and financial support in one way or the other.

Conflict of interest

The author declares that there is no conflict of interests regarding the publication of this paper.

Other declarations

This chapter was extracted from the thesis (unpublished) of my research for PhD, which was undertaken in 2014 with University of North West, Mafikeng Campus in South Africa.

Author details

Spar Mathews* and Patricia Sithebe

*Address all correspondence to: sparmat@gmail.com

North West University, Mafikeng Campus, South Africa

References

[1] Khadhraoui M, Belaid C. Wastewater treatment for a possible water reuse in semi-arid climate zone. Journal of Arid Land Studies. 2012;**22**(1):333-336

[2] Ateba CN, Maribeng MD. Detection of enterococcus species in groundwater from some rural communities in the Mmabatho area, South Africa: A risk analysis. African Journal of Microbiology Research. 2011;**5**(23):3930-3935

[3] Department of Water Affairs (DWA). The Annual National State of Water Resources Report: October 2011 to September 2012. Water Resource Information Programmes. South Africa: Department of Water Affairs; 2012

[4] Guillen D, Ginebreda A, Farre M, Darbra RM, Petrovic M, Gros M, Barcelo D. Prioritization of chemicals in the aquatic environment based on risk assessment: Analytical, modeling and regulatory perspective. Science of the Total Environment. 2012;**440**:236-252. DOI: 10.1016/j.scitotenv.2012.06.064

[5] Urbaniak M. Biodegradation of PCDDs/PCDFs and PCBs. Biodegradation—Engineering and Technology. 2013. pp. 73-100

[6] Ying G, Kookana RS, Kolpin DW. Occurrence and removal of pharmaceutically active compounds in sewage treatment plants with different technologies. Journal of Environmental Monitoring. 2009;**11**:1498-1505

[7] Gumaa NHH, Potrus WM, Mohammed SI. The effect of cultural and environmental conditions on biodegradation and biosurfatant production by Serratiamarcescens utilizing weathered diesel oil. Journal of Al-Nahrain University. 2010;**13**(1):112-120

[8] Pacwa-Plociniczak M, Plaza GA, Piotrowska-Seget Z, Cameotra SS. Environmental applications of biosurfactants: Recent advances. International Journal of Molecular Science. 2011;**12**:633-654

[9] Md F. Biosurfactant: Production and application. Journal of Petroleum and Environmental Biotechnology. 2012;**3**(4):124-129

[10] Kapadia SG, Yagnik BN. Current trend and potential for microbial biosurfactants. Asian Journal of Experimental Biological Sciences. 2013;**4**(1):1-8

[11] Blokesch M. Chitin colonization, chitin degradation and chitin-induced natural competence of vibrio cholera are subject to catabolite repression. Journal of Environmental Microbiology. 2012;**14**(8):1898-1912

[12] Environmental Protection Agency. Health Effects of Polychlorinated Biphenyls (PCBs). Washington, DC: United States of America EPA; 2013

[13] Anyasi RO, Atagana HI. Biological remediation of polychlorinated biphenyls (PCB) in the soil and sediments by microorganisms and plants. African Journal of Plant Science. 2011; **5**(7):373-389

[14] Barbalace RC. The Chemistry of Polychlorinated Biphenyls.Environmental Chemistry. com. 2003. [Accessed 21/09/2013]

[15] Jensen WB. The origins of the ortho-, meta-, and para- prefixes in chemical nomenclature. Journal of Chemical Education. 2006;**83**(3):356

[16] Arsalan J, Stuart H, Sadegh H, Stuart H. Concentrations and chiral signatures of polychlorinated biphenyls in outdoor and indoor air and soil in major UK conurbation. Environmental Science and Technology. 2007;**41**(7):2153-2158

[17] Ross G. The public health implications of polychlorinated biphenyls (PCBs) in the environment. Ecotoxicology and Environmental Safety. 2004;**59**(2004):275-291

[18] Rudel RA, Seryak LM, Brody JG. PCB containing wood floor finish is a likely source of elevated PCBs in residents blood, household air, and dust: A case study of exposure. Journal of Environmental Health. 2008;**7**(21):1-8

[19] Wethington DM, Hornbuckle KC. Milwaukee WI as a source of artmospheric PCBs to LAKE Michigan. Environmental Science and Technology. 2005;**39**(1):57-63

[20] Muir D, Lohmann R. Water as a new matrix for global assessment of hydrophilic POPs. Trends in Analytical Chemistry. 2013;**46**(2013):163-172

[21] Nwinyi OC. Enrichment and identification of Askarel oil (PCB blend) degrading bacteria enriched from landfill sites in Edo state, Nigeria. Agriculture and Biology Journal of North America. 2011;**2**(1):89-100

[22] Schafer KS, Kegley SE. Persistent toxic chemicals in the US food supply. Journal of Epidemiology Community Health. 2002;**56**:813-817

[23] Andrews W. Manual of Food Control.4 Rev. 1. Rome: Microbiological Analysis Food and Agriculture Organisation of the United Nations (FAO); 1992

[24] Teran T, Lamon L, Marcomini A. Climate change effects on POPs environmental behaviour: A scientific perspective for future regulatory actions. Atmospheric Pollution Research. 2012;**3**(2012):466-476

[25] Van Leeuwen SPJ, Van Bavel B, DeBoer J. First worldwide UNEP interlaboratory study on persistent pollutants (POPs), with data on polychlorinated biphenyls and organochlorine pesticides. Trends in Analytical Chemistry. 2013;**46**(2013):110-117

[26] Van Leeuwen SPJ, Van Bavel B, Abad E, Leslie HA, Fiedler H, DeBoer J. POPs analysis reveals issues in bringing laboratories in developing countries to a higher quality level. Trends in Analytical Chemistry. 2013;**46**(2013):198-206

[27] Leigh MB, Prouzova P, Mackova M, Macek T, Nagle DP, Fletcher JS. Polychlorinated biphenyl (PCB) – degrading bacteria associted with trees in a PCB-contaminated site. Applied and Environmental Microbiology. 2006;**72**(4):2331-2342

[28] Lynch CD, Jackson LW, Kostyniak PJ, BM MG, GMB L. The effect of prenatal and postnatal exposure to polychlorinated biphenyls and child neurodevelopment at age twenty four months. Reproductive Toxicology. 2012;**34**:451-456

[29] Pavuk M, Cerhan JR, Lynch CF, Schecter A, Petrik J, Chovancova J, Kocan A. Environmental exposure to PCBs and cancer incidence in Eastern Slovakia. Chemosphere. 2004; **54**(2004):1509-1520

[30] Rogan WJ, Ragan NB. Some evidence of effects of environmental chemicals on the endocrine system in children. Journal of Hygiene and Environmental Health. 2007;**210**(2007):659-667

[31] Man YB, Lopez BN, Wang HS, Leung AOW, Chow KL. Cancer risk assessment of polybrominateddiphenyl ethers (PBDEs) and polychlorinated biphenyls (PCBs) in former agricultural soils of Hong Kong. Journal of Hazardous Materials. 2011;**195**(2011): 92-99

[32] Zhao G, Wang Z, Zhou H, Zhao Q. Burdens of PBBs, PBDEs, and PCBs in tissues of the cancer patients in the e-waste. Science of the Total Environment. 2009;**407**(2009):4831-4837

[33] Martins LF, Peixoto RS. Biodegradation of petroleum hydrocarbons in hypersaline environments. Brazillian Journal of Microbiology. 2012;**2012**:865-872

[34] Linderholm L, Biague A, Mansson F, Norrgren H, Bergman A, Jakobsson K. Human exposure to persistent organic pollutants in West Africa—A temporal trend study from Guinea-Bissau. Environmental International. 2010;**36**:675-682

[35] Dhall P, Kumar R, Kumar A. Biodegradation of sewage water using autochthonous bacteria. The Scientific World Journal. 2012;**861903**:1-8

[36] Hamzah A, Rabu A, Azmy RFHR, Yussoff NA. Isolation and characterisation of bacteria degrading Sumandak and South Angsi oils. Sains Malaysiana. 2010;**39**(2):161-168

[37] Petric I, Hrsak D, Fingler S, Voncina E, Cetcovik H, Kolar AB, Kolic NU. Enrichment and characterization of PCB-degrading bacteria as potential seed cultures for bioremediation of contaminated soils. Food Technology and Biotechnology. 2007;**45**(1):11-20

[38] Heider J, Rabus R. Genomic Insights in the Anaerobic Biodegradation of Organic Pollutants. Microbial Biodegradation: Genomics and Molecular Biology. Caister: Academic Press; 2008. http://www.link.springer.com/referenceworkentry [Accessed: November 04, 2014]

[39] Cyon M, Zmijowska A, Wojcik M, Piotrowska-Seget Z. Biodegradation and bioremediation potential of diazinon-degrading Serratiamarcescens to remove other organophosphorus pesticides from soils. Journal of Environmental Management. 2013; **117**(2013):7-16

[40] Abor-Amer AE. Biodegradation of diazinon by Serratiamarcescens DI101 and its use in bioremediation of contaminated environment. Journal of Microbiology and Biotechnology. 2011;**21**(1):71-80

[41] Dalen MB, Pam JS, Izang A, Ekele R. Synergy between Moringaoleifera seed powder and alum in the purification of domestic water. Science World Journal. 2009;**4**(4):6-11

[42] Kawo AH, Daneji IA. Bacteriological and physcio-chemical evaluation of water treated with seed powder of Moringaoleifera LAM. Bayero. Journal of Pure and Applied Sciences. 2009;**4**(2):208-212

[43] Mumuni A, Oloruntoba EO, Sridhar MKC. Use of Moringaoleifera (LAM) seed powder as a coagulant for purification of water from unprotected sources in Nigeria. European Scientific Journal. 2013;**9**(24):214-229

[44] Lea M. Bioremediation of Turbid surface water using seed extract from *Moringa oleifera* (LAM.) (Drumstick) Tree. Current Protocols in Microbiology. 2014;**1G.2.1-1G.2.8**

[45] Mangale SM, Chonde SG, Jadhav AS, Raut PD. Study of *Moringa oleifera* (drumstick) seed as natural absorbent and antimicrobial agent for river water treatment. Journal of National Production and Plant Resources. 2012;**2**(1):89-100

[46] Roy M, Khara P, Basu S, Dutta TK. Catabolic versatility of sphingobiumspstrain PNB capable of degrading structurally diverse aromatic compounds. Journal of Bioremediation and Biodegradation. 2013;**4**(1):1-6. http://www.academia.edu/ [Accessed: November 04, 2014]

[47] Seeger M, Hernandez M, Mendez V, Ponce B, Cordova M, Gonzalez M. Bacterial degradation and bioremediation of chlorinated herbicides and phenyls. Journal of Soil Science & Plant Nutrition. 2010;**10**(3):320-332

[48] Forbes WF. Light absorption studies: The ultraviolet absorption spectra of chlorobenzenes. Canadian Journal of Chemistry. 1960;**38**(7):1104-1112

[49] Vrchotova B, Mackova M, Macek T, Demnerova K. Bioremediation of chlorobenzoic Acids. Agricultural and Biological Sciences. "Applied Bioremediation—Active and Passive Approaches". 2013. http://www.intechopen.com/books/applied-bioremediation [Accessed: November 04, 2014]

[50] Raja CE, Selvam GS, Omine K. Isolation, Identification and Characterisation of heavy metals resistant bacteria from sewage. In: Fukuoka JS, editor. International Joint Symposium on Geo-disaster Prevention and Geo-environment in Asia. 2009. pp. 205-211. http://www7.civil.kyushu-u.ac.jp/jeotech [Accessed: November 04, 2014]

[51] Martinkova L, Uhnakova B, Patek M, Nesvera J, Kren V. Biodegradation potential of the genus Rhodococcus. Environment International. 2009;**35**:162-177

[52] Farhadian M, Duchez D, Vachelard C, Larroche C. Monoaromatics removal from polluted water through bioreactors—A review. Journal of Water Research. 2008;**42**:1325-1341

Chapter 9

Distributed Control Systems for a Wastewater Treatment Plant: Architectures and Advanced Control Solutions

Dan Selișteanu, Ion Marian Popescu, Emil Petre,
Monica Roman, Dorin Șendrescu and Bogdan Popa

Additional information is available at the end of the chapter

http://dx.doi.org/10.5772/intechopen.74827

Abstract

This chapter is focused on the development and implementation of a distributed and hierarchized control system for the wastewater treatment plant (WTP) Calafat, Romania. The primary control loops for both treatment lines (water and activated sludge) are developed and analyzed. Also, the distributed control system (DCS) architecture of the wastewater treatment plant is presented, and the advantages of the proposed control structure are highlighted. In order to increase the performance of the overall control system, some advanced control solutions are investigated. More precisely, multivariable adaptive and robust control algorithms are proposed for the activated sludge bioprocess. Several realistic simulation experiments are performed, and the obtained results are analyzed.

Keywords: wastewater treatment, activated sludge, control systems, distributed control, adaptive control

1. Introduction

In this chapter, a control architecture developed at the wastewater treatment plant (WTP) Calafat (located in Oltenia region, Romania) is presented. This control structure was developed in the frame of research project ADCOSBIO (no. 211/2014, UEFISCDI) [1] and contract no. 168/2017, University of Craiova-Water Company Oltenia (WCO). More precisely, a distributed control system (DCS)-supervisory control and data acquisition (SCADA) architecture was proposed, which is organized as a distributed and hierarchized control system. This control

solution envisaged the wastewater treatment plant Calafat but can be adapted and implemented for other similar wastewater treatment plants from the WCO.

The wastewater treatment is a process operated to convert wastewater into an effluent that can be returned to the water cycle with minimal impact on the environment. This process takes place in a wastewater treatment plant (WTP) [2]. In a WTP, the treatment usually comprises three stages, called primary, secondary, and tertiary treatments [3]. Primary treatment consists in the mechanical removing of settled and floating materials, and the remaining liquid can be discharged or directed to secondary treatment. Secondary treatment removes dissolved and suspended biological matter, and it is typically performed by microorganisms in a special habitat. The goal of tertiary treatment is to provide a final treatment stage to improve the effluent quality before it is released to the environment. The treatment method used at the WTP Calafat is a classical one, with a mechanical stage for the impurity removal and a biological stage based on activated sludge. The proposed control solution for this WTP is based on a DCS structure.

The paradigm of DCSs is related to the control of medium and high complexity processes, and it consists in the implementation of distributed and hierarchized systems in a number of four to five levels [4]. The two main attributes of the DCS should be mentioned here: the horizontal functionality in each level is managed by a real-time operating system, and the communication between levels is characterized by the network used in the DCS. Currently, some modern technologies from the networks and processing devices are incorporated into the DCSs [5, 6]. The DCS-SCADA solution for the WTP Calafat consists in four levels: the field level (level 0), the direct control level (level 1), the plant supervisory level (level 2), and the production control/regional coordination level (level 3). In this chapter, the structure of the first three levels and their functionality are presented. The primary control loops implemented at level 1 of DCS-WTP Calafat are described. Also, due to the fact that the performance improvement of the WTP control system is possible only by managing the activated sludge bioprocess, some advanced control solutions based on nonlinear adaptive and robust control algorithms are proposed for level 2 of the DCS.

The activated sludge process implemented at WTP Calafat is an aerobic process, highly nonlinear and characterized by parametric uncertainties [3, 7–11]. The best-known model that tries to describe the activated sludge processes is ASM1 (Activated Sludge Model No. 1) [3, 10–12]. The main drawback of ASM1 is its complexity, such that it becomes unfeasible for control. Thus, in this chapter a simplified model of the activated sludge process will be used. The model is based on the model of Nejjari et al. [8], adapted for WTP Calafat.

Several control strategies were developed for bioprocesses, such as linearizing strategy, adaptive approach [3, 7–9], robust and optimal control, sliding mode control [13], model predictive control [14], etc. Yet, in all these schemes, the knowledge of all inputs is required. Unfortunately, for wastewater treatment processes, usually, the complete knowledge of inputs is not available. For these cases, interval observers (or set observers) were developed in the last period, allowing the reconstruction of a guaranteed interval for the unmeasured states instead of estimating their precise numerical values. The only requirement is to know an interval in which the unmeasured inputs of the process evolve. These robust observers are capable of

coping with the problems posed by both the uncertainties in the inputs and the incomplete knowledge of process kinetics [15–18].

In this chapter, some of our previous results [12] are extended for WTP Calafat in order to design multivariable adaptive and robust control algorithms. The proposed control strategies are able to handle the model uncertainties of an activated sludge process used for removal of two pollutants carried out in a continuous recycle reactor. The main control objective is to maintain the pollution level at a desired low value despite the load and concentration variations of the pollutant. The adaptive control scheme is designed by combining a linearizing control law with a state asymptotic observer and with an estimator used for online estimation of unknown kinetics. The robust control structure is designed as a linearizing control law plus an interval observer able to estimate lower and upper bounds in which the unmeasured states are guaranteed to lie. Moreover, the uncertain process parameters are replaced by their lower and upper bounds assumed known.

The chapter is organized as follows. In Section 2, the general characteristics of the WTP Calafat and the process flow are presented. Section 3 proposes a distributed control solution for the wastewater treatment process from WTP Calafat. The control architecture and the primary control loops are analyzed. In Section 4, the design of multivariable adaptive and robust control schemes for the activated sludge process is provided. The behavior of the proposed control algorithms is analyzed by performing realistic simulation experiments. The final conclusions are presented in Section 5.

2. Description of the technological process flow

The general characteristics of the wastewater treatment plant (WTP) Calafat and the process flow will be presented. The process flow comprises two stages: the pretreatment (which is the so-called mechanical stage) and the biological stage. **Figure 1** presents the general block diagram of the WTP, and **Figure 2** shows an aerial photography of the WTP.

The WTP was designed for the treatment of a daily average flow of 8366 m^3/day and of a maximum flow of 530 m^3/h. The WTP size was chosen in order to solve the needs of a number of maximum 29,000 inhabitants of Calafat town, predicted for 2020. The treatment method is a classical one, with a mechanical stage for the impurity removal and a biological stage based on activated sludge. The wastewater enters in a tank; it is lifted with special pumps to the pretreatment area and after that is gravitationally discharged in the biological tanks, where the water is aerated and mixed with the activated sludge. Thus, the biodegradation of the water occurs. Finally, the effluent is discarded through decantation.

2.1. Process flow: pretreatment

The process technological lines will be succinctly described. After the entering in the WTP, the influent wastewater passes through a bar screen (the gross filter) to remove all large objects, and after that it flows in a gravitationally way through a slit in the pump room. This unit is

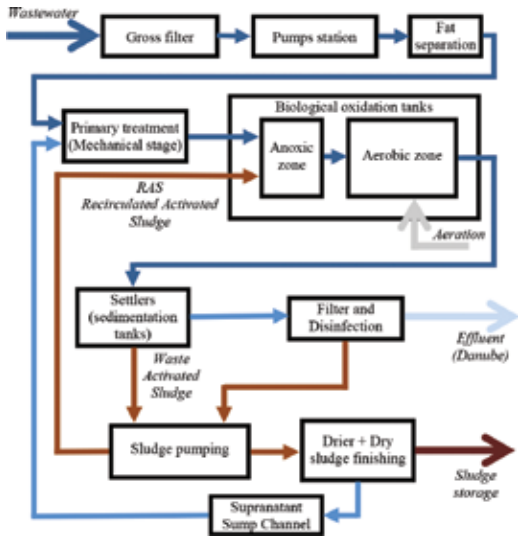

Figure 1. Block diagram (WTP Calafat).

Figure 2. WTP Calafat (aerial photo).

equipped with three Flygt submersible centrifugal pumps P1.A, P1.B, and P1.S (two active pumps (A and B) and one for backup (S)). The water level is measured by using an ultrasonic transducer L1 and is kept between two limits (preestablished limits depending on average water flow). By using the level information, the pumps act to keep the level into the limits. Also, the level information is transmitted to the process computer in the central control room. The water exits from the pumps P1.A, P1.B, and P1.S through three vertical pipes, which at the superior part of the tank (in the valve room) pass to a horizontal configuration and after that merge into a collector. From the valve room, a pipeline goes to the preliminary treatment

(pretreatment: mechanical stage). This plant is placed on a metallic structure at the +6.40 m elevation.

An electromagnetic flow meter is placed on the vertical part of the pipe, and it is used to measure the hourly flow of the wastewater provided by the pumps P1.A, P1.B, and P1.S. By opening two sluice valves located at the entrance of the channels used for thin filtering, the wastewater resulted from the pumps P1.A, P1.B, and P1.S passes through the channels and is filtrated by using some rotational filters. The thin impurities which are separated by the filters are then discharged on a conveyer belt and stored into a special tank.

The wastewater enters in a tangential manner in the workers, and, under the mixer action, the water has a descendant spiral movement. After that, the wastewater is lifted through a central pipe, and finally it is evacuated through a radial pipe. This movement, due to the gravitational and centrifugal forces, allows the sedimentation of the solids in the lower part of the workers. The fat and grease floating on the surface are collected by the skimmers. The solid particles are removed by opening the sliding valves, and thus these particles are periodically drained via a spiral conveyer. The grit is cleared into a special tank. After the pretreatment, the water passes via a pipeline which ramifies at the superior part of the biological tanks in the anoxic zones.

2.2. Process flow: biological stage

The biological tanks consist of two biological reactors (bioreactors) and two settlers (sedimentation tanks). These are circular tanks, positioned in a concentric manner, with the settler in the inner part and the biological reactor in the exterior. The walls of the tanks (5 m height) are from special glassed steel. The walls are embedded into concrete structures plated with Izocor hydro-isolation. The external diameter is $d_1 = 35.16$ m, the volume is $V = 3800$ m^3, and the inner diameter is $d_2 = 18.86$ m. At the biological reactor, the bottom is plane, but the bottom of the settler is in the shape of a truncated cone. The bioreactor is divided in two zones, anoxic and aerobic, by using two steel walls, radially disposed. The ratio of the volumes is 30% anoxic/70% aerobic.

In the anoxic zone of each bioreactor, the wastewater from the pretreatment is mixed with the activated sludge which is recirculated by the Flygt pumps RAS/SAS P3.A, P3.B, P3.S. These pumps are controlled with frequency converters, and the flow ratio is 1:1. An equal flow of mixture from the aerobic zone is pumped through a slit from the zone separation wall by the internal recirculation pumps P2.A and P2.B (Flygt type, with frequency converters). The mixers placed in this anoxic zone achieve the homogenization of the three inputs (wastewater, activated sludge, aerobic mixture). In the anoxic zone, the next actions are achieved:

- An appropriate ratio between the substrate (the organic content of the wastewater + nutrients) and the microorganisms (the active content of the sludge)
- The denitrification process (the nitrogen removal)

From the anoxic zone, the compound passes into the aerobic zone, where the biochemical oxidation of the organic matter is achieved. The needed oxygen is provided from the air delivered by the BOC Edwards air blowers A1.A, A1.B, and A1.S and bubbled as thin bubbles

by using polymeric membranes. Two technological variables are very important for the aerobic process: the dissolved oxygen (DO) and the pH of the mixture. These are measured and indicated by using the transducers Q1 and Q2 (for DO concentration) and Q3 and Q4, respectively, (for pH). The air is blown by the air blowers A1.A, A1.B, and A1.S (two active and one for backup) through galvanized steel pipes. The air pressure and temperature can be monitored by using the local devices. The airflows at the two tanks are measured by using the flow meters F1 and F2. The flow control is necessary in order to maintain the DO concentration between the specified values. The DO is measured by using the sensors Q1 and Q2, and the information is used to control the air blower speed by using frequency converters.

The mixture from the aerobic zone arrives at the partition wall where one-third from the flow is taken by the recirculation pumps P2.A and P2.B and delivered to the anoxic zones and two-thirds from the flow is passed through a pipeline (via the communicating vessel principle) into the central pipe of the settler. From here the mixture exits in a radial and uniform way at the superior part. The effluent is separated from the sludge and after that is gravitationally removed through a circular drain. Finally, the effluent is flushed in the Danube through a channel. The settlers are equipped with radial scrapper bridges, which have a double goal:

- The superior scrapper collects the foam and directs it to a foam-collecting chamber.
- The inferior scrapper cleans the sediments and directs the sludge to a discharge whirl.

The activated sludge is transported to a collector from which is exhausted through three ramifications by the pumps RAS/SAS P3.A, P3.B, P3.S (RAS is the recirculated activated sludge at the anoxic zones; SAS is the surplus activated sludge, which is carried to a special tank).

As a conclusion, in the biological tanks, the following processes occur:

- The decomposition of the organic matters by using enzymes (enzymatic reactions)
- Assimilation of some components by the microorganisms
- Microorganism growth (increase of the activated sludge mass)
- Oxygen consumption for endogenic respiration and biochemical oxidation
- Nitrification and denitrification
- The removal of the excess sludge

3. A distributed control solution for the wastewater treatment process: WTP Calafat

3.1. The control architecture

The proposed DCS-SCADA solution for the WTP Calafat is presented in **Figure 3**. The levels of the DCS and their functionality are described in the next paragraphs.

http://dx.doi.org/10.5772/intechopen.74827

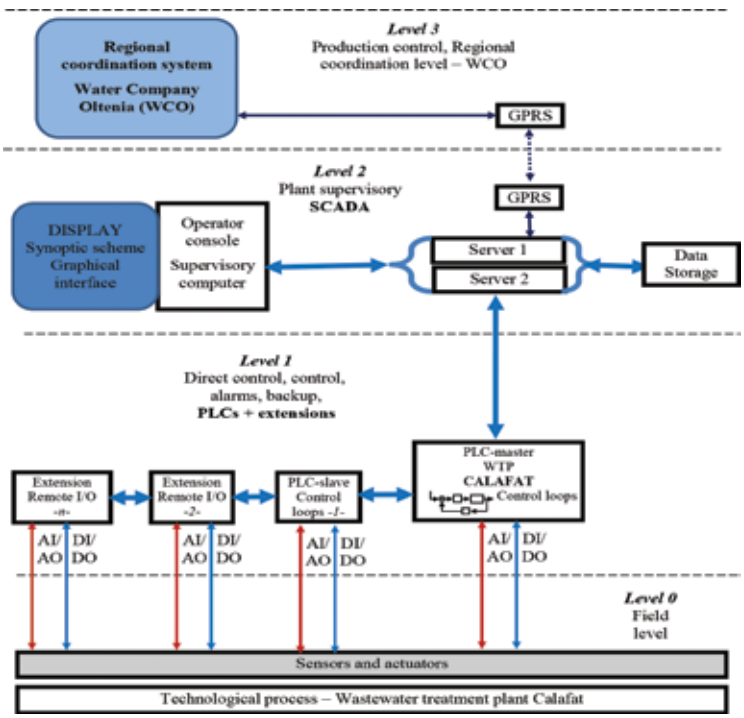

Figure 3. The structure of the DCS with four levels (WTP Calafat).

Level 0 contains all the field devices placed at the technological process level. Classically, at this level we have the measurements of various variables and the final control elements. The components of this level are:

- Sensors (analogic) for flows, levels, pressures, pH, and DO concentrations, such as electromagnetic sensors (Siemens, 0–10 m/s water speed) for flows, ultrasonic sensors (Siemens, 0.3–8 m) for level measurements, pH, and DO concentrations measured via integrated measurement systems (4–20 mA) for dosing devices, etc.
- Contact sensors that provide data about the state of some equipment and operations
- Final control elements (actuators) such as control valves, pumps, etc.
- Dedicated devices for various operations such as dosages, recipes, and technological processing, which will interact with the DCS at the monitoring level
- On/off elements for various actions such as pump starting, etc.

Level 1 comprises the data acquisition devices and the controllers, including the real-time data processing. The analogic signals from sensors and also the control inputs to the actuators are unified signals (e.g., currents in the range 4–20 mA). Due to the geographical distribution, the WTP control system is implemented with several PLCs (programmable logic controllers). These PLCs are connected into a master-slave network with extensions, which handles the

information and takes the required decisions for the coordination of the entire technological process. The acquired data, the decisions, and the events occurred in the process are communicated to the next level (SCADA) in order to be used and displayed on the graphical monitoring interface. The information flow is bidirectional; that is, the PLCs receive information about global decisions or optimization, such as set points for the control loops, switches between operational regimes, etc. The decisions at this level are taken in real time and such that the operation of the overall process is managed. The primary control loops are implemented at the PLC level, but the set point of each loop is provided by the superior hierarchic level (SCADA). The PLCs also achieve the implementation of the direct commands delivered by the control algorithms and function of various operational regimes.

Level 2 contains the equipment and the devices from the control room, which receive the information from level 1 (PLC level) and supervise the global operation of the WTP. This level is represented by the SCADA/HMI (human-machine interface) system. The main functions achieved at this level consist in operation optimization, implementation of adaptive and robust control algorithms (proposed in Section 4), operation monitoring via graphical interfaces, remote operation mechanisms, data/event storage, achievement of a data historian, etc. Also, the SCADA ensures the communication between the local dispatcher room (WTP Calafat) and the regional dispatcher of Water Company Oltenia, by using a GSM/GPRS system. The SCADA/HMI runs on two redundant servers. The SCADA supervises the direct control system (real time). If the SCADA system stops, the process will be automatically operated by using the PLCs. Several protection and backup procedures are incorporated in the operation and supervisor programs. The most of control and data acquisition devices used for levels 1 and 2 are provided by Siemens, Telemecanique, etc.

Level 3 is the regional dispatcher of the WCO, and it will coordinate the activity of the WTP with respect of the performance and of extended monitoring of the geographical area.

The operation regimes allowed by the DCS are as follows: automatic, manual via the computer, and locally manual. *Automatic*: The WTP control is achieved exclusively through the command/decision provided by the DCS (PLCs + SCADA/HMI). *Manual via the computer*: The DCS works only as a data acquisition system, but the decisions are taken by the human operator and are transmitted via PLCs and SCADA to the actuators. The system offers all the information and keeps the inter-blockings at the software and hardware levels. This regime can be achieved for the entire WTP or only for some components. *Locally manual*: This regime implies the local operation, no matter what regime is set at the PLCs or SCADA levels. This regime is of high priority, but the SCADA will signalize at the dispatcher level in this situation, and the event will be stored. This regime is useful when failures occur or in the case of network communication problems, startups, and maintenance.

The integration of local SCADA in regional SCADA. The regional SCADA system is a regional centralized structure, which implies the organization of a regional dispatcher, equipped with reliable industrial devices, disposed in a redundant topology in order to ensure a continuous operation. The regional dispatcher role is to coordinate all the subnetworks from the urban areas. The local dispatchers are in fact local process networks from each urban area, which acquire and handle the primary information from the process (levels, flows, concentrations, telemetry, diagnostic signals, etc.). This information is available for the local operator but also at the regional level.

3.2. Level 1: primary control loops

In this section, a few numbers of primary control loops that are implemented at level 1 of DCS-WTP Calafat will be described.

The control loop 1 ensures the level control in the admission room. The level is measured with the sensor L1, and the control action is achieved via the wastewater pumps P1.A, P1.B, and P1.S (two active pumps (A and B) and one for backup (S)). The block diagram of this control loop is presented in **Figure 4**. The level set point is preestablished, since the influent flow in the WTP fluctuates. If the level decreases under a limit, the pumps are shut down (decision at the PLC level). This critical situation is transmitted to the SCADA system, where a warning signal will be displayed/stored. The control loop is a classical feedback loop, with a possible PID control law plus a switching mechanism. The control loop is implemented at level 1 of DCS, but the set point (the reference) is provided by level 2. The actuators are the three pumps P1.A, P1.B, and P1.S that have the motors controlled with static frequency converters in order to provide a variable flow. The switching mechanism (switching logic) of the pumps is designed to ensure a rotation in the operation of the pumps. This fact is done to avoid the unevenly wear of the pumps but also for the failure situations. The influent wastewater flows are disturbances for the loop and will be rejected by the control law.

The control loop 2 is designed for the control of dissolved oxygen (DO) concentrations, which are measured with the transducers Q1 and Q2, and the control is provided by the air blowers A1.A, A1.B, and A1.S. The control loops are presented in **Figure 5** and are dedicated to the DO concentration control in the biological tanks (aerators).

The control laws are PIDs (with self-tuning facilities), but also some advanced control laws can be implemented. As in the previous case, the control loop is implemented at level 1 of DCS, but the set point is provided by level 2. The actuator for the technological line A is the air blower A1.A and for the line B is A1.B (A1.S is a backup air blower).

The control loop 3 is dedicated to the regulation of the recirculated flow percentage calculated from the aerated water flow (from the input of the distribution room). This process variable (percent) is processed by using an algorithm with several input arguments such as dissolved

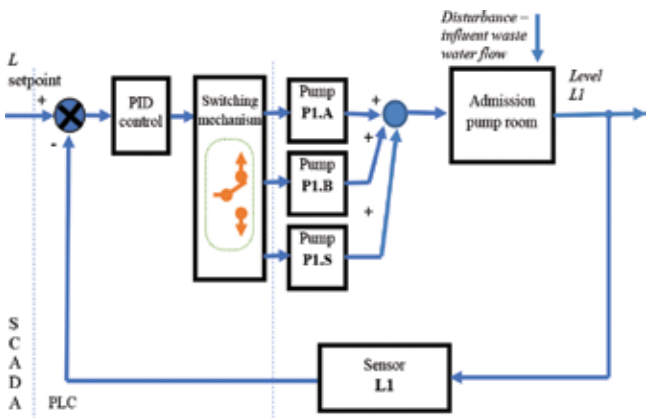

Figure 4. Level control loop: pumps room from the WTP admission.

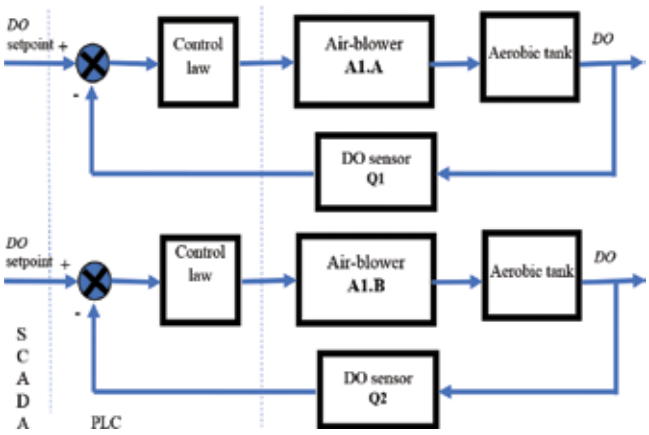

Figure 5. Control loops for the dissolved oxygen concentration.

oxygen, suspended solids, nitrogen, and phosphorus provided by the automated extraction probe system. The set point is given by the operator via the SCADA system, and the control action is based on the emulsion sludge pumps P2.A and P2.B from the aerators. These two control loops (block diagrams in **Figure 6**) are independent because we have two biological treatment tanks. The control loop is implemented at level 1 of DCS, and the set point is provided by level 2. The actuator for the technological line A is the recirculation pump P2.A, and for the line B is the pump P2.B.

The control loop 4 is designed to control the ratio (flow F1)/(flow F2), which is the activated sludge flow introduced in the influent wastewater flow, by using the submersible pumps P3.A, P3.B, and P3.S. This control loop is presented in **Figure 7**. The backup pump P3.S will act:

- Periodically (scheduled by the operator), to ensure a uniform usage of the pumps
- When additional flows of wastewater occur and the active pumps cannot provide the required activated sludge flow
- When some failures occur at the active pumps

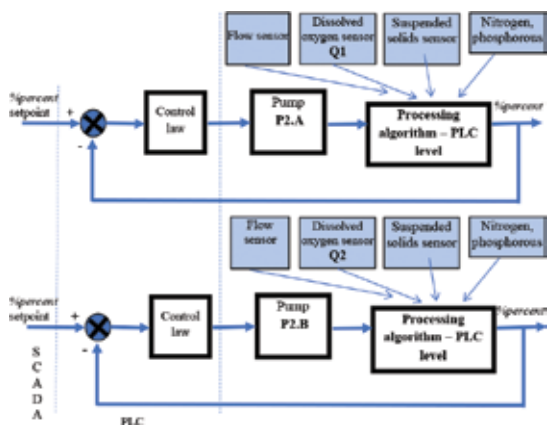

Figure 6. Control loops for the recirculation flows.

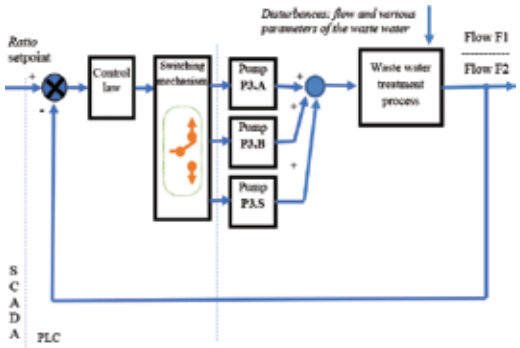

Figure 7. Control loop for the ratio: activated sludge flow/wastewater flow.

As in the previous cases, the control loop is implemented at level 1 of DCS, and the set point is provided by level 2. The actuators are the submersible pumps P3.A, P3.B, and P3.S. The switching mechanism (switching logic) of the pumps is designed in order to cover the above-described scenarios. The influent wastewater flows and their parameters are disturbances for the control loop and will be rejected by the control law.

4. Advanced control solutions for the activated sludge bioprocess

In the following sections, some advanced control solutions are proposed in order to be implemented at level 2 of the DCS-WTP Calafat. More precisely, multivariable adaptive and robust control algorithms are proposed for the activated sludge process that takes place at WTP Calafat. The main control objective at this level is to maintain the pollution level at a desired low value despite the load and concentration variations of the pollutant. The controlled variables are the concentrations of pollutant and dissolved oxygen inside the aerator. Therefore, some of the control loops described in the previous section will be used, and other loops will be modified. The simulations performed in realistic conditions and using an adapted model of the activated sludge process showed that the performance of the overall control system can be increased. The implementation of the proposed control algorithms at WTP Calafat will be ensured within the research project TISIPRO [19].

4.1. Dynamical model of the activated sludge bioprocess and control objective

The activated sludge process which works at WTP Calafat is an aerobic process of biological wastewater treatment. As it was mentioned above, this process is operated in at least two interconnected tanks: a bioreactor (aerator) in which the biodegradation of the pollutants takes place and a sedimentation tank (settler) in which the liquid is clarified (the biomass is separated from the treated wastewater) (**Figure 8**). This bioprocess is very complex, highly nonlinear, and characterized by parametric uncertainties. In the literature there are many models that try to describe the activated sludge processes. The best-known model is ASM1 (Activated Sludge Model No. 1) [3, 10–12]. The main drawback of ASM1 is its complexity, such that it becomes unusable in control issues. Thus, in this chapter a simplified model of a process

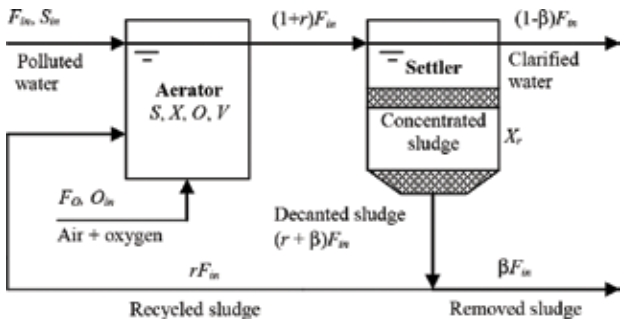

Figure 8. Schematic view of an activated sludge process.

for the removal of the pollutant S from the treated water will be used. The model is based on the model of Nejjari et al. [8], adapted for WTP Calafat. The dynamics of the plant (aerator + settler) is described by the mass balance equations [8, 9]:

$$\begin{aligned}
\dot{X}(t) &= \mu(t)X - \mu_S X - D(1+r)X + rDX_r,\\
\dot{S}(t) &= -(1/Y)\big(\mu(t)X - \mu_S X\big) - D(1+r)S + DS_{in},\\
\dot{O}(t) &= -(K_0/Y)\big(\mu(t)X - \mu_S X\big) - D(1+r)O + \alpha F_O(O_{sat} - O) + DO_{in},\\
\dot{X}_r(t) &= (1+r)DX - \big(r+\beta\big)DX_r,
\end{aligned} \tag{1}$$

where X, S, O, and X_r are the concentrations of biomass (active sludge) in the aerator, of substrate (pollutant), of dissolved oxygen, and of recycled biomass, respectively, O_{sat} is the saturation concentration of dissolved oxygen, $D = F_{in}/V$ is the dilution rate (F_{in} is the influent flow rate, V is the constant aerator volume), μ is the specific growth rate, μ_S is the decay coefficient for biomass, Y is the consumption coefficient of substrate S, r is the rate of recycled sludge, β is the rate of removed sludge, F_O is the aeration rate, and α is the oxygen transfer rate. S_{in} and O_{in} are the substrate and dissolved oxygen concentrations in influent substrate.

If we define $\xi = [X \;\; S \;\; O \;\; X_r]^T$ the state vector of model (1), $\phi = \big(\mu(\cdot) - \mu_S\big)X$ the reaction rate, $v = [0 \quad DS_{in} \quad DO_{in} + \alpha F_O O_{sat}) \quad 0]^T$ the vector of mass inflow rates and gaseous transfer rates, and $K = [1 \quad -1/Y \quad -K_0/Y \quad 0]^T$ the yield vector, then model (1) can be written as

$$\dot{\xi} = K\phi(\xi) - \overline{D}\xi + v \tag{2}$$

where $\overline{D}$ is the matrix of dilution rates, whose structure is the next one:

$$\overline{D} = \begin{bmatrix} D(1+r) & 0 & 0 & -rD \\ 0 & D(1+r) & 0 & 0 \\ 0 & 0 & D(1+r) + \alpha F_O & 0 \\ -D(1+r) & 0 & 0 & D\big(r+\beta\big) \end{bmatrix}. \tag{3}$$

In fact, model (2) describes the dynamics of a large class of bioprocesses carried out in stirred tank reactors and is referred as *general dynamic state-space model* of this class of bioprocesses [3, 7],

with $\xi \in \Re^n$, $\phi(\cdot) \in \Re^m$, $K \in \Re^{n\times m}$, $\overline{D} \in \Re^{n\times n}$, and $v \in \Re^n$. The nonlinear character of model (2) is given by the reaction kinetics, its modeling being the most difficult task.

The main *control objective* is to maintain the pollution level at a desired low value despite the load and concentration variations of the pollutant. Because in any aerobic fermentation a proper aeration is essential in order to obtain an efficient process, then an adequate control of dissolved oxygen concentration in aerator is very important [3, 8, 11]. Thus, the *controlled variables* are concentrations of pollutant S and dissolved oxygen O inside the aerator, that is, $y = [S \;\; O]^T$. As *control inputs* we chose the dilution rate D and the aeration rate F_O, that is, $u = [D \;\; F_O]^T$. So, we have a multivariable control problem of a squared process with two inputs and two outputs [12]. Since in model (1) the relative degrees [20] of both controlled variables S and O are equal to one, then the dynamic of output y can be written as

$$\dot{y} = \Psi(\xi) + \Phi^T(\xi)\,\theta + B(\xi)\,u, \tag{4}$$

where $\Psi(\xi)$, $\Phi^T(\xi)$, θ, and $B(\xi)$ are given by.

$$\Psi(\xi) = \begin{bmatrix} (1/Y)\cdot \mu_S X \\ (K_0/Y)\cdot \mu_S X \end{bmatrix}, \Phi^T(\xi) = \begin{bmatrix} -1/Y \\ -K_0/Y \end{bmatrix}, \theta = \mu X, B(\xi) = \begin{bmatrix} S_{in} - (1+r)S & 0 \\ O_{in} - (1+r)O & \alpha(O_{sat} - O) \end{bmatrix} \tag{5}$$

Model (4) is linear with respect to control input $u(t)$.

The matrix $B(\xi)$ is nonsingular and so invertible as long as $S_{in} - (1+r)S$ and $\alpha(O_{sat} - O)$ are different from zero, conditions that are satisfied in a normal operation of the reactor.

We consider that the specific growth rate μ is a double Monod-type model, i.e., [8]

$$\mu(t) = \mu_{\max} \frac{S(t)}{K_S + S(t)} \cdot \frac{O(t)}{K_O + O(t)} \tag{6}$$

where $\mu_{\max}$ is the maximum specific growth rate of microorganisms and K_S and K_O are the saturation constants for substrate S and for oxygen, respectively.

Consequently, based on the input-output model (4), the main *control objective* is to make output y to asymptotically track some desired trajectories denoted $y^* \in \Re^2$ despite any influent pollutant variation and uncertainty and time-varying of some process parameters and also of unavailability of some process states.

4.2. Control strategies

4.2.1. Exact feedback linearizing control

Firstly, we consider the ideal case where maximum prior knowledge concerning the process is available; that is, model (2) is completely known (i.e., μ is assumed completely known and all the state variables, and all the inflow rates are available by online measurements). Then, a *multivariable decoupling exact feedback linearizing control law* can be designed. Since the relative degree of the input-output model (4) is equal to 1, then for the closed loop system, we impose the following first-order linear stable dynamical behavior:

$$(\dot{y}^* - \dot{y}) + \Lambda \cdot (y^* - y) = 0, \tag{7}$$

where $y^* = [S^* \;\; O^*]^T$ is a desired piecewise constant output, $\Lambda = \text{diag}\{\lambda_i\}$, $\lambda_i > 0$, and $i = 1, \;\; 2$.

Then, from models (4) and (7), one obtains a *multivariable decoupling feedback linearizing control law*:

$$u = B(\xi)^{-1}\left[\Lambda(y^* - y) - \Psi(\xi) - \Phi^T(\xi)\,\theta + \dot{y}^*\right]. \tag{8}$$

The control law (8) leads to a linear error model described as $\dot{e} = -\Lambda e$, where $e = y^* - y$ is the tracking error, which for $\lambda_i > 0, \quad i = 1, 2$ has an exponential stable point at $e = 0$.

This controller will be used both for developing of the adaptive and robust controllers and as benchmark, because it yields the best behavior and can be used for comparison.

4.2.2. Adaptive control strategy

Since the prior knowledge concerning the process previously assumed is not realistic, we will design *an adaptive control strategy* under the following conditions:

- The specific growth rate μ is time-varying and completely unknown.
- The variables X and X_r are not accessible.
- The inflow rate F_{in} and the rate of recycled sludge r are time-varying.
- The online available measurements are the output pollution level S; the oxygen concentrations O_{in} and O, respectively; and the influent substrate concentration S_{in}.
- All the other kinetic and process coefficients are known.

Recall that the control objective is to make output y to asymptotically track some specified references $y^* \in \Re^2$ despite the unknown kinetics, any time variation of S_{in}, O_{in}, and F_{in} and time-varying of some process parameters. Under the above conditions, an *adaptive controller* is obtained as follows. The unmeasured variables X and X_r can be estimated by using an appropriate form of the *reaction rate-independent asymptotic observer* developed in [12], described by the next equations (for details, see [12, 15–17]):

$$\dot{\widehat{w}}\,(t) = W(t)\,\widehat{w}(t) + Z(t)\,\zeta_1(t) + N b(t), \quad \widehat{w}(0) = N\,\widehat{\xi}(0) \quad \widehat{\zeta}_2(t) = N_2^{-1}(\widehat{w}(t) - N_1\zeta_1(t)) \tag{9}$$

with

$$W(t) = (N_1 A_{12}(t) + N_2 A_{22}(t))N_2^{-1}, \quad Z(t) = N_1 A_{11}(t) + N_2 A_{21}(t) - W(t)N_1 \tag{10}$$

This observer was developed for the following class of nonlinear models [12, 15–17]:

$$\dot{\xi}(t) = K\phi(\xi, t) + A(t)\xi(t) + b(t), \tag{11}$$

that can describe the dynamics of numerous bioprocesses, with $x \in \Re^n$, $\phi(\cdot) \in \Re^m$, $K \in \Re^{n\times m}$, $A \in \Re^{n\times n}$, and $b \in \Re^n$. Note that the aerobic process modeled by model (2) belongs to this class.

For a good understanding, we resume here only some aspects. If in model (11) $q \le n$, states are measured online, and then model (11) can be rewritten as [12, 15–17]:

$$\dot{\zeta}_1(t) = K_1\phi(\xi,t) + A_{11}\zeta_1 + A_{12}\zeta_2 + b_1(t), \quad \dot{\zeta}_2(t) = K_2\phi(\xi,t) + A_{21}\zeta_1 + A_{22}\zeta_2 + b_2(t), \quad (12)$$

where ζ_1 ($\dim\zeta_1 = q$) denotes the measured variables and ζ_2 ($\dim\zeta_2 = n - q = s$) represents the variables that have to be estimated, and the matrices K_1, K_2, A_{11}, A_{12}, A_{21}, A_{22}, b_1, and b_2, with suitable dimensions, are the corresponding partitions of K, A, and b, respectively.

The observers (9) and (10) were developed under the next assumptions about model (11) [12, 15–17]: (H1) K, $A(t)$, and $b(t)$ are known, $\forall t \ge 0$; (H2) $\phi(\xi,t)$ is unknown, $\forall t \ge 0$; (H3) rank $K_1 =$ rank $K = p$ with $p \le m < n$; and (H4) $A(t)$ is bounded, i.e., there exist two constant matrices A^- and A^+ such as $A^- \le A(t) \le A^+$ and $\forall t \ge 0$.

The auxiliary variable w ($\dim w = s$) is defined as $w(t) = N\xi(t)$, with $N = [N_1 \vdots N_2] \in \Re^{s\times n}$, where $N_1 \in \Re^{s\times q}$ and $N_2 \in \Re^{s\times s}$ checks the equation $N_1K_1 + N_2K_2 = 0$. If N_2 can be arbitrarily chosen, then $N_1 = -N_2K_2K_1^*$, where K_1^* is a generalized pseudo-inverse of K_1 [15, 21]. Moreover, if N_2 is invertible, then the unmeasured states ζ_2 can be calculated from $w(t) = N_1\zeta_1(t) + N_2\zeta_2(t)$ as $\zeta_2 = N_2^{-1}(w - N_1\zeta_1)$. This condition is satisfied if N_2 is chosen as $N_2 = kI_s$, where $k > 0$ is a real arbitrary parameter and I_s is the s-dimensional unity matrix.

The stability of the observers (9) and (10) can be analyzed by using the observation error $\tilde{\zeta}_2 = \zeta_2 - \widehat{\zeta}_2$, whose dynamics obtained from models (9) and (12) is given by $\dot{\tilde{\zeta}}_2(t) = W_\zeta(t)\tilde{\zeta}_2(t)$, with

$$W_\zeta(t) = N_2^{-1}W(t)N_2 = A_{22}(t) - K_2K_1^*A_{12}(t). \quad (13)$$

It was proven (see [21]) that whatever K_1^* is, the observers (9) and (10) are asymptotically stable if the next conditions hold [15]: (a) $W_{\zeta,ij}(t) \ge 0$ and $\forall i \ne j$, that is, W_ζ is a Metzler matrix [22]; (b) W_ζ^- and W_ζ^+ are Hurwitz stable matrices, with $W_\zeta^\pm(t) = A_{22}^\pm(t) - K_2K_1^*A_{12}^\pm(t)$, where A_{12}^+ and A_{22}^+ and A_{12}^- and A_{22}^- are the corresponding partitions of A^- and A^+, specified in (H4). Since in model (2) rank $K = 1$, under the above conditions, let us consider the next state partitions:

$$\zeta_1 = [S \;\; O]^T \text{ and } \zeta_2 = [X \;\; X_r \;\;]^T. \quad (14)$$

which are induced on the matrices K, A, and b from model (11) the following partitions:

$$K = \left[K_1^T \vdots K_2^T\right] = [-1/Y \quad -K_0/Y \;\vdots 1 \quad 0]^T, \phi(\xi,t) = \left(\mu(S,O) - \mu_S\right)X,$$

$$A(t) = \begin{bmatrix} A_{11} & \vdots & A_{12} \\ \cdots & \vdots & \cdots \\ A_{21} & \vdots & A_{22} \end{bmatrix} = \begin{bmatrix} -D(1+r) & 0 & \vdots & 0 & 0 \\ 0 & -D(1+r) - \alpha F_O & \vdots & 0 & 0 \\ \cdots\cdots & \cdots\cdots\cdots & \vdots & \cdots\cdots & \cdots\cdots \\ 0 & 0 & \vdots & -D(1+r) & rD \\ 0 & 0 & \vdots & D(1+r) & -D(r+\beta) \end{bmatrix}, \quad (15)$$

$$b(t) = \left[b_1^T \vdots b_2^T\right]^T = [DS_{in} \;\; \alpha F_O O_{sat} + DO_{in} \;\vdots\; 0 \;\; 0]^T.$$

If the matrix N_2 is chosen as $N_2 = I_2$, then the matrix N_1 from $N = [N_1 \vdots N_2]$ takes the form:

$$N_1 = -N_2 K_2 K_1^* = \frac{1}{(1/Y)^2 + (K_0/Y)^2} \cdot \begin{bmatrix} 1/Y & K_0/Y \\ 0 & 0 \end{bmatrix}. \tag{16}$$

The unmeasured states X and X_r are obtained by using the asymptotic observers (9) and (10) where $W(t)$ and $Z(t)$ are described by the following matrices:

$$W(t) = \begin{bmatrix} -D(1+r) & rD \\ D(1+r) & -D(\beta + r) \end{bmatrix}, \tag{17}$$

$$Z(t) = \frac{1}{(1/Y)^2 + (K_0/Y)^2} \begin{bmatrix} 0 & -(K_0/Y)\alpha F_O(1+r) \\ -(1/Y)D(1+r) & -(K_0/Y)D(\beta + r) \end{bmatrix}. \tag{18}$$

Since $N_2 = I_2$, then $W_\zeta(t) = W(t)$. It is obvious that if $0 < D^- \le D \le D^+$ and $0 \le r^- \le r \le r^+$, where D^- and D^+ and r^- and r^+ represent a lower and, respectively, an upper bound of D and r, and $1 \ge \beta \ge 0$, then two stable bounds denoted W_ζ^- and W_ζ^+ can be calculated for the stable matrix $W_\zeta(t)$.

To obtain the online estimates $\widehat{\mu}$ of the unknown rate μ, we will use an observer-based parameter estimator (OBE) (for details, see [3, 7, 21]).

Since for the aerobic digestion we must estimate only one incompletely known reaction rate, using only the dynamics of S and O, then the OBE is particularized as [3, 7, 12]

$$\begin{aligned} \dot{S}(t) = -(1/Y)(\widehat{\mu} - \mu_S)\widehat{X} - D(1+r)S + DS_{in} + \omega_1\left(S - \widehat{S}\right), \dot{O}(t) = -(K_0/Y)(\widehat{\mu} - \mu_S)\widehat{X} \\ -D(1+r)O + \alpha F_O(O_{sat} - O) + DO_{in} + \omega_2\left(O - \widehat{O}\right), \dot{\widehat{\mu}}(t) = -(1/Y)\widehat{X} \cdot \gamma_1 \cdot \left(S - \widehat{S}\right) \\ -(K_0/Y)\widehat{X} \cdot \gamma_2 \cdot \left(O - \widehat{O}\right), \end{aligned} \tag{19}$$

where $\widehat{X}$ is the online estimate of X, calculated by using the state asymptotic observer given in Eqs. (9) and (10), and $\omega_1,\ \omega_2 < 0$ and $\gamma_1,\ \gamma_2 > 0$ are design parameters at the user's disposal to control the stability and the tracking properties of the estimator.

Finally, the complete adaptive control algorithm is made up by combination of the observer Eqs. (9), (10), and (14)–(18) and parameter estimator Eq. (19) with the linearizing control law (8) rewritten as

$$\begin{aligned} \begin{bmatrix} D \\ F_O \end{bmatrix} = \begin{bmatrix} S_{in} - (1+r)S & 0 \\ O_{in} - (1+r)O & \alpha(O_{sat} - O) \end{bmatrix}^{-1} \left(\begin{bmatrix} \lambda_1 & 0 \\ 0 & \lambda_2 \end{bmatrix} \cdot \begin{bmatrix} S^* - S \\ O^* - O \end{bmatrix} \right. \\ \left. - \begin{bmatrix} -(1/Y) \cdot (\widehat{\mu} - \mu_S) \cdot \widehat{X} \\ -(K_0/Y) \cdot (\widehat{\mu} - \mu_S) \cdot \widehat{X} \end{bmatrix} + \begin{bmatrix} \dot{S}^* \\ \dot{O}^* \end{bmatrix} \right). \end{aligned} \tag{20}$$

A block diagram of the designed multivariable adaptive system is shown in **Figure 9**.

http://dx.doi.org/10.5772/intechopen.74827

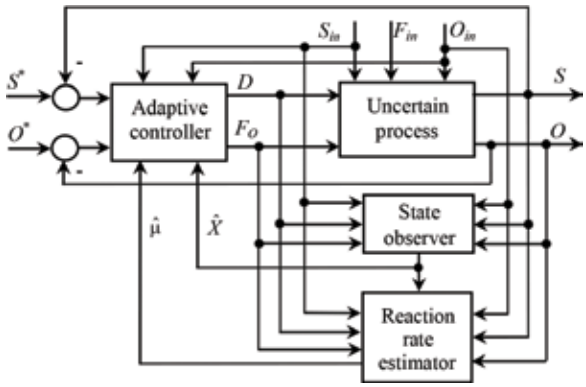

Figure 9. Structure of the adaptive controlled bioprocess.

4.2.3. Robust control strategy

We will develop *a robust control strategy* under realistic conditions as follows:

- S_{in} and O_{in} are not measurable; that is, in model (11) the vector $b(t)$ is incompletely known, but some lower and upper bounds, possible time-varying, denoted by S_{in}^- and S_{in}^+ and O_{in}^- and O_{in}^+, respectively, are given.
- The variables X and X_r are not accessible.
- μ is uncertain and time-varying, because both $\mu_{\max}$ and K_S are uncertain and time-varying, but for these, the bounds $\mu_{\max}^-$ and $\mu_{\max}^+$ and K_S^- and K_S^+, respectively, are known.
- The inflow rate F_{in} is time-varying.
- r is time-varying, but $r \in [r^-,\ r^+]$, where the bounds $r^{\mp}$ are given.
- The available online measurements are S and O.
- All the other kinetic and process coefficients are known.

To control process (1) under the above conditions, we will develop a robust control strategy as follows. First, the components D and F_O of the control law (8) are written as

$$D = \frac{1}{S_{in} - (1+r)S}\left(\lambda_1(S^* - S) + f_D\right), \tag{21}$$

$$F_O = -\frac{O_{in} - (1+r)O}{(S_{in} - (1+r)S)\cdot\alpha(O_{sat} - O)}\left(\lambda_1(S^* - S) + f_D\right) + \frac{1}{\alpha(O_{sat} - O)}\left(\lambda_2(O^* - O) + f_O\right), \tag{22}$$

where

$$f_D = (1/Y)\left(\mu - \mu_S\right)X, f_O = (K_0/Y)\left(\mu - \mu_S\right)X. \tag{23}$$

To estimate the unknown variable X from Eq. (23), we cannot use anymore the asymptotic observers (9) and (10) because S_{in} and O_{in} are not measurable. Hence, by using a suitable

observer interval, based on the known lower and upper bounds of S_{in} and O_{in}, we estimate lower and upper bounds of X, in-between it evolve. The interval observer is achieved by using the designed asymptotic observers (9) and (10). For this purpose, the hypothesis (H1) is modified into (H1′) as follows: (H1′) K and $A(t)$ are known, $\forall t \geq 0$, and the next additional hypotheses are introduced [15, 16, 21]: (H5) the input vector $b(t)$ is unknown, but guaranteed bounds, possibly time-varying, are given as $b^-(t) \leq b(t) \leq b^+(t)$; and (H6) the initial state conditions are unknown, but guaranteed bounds are given as $\xi^-(0) \leq \xi(0) \leq \xi^+(0)$.

Interval observers work as a bundle of two observers: an upper observer, which produces an upper bound of the state vector, and a lower observer producing a lower bound, providing this way a bounded interval in which the state vector is guaranteed to evolve [15–17, 23]. The design is based on properties of monotone dynamical systems or cooperative systems (see [15–16, 21, 24]). Then, under hypotheses (H1′)-(H6), a robust interval observer for the system (2) can be described as [12, 15–17, 21]

$$(\Sigma^+) = \begin{cases} \dot{w}^+(t) = W(t)w^+(t) + Z(t)\zeta_1(t) + Mv^+(t), \quad w(0)^+ = N\xi(0)^+, \\ \zeta_2^+(t) = N_2^{-1}(w^+(t) - N_1\zeta_1(t)), \end{cases}$$

$$(\Sigma^-) = \begin{cases} \dot{w}^-(t) = W(t)w^-(t) + Z(t)\zeta_1(t) + Mv^-(t), \quad w(0)^- = N\xi(0)^-, \\ \zeta_2^-(t) = N_2^{-1}(w^-(t) - N_1\zeta_1(t)), \end{cases} \tag{24}$$

where $W(t)$ and $Z(t)$ are given by (10), $\zeta_2^+(t)$ and $\zeta_2^-(t)$ are upper and lower bounds of the estimated state $\zeta_2(t)$ and $M = \left[N_1 \vdots |N_{1,ij}| \vdots N_2\right]$, and $v^+(t) = \left[\left(b_1^+ + b_1^-\right)/2 \quad \left(b_1^+ - b_1^-\right)/2 \quad b_2^+\right]^T$ and $v^-(t) = \left[\left(b_1^+ + b_1^-\right)/2 \quad -\left(b_1^+ - b_1^-\right)/2 \quad b_2^-\right]^T$, with b_1^+, b_2^+ and b_1^-, b_2^-, are the partitions of the known upper and lower bounds of the input vector $b(t)$. Since N_2 must have to be invertible, then it is chosen as $N_2 = kI_s$, where I_s is the identity matrix and $k > 0$ is a real arbitrary parameter.

If the matrix $W_\zeta(t)$ defined in Eq. (13) is cooperative [15–16, 23], then under hypotheses (H1′)–(H6), the pair of systems $(\Sigma^+, \ \Sigma^-)$ constitutes a stable robust interval observer generating trajectories $\zeta_2^+(t)$ and $\zeta_2^-(t)$, and it guarantees that $\zeta_2^-(t) \leq \zeta_2(t) \leq \zeta_2^+(t)$ and $\forall t \geq 0$ as soon as $\xi^-(0) \leq \xi(0) \leq \xi^+(0)$ [15–16, 21]. The convergence of observer (24) can be proven like in [21].

Since the *control objective* is to maintain the wastewater degradation S at a desired low-level S^* with a proper aeration, then under the next realistic conditions $S_{in}^- \leq S_{in} \leq S_{in}^+$, $O_{in}^- \leq O_{in} \leq O_{in}^+$, $\mu_{\max}^- \leq \mu_{\max} \leq \mu_{\max}^+$, $K_S^- \leq K_S \leq K_S^+$, $r^- \leq r \leq r^+$, and $\widehat{X}^- \leq \widehat{X} \leq \widehat{X}^+$ (where $\widehat{X}$ is the estimated value of X, but $\widehat{X}^-$ and $\widehat{X}^+$ are its lower and upper bounds achieved by using the interval observer (24)), we can define the following *robust control strategy.*

If $S < (1-\varepsilon)S^*$ and $O < (1-\varepsilon)O^*$, where $0 < \varepsilon \leq 0.05$, represent a dead zone, then***

$$D = \frac{1}{S_{in}^- - (1+r^+)S}\left(\lambda_1(S^* - S) + f_D^+\right),$$

$$F_O = -\frac{O_{in}^- - (1+r^+)O}{\left(S_{in}^+ - (1+r^-)S\right)\cdot\alpha(O_{sat} - O)}\left(\lambda_1(S^* - S) + f_D^+\right) + \frac{1}{\alpha(O_{sat} - O)}\left(\lambda_2(O^* - O) + f_O^-\right)$$

else if $(1-\varepsilon)$ and $O > (1+\varepsilon)O^*$, then

$$D = \frac{1}{S_{in}^- - (1+r^+)S}\left(\lambda_1(S^* - S) + f_D^+\right),$$

$$F_O = -\frac{O_{in}^+ - (1+r^-)O}{\left(S_{in}^- - (1+r^+)S\right)\cdot\alpha\left(O_{sat} - O\right)}\left(\lambda_1(S^* - S) + f_D^-\right) + \frac{1}{\alpha\left(O_{sat} - O\right)}\left(\lambda_2(O^* - O) + f_O^+\right)$$

else if $S > (1+\varepsilon)S^*$ and $O < (1-\varepsilon)O^*$, then

$$D = \frac{1}{S_{in}^+ - (1+r^-)S}\left(\lambda_1(S^* - S) + f_D^-\right), \tag{25}$$

$$F_O = -\frac{O_{in}^- - (1+r^+)O}{\left(S_{in}^+ - (1+r^-)S\right)\cdot\alpha\left(O_{sat} - O\right)}\left(\lambda_1(S^* - S) + f_D^+\right) + \frac{1}{\alpha\left(O_{sat} - O\right)}\left(\lambda_2(O^* - O) + f_O^-\right)$$

else if $S > (1+\varepsilon)S^*$ and $O > (1+\varepsilon)O^*$, then

$$D = \frac{1}{S_{in}^+ - (1+r^-)S}\left(\lambda_1(S^* - S) + f_D^-\right),$$

$$F_O = -\frac{O_{in}^+ - (1+r^-)O}{\left(S_{in}^- - (1+r^+)S\right)\cdot\alpha\left(O_{sat} - O\right)}\left(\lambda_1(S^* - S) + f_D^-\right) + \frac{1}{\alpha\left(O_{sat} - O\right)}\left(\lambda_2(O^* - O) + f_O^+\right),$$

where.

$$f_D^{\pm} = (1/Y^{\mp})\left(\mu^{\pm} - \mu_S\right)\widehat{X}^{\pm}, f_O^{\pm} = (K_0/Y^{\mp})\left(\mu^{\pm} - \mu_S\right)\widehat{X}^{\pm} \tag{26}$$

In Eq. (26) the values of μ^+ and μ^- of μ are calculated as $\mu^{\pm} = \mu_{\max}^{\pm} S/\left(K_S^{\mp} + S\right)\cdot O/(K_O + O)$, and $\widehat{X}^-$ and $\widehat{X}^+$ correspond to S_{in}^- and O_{in}^- and S_{in}^+ and O_{in}^+, respectively.

Remark 1. Note that in a normal operation of the bioreactor the terms $S_{in}^+ - (1+r^-)S$, $S_{in}^- - (1+r^+)S$, and $\alpha(O_{sat} - O)$ from control law (25) are different from zero.◆

As can be observed from the structure of the control scheme (25) (block diagram in **Figure 10**) and from the simulation results presented in the next section, this control strategy forces the controlled variables to be as close as possible to their desired values.

4.3. Simulation results and discussions

The performance of adaptive controller given by Eq. (20) and of robust controller given by Eqs. (25) and (26) by comparison to the exact linearizing controller (8) (used as benchmark) has been tested by performing extensive simulation experiments. For a proper comparison, the simulations were carried out by using the process model (1) under identical conditions. The values of process and kinetic parameters [8, 12] are adapted for WTP Calafat as in **Table 1**. Two simulation scenarios were taken into consideration:

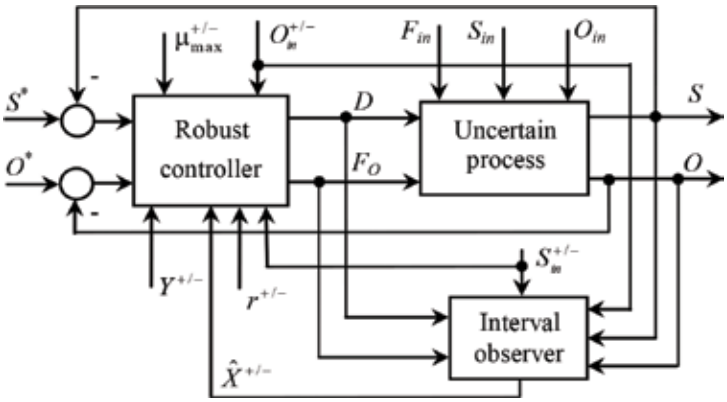

Figure 10. Structure of the multivariable robust controlled system.

Parameter	Value	Parameter	Value
$\mu_{\max}^0$	0.15 h^{-1}	α	0.018
K_S^0	100 g/l	β	0.2
K_O	2 mg/l	r^0	0.6
Y	65 g/g	F_{in}^0	6.75 m^3/min
K_0	0.5 mg/g	V	3800 m^3
μ_S	0. 0002 h^{-1}	S_{in}^0	200 mg/l
O_{sat}	10 mg/l	O_{in}^0	0.025 h^{-1}

Table 1. Kinetic and process parameters values.

Case 1. We analyzed the behavior of closed-loop system using the adaptive controller (20), by comparison to exact linearizing control law (8) under the following conditions:

- S_{in} and O_{in} are time-varying (**Figures 11** and **12**), but they are assumed measurable.
- The specific growth rate μ is unknown and time-varying.
- The kinetic coefficients $\mu_{\max}^0$ and K_S^0 are time-varying parameters described as $\mu_{\max}(t) = \mu_{\max}^0 (1 + 0.5 \sin(\pi t/10))$, $K_S(t) = K_S^0(1 + 0.25 \sin(\pi t/12 + \pi/2))$.
- The rate of recycled sludge r is time-varying as $r(t) = r^0(1 + 0.5 \sin(\pi t/36))$.
- The influent flow rate F_{in} is time-varying as $F_{in}(t) = F_{in}^0(1 + 0.2 \sin(\pi t/25) + 0.05 \sin(\pi t/4))$.
- All the other coefficients (Y, K_O, μ_S, β, α) are constant and known.
- The variables S and O are known (measurable).
- The states X and X_r are unmeasurable (X and X_r will be estimated).

http://dx.doi.org/10.5772/intechopen.74827

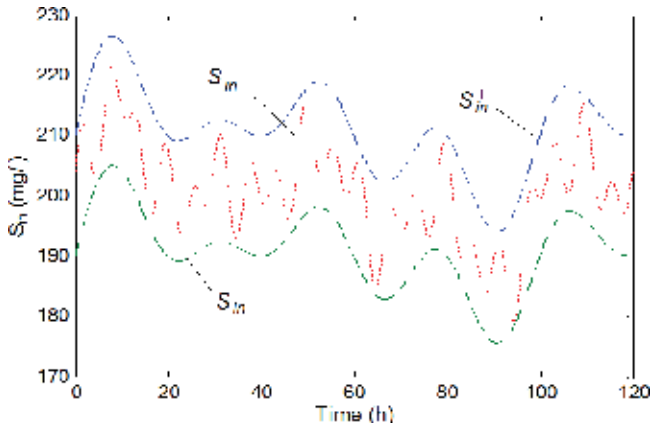

Figure 11. Evolution of S_{in} and of its bounds.

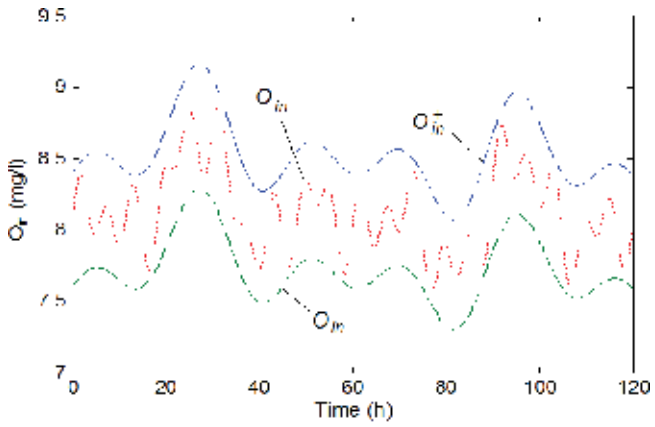

Figure 12. Evolution of O_{in} and of its bounds.

The behavior of closed-loop system using adaptive controller (20), by comparison to exact linearizing control law (8), is presented in **Figures 13–16**. To verify the regulation properties, for references S^* and O^*, some piece-wise constant variations were considered.

To be close to reality, we considered that the measurements of controlled variables S and O are corrupted with additive zero mean white noises (2.5% from their nominal values), as well as the measurements of the influent variables S_{in} and O_{in} are corrupted with an additive zero mean white noise (2.5% from their nominal values). The gains of control laws (8), respectively, (20) are $\lambda_1 = \lambda_2 = 2$, and the tuning parameters of adaptive controller have been set to the values $\omega_1 = \omega_2 = 0.5$ and $\gamma_1 = \gamma_2 = 0.75$.

The evolution of the estimate of unknown variable X provided by the observers (9), (10), and (14)–(18) is presented in **Figure 17**, and the profile of estimate of unknown specific growth rate μ provided by the OBE (19) is given in **Figure 18**. It can be noticed that both state observer and parameter estimator provide proper results. From graphics in **Figures 13** and **14**, it can be seen

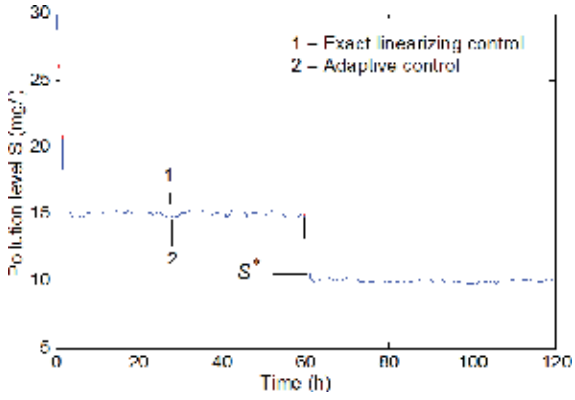

Figure 13. Time evolution of output *S* (Case 1).

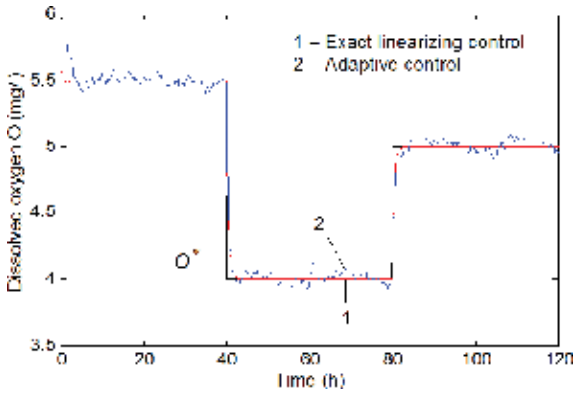

Figure 14. Time evolution of output *O* (Case 1).

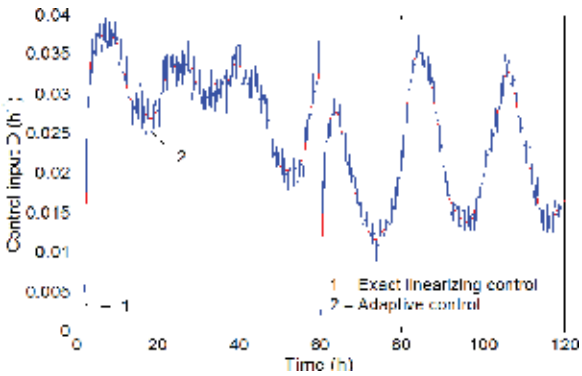

Figure 15. Profile of control input *D* (Case 1).

that the behavior of overall system with adaptive controller (20) is correct, being very close to the behavior of closed-loop system in the ideal case obtained using the linearizing controller (8) when the model is known. Note also the regulation properties and ability of the controller

http://dx.doi.org/10.5772/intechopen.74827

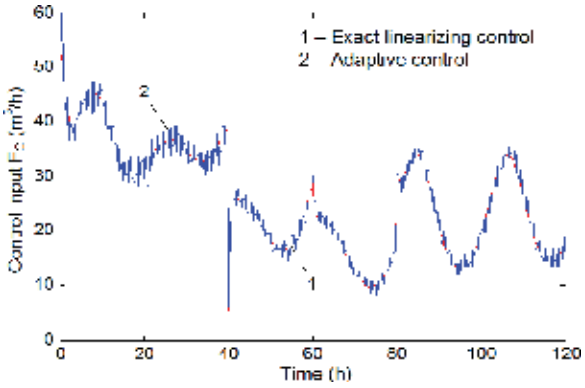

Figure 16. Profile of control input F_O (Case 1).

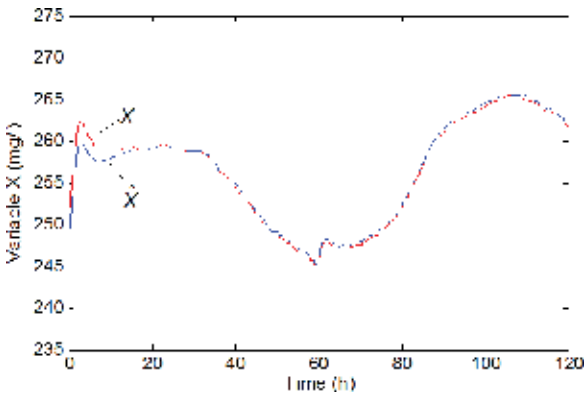

Figure 17. Estimate of unknown X (Case 1).

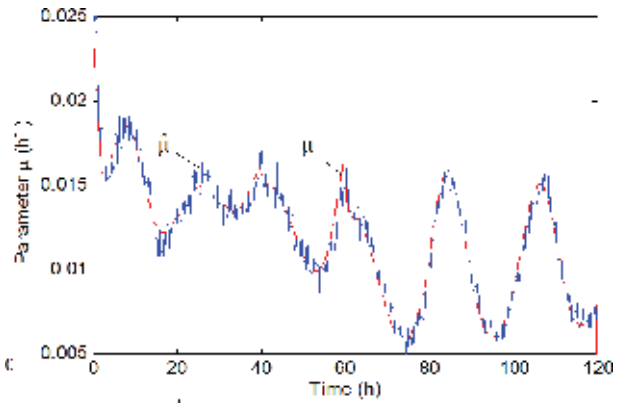

Figure 18. Estimate of unknown rate μ (Case 1).

to maintain the controlled output y very close to its desired value, despite the high variation of S_{in} and F_{in} as well as of the unmeasurable influent dissolved concentration O_{in} and time variation of some process parameters. Even if the control inputs are more affected by noisy measurements, the behavior of the controlled system remains satisfactory.

Case 2. In this case the closed-loop system is based on the structure of robust controllers (25) and (26) under the following assumptions:

- S_{in} and O_{in} are not measurable, but some lower and upper bounds, denoted by S_{in}^{-} and O_{in}^{-} and S_{in}^{+} and O_{in}^{+}, respectively, as in **Figures 11** and **12**, are given.
- $\mu_{\max}^{0}$ and K_S^0 are two uncertain and time-varying parameters, but some lower and upper bounds of them are known, i.e., $\mu_{\max}^{-} \le \mu_{\max}(t) \le \mu_{\max}^{+}$ and $K_S^{-} \le K_S(t) \le K_S^{+}$.
- F_{in} is time-varying as in Case 1, and the variables S and O are known (measurable).
- The rate of recycled sludge r and the yield coefficient Y are time-varying, but some lower and upper bounds of them are known, i.e., $r^{-} \le r(t) \le r^{+}$ and $Y^{-} \le Y(t) \le Y^{+}$.
- All the other kinetics and process coefficients are constant and known; states X and X_r are unmeasurable (the lower and upper bounds X^{-}, X_r^{-} and X^{+}, X_r^{+} will be estimated, corresponding to S_{in}^{-} and O_{in}^{-} and S_{in}^{+} and O_{in}^{+}, respectively).

In our analysis we assume that the time variations of $\mu_{\max}$ and K_S are those from Case 1, that is $\mu_{\max} \in \left[\mu_{\max}^{-},\ \mu_{\max}^{+}\right] = \left[0.5\mu_{\max}^{0},\ 1.5\mu_{\max}^{0}\right]$, and $K_S \in \left[K_S^{-},\ K_S^{+}\right] = \left[0.75K_S^{0},\ 1.25K_S^{0}\right]$.

We assume also that the time variation of r is like in Case 1, that is, $r \in [r^{-},\ r^{+}] = \left[0.5r^{0},\ 1.5r^{0}\right]$. As we mentioned above, in the control laws (25) and (26), the values of μ^{+} and μ^{-} are calculated as $\mu^{\pm} = \mu_{\max}^{\pm} S/\left(K_S^{\mp} + S\right) \cdot O/(K_O + O)$.

The behavior of closed-loop system using robust controllers (25) and (26) by comparison to the linearizing law (8) is presented in **Figures 19–22**. The gains of control laws (25) are the same as in the first case, i.e., $\lambda_1 = \lambda_2 = 2$. The estimates of lower and upper bounds of variable X are presented in **Figure 23**. The estimated values $\widehat{X}^{+}$ and $\widehat{X}^{-}$ are obtained by using the interval observers (24) and (14)–(18), where the input vectors v^{+} and v^{-} contain the known bounds S_{in}^{-} and O_{in}^{-} and S_{in}^{+} and O_{in}^{+}, respectively. The state initial conditions are unknown, but some

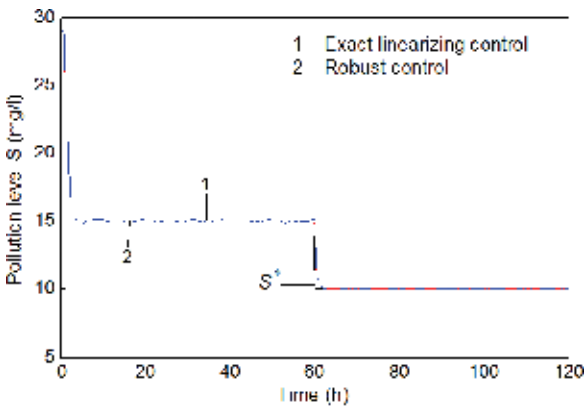

Figure 19. Time evolution of output S—Case 2.

http://dx.doi.org/10.5772/intechopen.74827

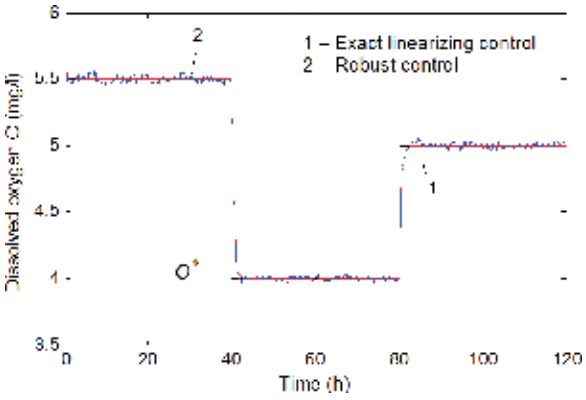

Figure 20. Time evolution of output O—Case 2.

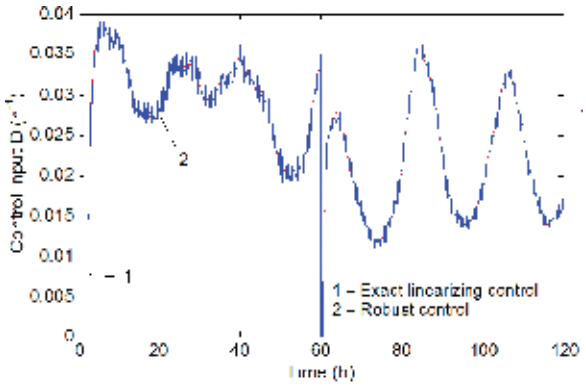

Figure 21. Profile of control input D—Case 2.

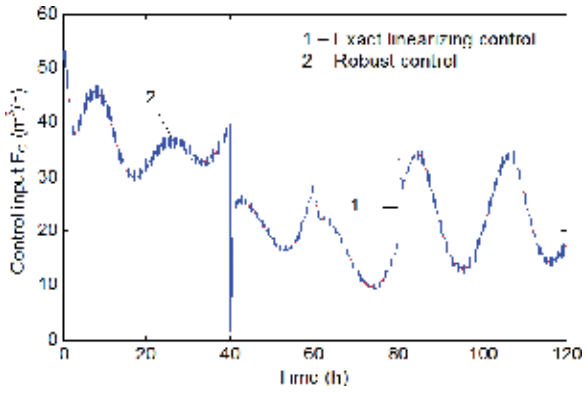

Figure 22. Profile of control input F_O—Case 2.

guaranteed lower and upper bounds are assumed as $245 = X^{-}(0) \leq X(0) \leq X^{+}(0) = 255$ (g/l). The time evolution of the uncertain but bounded time-varying parameter μ as well as of its bounds is shown in **Figure 24**.

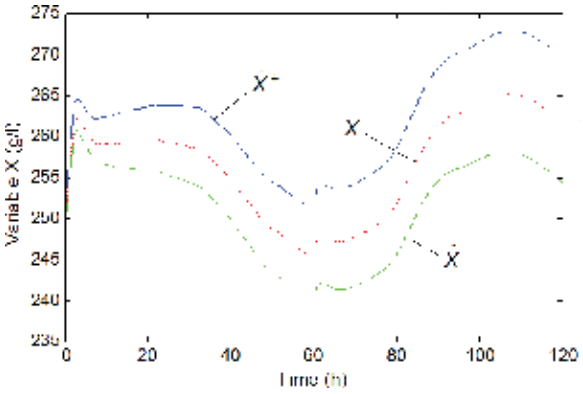

Figure 23. Estimates of bounds of X—Case 2.

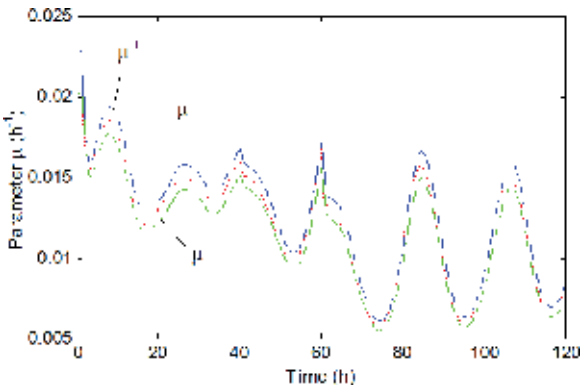

Figure 24. Profiles of μ and its bounds—Case 2.

Note that the reference profiles of S^* and O^* are the same as in the first case. As in the adaptive case, the measurements of controlled variable S and O are corrupted with additive zero mean white noises (2.5% from their nominal values). From **Figures 19–22**, it can be seen that the behavior of overall system with robust controllers (25) and (26), even if this controller uses much less a priori information and is affected by measurement noises, is correct, being close to the behavior of closed-loop system with adaptive controller (20) as well as to the behavior of closed-loop system in the ideal case (process completely known).

5. Conclusions

In this chapter, a distributed and hierarchized control system implemented at WTP Calafat was presented and analyzed. Also, advanced control solutions for the activated sludge bioprocess taking place in the WTP were proposed.

The implemented DCS-SCADA architecture of the WTP was organized as a distributed and hierarchized control system, developed on four levels. The first three levels were approached in this chapter: the field level, the direct control level, and the plant supervisory level. The structure and the functionality of these levels were described. The primary control loops were dedicated to the control of main technological variables such as levels, dissolved oxygen concentrations, recirculation flows, activated sludge flows, etc.

The analysis of the WTP behavior showed that the performance improvement of the control system is possible by developing advanced control solutions for the activated sludge bioprocess that takes place in the WTP. Therefore, multivariable adaptive and robust control algorithms were proposed and will be implemented at level 2 of the DCS.

The main control objective for the activated sludge process is to maintain the pollution level at a desired low value in spite of load and concentration variations of the pollutant. The controlled variables were the concentrations of pollutant and dissolved oxygen. Two nonlinear control strategies were proposed: an adaptive control scheme and a robust control structure. The adaptive control law was developed under the assumption that the growth rates were unknown but the influent flow rate was measurable. The robust control structure was designed under more realistic suppositions that the growth rates are uncertain and the influent concentrations are completely unknown, but lower and upper bounds of growth rates and of influent organic load (possibly time-varying) are known. Also, the uncertain process parameters were replaced by their lower and upper bounds assumed known.

The proposed control strategies were tested in realistic simulation scenarios, by using noisy measurements of the available states. Taking into account all the uncertainties, disturbances, and noisy data acting on the bioprocess, the conclusion is that the adaptive and especially the robust controllers can constitute a good choice for the control of such class of wastewater treatment bioprocesses. As future research, the implementation of the proposed control algorithms for the activated sludge process at WTP Calafat will be ensured within the project TISIPRO. The proposed control architecture and solutions envisaged the WTP Calafat but can be adapted and implemented for other similar WTPs from the WCO.

Acknowledgements

This work was supported by UEFISCDI, project ADCOSBIO no. 211/2014 (2014–2017); by the University of Craiova and Water Company Oltenia, contract no. 168/2017; and by the Competitiveness Operational Program, project TISIPRO no. P_40_416/105736 (2016–2021).

Conflict of interest

The authors declare that there is no conflict of interest about the publication of this chapter.

Author details

Dan Selișteanu, Ion Marian Popescu*, Emil Petre, Monica Roman, Dorin Șendrescu and Bogdan Popa

*Address all correspondence to: pmarian@automation.ucv.ro

Department of Automatic Control and Electronics, University of Craiova, Craiova, Romania

References

[1] ADCOSBIO. Final research report [project report]. Univ. of Craiova—UEFISCDI; 2017

[2] Tchobanoglous G, Burton FL, Stensel HD. Wastewater Engineering: Treatment and Reuse. 4th ed. Metcalf & Eddy, Inc. New York: McGraw-Hill; 2003

[3] Dochain D, Vanrolleghem P. Dynamical Modelling and Estimation in Wastewater Treatment Processes. London: IWA Publishing; 2001

[4] Galloway B, Hancke GP. Introduction to industrial control networks. IEEE Communications Surveys and Tutorials. 2013;**15**(2):860-880

[5] Knapp ED, Langill JT. Industrial Network Security: Securing Critical Infrastructure Networks for Smart Grid, SCADA, and Other Industrial Control Systems. 2nd ed. Waltham: Syngress, Elsevier; 2015

[6] Gupta RA, Chow MY. Networked control system: Overview and research trends. IEEE Transactions on Industrial Electronics. 2010;**57**(7):2527-2535

[7] Bastin G, Dochain D. On-Line Estimation and Adaptive Control of Bioreactors. Amsterdam: Elsevier; 1990

[8] Nejjari F, Dahhou B, Benhammou A, Roux G. Non-linear multivariable adaptive control of an activated sludge waste-water treatment process. International Journal of Adaptive Control and Signal Processing. 1999;**13**(5):347-365

[9] Petre E, Marin C, Selişteanu D. Adaptive control strategies for a class of recycled depollution bioprocesses. Journal of Control Engineering and Applied Informatics. 2005;**7**(2):25-33

[10] Luca L, Barbu M, Caraman S. Modelling and performance analysis of an urban wastewater treatment plant. In: Proceedings of International Conference on System Theory, Control and Computing; 17-19 October 2014; Sinaia. IEEE; 2014. p. 285-290

[11] Henze M, Gujer W, Mino T, van Loosdrecht MCM. Activated Sludge Models ASM1, ASM2, ASM2d and ASM3. IWA Task Group on Benchmarking on Mathematical Modeling for Design and Operation of Biological Wastewater Treatment. London: IWA Publishing; 2000

[12] Petre E, Selişteanu D. A multivariable robust-adaptive control strategy for a recycled wastewater treatment bioprocess. Chemical Engineering Science. 2013;**90**:40-50

[13] Selişteanu D, Petre E, Răsvan V. Sliding mode and adaptive sliding-mode control of a class of nonlinear bioprocesses. International Journal of Adaptive Control and Signal Processing. 2007;**21**(8–9):795-822

[14] Şendrescu D, Popescu D, Petre E, Bobaşu E, Selişteanu D. Nonlinear model predictive control of a lipase production bioprocess. In: Proceedings of International Carpathian Control Conference (ICCC'11); 25-28 May 2011; Velké Karlovice. IEEE; 2011. p. 341-345

[15] Alcaraz-González V, Harmand J, Dochain D, Rapaport A, Steyer JP, Pelayo Ortiz C, González-Alvarez V. A robust asymptotic observer for chemical and biochemical reactors. In: Proceedings of IFAC Symposium on Robust Control Design (ROCOND 2003), 25–27 June 2003; Milan. IFAC; 2003. 6 p

[16] Rapaport A, Dochain D. Interval observers for biochemical processes with uncertain kinetics and inputs. Mathematical Biosciences. 2005;**193**(2):235-253

[17] Alcaraz-González V, Steyer JP, Harmand J, Rapaport A, González-Alvarez V, Pelayo-Ortiz C. Application of a robust interval observer to an anaerobic digestion process. Asia-Pacific Journal of Chemical Engineering. 2005;**13**(3–4):267-278

[18] Selişteanu D, Tebbani S, Roman M, Petre E, Georgeanu V. Microbial production of enzymes: Nonlinear state and kinetic reaction rates estimation. Biochemical Engineering Journal. 2014;**91**:23-36

[19] TISIPRO. Research portfolio no. 4 [project report]. University of Craiova; 2017

[20] Isidori A. Nonlinear Control Systems. 3rd ed. Berlin: Springer-Verlag; 1995

[21] Petre E, Selişteanu D, Şendrescu D. Adaptive and robust-adaptive control strategies for anaerobic wastewater treatment bioprocesses. Chemical Engineering Journal. 2013;**217**: 363-378

[22] Aviles JD, Moreno JA. Cooperative observers for nonlinear systems. In: Proceedings of Joint IEEE Conference on Decision and Control and Chinese Control Conference; 15–18 December 2009; Shanghai: IEEE; 2009. pp. 6125-6130

[23] Moisan M, Bernard O. Interval observers for non monotone systems. Application to bioprocess models. In: Proceedings of IFAC World Congress; 3-8 July 2008; Prague: IFAC; 2008. 6 p

[24] Smith HL. Monotone dynamical systems: An introduction to the theory of competitive and cooperative systems. AMS Mathematical Surveys and Monographs. Vol. 41. Providence, Rhode Island: American Mathematical Society; 1995. 174 pp

Chapter 10

State-of-the-Art Design Technique of a Single-Channel Pump for Wastewater Treatment

Jin-Hyuk Kim and Young-Seok Choi

Additional information is available at the end of the chapter

http://dx.doi.org/10.5772/intechopen.75171

Abstract

A single-channel pump, which is commonly used for wastewater treatment, with a single-channel impeller can effectively prevent performance reduction or damage caused by foreign substances. However, the design methods for this special type of pump are different and more difficult to realize than those for general pumps. In this chapter, a state-of-the-art design technique for a single-channel pump is introduced for realizing high efficiency and low-fluid-induced vibration. In other words, advanced multidisciplinary design optimization techniques combined with unsteady flow analysis are introduced and discussed in detail to simultaneously improve hydraulic efficiency and reduce flow-induced vibration, considering the impeller-volute interaction of a single-channel pump.

Keywords: single-channel pump, wastewater treatment, hydraulic efficiency, flow-induced vibration, radial force, optimization

1. Introduction

The most common fault in a submerged pump is due to waste clogging. This phenomenon causes not only motor overload but also serious damage to a pump system. Hence, this type of pump requires unique design features for preventing losses in performance due to factors such as waste clogging, damage, and failure, unlike general submerged pumps.

Representative types of submerged pumps for wastewater treatment consist of the crushing type and flow-path-securing type. A crushing-type pump mostly crushes and transfers foreign substances with a disintegrator installed in front of the impeller. However, as such types of pumps require the installation of an additional crusher, large-sized solid particles cannot be

driven perfectly along the flow path. Moreover, it has a complex structure, high cost, low capacity, and frequent replacement cycle. On the other hand, as a single-channel pump is a representative case of a flow-path-securing type, it has different mechanism features compared with general pumps pressurized by multiblades. A single-channel impeller has one free annulus passage and does not have multiple blades. Further, it is driven by the centrifugal force generated from the rotating annulus passage [1]. Therefore, a single-channel pump is very robust, especially against failure and damage due to waste clogging.

Because of these advantages, the demand for single-channel pumps has increased rapidly in recent times in the field of wastewater treatment. Nevertheless, only a few studies have been published on the design of a single-channel pump [1–4]. To the best of the author's knowledge, the lack of studies can be attributed to the difficulties in establishing a theoretical design methodology, manufacturing, and especially, solving the balancing problem related to the fluid-induced vibration between the impeller and volute of a single-channel pump. In fact, because the mass distribution of a single-channel impeller is not rotationally symmetric, it is difficult to stabilize the fluid-induced vibration between the impeller and volute. Furthermore, unsteady radial forces, which rotate at a frequency generally determined by the rotating speed, are generated in the single-channel impeller [5]. These unsteady sources are generated by the interaction between the rotating impeller and volute, and these adversely affect the overall performance of a single-channel pump, especially its life expectancy and durability.

Over the past several years, there has been growing interest on the effects of unsteady dynamic radial forces due to impeller-volute interaction in centrifugal pumps [6–8]. However, no systematic studies on single-channel pumps have yet been attempted, except for several concepts and patents. To this end, this work presents a state-of-the-art design technique for a single-channel pump for wastewater treatment based on a theoretical approach and three-dimensional steady and unsteady numerical analyses. Moreover, advanced multidisciplinary numerical design optimization techniques are introduced and discussed in detail to simultaneously improve hydraulic efficiency and reduce the flow-induced vibration due to the impeller-volute interaction in a single-channel pump. The objective of this chapter is to provide practical guidelines for optimizing the design of a single-channel pump with the proposed design approach.

2. Basic design approach of single-channel pump

The single-channel pump with an impeller and a volute for wastewater treatment is initially designed according to the Stepanoff theory [9]. The pump can then be modeled as a three-dimensional shape, as shown in **Figure 1** [10]. The three-dimensional model can be developed using commercial modeling software such as SOLIDWORKS and CATIA. Because the Stepanoff theory generally minimizes the flow loss due to flow speed differences by increasing the cross-sectional area of internal flow at a fixed rate according to the theta angle position, it is especially useful for designing a stationary volute. Nonetheless, the impeller of a single-channel pump can be designed based on this concept because it has a free annulus passage

http://dx.doi.org/10.5772/intechopen.75171

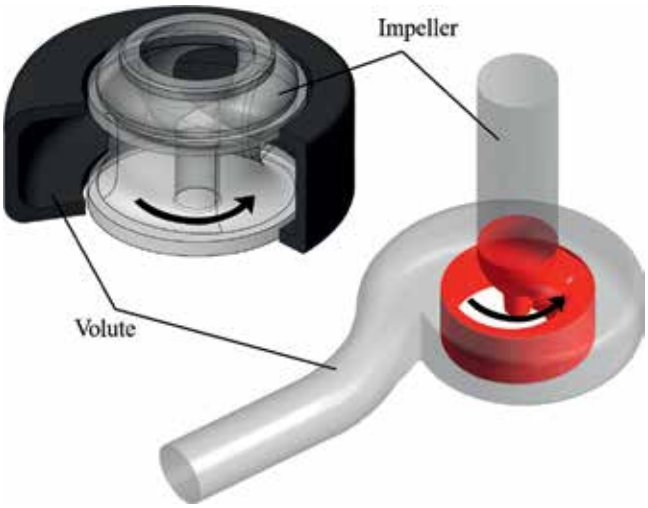

Figure 1. Three-dimensional shape of a single-channel pump [10].

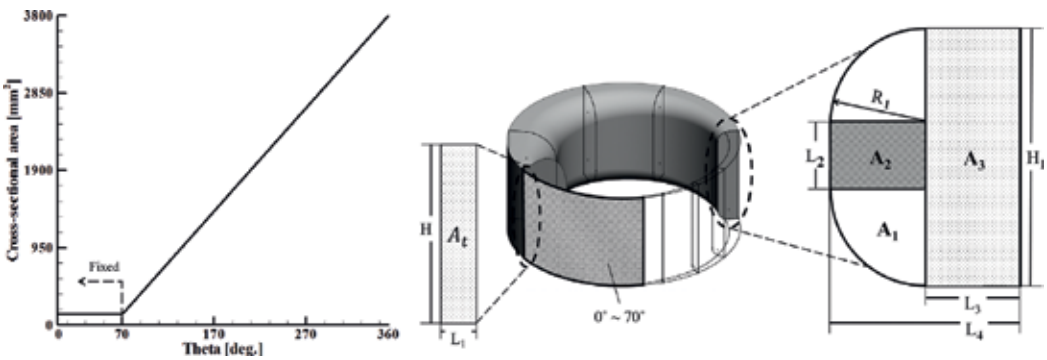

Figure 2. Cross-sectional area distribution and definition of the impeller [10].

and does not contain multiple blades. Further, the impeller is driven by the centrifugal force generated from the rotating annulus passage. Thus, the internal flow distribution in the cross-sectional area of the impeller and volute is changed proportionally with the theta angle position in order to maintain a constant flow velocity. **Figures 2** and **3** show the distribution of internal flows in the cross-sectional area of the impeller and volute generated from the Stepanoff theory. In the authors' previous work, for example, the reference volume flow rate and total head at the design point were 1.42 m^3/min and 10 m, respectively, with a rotational speed of 1760 rpm [11].

When the distribution of internal flows in the cross-sectional area is determined according to the theta angle, the shape of the area should be defined. This shape is very important for deciding the hydraulic performance and size of solid matter in a single channel. In the previous work, the authors proposed a novel design method for defining the cross section of the

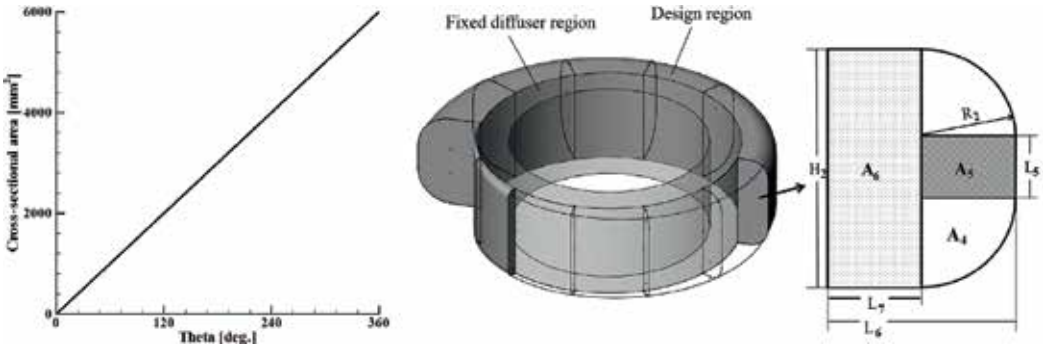

Figure 3. Cross-sectional area distribution and definition of the volute [10].

impeller and volute of a single-channel pump with high performance, as shown in **Figures 2** and **3**, respectively. The cross-sectional area is determined as follows:

The given total area (A_t) in the impeller part,

$$H_1 = 0.835 \times D_1 \tag{1}$$

where the impeller height (H_1) is fixed along theta angle and D_1 represents the inlet diameter of the impeller.

$$A_t\left(@0^\circ \sim 70^\circ\right) = 0.013 \times {D_1}^2 \tag{2}$$

$$L_1 = A_t/H_1 \tag{3}$$

$$A_t\left(@360^\circ\right) = 0.38 \times {D_1}^2 \tag{4}$$

$$A_t = 2A_1 + A_2 + A_3 \tag{5}$$

$$R_1 = \left\{\text{theta}\left(^\circ\right)\text{–}70\ (\text{value of fixed area angle})\right\} \times C_1\ \left(\text{here}, 70^\circ < \text{theta}\left(^\circ\right) \leq 360^\circ\right) \tag{6}$$

where $C_1 = 0.1 \times H_1/83.5$ is the expansion coefficient.

$$A_1 = \pi {R_1}^2/4 \tag{7}$$

$$A_2 = R_1 \times L_2 \tag{8}$$

$$A_3 = A_t\text{–}A_2\text{–}2A_1 \tag{9}$$

$$L_3 = A_3/H_1\ (\text{here}, L_3 > 0) \tag{10}$$

The given total area (A_t) in the volute part,

$$H_2 = 0.01 \times A_t\left(@360^\circ\right) \tag{11}$$

where the volute height (H_2) in fixed along theta angle.

$$A_t = 2A_4 + A_5 + A_6 \tag{12}$$

$$R_2 = \text{theta}(^\circ) \times C_2 \tag{13}$$

where $C_2 = 0.1 \times H_2/89.5$ is the expansion coefficient.

$$A_4 = \pi {R_2}^2/4 \tag{14}$$

$$A_5 = R_2 \times L_5 \tag{15}$$

$$A_6 = A_t - 2A_4 - A_5 \tag{16}$$

$$L_7 = A_6/H_2 \ (\text{here}, L_7 > 0) \tag{17}$$

The cross sections of the impeller and volute are defined as mentioned above. The three-dimensional shape can then be modeled as shown in **Figure 1**. The more detailed explanation can be found in the previous works of the authors [12, 13].

3. Steady and unsteady numerical analyses

In the computation domain generated from the basic design approach, the internal flow field is analyzed by solving three-dimensional steady and unsteady incompressible Reynolds-averaged Navier–Stokes (RANS) equations with a k-ω-based shear stress transport (SST) turbulence model by using a finite volume solver. In this work, the commercial computational fluid dynamics (CFD) code ANSYS CFX 14.5 is used, and ICEM CFD is applied to generate computational meshes for the impeller and volute. The numerical analysis is carried out with boundary conditions, solved, and post-processed using ANSYS CFX-Pre, CFX-Solver, and CFX-Post, respectively.

For the turbulence closure model, the k-ω-based SST model [14] is employed to accurately predict flow separation under an adverse pressure gradient. In this model, the k-ω and k-ε models are applied in the near-wall region and bulk domain, respectively, and a blending function ensures smooth transitions between these two models. The accuracy of the numerical analyses of turbulent flows significantly depends on treating the wall shear stress. In this chapter, the near-wall grid resolution is adjusted to maintain $y + \leq 2$ to accurately capture the wall shear stress and to implement a low-Reynolds-number SST model.

A tetrahedral grid system is constructed in the computational domain with a prism mesh near the surfaces, as shown in **Figure 4** [15]. The rotating single-channel impeller and the volute domains are each constructed using approximately 1,300,000 and 1,200,000 grid points. Hence, the optimum grid system selected using the grid independency test has approximately 2,500,000 grid points, as previously reported [15, 16].

For the boundary condition, water is considered as the working fluid, and the total pressure and designed mass flow rate are set to the inlet and outlet of the computational domain, respectively. The solid surfaces in the computational domain are considered to be hydraulically smooth under

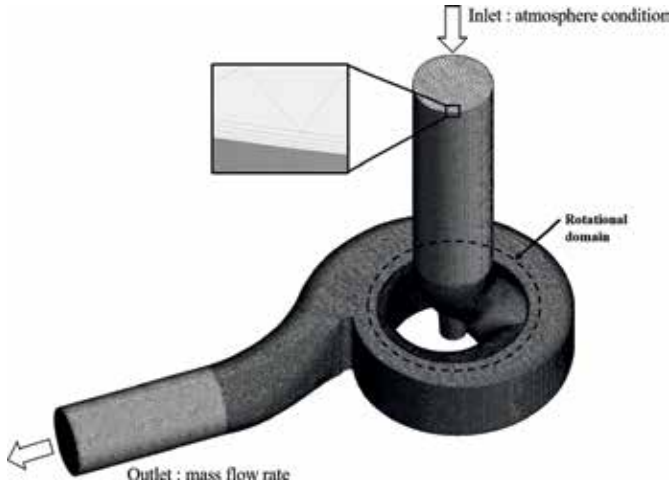

Figure 4. Computational domain and grids.

adiabatic and no-slip conditions. The stage average and transient-rotor-stator methods are respectively applied to connect the interface between the rotating impeller and volute domains in the steady and unsteady analyses.

The convergence criteria in a steady computation consist of the root-mean-square (RMS) values of the residuals of the governing equations, which are set to less than 10^{-5} for all equations. The physical time scale was set to $1/\omega$, where ω is the angular velocity of the impeller. The computations are carried out using an Intel Xeon CPU with a clock speed of 2.70 GHz, and the converged solutions are obtained after 1000 iterations with a computational time of approximately 4 h.

The results of the steady RANS analysis are used in the unsteady RANS analysis to obtain the characteristics of the radial force sources in the region of the exit surface of the impeller according to the impeller-volute interaction in the single-channel pump. In an unsteady simulation, the time step and coefficient loop for the time scale control are set to 0.000947 s and three times, respectively. The solutions are obtained after 180 iterations with an unsteady total time duration of 0.170478 s (five revolutions), and the computational time for the unsteady calculation was approximately 8 h.

4. Optimization techniques

In this chapter, the geometric parameters related to the internal flow through the cross-sectional area of the impeller and volute are selected as design variables to simultaneously optimize the hydraulic efficiency and radial force sources, considering the interaction between the rotating impeller and volute of the single-channel pump. The distribution of internal flow in the cross-sectional area of the impeller and volute can be changed smoothly by adjusting the control points represented by third-order and fourth-order Bezier-curves, respectively, as shown in **Figure 5**. Therefore, the variations in the *y*-axes for five control points (CP1, CP2,

CP3, CP4, and CP5) of both the impeller and volute are selected as design variables to obtain the most sensitive results for the variation in curve among the control points [17].

The aim of the current optimization problem is to simultaneously improve the hydraulic efficiency (η) and reduce the radial force sources considering the impeller-volute interaction in the single-channel pump. Here, one of the three objective functions, that is, the hydraulic efficiency, is defined as follows.

$$\eta = \frac{\rho g H Q}{\tau \omega} \tag{18}$$

where ρ, g, H, Q, τ, and ω denote the density, acceleration of gravity, total head, volume flow arte, torque, and angular velocity, respectively.

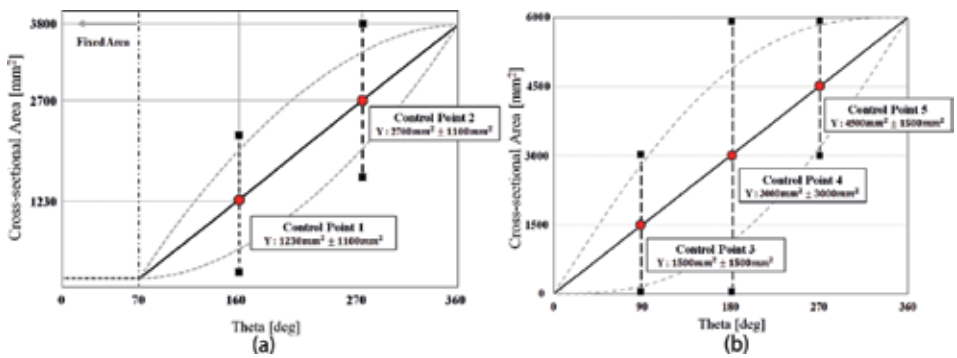

Figure 5. Definition of the design variables. (a) Impeller part (b) Volute part.

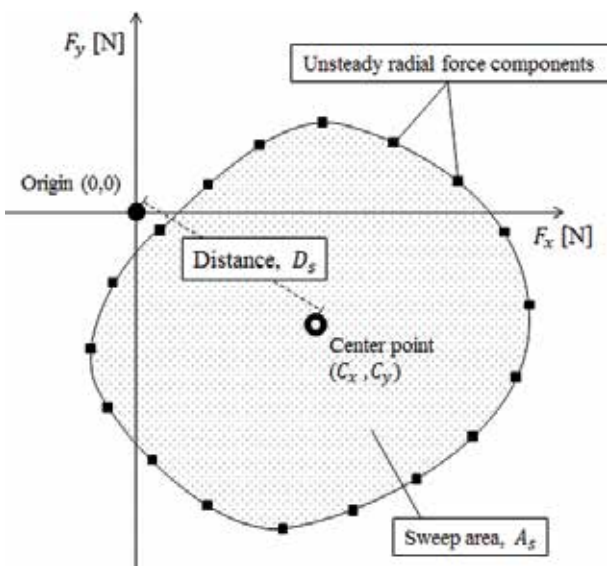

Figure 6. Definition of objective functions related to the radial force sources [10].

The other objective functions related to the radial force sources are defined as the sweep area (As) of the radial force during one revolution of impeller and the distance (Ds) of the mass center of the sweep area from the origin, as shown in **Figure 6**. These functions are defined as follows:

$$A_s = \frac{1}{2}\sum_{i=0}^{n-1}\left(x_i y_{i+1} - x_{i+1} y_i\right) \tag{19}$$

where A_s is the signed area of the polygon as the sweep area of the radial force during one revolution of impeller. The centroid of a non-self-intersecting closed polygon, defined by n vertices (x_0, y_0), (x_1, y_1), …, (x_{n-1}, y_{n-1}), is defined as the point (C_x, C_y) as follows:

$$C_x = \frac{1}{6A_s}\sum_{i=0}^{n-1}\left(x_i + x_{i+1}\right)\left(x_i y_{i+1} - x_{i+1} y_i\right) \tag{20}$$

$$C_y = \frac{1}{6A_s}\sum_{i=0}^{n-1}\left(y_i + y_{i+1}\right)\left(x_i y_{i+1} - x_{i+1} y_i\right) \tag{21}$$

In these formulas, the vertices are assumed to be numbered in the order of their occurrence along the perimeter of the polygon. Therefore, the distance of the mass center of the sweep area from the origin is finally defined as follows:

$$D_s = \sqrt{{C_x}^2 + {C_y}^2} \tag{22}$$

The Latin hypercube sampling (LHS) is employed to generate 54 design points that are used as the initial base data for constructing the response surface from five design variables. LHS, as an effective sampling method for designing and analyzing computer experiments (DACE) [18], is a matrix of order $i \times j$, where i is the number of levels to be examined and j is the number of design variables. Each of the j columns of the matrix containing levels 1, 2, …, i is randomly paired. LHS generates random sample points, ensuring that all portions of the design space are represented. Finally, the objective function values at these design points are evaluated by steady and unsteady numerical analyses.

The response surface approximation (RSA) model is applied as a surrogate model to predict the objective function values based on the 54 design points generated in the design space by using LHS. The RSA model, as a methodology of fitting a polynomial function to discrete responses obtained from numerical calculations, represents the association between the design variables and response functions [19]. The construction function for a second-order polynomial RSA can be expressed as follows:

$$f(x) = \beta_0 + \sum_{j=1}^{N}\beta_j x_j + \sum_{j=1}^{N}\beta_{jj} x_j^2 + \sum\sum_{i\neq j}^{N}\beta_{ij} x_i x_j \tag{23}$$

where β, N, and x represent the regression analysis coefficients, number of design variables, and a set of design variables, respectively, and the number of regression analysis coefficients (β_0, β_i, etc.) is $[(N + 1) \times (N + 2)]/2$.

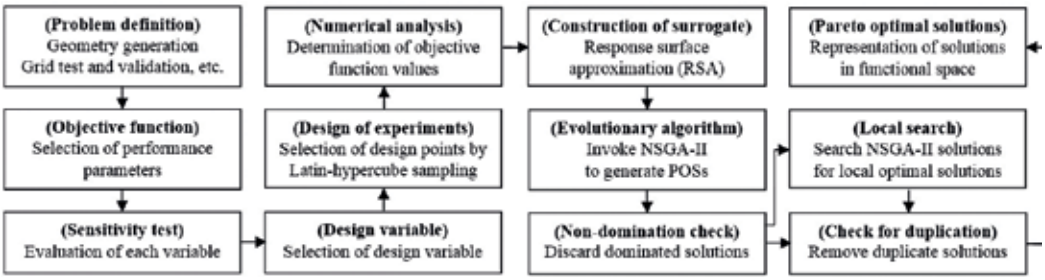

Figure 7. Multiobjective optimization procedure [22].

The RSA models are employed to construct the response surfaces based on the objective function values at the 54 design points generated in the design space using LHS. A hybrid multiobjective genetic algorithm (MOGA) is used to obtain the global Pareto-optimal solutions (POSs). The approximate POSs are obtained using a controlled elitist genetic algorithm (a variant of NSGA-II [20] as the MOGA function for three objective functions. The optimization algorithm and functions in the MATLAB OPTIMIZATION TOOLBOX [21] are used to finally generate the global POSs. **Figure 7** shows an example of the multiobjective optimization procedure [22]. The detailed optimization procedure can be referred to in the previous literatures [23, 24].

5. Results of multiobjective optimization

A hybrid MOGA based on the response surface constructed from the RSA model is employed to obtain the global POSs by using a controlled elitist genetic algorithm (a variant of NSGA-II) for three objective functions. **Figure 8** shows the three-dimensional POSs based on the three objective functions obtained using a hybrid MOGA combined with the RSA model. Here, the values of all the objective function are normalized according to the corresponding values in the reference design. Three-dimensional POSs are obviously the trade-off among the conflicting objective functions. As a result, a trade-off analysis shows an obvious correlation between the hydraulic efficiency and radial force sources. The arbitrary optimum design (AOD) is randomly extracted near the end of the POSs, which exhibits the best performance in terms of all objective functions, as shown in **Figure 8**. The AOD has objective function values that are remarkably improved relative to those in the reference design. Consequently, the value of each objective function in the AOD shows improvements of approximately 49%, 80%, and 4% in the sweep area (As) of the radial force during one revolution, the distance (Ds) of the mass center of the sweep, and the hydraulic efficiency (η), respectively, in comparison with the reference design. On the other hand, a relatively large error among the three objective functions is observed, especially for the distance of the mass center of the sweep. Nevertheless, the values obtained by the numerical analysis are better compared with the reference design.

To understand the optimization results, the trade-off of the POSs in each two-dimensional functional space is shown in **Figure 9**. As shown in **Figure 9(a)** and **(b)**, the decrement in the distance of the mass center of the sweep clearly leads to deterioration in the other objective

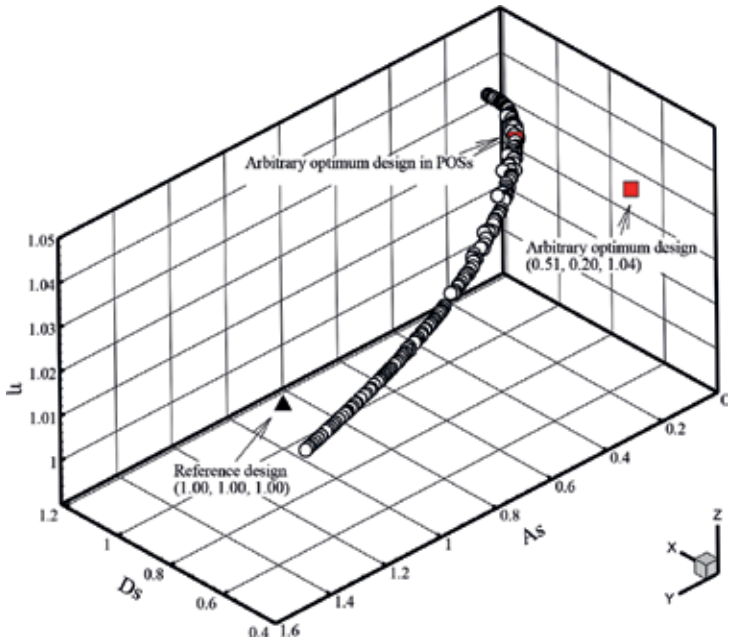

Figure 8. Three-dimensional POSs based on three objective functions. (a) ds-as (b) ds-eff. (c) as-eff.

functions. Specifically, the reduced distance of the mass center of the sweep is obtained at a lower efficiency and higher sweep area of the radial force during one revolution. However, the efficiency and sweep area of the radial force during one revolution shows a positive relation, as shown in **Figure 9(c)**. The trade-off analysis of the POSs therefore allows an engineering designer to choose any economic solution according to the required design conditions.

Figure 10 shows the isosurfaces having a low velocity of 2 m/s. As shown in **Figure 10(a)**, an extremely low-velocity region is formed along the internal wall in the impeller flow path in the reference design, whereas a similar low velocity isosurface is reduced considerably in the arbitrary optimum model (**Figure 10(b)**). These results illustrate the enhancement of hydraulic efficiency in the arbitrary optimum model as a result of optimization.

Figure 11 shows the distributions of unsteady radial force sources, averaged at the boundary surface near the impeller outlet, during one revolution of the impeller for both the reference and AODs. Here, both values are normalized by the value of the maximum radial force in the reference design. The sweep area constructed from the unsteady radial force sources in the reference design leans slightly toward the four quadrant directions from the origin, whereas it is formed near the origin in the AOD. Furthermore, the sweep area in the AOD is remarkably decreased compared with that in the reference design. Consequentially, as discussed already, the sweep area and the distance of the mass center of the sweep in the AOD are decreased by 49% and 80%, respectively, compared with those in the reference design.

Figure 12 shows the unsteady fluctuations of the net radial forces for the reference and AODs during one revolution. Both values are also normalized by the maximum value in the reference

http://dx.doi.org/10.5772/intechopen.75171

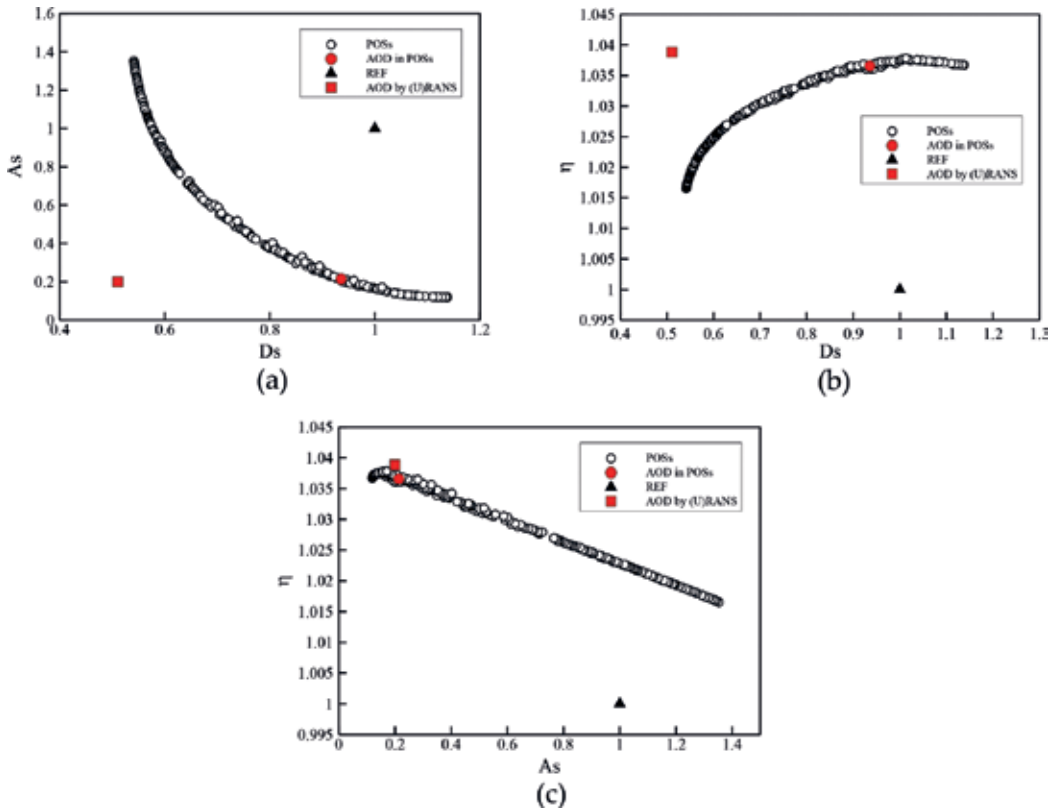

Figure 9. POSs on two-dimensional functional space.

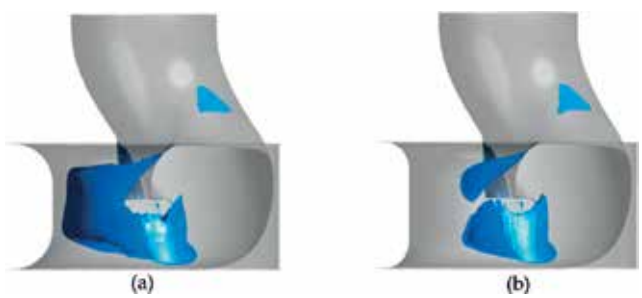

Figure 10. Isosurfaces having a low velocity of 2 m/s. (a) Reference design (b) Arbitrary optimum design.

design. As shown in **Figure 12**, the amplitude values of the fluctuation of the net radial forces in the AOD decrease considerably for most theta angle positions, especially in the region where the value of theta is 100°. In addition, its level is also less than the normalized value of 0.5 and mostly flat compared with the reference design. These phenomena clearly highlight the considerable decrease in the radial force sources as a result of optimization.

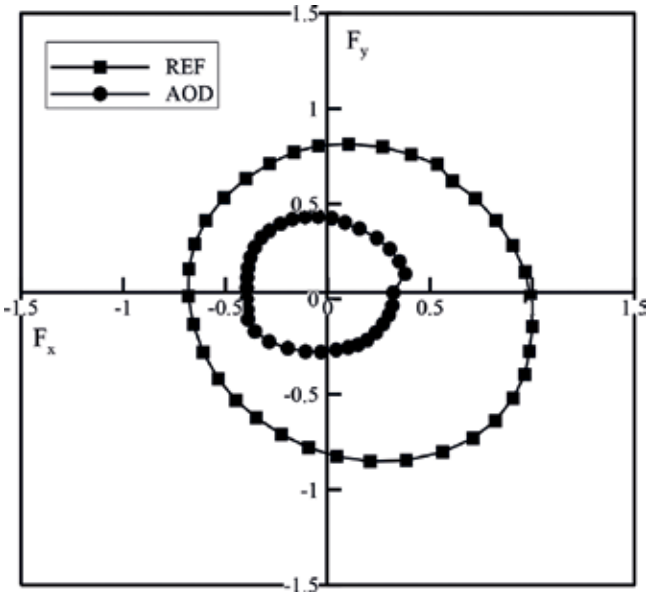

Figure 11. Unsteady radial force distributions during one revolution of the impeller.

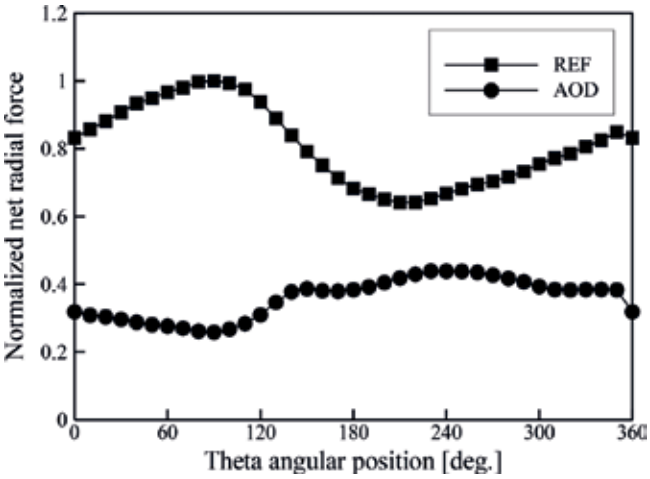

Figure 12. Unsteady net radial force fluctuations during one revolution of the impeller.

Figure 13 shows the time history of instantaneous unsteady pressure contours at the boundary surface near the impeller outlet for both the reference and AODs. Here, both values are normalized by the maximum pressure value in the pressure contours. Both the instantaneous unsteady pressure contours are compared for one rotation τ of the single-channel pump impeller. This rotation is divided into six steps to clarify changes in flow structure with time during one revolution of the impeller, as shown in **Figure 13**. In the reference design, high-pressure zones occur widely on the boundary surface near the impeller outlet, as shown in

http://dx.doi.org/10.5772/intechopen.75171

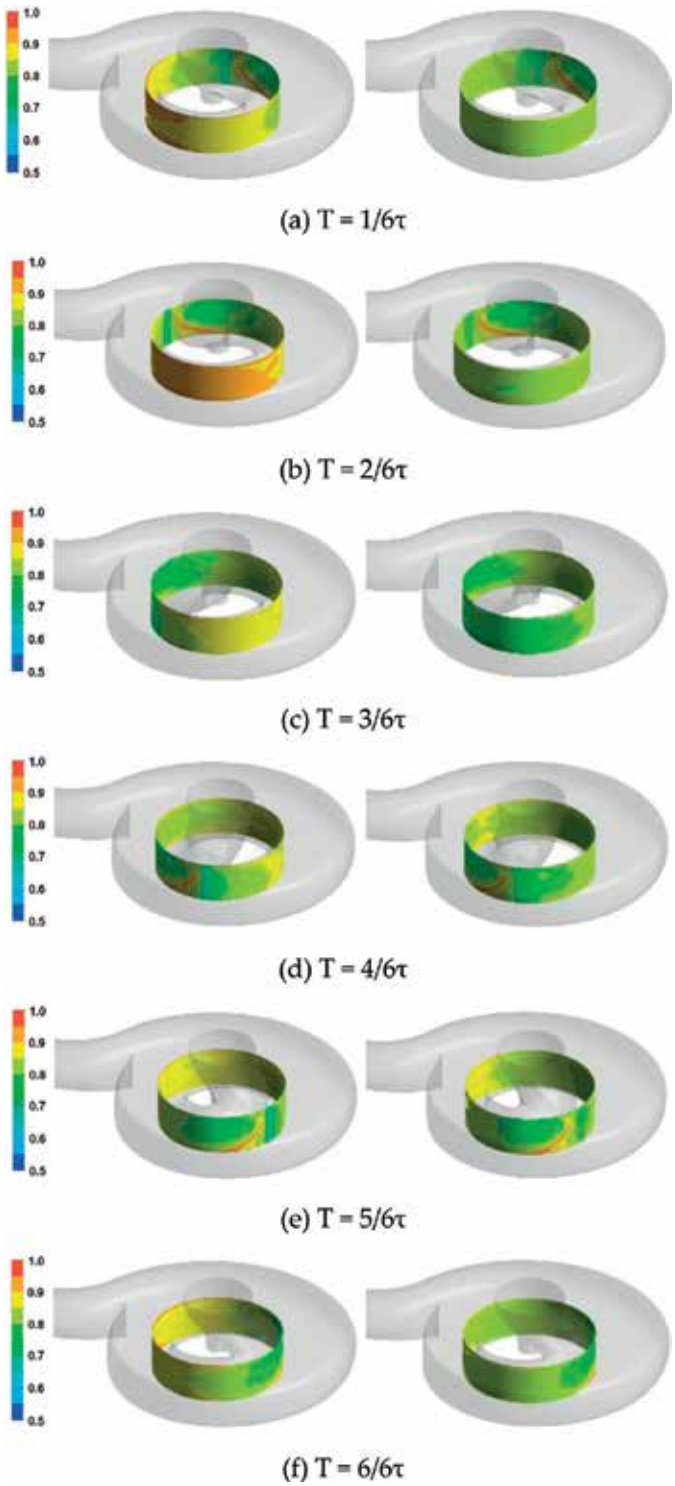

Figure 13. Unsteady pressure contours during one revolution of the impeller. (a) T = 1/6τ. (b) T = 2/6τ. (c) T = 3/6τ. (d) T = 4/6τ. (e) T = 5/6τ. (f) T = 6/6τ.

Figure 13(b), and a high-pressure zone caused by impeller-volute interactions becomes gradually larger. Consequently, this results in the unbalancing phenomena, along with the fluid-induced vibrations caused by unsteady radial forces, throughout the annulus passage area of the pump. Thus, the sweep area constructed from the unsteady radial force sources leans slightly toward the four quadrant directions from the origin, as shown in **Figure 11**. In the AOD, the pressure distribution is generally uniform; especially, at the same instantaneous time, the large high-pressure zone caused by impeller-volute interactions is obviously

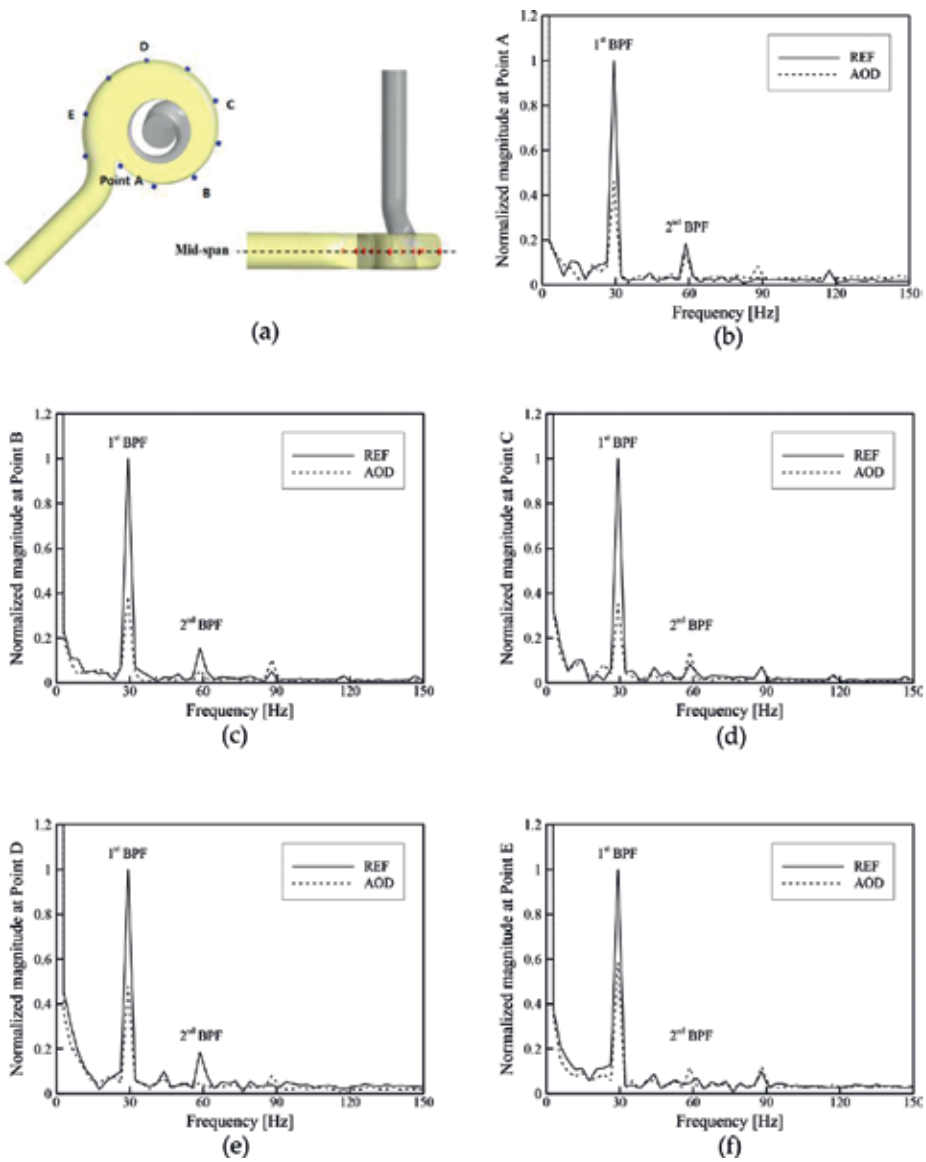

Figure 14. Spectra of the magnitude values at observation points on the casing wall. (a) Location of the observation points (b) Point A. (c) Point B. (d) Point C. (e) Point D. (f) Point E.

suppressed, as shown in **Figure 13(b)**. The AOD results in mostly stable flows throughout the annulus passage area of the pump. This explains the considerable decrease in the fluid-induced vibration caused by impeller-volute interaction owing to optimization.

Figure 14 shows the spectra of the magnitude values at observation points on the casing wall for the reference and AODs. Here, the spectra are calculated based on the wall pressure fluctuation time history by using a fast Fourier transformation algorithm. Both magnitude values are normalized by the first blade passing frequency (BPF) in the reference design, and these values are also related to the vibration of pump. As shown in **Figure 14**, the BPF is approximately 30 Hz (BPF = Blade number × rpm/60). The peak magnitude values are clearly seen at every harmonic BPF in steps of 30 Hz, which are due to the periodic motion of pump impeller rotation. In the AOD, a considerable decrease in the magnitude values at the first BPF is observed specifically, as well as at all observation points, especially for points B and C. It clearly shows that the large high-pressure zone caused by impeller-volute interactions is obviously suppressed, as shown in **Figure 13(b)**. Consequently, the considerable decreases in these magnitude values reduce the vibration caused by impeller-volute interaction.

6. Conclusions

A state-of-the-art design technique was introduced for a single-channel pump for realizing both high efficiency and low-fluid-induced vibration. The technique is based on a theoretical approach and three-dimensional steady and unsteady numerical analyses. Furthermore, advanced multidisciplinary numerical design optimization techniques were discussed in detail to simultaneously improve hydraulic efficiency and reduce the flow-induced vibration caused by impeller-volute interaction in the single-channel pump. The CFD studies conducted in the last decades, along with an increase in computing power systems, have significantly contributed to the development of various turbomachines with a deep understanding of flow physics and mechanism. Of course, it was possible to suggest a state-of-the-art design technique for a single-channel pump because of the rapid increase in the computing power system and development of computational methods. The authors expect that the practical design technique introduced in this chapter will be useful for engineers designing various single-channel pumps in the near future.

Acknowledgements

This work was supported by the Demand-based-Manufacturing Technique Commercialization R&D Project of the Korea Institute of Industrial Technology (KITECH) (No. JB180001), which was funded by the Ministry of Science and ICT (MSIT). The authors wish to express gratefully our thanks to Ms. Bo-Min Cho (former master student in UST and currently CFD engineer in Anflux Co., Ltd., Korea) and Mr. Wang-Gi Song (currently master student in UST) for their cooperation in the numerical simulation.

Conflict of interest

The author(s) declare no potential conflicts of interest with respect to the research, authorship, and/or publication of this article.

Author details

Jin-Hyuk Kim[1,2]* and Young-Seok Choi[1,2]

*Address all correspondence to: jinhyuk@kitech.re.kr

1 Korea Institute of Industrial Technology (KITECH), Cheonan, Republic of Korea

2 University of Science and Technology (UST), Daejeon, Republic of Korea

References

[1] Hansen BF, Henning PJ. Waste water pump. US patent application no. 13. 2013;**886**:479

[2] Zhang H, Chen B, Shi WD, Pan ZY, Cao WD. Effects of contraction-type impeller on non-overloaded performance for low-specific-speed sewage pump. Journal of Mechanical Science and Technology. 2014;**28**(3):937-944

[3] Pei J, Benra FK, Dohmen HJ. Application of different strategies of partitioned fluid–structure interaction simulation for a single-blade pump impeller. Proceedings of the Institution of Mechanical Engineers, Part E: Journal of Process Mechanical Engineering. 2012;**226**(4):297-308

[4] Keays J, Meskell C. A study of the behaviour of a single-bladed waste-water pump. Proceedings of the Institution of Mechanical Engineers, Part E: Journal of Process Mechanical Engineering. 2006;**220**(2):79-87

[5] Gulich JF. Centrifugal pumps. 2nd ed. Berlin: Spring-Verlag; 2008. pp. 548-549

[6] Gonzalez J, Fernandez J, Blanco E, Santolaria C. Numerical simulation of the dynamic effects due to impeller-volute interaction in a centrifugal pump. Transactions of the ASME—Journal of Fluids Engineering. 2002;**124**:348-355

[7] Gonzalez J, Parrondo J, Santolaria C, Blanco E. Steady and unsteady radial forces for a centrifugal pump with impeller to tongue gap variation. Transactions of the ASME—Journal of Fluids Engineering. 2006;**128**:454-462

[8] Baun DO, Köstner L, Flack RD. Effect of relative impeller-to-volute position on hydraulic efficiency and static radial force distribution in a circular volute centrifugal pump. Transactions of the ASME—Journal of Fluids Engineering. 2000;**121**:598-605

[9] Kelder JDH, Dijkers RJH, Van Esch BPM, Kruyt NP. Experimental and theoretical study of the flow in the volute of a low specific-speed pump. Fluid Dynamics Research. 2001;**28**(4):267-280

[10] Cho BM. A study on numerical optimization of flow path cross-sectional area to improve the hydraulic performance of a single-channel pump [thesis]. Daejeon, Republic of Korea, University of Science and Technology; 2017

[11] Kim JH, Cho BM, Kim YS, Choi YS, Kim KY, Kim JH, Cho Y. Optimization of a single-channel pump impeller for wastewater treatment. International Journal of Fluid Machinery and Systems. 2016;**9**(4):370-381

[12] Kim JH, Choi YS, Lee KY, Cho BM. Single channel pump impeller and centrifugal pump having the same. Korea patent application no. 10–2016-0115198. 2016

[13] Kim JH, Choi YS, Lee KY, Cho BM. Single channel pump volute and centrifugal pump having the same. Korea patent registration no. 10–1784561. 2017

[14] Menter FR. Two-equation eddy-viscosity turbulence models for engineering application. AIAA Journal. 1994;**32**(8):1598-1605

[15] Kim JH, Cho BM, Choi YS, Lee KY. Multi-objective optimization based on unsteady analysis considering the efficiency and radial force of a single-channel pump for wastewater treatment. Journal of Mechanics Engineering and Automation. 2016;**6**:234-245

[16] Kim JH, Cho BM, Choi YS, Lee KY, Peck JH, Kim SC. Optimized reduction of unsteady radial forces in a single-channel pump for wastewater treatment. IOP Conf. Series: Earth and Environmental Science. 2016;**49**:032008

[17] Cho BM, Kim JH, Choi YS, Kim JW, Kim YS, Kim KY, Ahn TS, Kim JH. Surrogate based optimization of a single-channel pump impeller. Proceedings of the 7th International Conference on Pumps and Fans 2015 (ICPF 2015); 18–21 October; Hangzhou. China: 2015. ICPF-121

[18] Sacks J, Welch WJ, Mitchell TJ, Wynn HP. Design and analysis of computer experiments. Statistical Science. 1989;**4**(4):409-435

[19] Myers RH, Montgomery DC. Response Surface Methodology: Process and Product Optimization Using Designed Experiments. New York, USA: Wiley; 1995

[20] Deb K. Multi-Objective Optimization Using Evolutionary Algorithms. 1st ed. Chichester, England, UK: John Wiley & Sons Inc; 2001

[21] MATLAB®. The language of technical computing. Release 14. The Math Work Inc; 2004

[22] Kim JH, Kim JW, Kim KY. Axial-flow ventilation fan design through multi-objective optimization to enhance aerodynamic performance. Transactions of the ASME—Journal of Fluids Engineering. 2011;**133**:101101

[23] Afzal A, Kim KY. Three-objective optimization of a staggered herringbone micromixer. Sensors and Actuators B: Chemical. 2014;**192**:350-360

[24] Shim HS, Afzal A, Kim KY, Jeong HS. Three-objective optimization of a centrifugal pump with double volute to minimize radial thrust at off-design conditions. Proceedings of the Institution of Mechanical Engineers, Part A: Journal of Power and Energy. 2016;**230**(6): 598-615

Chapter 11

Sustainable Sorbent Materials Obtained from Orange Peel as an Alternative for Water Treatment

Irma Robles Gutierrez, Ana K. Tovar and
Luis A. Godínez

Additional information is available at the end of the chapter

http://dx.doi.org/10.5772/intechopen.76137

Abstract

The presence of pollutants in water promotes negative impacts on aquatic organisms. Among the methods of wastewater treatment, the use of sorbent materials is one of the most outstanding due to its efficiencies and easy implementation. Orange peels had become value-added products for these purposes. Activated carbon as a sorbent material was prepared using orange peel as a precursor. The resulting material was physicochemically characterized by scanning electron microscope (SEM) and Fourier transform infrared radiation (FTIR); structural changes were identified and related to sorption capacity using a model pollutant. Results of sorption indicated natural dried orange peel which presented a sorption capacity of 149.26 mg/g, while sorbent-activated carbon presented a sorption capacity of 2342.91 mg/g. The recovery of orange peel to obtain potential interest materials provided benefits for wastewater treatment.

Keywords: orange peel, sorbent material, activated carbon, valorization, wastewater treatment

1. Introduction

The industry of agricultural products processing, or agribusiness, is defined as the economic activity that combines the agricultural productive process with the industrial processing to obtain food or semi-processed raw materials. Among the industrialized products are fruits, vegetables, seeds, tubers and pods; some are marketed fresh and others are transformed into nectars, juices, jams, flours, oils, and wines, among others.

After the processing of these products, agroindustrial waste is obtained. Agroindustrial waste is solid or liquid materials generated from the direct consumption of primary products or its industrialization. Those residues are no longer useful for the process that generated them, but they are susceptible to transformation to obtain another product with economic value, of commercial and social interest [1].

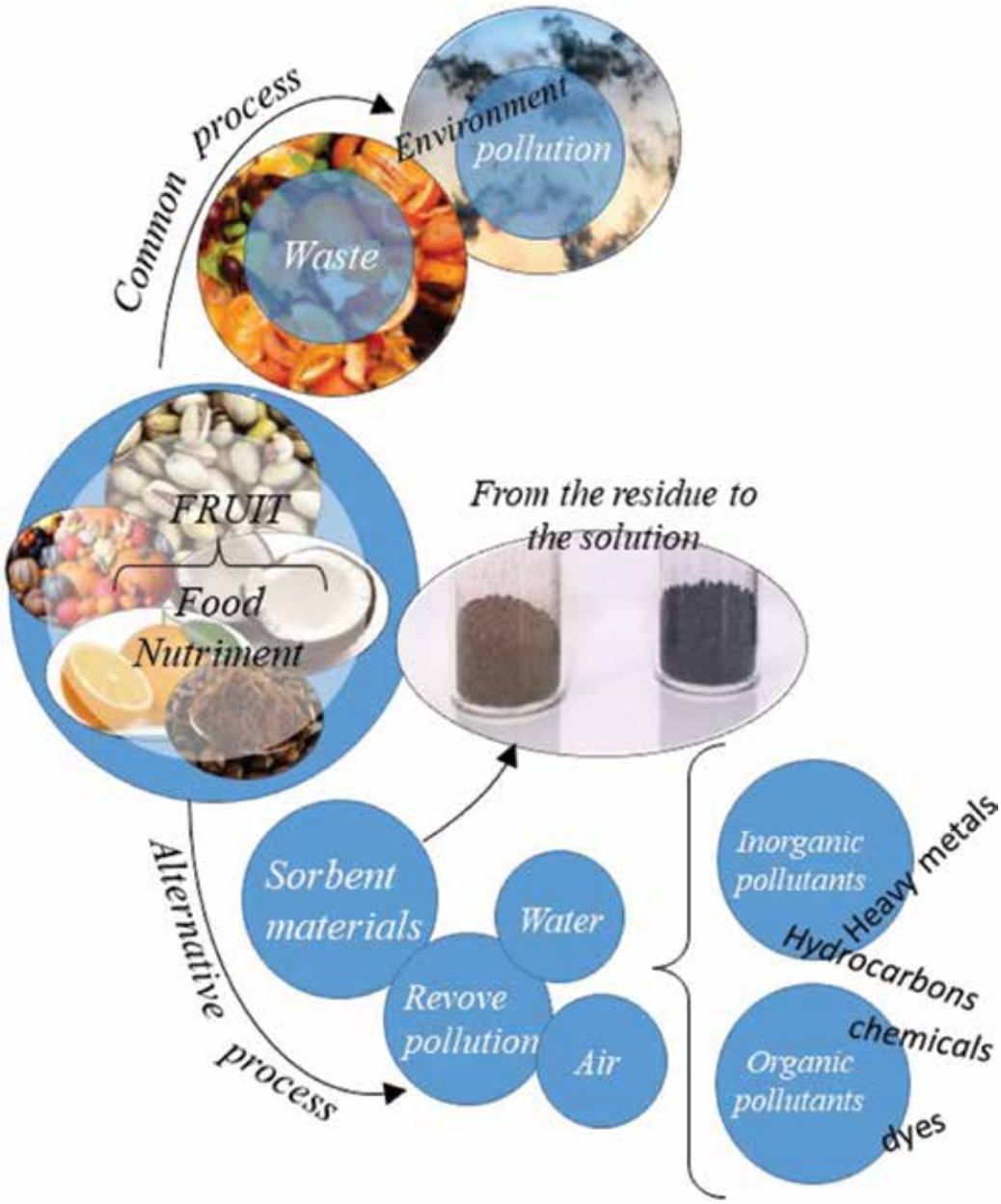

Figure 1. Alternatives for organic residue waste management.

The food industry is characterized by a considerable generation of waste and byproducts. Despite the environmental repercussions that this represents, the amount of agroindustrial waste has increased continuously. Orange peels represent a clear example of agroindustrial waste, which is the result of fruit processing for the production of juices. Due to the large volume of generation and the environmental risk they represent, some investigations have focused on the valorization of this waste through extraction of value-added products or even transformation to other materials.

Valorization of waste is an attractive approach that offers potentially useful alternatives to treat waste, instead of disposal or landfill deposition. In general, agroindustrial waste possesses varied characteristics, which depend on the raw material and the process that generated those residues; however, they share a similar characteristic, that is the organic matter content, constituted by different percentages of cellulose, lignin, hemicellulose, and pectin. The valorization of food waste components could give numerous possibilities for obtaining value-added products [2]. **Figure 1** represents different alternatives for organic residue waste management, on the one hand, the common use of waste that implies it's wasted, and even its contribution to the environment and, on the other hand, some possibilities to use them as materials for environment protection from the use of sorbent materials.

2. Orange fruit

In the orange Mexican harvest, the volume of production has averaged 4.3 million tons in the last 6 years. The national market is the main trade of Mexican orange; an average of 67.53% of the supply of fresh oranges is destined for national production; most of them are designated to homes, restaurants, street vendors, and hotel chains, among others [3, 4].

Since orange has a high production in the country, as well as in the world, and serves as the main raw material for agroindustrial processing, the amount of fruit marketed to the juicing industry has increased [3].

The orange processing industry accommodates a small percentage of 32% in the last years [4]. Since 2004, the percentage of fruit destined to the juice agroindustry increased significantly due to government programs which allowed the recovery of the freight and collection costs of the fruit marketed to the Mexican agroindustry of oranges (**Table 1**). Simple juice and concentrated juice are the main products in the processing of citrus fruits [3].

Production	2011	2012	2013	2014	2015	2016
Mexico	83	151	126	159	165	170
EUA	681	607	476	438	383	355
Brazil	1263	980	1230	1006	848	1222

Table 1. Main producing countries of orange juice, considering 1000 metric tons at 65° BRIX.

The oranges processed in the industry are destined in its majority to the juice export market (**Table 2**). Studies show that Mexico, in comparison with large producing countries, has been increasing the amount of juice produced over the years. Mexico has had a great inclusion in the international market, satisfying the demand of countries such as the United States, Canada, and Japan, among others [3, 4].

Production	2011	2012	2013	2014	2015	2016
Mexico	2011	2012	2013	2014	2015	2016
EUA	79	143	121	153	158	163
Brazil	110	114	113	81	66	65

Table 2. Export data of orange juice, considering 1000 metric tons at 65° BRIX.

3. Orange peels

Orange peels are waste generated mainly by the juicing industry that can cause environmental problems due to its large volume of generation and physicochemical characteristics, such as soil and water pollution. For this reason, the recovery and transformation of orange peels has become a topic of interest for recent investigations; one important alternative is the preparation of sorbent materials.

The waste material of the orange industry is constituted mainly by peels, shells, seeds, and capillary membranes. When leaving the industry, the orange peels have a high level of organic matter and low pH; such indicators demonstrate the potential polluting. Since the composition of orange peels can be transformed to use as raw material for the production of national interest products, in this way, value-added products can be obtained due to the valorization process, and, at the same time, it is possible to reduce the environmental impact [5, 6].

3.1. Physicochemical composition of orange peel

The chemical composition of orange peels, shown in **Table 3**, makes them an attractive source of industrial products. Soluble sugars present in orange peels are composed mostly of sucrose, glucose, and fructose, while organic acids are composed of citric, oxalic, and succinic acid. The fiber is the portion of the shell where the pectin is contained. The pectins contained in the orange fiber are soluble and insoluble in the form of protopectin [5].

However, resent investigations of citrus waste focus on the recovery of a single component, such as d-limonene, pectin, or bioethanol [8].

Recent investigations have shown that orange peel is a potentially valuable resource that can be transformed into value-added products; the most common alternatives have reported the use of this material as livestock feed, source of heat generation, biomethanization, and compost [9, 10].

Parameter	Value
Soluble solids (°Brix)	7.10 ± 1.2
pH	3.93 ± 0.003
Acidity[1]	0.29 ± 0.003
Formaldehyde	34.00 ± 2.4
Moisture (%)	60.5
Ash (%)[2]	3.29 ± 0.19
Fat content (%)[2]	0.2
Protein (%)[2]	1.5
Carbohydrates (%)[2]	89.00 ± 1.1
Pectin (%)[2]	170.00 ± 5
Lignin	3.20 ± 0.4
Essential oils (mL/kg)	1.45 ± 0.16

[1]g of citric acid/100 mL.
[2]db = dry basis.

Table 3. Physicochemical composition of the orange peel [7].

4. Sorbent materials obtained from orange peels

The elaboration of high-quality sorbent materials from agroindustrial waste opens an effective path for the conversion of these residues into high value added products [11].

Activated carbons are commonly used as sorbent materials due to their sorption capacity; those activated carbons are produced from a wide variety of carbon-based materials. Those materials used for the production of activated carbon are carbon-based organic materials, such as coal, lignite, and wood. Although natural coal is the most used precursor, agroindustrial waste is considered as a good alternative; in this way, the activated carbon produced from waste would reduce the demand of forests since wood is also used for this purpose [12].

According to International Union of Pure and Applied Chemistry (IUPAC), an activated carbon is a porous carbonaceous material that has been subjected to gas reaction, sometimes with chemical agents, during or after carbonization process in order to increase its sorption properties.

The use of carbon-based materials goes so far back in history, since charred wood and mineral coal or simply partially volatilized coal materials were already used for similar purposes.

From 1901, several patented methods of activated carbon production were registered. In this way, R. Von Ostrejko patented two methods to produce activated carbon: one based on the carbonization of lignocellulosic materials with metal chlorides (the basis of chemical activation) and the second method based on a gentle gasification of coals with water vapor or carbon dioxide (basis of physical activation) [13].

Nowadays the activated carbons are prepared from a carbon precursor such as lignite, wood, or synthetic precursors, mainly of polymeric type such as resins.

A typical carbonization process produces around 20–30% carbonization yield, where the activating agent is a dehydrating compound, which would increase the amount of active sites, favored by the thermal degradation of the precursor, modifying in this way the porosity of the obtained material. Precursors such as lignocellulosic materials reflect the botanical texture of the precursor [14].

Many of the laboratory uses and industrial applications of activated carbons are based on the high sorption capacity of the material. This capacity depends on the physical properties of the coal, as well as its chemical structure [15].

4.1. Chemical structure of activated carbons

The structure of the activated carbon is considered as a continuous descent in the degree of ordering of the planes in the graphite. However, activated carbon also has a three-dimensional structure of carbon atoms in flat sheets of hexagonal rings. However, unlike graphite, there is no crystallographic order in the third dimension, and the cross-linking of the plates can occur [13].

The spaces between the graphite planes of crystals create the microporous structure, with a high internal surface area [16]. According to IUPAC, pores of activated carbons can be classified into micropores (pore diameter <2 nm), mesoporous (pore diameter between 2 and 50 nm), and macropores (pore diameter >50 nm) [13].

In addition to the porous structure, activated carbons have a chemical structure, since they contain small amounts of heteroatoms. The presence of heteroatoms (O, N, H, S, etc.) attached to the edges of the graphene layers gives rise to a variety of surface functional groups [16], which allow polar substances to be weakly retained on the surface of activated carbon. This is because the carbon atoms located at the edges of the planes have a high available activity, since they are not saturated with carbon atoms and have free electrons [13].

Oxygenated functionalities are the most important due to their surface properties and can also be developed spontaneously through the exposure of the material to the inert atmosphere. Chemisorbed oxygen can only be removed from the surface as CO or CO_2 at temperatures above 120°C. The unsaturated carbon atoms at the edges of the basal crystal planes are associated with high concentrations of mismatched electrons, which play a very important role in the chemisorption process [16].

Oxygenated functional groups are not formed exclusively by the reaction with oxygen; these groups can also be the results of the reaction with other oxidizing gases (O_3, N_2O, CO_2) and oxidizing solutions (HNO_3, H_2O_2). In addition, the electron density π of the basal carbon planes is considered as chemically active [16]. The surface chemistry of activated carbon has an amphoteric nature due to the coexistence of acidic and basic surface groups. An activated carbon is globally acidic or basic depending on the surface concentration of these groups and also on the strength of acidic or basic compounds [13]. Therefore, the oxygenated surface groups are classified into the categories mentioned in the following sections.

4.1.1. Basic surface groups

These groups are formed when the oxidized surface is reduced by an inert or hydrogen atmosphere, at high temperatures. The decomposition of acidic groups creates active sites at the edges of graphene plates, which can attract oxygen during the cooling stage in an inert atmosphere, and after a process of reexposure to air, forming basic functional groups such as chromene and pirona.

4.1.2. Acidic surface groups

These groups are formed when the carbon surface is exposed to oxygen through reactions with oxidizing agents in solutions or the gas phase; this process can be carried out at room temperature or even at high temperatures, these parameters are responsible for the amphoteric characteristic of the activated carbons, which depend on the pH of the aqueous phase.

4.1.3. Hydrogenated groups

Hydrogen atoms are usually present in the surface of activated carbons such as chemisorbed water, as part of other surface groups such as carboxylic acids, phenols, amines, or even directly attached to carbon atoms as part of aromatic or aliphatic structures.

4.1.4. Phosphorus groups

Phosphorus atoms contained in activated carbons generally come from the phosphoric acid used as an activating agent in the preparation stage. Once phosphorus is located in the carbon matrix, it can be stable between 500 and 1000°C; this atom can be found as red phosphorus or chemically bonded as —C—P— or —C—O—P—. Phosphorus-containing species can be formed during carbonization at low temperature ranges [16].

4.1.5. Activated carbon preparation

The physicochemical properties of each activated carbon depend mainly on the source of the starting material, since it essentially determines the structural characteristics of the resulting material [14].

Through the carbonization process, it is possible to obtain a low surface area, as elements such as oxygen and hydrogen are eliminated by decomposition of the starting material in an inert atmosphere, usually nitrogen. The resulting material is formed by unions of elementary graphitic microcrystals, usually plugged by tars and carbonization residues, which notably decrease the sorption capacity. In order to increase the sorption capacity of this coal, it will be necessary to resort to some method that allows eliminating tars, by means of some oxidizing agent as the activating agent [14]. There are two activation processes, called physical activation and chemical activation, described below [13].

4.1.6. Physical activation

This method consists of an oxidation step that is usually carried out in the presence of water vapor, carbon dioxide, or air; the activation treatment is carried out at high temperatures

(>700°C) [15]. These agents are capable of extracting carbon atoms from the porous carbon structure according to the following stoichiometry equations; these equations describe the endothermic reactions. This method of activation is known as physical or thermal activation [14].

$$C + CO_2 \rightarrow 2CO \quad (1)$$

$$C + H_2O \rightarrow CO + H_2 \quad (2)$$

In this process, two differentiated stages can be considered: a first one, in which all the disorganized materials are burned, and a second one, in which the pores that were initially closed or blocked are opened. As a result of that, a new material with a high surface is produced, due to the presence of large porosity [17].

4.1.7. Chemical activation

Chemical activation involves the carbonization of the precursor in the presence of an alkali, hydroxides (KOH, NaOH), or inorganic acids (H_3PO_4, HNO_3, H_2SO_4) [16].

The yield of activated carbon prepared by chemical activation method is usually higher than those activated carbons prepared under physical activations. In order to compare physical and chemical methods, it is possible to emphasize that, while in the physical activation method, the development of pores is mainly promoted by the removal of carbon atoms by a gasification process; in the chemical activation method, the activation agents promote dehydrogenation reactions in the precursor that promote bonds' formation between carbon atoms and also the creation of pores on the surface.

Unlike physical activation, the preparation of activated carbons by chemical activations is carried out in a single stage; the carbonization and activation process are carried out simultaneously. Chemical activation requires lower carbonization temperatures than physical activation. In addition, chemical activation leads to a better formation of the porous structure.

As a result of the carbonization and activation processes, activated carbons with porous characteristics are obtained which are determined by various factors such as starting material (precursor), size of the precursor particles, activating agent, activation temperature, heating rate, temperature and carbonization time, etc. [12, 16].

4.2. Sorption on solid surfaces

The forces that hold a solid bonded to the surface of activated carbons produce a field force around each ion, atom, or molecule. At the surface of the solid, these forces cannot suddenly disappear, and due to these unsaturated and unbalanced forces, the solid has the tendency to attract and retain on its surface molecules and ions of other substances with which it is in contact. Thus, when the surface of the solid is in contact with a gas or a liquid, the concentration of the gas or liquid is always greater in the surface of the solid than in the interior of the gas or liquid phase. The substance adhered to the surface is called sorbate, and the material in which it is sorbed is called sorbent. Depending on the nature of the forces involved, the sorption process is classified into two main types [18]:

4.2.1. Physical sorption

The sorbate is bounded to the surface of the activated carbon by relatively weak Van der Waals forces, identical to the molecular forces of cohesion that are involved in the condensation of vapor on liquids.

4.2.2. Chemical sorption or chemisorption

This process involves electron exchange between the sorbate molecules and the surface of the sorbent, resulting in a chemical reaction. The bond formed between the sorbate and the sorbent is essentially a chemical bond and is stronger than in a physical sorption.

The nature of the forces involved in each of the sorption processes is significantly different. In the physisorption process, no activation energy is required; therefore, the sorption rate is higher even at low temperatures. While chemisorption requires activation energy, the sorption rate is low and depends on the sorption temperature [18].

In the study of new sorbents, it is essential to establish the most appropriate sorption equilibrium correlation, which is indispensable for the reliable prediction of sorption parameters and the quantitative comparison of the sorbent behavior for different sorbent systems, for varied experimental conditions [19].

The most common way to study the behavior of activated carbon is through kinetic and sorption equilibrium models. The first model is related to the study of the kinetics, while the second type is related to the studies of isotherm processes [16].

As a result of activation and carbonization processes, activated carbons with porous characteristics are obtained, which are determined by factors such as starting material, temperatures and carbonization and activation times, heating rate, particle size of the starting material, and so on [12].

In the preparation of an activated carbon, it is necessary to look for the appropriate ratio, as can be deduced from the information earlier, between the transport pores and the sorption pores, that is, it is necessary to achieve a rapid transport of the sorbate to the internal surface and, at the same time, obtain an internal surface sufficiently developed to ensure a high sorbent capacity. In each case, the properties of activated carbon will depend on the raw material, its previous treatment, and activation conditions [17].

Nowadays, a strong demand for activated carbons can be expected in two very important fields in developed countries: atmospheric pollution and wastewater, they are also used for other applications such as elimination of organic matter and toxic substances from industrial gases and drinking water, elimination of chlorine from water, etc. This promising future of activated carbons requires the development of alternative materials that may face the requirement of sorbent materials in the depollution area, especially as regards the search for new raw materials and obtaining very selective activated carbons. Actually, activated carbons with properties like molecular sieve are being prepared in recent years; the object of these materials is the selective sorption of molecules of specific size, a process in which the activated carbons

are displacing the zeolites, used frequently for this purpose. Another important application, which takes advantage of the properties of a molecular sieve of activated carbons, is the retention of nitrogen oxides (NOx) from different sources and sulfur that coals and oils contain and that when heated is transformed into toxic products, such as sulfur dioxide (SO_2), hydrogen sulfide (SH_2), carbon sulfide (S_2C), and so on [17].

Recently, fruit husks as agroindustrial waste have been implemented in the production of activated carbons; investigation of sorption about selective specific size molecules has been done regarding these materials. The use of agroindustrial residues is a new alternative that provides a proposal of integral valorization, taking advantage of the waste abundance and the low cost of the material [17].

Table 4 shows the results of some reports from which activated carbons have been elaborated; elaborating parameters as well as surface areas are shown. It is possible to see surface area values from 200 to 1800 m^2/g; these values are comparable to those reported in literature for lignite of 1300 m^2/g [23], as well as 1853 m^2/g [24]. These values are also comparable to commercial materials: PET activated carbons have 1170 m^2/g [25], Darco KB-B of 1608 m^2/g [26], Fluka 05120 of 1110 m^2/g [26], activated carbon MT40 of 528 m^2/g [27], activated carbon BW of 300 m^2/g [27], and Fluka 03866 of 179 m^2/g [26].

4.3. Activated carbons obtained from orange peels

Some studies have been done for the preparation of activated carbon from orange peel, **Table 5** shows some reports and it is possible to appreciate the different activating agents used, temperature, and time of carbonization, as well as the surface area reported for those materials.

Some studies for the elaboration of activated carbons from orange peel are described below; these materials have been used for the removal of metals, dyes, among others. These reports indicate sorption capacities from 7.9 to 982 mg/g.

Quijano and Mejía [31] elaborated activated carbons from the residue obtained after pectin extraction from orange peels; they analyzed the effect of time and carbonization temperature on the carbonization percentage, using a 2^2 factorial design. They determined that temperature has significant influence on the carbonization yield; the optimum condition was obtained at 400°C and 0.5 h for a 34.8% yield and a sorption capacity of methylene blue of 149.4 mg/g.

Annadurai et al. [32] prepared low-cost sorbents from orange peels for the sorption of several dyes in aqueous solution. The concentrations of dye and pH were varied and after the study they determined that sorption capacities decrease as follows: methyl orange > methylene blue > rhodamine B > red congo > methyl violet > black amino 10B, from 20.5 to 7.9 mg/g.

Khaled et al. [33, 34], in different studies, evaluated different conditions to obtain activated carbon; they used H_2SO_4 as an activating agent; a solution of this acid was in contact with the material for 96 h at 105°C; after that, the sample was carbonized at 120°C and 180°C. Obtained activated carbons were evaluated using direct blue dye-106 and direct yellow-12, for which sorption capacities were 107.5 and 75.8 mg/g, respectively.

Material[a]	Particle size (mm)	Temperature (°C)	Time (h)	Activation	Agent	Temperature (°C)	Time (h)	Surface area (m^2/g)	Pore volume (cm^3/g)	Pore size (nm)	Sorption capacity (mg/g)	Reference
Grapefruit	—	450	2	CH	KOH	450, 800	1.5, 2.5	1892.1	1.095	1.92	680	[20]
Banana	—	1000	8		ZnCl	—	—	1650	1.26	3.01	—	[11]
Yaca	—	350	0.5		H_3PO_4	350	0.5	5	—	—	—	[12]
						450	0.5	1033	0.664	1.7	—	
						550	0.5	1260	0.733	2	—	
Almond	1–5	300	1	P	CO_2	—	1	322	19.5	8–12	288.5	[21]
		700	1			—	1	385	16.92	10		
		1200	1			—	1	342	15.5	15–25		
Orange		300	1			—	1	225.6	14.5	7–14	166.7	
		700	1			—	1	248	15	10		
		1200	1			—	1	240	13.5	12–14		
Rice	6×10^{-3}	650	1	CH	NaOH	—	—	253.4	0.17	2.62	0.17	[22]

[a]Materials were considered as the husks of the mentioned fruits. CH: chemical activation and P: physical activation.

Table 4. Organic waste used for the production of activated carbon.

http://dx.doi.org/10.5772/intechopen.76137

Activation type	Agent	Atmosphere	Temperature (°C)	Carbonization time (h)	Time of mixing material-agent	Surface area (m^2/g)	Reference
Physical	CO_2	Nitrogen	700	1 h	—	248	[21]
Chemical	H_3PO_4	Autogenerated	850	1 h	—	1090	[28]
Chemical	H_3PO_4	Nitrogen	450	2 h	2 h	1203	[29]
Chemical	ZnCl	Nitrogen	550	1 h	36 h	1477	[30]

Table 5. Preparation of activated carbon using orange peels.

Fernandez et al. [35] studied the effect of H_3PO_4 as an activating agent to prepare activated carbon; the carbonization procedure was carried out at 475°C in 0.5 h. Authors report surface areas of 1090 m^2/g for the obtained materials. Methylene blue and rhodamine B were used to characterize sorption capacities and the values obtained were 320 and 522 mg/g, respectively.

Li et al. [20], studied the effect of KOH as an activating agent and the process of carbonization in an inert atmosphere, at 800°C; the activated carbon obtained had a surface area greater than 1800 m^2/g, and a sorption capacity of 680 m/g was obtained using methyl orange as a model pollutant.

Ashtaputrey and Ashtaputrey [36] prepared activated carbon from orange peels by chemical activation using HCl; they also varied the carbonization temperature from 300 to 500°C for 1 h. They analyzed the sorption capacity of iodine, and finally, they concluded that a carbonization temperature of 300°C promotes a sorption capacity of up to 983 mg/g.

5. Preparation and characterization of orange peel-activated carbon

Our results of the preparation of activated carbon from orange peel let us characterize the material. This material was prepared under the following conditions: activation agent, H3PO4, carbonization temperature of 400°C, and carbonization time of 1 h. Methyl orange was used as

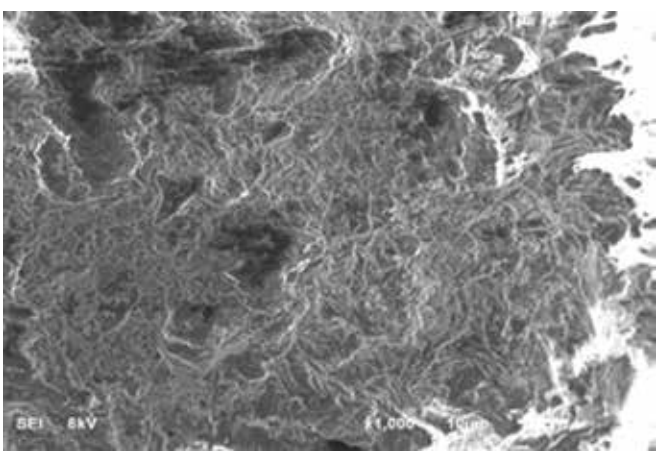

Figure 2. SEM micrography of orange peel at 1000×.

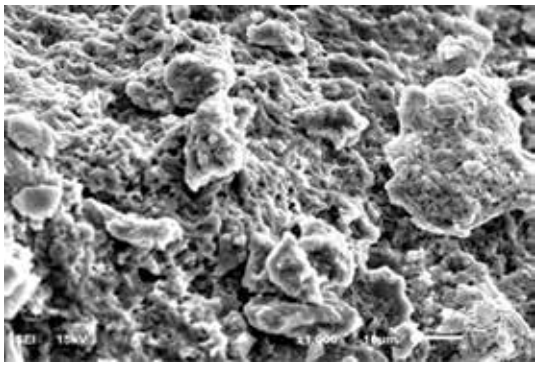

Figure 3. SEM micrography of activated carbon obtained from orange peel at 1000×.

the model pollutant in order to analyze sorption capacity of 2342.91 mg/g. This result was compared to dried orange peel that showed a sorption capacity of 149.26 mg/g.

Figures 2 and **3** show a comparison of the surface morphology of orange peel and activated carbon obtained from orange peel. It can be seen that after the carbonization treatment the surface was modified, given by the thermal process and by the activation agent. The carbonization process promotes the formation of new surface sites.

On the other hand, Fourier Transform Infrared Spectroscopy (FTIR) was used to identify the surface groups of activated carbon obtained from orange peel. **Figure 4** shows the comparison of orange peel and activated carbon. It is possible to appreciate that the intensity of some signals decreases after carbonization process. **Table 6** identifies functional groups associated with the FTIR spectra of **Figure 4**.

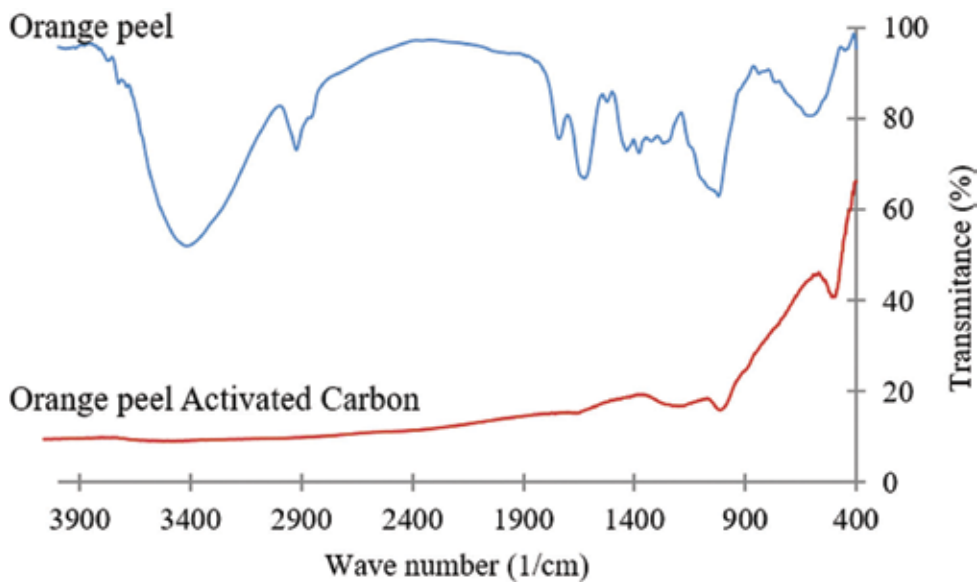

Figure 4. Comparison of the FTIR spectrum of orange peel and orange peel-activated carbon.

Wave number (1/cm)	Functional group
3422.8	—OH
2925.62	C—H
1741.27	C═O
1626.83	C═C
1435.53	$—CH_2$ $—CH_3$ $O—CH_3$
1379.24	C—O
1070	P—O
1020.77	C—O—H C—O—R
596.19	C—H

Table 6. Functional groups of FTIR spectrum.

Activated carbon prepared from orange peel has higher sorption capacity compared to the precursor (dried orange peel), which means that the transformation of a residence is a great advantage. The resulting material possesses the ability to be used for the treatment of water contaminated with colorants as an alternative principal.

However, it is necessary to continue the study of this material for the removal of heavy metals, organochloride compounds, and so on in order to provide greater alternatives for better care for the environment.

6. Sustainable materials

The concept of sustainability arises in 1987, when the World Commission on Environment and Development from the United Nations published a report titled "Our common future" [37], that is focused on the idea of sustainability or sustainable development.

Sustainability is a process that aims to find a balance between the environment and the use of natural resources. Humanity has degraded natural resources in such a way that currently it is necessary to conscientiously procure and plan its consumption to guarantee the existence to future generations.

That is why the use of innovative alternatives for the development of materials allows us to offer better conditions for the care of the environment. Therefore, if a strategy is generated to collect, characterize, and even take advantage of waste materials that currently contribute to the contamination of the environment, in the future, people tend to think of integral use of consumption products. It represents a change in how our society thinks about the use of natural resources and environmental protection.

This is the case of agroindustrial waste, since they have a physicochemical composition that can be used for different purposes, both for the recovery of different raw materials and for their transformation into sustainable materials useful to reduce water pollution.

7. Conclusion

Orange peels are good alternatives as raw materials for the production of activated carbons. Activated carbons obtained from this precursor have high surface areas and high sorption capacities, compared to commercial materials used for water treatment.

Orange peel-activated carbon is a sustainable alternative to replace activated carbons obtained from lignite materials that come from non-renewable sources.

Acknowledgements

Authors thank the Centro de Investigación y Desarrollo Tecnológico en Electroquímica, CIDETEQ (www.cideteq.mx), for the facilities provided for the development of this research.

Author details

Irma Robles Gutierrez*, Ana K. Tovar and Luis A. Godínez

*Address all correspondence to: irobles@cideteq.mx

Center for Electrochemical Science and Technology (CIDETEQ), Pedro Escobedo Queretaro, Pedro Escobedo, Mexico

References

[1] Saval S. Aprovechamiento de residuos agroindustriales: Pasado, presente y futuro. Biotecnología. 2012;**16**:14-46

[2] Luque R, Clark JH. Valorisation of food residues: Waste to wealth using green chemical technologies. Sustainable Chemical Processes. 2013;**1**. DOI: 10.1186/2043-7129-1-10

[3] Comité Sistema Producto Cítricos del Estado de Veracruz. Sagarpa [Internet]. 2009. Available from: http://www.sagarpa.gob.mx/agronegocios/Documents/Estudios_promercado/SISTPROD_CITRICOS.pdf [Accessed: November 2017]

[4] Foreign Agricultural Service. United States Department of Agriculture [Internet]. January 2018. Available from: https://apps.fas.usda.gov/psdonline/circulars/citrus.pdf [Accessed: February 2018]

[5] Castro ME, Sepúlveda A. Estudio de factibilidad técnica y económica de una planta extractora de pectina a partir de los residuos generados por el proceso de industrialización de la naranja (*Citrus sinensis*) [thesis]. Santander: Universidad Industrial de Santander; 2012

[6] Cerón-Salazar I, Cardona Alzate C. Evaluación del proceso integral para la obtención de aceite esencial y pectina a partir de cáscara de naranja. Ingeniería y Ciencia. 2011;**7**(13):65-86

[7] Espachs-Barroso A, Soliva-Fortuny RC, Martín-Belloso O. A natural clouding agent from orange peels obtained using polygalacturonase and cellulase. Food Chemistry. 2005;**92**(1): 55-61. DOI: 10.1016/j.foodchem.2004.04.047

[8] Balu AM, Budarin V, Shuttleworth PS, Pfaltzgraff LA, Waldron K, Luque R. Valorisation of Orange peel residues: Waste to biochemicals and nanoporous materials. ChemSusChem. 2012;**5**:1694-1697. DOI: 10.1002/cssc.201200381

[9] Siles JA, Vargas F, Gutiérrez MC, Chica AF, Martín MA. Integral valorisation of waste orange peel using combustion, biomethanisation and co-composting technologies. Bioresource Technology. 2016;**211**:173-182. DOI: 10.1016/j.biortech.2016.03.056

[10] Miranda R, Bustos-Martineza D, Sosa C, Gutiérrez MH, Rodriguez ME. Pyrolysis of sweet orange (Citrus sinensis) dry peel. Jurnal of Analytical and Applied Pyrolysis. 2009;**86**(2): 245-251. DOI: 10.1016/j.jaap.2009.06.001

[11] Lv y, Gan L, Liu M, Xiong W, Xu Z, Zhu D, Wright D. A self-template synthesis of hierarchical porous carbon foams based on banana peel for supercapacitor electrodes. Journal of Power Sources. 2012;**209**:152-157. DOI: 10.1016/j.jpowsour.2012.02.089

[12] Prahas D, Kartika Y, Indraswati N, Ismadji S. Activated carbon from jackfruit peel waste by H_3PO_4 chemical activation: Pore structure and surface chemistry characterization. Chemical Engineering Journal. 2008;**140**(1–3):32-42. DOI: 10.1016/j.cej.2007.08.032

[13] Álvarez MA, Carrasco F, Maldonado FJ. Desarrollo y aplicaciones de materiales avanzados de carbón. 1st ed. Sevilla|: Universidad Internacional de Andalucía; 2014. 428 p

[14] Marsh H, Rodríguez F, editors. Activated Carbon. 1st ed. Amsterdam: Elsevier; 2006.554 p

[15] Gómez-Serrano V, Piriz-Almeida F, Durán-Valle CJ, Pastor-Villegas J. Formation of oxygen structures by air activation. A study by FT-IR spectroscopy. Carbon. 1999;**37**(10):1517-1528. DOI: 10.1016/S0008-6223(99)00025-1

[16] Kwiatkowski JF, editor. Activated Carbon: Classifications, Properties and Applications. 1st ed. New York: Nova Science Publishers; 2011 572 p

[17] Martinez JMM. Adsorción física de gases y vapores por carbones. 1st ed. Universidad de Alicante; 2009. 116 p

[18] Chand RB, Goyal M. Activated Carbon Adsorption. 1st ed. Boca Raton: CRC Press; 2005. 520 p

[19] Foo KY, Hammed BH. Insights into the modeling of adsorption isotherm systems. Chemical Engineering Journal. 2010;**156**(1):2-10. DOI: 10.1016/j.cej.2009.09.013

[20] Li H, Sun Z, Zhang L, Tian Y, Cui G, Yan S. A cost-effective porous carbon derived from pomelo peel for the removal of methyl orange from aqueous solution. Colloids and Surfaces A: Physicochemical and Engineering Aspects. 2016;**489**:191-199. DOI: 10.1016/j.colsurfa.2015.10.041

[21] Hashemian S, Salari K, Atashi Z. Preparation of activated carbon from agricultural wastes (almond shell and orange peel) for adsorption of 2-pic from aqueous solution. Journal of Industrial and Engineering Chemistry. 2014;**20**(4):1892-1900. DOI: 10.1016/j.jiec.2013.09.009

[22] Mohd TF, Muhammad I, Maizatul S, Chong FK. Adsorptive removal of Zn(II) ion from aqueous solution using rice husk-based activated carbon. In: American Institute of Physics, editor. International Conference on Fundamental and Applied Sciences 2012: (ICFAS2012). American Institute of Physics; 2012. p. 252-257. DOI: 10.1063/1.4757475

[23] Montané D, Torné-Fernández V, Fierro V. Activated carbons from lignin: Kinetic modeling of the pyrolysis of Kraft lignin activated with phosphoric acid. Chemical Engineering Journal. 2005;**106**(1):1-12. DOI: 10.1016/j.cej.2004.11.001

[24] Suhas CPJM, Ribeiro MML. Lignin – From natural adsorbent to activated carbon: A review. Bioresource Technology. 2007;**98**(12):2301-2312. DOI: 10.1016/j.biortech.2006.08.008

[25] László K, Podkościelny P, Dąbrowski A. Heterogeneity of polymer-based active carbons in adsorption of aqueous solutions of phenol and 2,3,4-Trichlorophenol. Langmuir. 2003; **19**(13):5287-5294. DOI: 10.1021/la026761s

[26] Schwickardi M, Johann T, Schmidt W, Schüth F. High-surface-area oxides obtained by an activated carbon route. Chemistry of Materials. 2002;**14**(9):3913-3919. DOI: 10.1021/cm0211857

[27] Podkościelny P, Browski AD, Marijuk OV. Heterogeneity of active carbons in adsorption of phenol aqueous solutions. Applied Surface Science. 2003;**205**(1–4):297-303. DOI: 10.1016/S0169-4332(02)01154-6

[28] Fernandez ME, Nunell G, Bonelli PR, Cukierman AL. Conversión de cáscaras de naranjas en carbón activado y su empleo en el tratamiento de aguas contaminadas por colorantes. In: SAASA, editor. Segundo Simposio sobre Adsorción Adsorbentes y sus Aplicaciones; 2013; SAASA; 2013

[29] Peña KJ, Giraldo L, Moreno JC. Preparation of activated carbon from orange peel by chemical activation physical and chemical characterization. Revista Colombiana de Química. 2012;**41**(2):311-323. DOI: 10.15446/rev.colomb.quim

[30] Xie Z, Guan W, Ji F, Song Z, Zhao Y. Production of biologically activated carbon from orange peel and landfill leachate subsequent treatment technology. Journal of Chemistry. 2014;**2014**:1-9. DOI: 10.1155/2014/491912

[31] Quijano MA, Mejía GM. Integrated utilization of orange peel. Bioresource Technology. 1993;**44**(1):61-63. DOI: 10.1016/0960-8524(93)90209-T

[32] Annadurai G, Juang RS, Lee DJ. Use of cellulose-based wastes for adsorption of dyes from aqueous solutions. Journal of Hazardous Materials. 2002;**92**(3):263-274. DOI: 10.1016/S0304-3894(02)00017-1

[33] Khaled A, El-Nemr A, El-Sikaily A, Abdelwahab O. Removal of direct N Blue-106 from artificial textile dye effluent using activated carbon from orange peel: Adsorption isotherm and kinetic studies. Journal of Hazardous Materials. 2009;**165**(1–3):100-110. DOI: 10.1016/j.jhazmat.2008.09.122

[34] Khaled A, El-Nemr A, El-Sikaily A, Abdelwahab O. Treatment of artificial textile dye effluent containing direct yellow 12 by orange peel carbon. Desalination. 2009;**238**(1–3):210-232. DOI: 10.1016/j.desal.2008.02.014

[35] Fernandez ME, Nunell GV, Bonelli PR, Cukierman AL. Activated carbon developed from orange peels: Batch and dynamic competitive adsorption of basic dyes. Industrial Crops and Products. 2014;**62**:437-445. DOI: 10.1016/j.indcrop.2014.09.015

[36] Ashtaputrey SD, Ashtaputrey PD. Preparation and characterization of activated charcoal derived from orange peel. Journal of Advanced Chemical Sciences. 2016;**2**(3):360-362

[37] NGO Committee on Education. Report of the World Commission on Environment and Development: Our Common Future [Internet]. 1987. Available from: http://www.un-documents.net/wced-ocf.htm [Accessed: January 2018]

Edited by Taner Yonar

Water is accepted as the most important source of life. It is assumed that life began in water and spread from there to the whole world. But water has been polluted anthropogenically since the beginning of the industrial revolution in the late 19th century. At the end of the 20th century, most water sources cannot be used for aquaculture, irrigation, and human use. Therefore, for sustainable development, we have to protect our water sources on Earth, because it's the only planet we have!

Published in London, UK

IntechOpen

ISBN 978-1-83881-539-4